THE ROLE OF ENDOGLIN IN ANGIOGENESIS AND ITS POTENTIAL AS AN ANTI-ANGIOGENIC THERAPEUTIC TARGET

ZHENHUA ZHAI MBBS, MSc

Thesis submitted for the degree of Doctor of Philosophy

Institute of Genetic Medicine

Newcastle University, UK

August 2011

Abstract

Tumour growth and metastasis depend on the vascularization of tumours by angiogenesis. This is regulated by the combined action of several growth factors (e.g. vascular endothelial growth factor, VEGF) that are secreted by the growing tumour, and activate VEGF receptors (VEGFR) expressed on the surface of endothelial cells to stimulate new blood vessel formation. Therapies that target VEGF/VEGFR signalling have indicated that anti-angiogenic therapy may be a useful supplementary anti-cancer treatment in the clinic. In addition to VEGF, malignant cells secrete transforming growth factor (TGF)-β, which is thought to stimulate new blood vessel formation by interacting with endoglin, an endothelial co-receptor for TGF-β that regulates angiogenesis. However, it is not yet clear whether this property could also be utilised to inhibit angiogenesis and metastasis, consistent with endoglin acting as a therapeutic target in a clinical setting.

Therefore, the aim of my project was to investigate the role of endoglin in tumour angiogenesis and metastasis and its potential as an anti-angiogenic therapeutic target. I used a conditional endoglin knockout mouse model, that was generated by combining a floxed endoglin allele with a tamoxifen inducible vascular specific Cre (*Cdh5*(PAC)Cre-ER^{T2}). Angiogenesis was tested using the matrigel subdermal plug assay and was significantly less in endoglin-deficient adult mice compared with tamoxifen treated control mice. Subsequently, angiogenesis and metastasis were investigated using a subdermal lewis lung carcinoma (LLC) model. The growth of the primary tumours was initially reduced, suggesting that targeting endoglin may delay tumour progression at an early stage. However, there was no significant effect of endoglin loss on primary tumour growth at later stages of tumour progression. Furthermore, loss of endoglin was associated with a significant increase in metastases, in a similar way to recent findings for other anti-angiogenesis treatments. The reasons for this are not yet clear.

In terms of animal health, endothelial specific loss of endoglin alone did not appear to cause any major adverse effects. Endoglin inducible knockout (Eng-iKO^{e}) mice did not lose weight and appeared healthy (over two months). However, Eng-iKO^{e} mice did exhibit abnormal venous enlargement close to matrigel plugs supplemented with angiogenic growth factors compared to control mice. There was no evidence for a similar response in the peritumoral vasculature.

In parallel to the *in vivo* studies, I took advantage of combining the conditional Eng- iKO line and the 'immortomouse' line to create conditionally immortalised Eng-iKO mouse lung endothelial cell lines (MLECs) to investigate the role of endoglin in regulating endothelial cell viability, proliferation and migration. In standard media, MLECs showed normal cell viability, proliferation and migration in the absence of endoglin. However, titration of the growth factor supplements did result in significant reduction in viability in the absence of endoglin, suggesting endoglin is important for maintaining endothelial cell viability.

Although the exact mechanisms regulating the role of endoglin in angiogenesis are still unclear, this study has increased our understanding of the endothelial cell phenotype in pathophysiological conditions in the absence of endoglin. In particular, the finding that endoglin depletion delays tumour progression in the early stage but is associated with increased metastatic risk is important when considering appropriate utilisation of anti-endoglin therapy, which is already being given to cancer patients in phase I/II clinical trials.

Declaration

This thesis is based on my studies in the Institute of Genetic Medicine (known as Institute of Human Genetics before March 2011), Newcastle University, from October 2006 to September 2009. The content of this thesis is original, some of these data were published and no part of this thesis has been submitted for the award of any other degree.

Acknowledgements

This thesis presents the results of my Ph.D. studies at the Institute of Genetic Medicine (IGM), Newcastle University. My student scholarship was funded by an Overseas Research Student (ORS) Award, and the later part of the work was funded by a project grant from Cancer Research UK (CRUK).

For my host laboratory, the work described in this thesis represents the first study in the field of tumour angiogenesis. My first thanks go to Dr. Helen Arthur, my supervisor for convincing me to join the laboratory in 2006 and opening the track for me. Also I am profoundly grateful to her for giving me the freedom to do so and she has been a constant support whatever in research and life through the years. In addition, I would like to extend my thanks to all the colleagues in the lab, since I can not be able to finish my lab work without their support and co-operation. Also I would like to extend my thanks to all the support staff at the IGM, particularly the FGU staff who have been carefully taking care of the mice and Lisa Hodgson for invaluable help with various aspects of microscopy.

Beyond the IGM, I wish to thank my secondary supervisor Dr. Ross Maxwell and Mr. Ian Wilson who work at the MRI and PET-CT imaging centre, Newcastle University. They have given me a lot of background knowledge and practical help during the tumour model scanning.

Finally, I would like to thank my parents, my family and my friends for their support throughout these years. In particular, I wish to thank my wife Mrs. Xiaomeng Zhang who gave massive supports and friends from all over China that help with me in the different fields of academic research and clinical study. I will always remember the time I spent with them as some of the best of my life.

List of abbreviations

ActRI	activin type I receptor
ActRII	activin type II receptor
AIs	angiogenic inhibitors
ALK	activin-like receptor kinase
AVM	arteriovenous malformation
bFGF	basic fibroblast growth factor
BMP	bone morphogenetic protein
BMPRI	bone morphogenetic protein type I receptor
BMPRII	bone morphogenetic protein type II receptor
BSA	bovine serum albumin
CAFs	cancer associated fibroblasts
CEPCs	circulating endothelial progenitor cells
Cdh5	cadherin5
Co-Smad	common mediator Smad
CPA	cyclophosphamide
CRPC	castrate resistant prostate cancer
CSC	cancer stem cell
CT	computed tomography
CTCs	circulating tumour cells
CV	coefficient of variation
DAB	3-3'-diaminobenzidine tetrahydrochloride
dATP	deoxyadenosine triphosphate
dCTP	deoxycytidine triphosphate
DH_2O	distilled water
DEPC	diethyl pyrocarbonate
DMEM	Dulbecco's modified Eagle's medium
DMSO	dimethyl sulphoxide
DNA	deoxyribonucleic acid
dNTPs	deoxyribonucleotide triphosphate

DPX	doxorubicin
dTTPs	deoxythymidine triphosphates
ECs	endothelial cells
ECM	extracellular matrix
EDTA	ethylenediaminetetraacetic acid
EGTA	ethylene glycol tetraacetic acid
EGF	epidermal growth factor
EMT	epithelial mesenchymal transition
Eng	endoglin
EndMT	endothelial mesenchymal transition
EPCs	endothelial progenitor cells
EtOH	ethanol
FCS	fetal calf serum
FDA	food and drug administration
FDG	fludeoxyglucose
FGF	fibroblast growth factor
FITC	fluorescein isothyocyanate
FMT	fluorescent mediated tomography
FSP1	fibroblast specific protein1
GEM	genetically engineered mice
GDF	growth differentiation factor
HE	haematoxylin eosin
HGF	hepatic growth factor
HHC	hepatocellular carcinoma
HHT	hereditary haemorrhagic telangiectasia
HIF	hypoxia inducible factor
HMEC1	human microvessel endothelial cell line-1
HNSCCS	head and neck squamous cell carcinomas
HPCs	haematopoietic progenitor cells
HRP	horseradish peroxidase

HSCs	haematopoietic stem cells
HUVEC	human umbilical vein endothelial cells
Id	inhibitor of differentiation
IFN	interferon
IGF	insulin-like growth factor
IHC	immunohistochemistry
iKO	inducible knockout
IL	interleukin
IMG	intussusceptive microvascular growth
IP	intraperitoneal
IQR	interquartile range
I-Smad	inhibitory Smad
JAM-1	junctional adhesion molecule
LLC	lewis lung carcinoma
LYVE	lymphatic vessel endothelial hyaluronan receptor
mAb	monoclonal antibody
MEEC	mouse embryonic endothelial cells
MeOH	methanol
MLECs	mouse lung endothelial cells
MMP	matrix metalloprotease
MRI	magnetic resonance imaging
mRNA	messenger RNA
MTT	3-(4,5-dimethylthiazol-2-yl)-2,5-diphenyltetratetrazolium bromide
MTD	maximum tolerated dose
MVD	microvessel density
NO	nitric oxide
NP40	nonidet p40
NSCLC	non-small cell lung cancer
OHT	hydroxy tamoxifen

PAC	P1 artificial chromosome
PAI-1	plasminogen activator inhibitor-1
PBS	phosphate buffered saline
PCs	pericytes
PCR	polymerase chain reaction
PDGF	platelet-derived growth factor
PDGFR	platelet-derived growth factor receptor
PECAM-1	platelet and endothelial cell adhesion molecule-1
PET	positron emission tomography
PFA	para-formaldehyde
PlGF	placental growth factor
PT	primary tumour
RCC	renal cell carcinoma
RFP	red fluorescent protein
RGD	arginine-glycine-aspartic acid
RNA	ribonucleic acid
R-Smad	receptor-regulated Smad
SCID	severe combined immunodeficiency
SD	standard deviation
SDS	sodium dodecyl sulphate
sEND-1	skin (dermal vascular) endothelial cells
SMCs	smooth muscle cells
SPECT	single-photo-emission computed tomography
SV40 TAg	simian virus 40 larger T antigen
TAE	Tris-acetate EDTA
TAK1	TGF-β activated kinase 1
TGFBR1	TGF-β type I receptor
TGFBR2	TGF-β type II receptor
TBS	tris buffered saline
TBST	tris buffered saline Tween

TGF	transforming growth factor
TKIs	tyrosine kinase inhibitors
TNF-α	tumour necrosis factor-α
TRIS	tris (hydroxymethyl) methylamine
VDAs	vascular disrupting agents
VE-	vascular endothelial
VEGF	vascular endothelial growth factor
VEGFR	vascular endothelial growth factor receptor
VPF	vascular permeability factor
VSMC	vascular smooth muscle cell
vWF	von Willebrand Factor
X-gal	5-bromo-4-chloro-3-inody-beta-D-galactopyranoside
ZP	zona pellucida

List of contents

List of figures

List of tables

Chapter 1. Introduction

1.1 Vasculogenesis and angiogenesis

Vessel growth can be classified in two distinct ways, vasculogenesis and angiogenesis (Figure 1.1). Vasculogenesis leads to the first primitive vascular plexus of the embryo and its yolk sac, via the in situ differentiation and growth of blood vessels from mesoderm-derived haemangioblasts. Subsequently, blood vessels are remodelled and expanded from pre-existing ones, which can occur by both sprouting and non-sprouting angiogenesis. The sprouting of vessels and intussusceptive microvascular growth (also known as splitting angiogenesis) are two distinct processes of angiogenesis. The sprouting angiogenesis includes endothelial cell (EC) migration, proliferation and tube formation (Carmeliet, 2005). Intussusceptive angiogenesis involves the capillary wall extending into the lumen to split a single vessel in two. This type of angiogenesis is totally different from sprouting angiogenesis since it is a reorganization of existing cells and does not require intense local EC proliferation (Djonov et al., 2000).

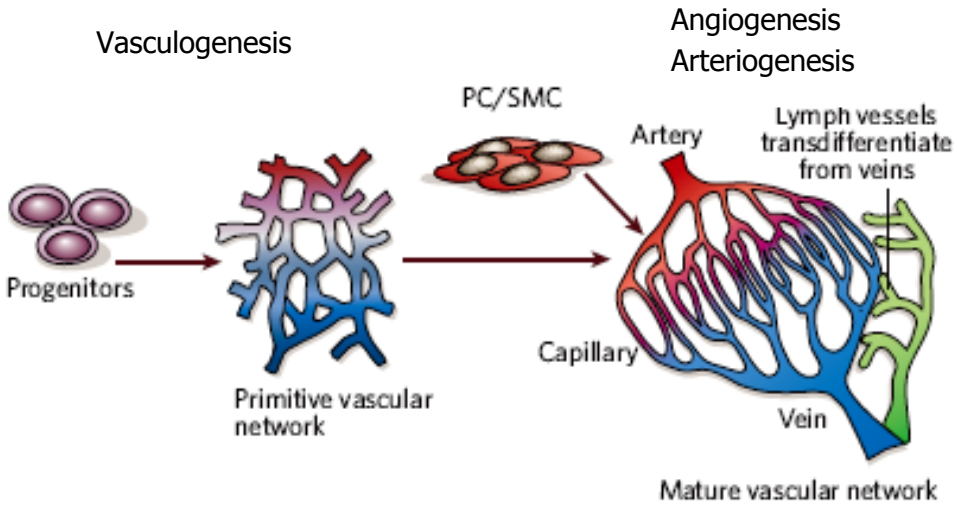

Figure 1.1 Formation of blood and lymph vessels.

Endothelial progenitors generate primitive vascular capillaries during vasculogenesis. Afterwards, the primitive vascular network expands by angiogenesis, the nascent endothelial channels are covered by pericytes (PCs) and smooth muscle cells (SMCs), and then a stereotypically organized vascular network of arteries and veins emerges. Arteriogenesis refers to the remodelling of an existing artery to increase its luminal diameter in response to increased blood flow. In addition, lymphatic vessels are transdifferentiated from veins. Adapted from (Carmeliet, 2005).

1.2 Tumour angiogenesis, tumour growth and metastasis

1.2.1 Carcinogenesis and cancer stem cells

Carcinogenesis is a dynamic process where cancer cells are transformed from normal cells. Mutations in DNA of normal cells can disturb the balance between normal cell proliferation and cell death leading to carcinogenesis. Typically, a number of serial mutations in critical genes including tumour suppressor genes, proto-oncogenes and DNA repair genes are required before a normal cell transforms into a cancer cell. More recently, carcinogenesis has been considered in the context of developmental biology and stem cells. The hypothesis of the cancer stem cell (CSC) proposes that misregulation of this pluripotent cell type can result in a variety of heterogeneous tumour cells. Either transformation of adult stem cells or differentiated cells within a tissue might generate CSCs. These cells still maintain the key features of stem cells such as differentiating into different kinds of cells and self-renewal capability and also function as a subcomponent of the tumour. Moreover, these cells may also contribute to cancerous relapse and metastatic emergence (Dalerba et al., 2007; Bomken et al., 2010).

1.2.2 Tumour angiogenesis and cancer progression

Tumour angiogenesis is basically the formation of new blood vessels from pre-existing vasculature, which is extremely important for the survival and proliferation of cancer cells since tumour-associated neovasculature supplies oxygen and nutrients and removes waste products (Figure 1.2). Tumour angiogenesis is a complicated process that is divided into several processes: vasculogenesis, vascular remodelling (co-option), angiogenesis (vascular sprouting and intussusception), vasculogenic mimicry (formation of tumour neovasculature partially contributed by tumour cells) and vessels formed partially by ECs that differentiated from cancer stem-like cells and is regulated by a number of pro-angiogenic and anti-angiogenic molecules (Chang et al., 2000; Carmeliet and Jain, 2011a).

The initiation of angiogenesis is largely determined by the balance between pro-angiogenic factors and anti-angiogenic factors. In most normal tissues the balance favours the anti-angiogenic factors and angiogenesis is inhibited. In contrast, many tumour cells switch toward an angiogenesis-stimulating phenotype associated with an increase in producing angiogenic factors. Cancer cells secrete pro-angiogenic growth factors that bind to receptors on the surface of endothelial cells (ECs) on neighbouring vessels. Then ECs that acquire an angiogenic phenotype as a result of this stimulation are capable of migration and proliferation to form new sprouts from the pre-existing vasculature. In fact, during tumour progression, genetic alterations of tumour oncogenes and suppressors and responses to oxygen reduction can lead to overexpression of pro-angiogenic growth factors. These include vascular endothelial growth factor (VEGF), fibroblast growth factor (FGF), epidermal growth factor (EGF), platelet-derived growth factor (PDGF) and transforming growth factor (TGF)β (Chung et al., 2010). The initial stimulation of tumour vasculature formation is termed the 'angiogenic switch' and can occur at any stage of tumour progression and also plays an important role in several steps of tumour progression including promoting a small avascular primary tumour to a large vascular tumour, activating a dormant lesion and in the conversion of micrometastases to macrometastases (Bergers and Benjamin, 2003). Hypoxia caused by insufficient oxygen supply in a rapidly growing tumour is one of the most important factors triggering the angiogenic switch. For example, stabilisation of hypoxia inducible factor (HIF)-1α in response to hypoxia leads to a major increase in the expression of vascular endothelial growth factor A (VEGFA) which promotes angiogenesis (Forsythe et al., 1996; Bergers and Benjamin, 2003; Manalo et al., 2005; Majmundar et al., 2010). Therefore, it will be useful to know whether the inhibition of the angiogenic switch can reduce the conversion of pre-angiogenic micrometastases to angiogenic macrometastases.

In addition to tumour vessels originating from the neighbouring vasculature by angiogenesis, two recent independent studies showed that glioblastoma stem-like

cells are capable of giving rise to their own blood vessels (Ricci-Vitiani et al., 2010; Wang et al., 2010a). It appears that glioblastoma cells with stem cell like features can make ECs as well as cancer cells. The anti-angiogenic drug Bevacizumab (Avastin, described below) did not affect the differentiation of cancer stem cells into endothelial progenitor cells (EPCs), however it did inhibit their further differentiation to ECs. Targeting endothelial cells generated by glioblastoma derived stem cells resulted in significant reduction of tumour growth. Although these studies were performed using a glioblastoma model, similar mechanisms may be involved in other tumours and their metastases. The findings describe a novel link between glioblastoma stem-like cells, endothelial progenitors and tumour derived endothelium. It is thus a new mechanism for tumour neovascularisation, which remains to be confirmed in a wide range of other tumours.

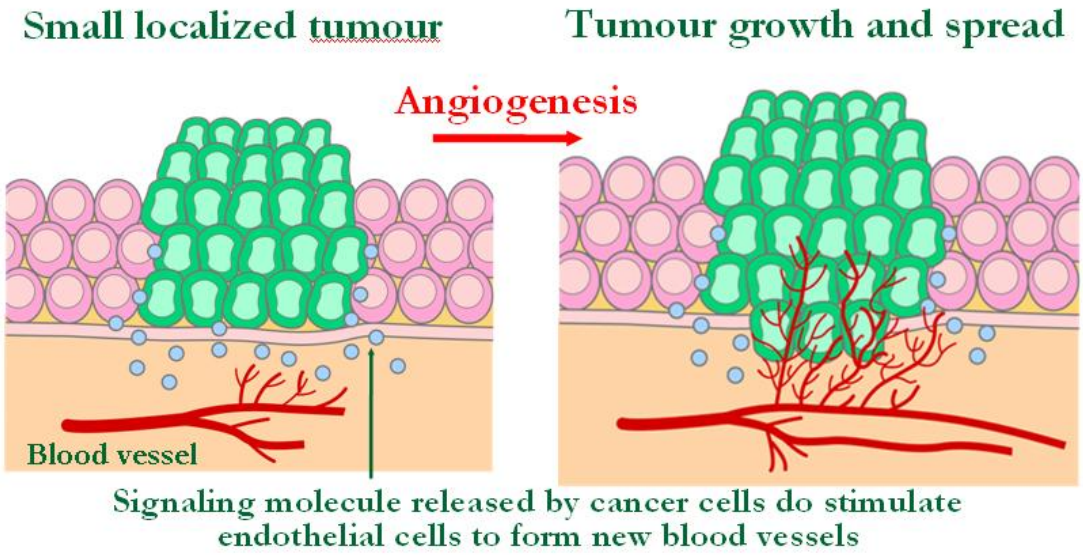

Figure 1.2 Schematic picture of tumour new blood vessel formation.

Tumour angiogenesis is the formation of new blood vessels that penetrates into a solid cancer mass, supplying nutrients and oxygen and removing waste products. Cancer cells release pro-angiogenic molecules to stimulate ECs to form new vessels to vascularise the growing tumour. These tumour vessels also provide an opportunity of tumour dissemination. Adapted from National Cancer Institute, NIH, http://www.cancer.gov/.

1.2.3 Tumour angiogenesis and lymphangiogenesis in the tumour metastatic cascade

The growth of secondary tumours that are seeded from and are distant to the primary tumour causes the majority of cancer patient mortality. The primary tumour may be removed surgically, but numerous secondary tumours may be present, for example in the liver, lung or bone tissues. A better understanding of the complex metastatic process that is responsible for the spread of the tumour is extremely important for exploring novel anti-cancer treatments. The formation of new blood vessels (angiogenesis) and new lymphatic vessels (lymphangiogenesis) are critical for cancer metastasis as these provide the 'conduits' for spread of the cancer cells (Figure 1.3). As mentioned above, tumour angiogenesis can be stimulated by VEGF-A (as well as by VEGF-C and VEGF-D). In addition, VEGF-C and VEGF-D can induce lymphangiogenesis of the primary tumour and subsequent metastatic spread of cancer cells to lymph nodes. Cancer cells may be disseminated using both the lymphatic and blood circulation systems. For instance, the spread of tumour cells could be via blood vessels from lymph nodes to distant organs (Achen and Stacker, 2008).

Interestingly, both clinical observations and experimental studies have found that certain tumours metastasize to specific organs (Langley and Fidler, 2007). It seems that these findings can be explained by the cross-talk between the 'seed and soil', which was proposed by Stephen Paget in 1889 (Fidler, 2003) and refined by Isaiah Fidler. Metastasis to specific organs is likely due to interactions between specific subpopulations of metastatic cancer cells (seed) and host homeostatic factors in specific organ microenvironments (soil) that include the vasculature. Though, the cellular and molecular mechanisms by which disseminating tumour cells metastasize to a pre-determined conducive location are largely unknown. There are a number of possibilities underpin the 'seed and soil' hypothesis, for example, bone marrow derived VEGFR1 (+)-haematopoietic progenitor cells (HPCs) in combination with the expression patterns of fibronectin at pre-determined

metastatic niches to generate a conducive microenvironment for tumour cell adhesion and extravasation (Kaplan et al., 2005). Furthermore, some adhesion molecules such as metadherin (a tumour cell surface adhesion molecule) mediates specific adhesion of breast cancer cells to the lung vasculature (Brown and Ruoslahti, 2004). Therefore, a new understanding of these issues should result in new therapeutic development against metastases by targeting metastatic cells and/or the specific organ microenvironment, such as organ-specific vasculature. It seems that anti-angiogenic therapy against metastases is an important area for future research (Langley and Fidler, 2007; Psaila and Lyden, 2009; Hanahan and Weinberg, 2011).

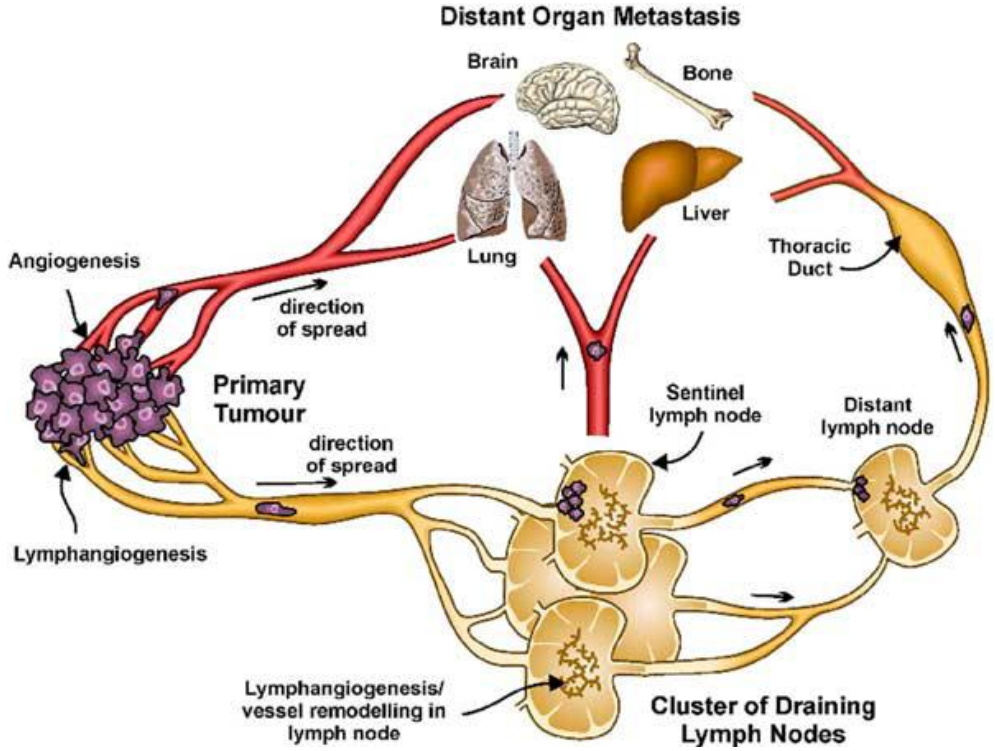

Figure 1.3 Summary of a metastatic cascade via blood and lymphatic vessels
Metastasis is a multistage process that consists of sequential, interlinked, and selective steps and requires cancer cells to escape from the primary tumour, survive in the circulation, seed at distant sites and grow. Primary tumour cells can spread to metastatic sites via blood vessels and/or lymphatic vessels. Adapted from (Achen and Stacker, 2008).

1.2.4 Tumour associated endothelium and vasculature

Tumour angiogenesis is associated with the formation of poorly muscularised and high permeable vasculature in a chaotic and disorganized pattern that enable

metastatic cancer cells to disseminate via the blood and/or lymphatic vessels. Tumour associated endothelium differs from the endothelium of normal vasculature- there are both morphological differences from normal ECs within the same organ, as well as changes at the molecular level (Charalambous et al., 2006; Bussolati et al., 2010). It was shown that cultured ECs derived from neuroblastomas, meningiomas and glioblastoma multiforme were morphologically characterized by a veil-like flat structure with large nuclei which was totally different from the typical cobblestone-like appearance of cultured normal ECs (Alessandri et al., 1999; Charalambous et al., 2005). It was also found that some endothelial cell-specific genes were expressed only in angiogenic blood vessels of tumours rather than in physiologically angiogenic blood vessels (Seaman et al., 2007). For example, Tie-2 (Fathers et al., 2005), endoglin (di Tomaso et al., 2005) and PECAM-1 (di Tomaso et al., 2005) may be heterogeneously expressed in some tumour-associated ECs. Coevolution of tumour cells and the tumour stroma and tumour-specific angiogenic growth factors may cause intratumoural differences in the endothelium (Langenkamp and Molema, 2009; Bussolati et al., 2010). In addition, tumour vasculature might be temporally and spatially different depending on tumour stage and tumour microenvironment (Hellebrekers et al., 2007; Langenkamp and Molema, 2009). A mosaic phenotype of tumour blood vessels results from discontinuities in the expression of EC-specific markers and gaps between adjacent ECs. Thus, the heterogeneity and alterations of tumour-associated ECs appear to be associated with specific stage and tumour type and these differences may contribute to the evasiveness of some tumours to anti-angiogenic drugs (Aird, 2009; Bussolati et al., 2010). Therefore, deciphering the molecular mechanisms that regulate tumour-associated ECs within the specific tumour microenvironment might lead to novel ways of overcoming tumour resistance to current therapies.

1.2.5 Anti-angiogenic therapy

It seems that targeting tumour-associated ECs has opened a new era in the field of cancer therapy. In the past four decades, a large number of anti-angiogenic therapeutic agents have been tested in the clinical settings, but currently only four anti-angiogenic drugs are approved by the Food and Drug Administration (FDA) for six tumour indications (Ebos and Kerbel, 2011). The humanized murine anti-vascular endothelial growth factor (VEGF) monoclonal antibody (mAb) bevacizumab (avastin; Genentech) was the first molecular-targeted anti-angiogenic therapy approved by the FDA. It was found to have a beneficial effect when used in combination with chemotherapy and has received FDA approval for the treatment of metastastic colorectal cancer (CRC) (Hurwitz et al., 2004; Ferrara and Kerbel, 2005). Afterwards, the FDA granted approval for the treatment of non-small cell lung cancer (NSCLC), metastatic HER2-negative breast cancer (MBC), glioblastoma mulifore (GBM) and metastatic renal cell carcinoma (mRCC) (The information originated from http://www.cancer.gov/cancertopics/druginfo/fda-bevacizumab). In patients with solid tumours, however, who are found to benefit from VEGF-targeted therapy, the improved overall survival is relatively short (Ellis and Hicklin, 2008). Moreover, it has been recently announced that FDA will take the first step to remove the usage of bevacizumab in metastatic breast cancer since the data from 4 clinical trials indicated there was almost no improvement in progression-free survival (PFS) or overall survival (OS) in patients with metastatic breast cancer with bevacizumab treatment. In addition, patients were at risk of serious side effects such as hypertension, stroke, organ damage and wound healing complications (The information was summarized on the Medscape Medical News website: http://www.medscape.com/viewarticle/734373).

The mammalian VEGF family is a large family of potent angiogenic regulators including VEGFA, VEGFB, VEGFC, VEGFD and placental growth factor (PIGF, also known as PGF). The well characterized member of VEGF family is VEGFA (commonly termed as VEGF), which is expressed as various isoforms (mature

121-, 165-, 189- and 206-amino-acid proteins), depending on alternative splicing. VEGF-A_{165} is the major isoform and is overexpressed in a wide range of human solid tumours. Binding of VEGFA to the VEGF receptor, VEGFR2 (primarily restricted to the vasculature), promotes EC differentiation, proliferation and sprouting. Also, the vascular response to VEGF is increased within the tumour due to the upregulation of VEGFR2 in response to hypoxia (Brekken and Thorpe, 2001). In addition, the pro-angiogenic and anti-angiogenic responses such as ECs proliferation, migration and tube formation are tightly regulated by different VEGF ligands. For instance, the pro-angiogenic isoform VEGF-A_{165} and the anti-angiogenic isoform VEGF-A_{165}b can be produced via alternative splicing of exon 8 (Bates et al., 2002). In addition, another member of the VEGF xxxb family, $VEGF_{121}$b, which is also a VEGF-A splice isoform, functions as an anti-angiogenic agent to inhibit tumour-associated neovascularisation and tumour progression (Rennel et al., 2009). Therefore, regulating splicing of the different VEGFA isoforms from pro-angiogenic to anti-angiogenic forms could provide a novel therapeutic strategy to regulate blood vessel growth (Nowak et al., 2010).

In addition to Bevacizumab, there are some other VEGF or VEGFR targeted agents that are being tested in current clinical trials. For instance, the multi-tyrosine kinase inhibitor (TKI) Sunitinib (Sutent, Pfizer), which is a small-molecule inhibitor with high affinity for VEGFR, PDGFR, receptor tyrosine kinase encoded by the ret proto-oncogene and c-Kit receptors. Another example is Sorafenib (Nexavar, Bayer/Onyx), which is a potent inhibitor of Raf-1 kinase and VEGFR-2. These kinase inhibitors are approved for use as single agents for patients with certain types of cancer such as renal cell carcinoma (RCC) and hepatocellular carcinoma (HHC). Recently, Pazopanib (Votrient, GlaxoSmithKline) has been approved to treat metastatic RCC by the FDA and supposed to inhibit VEGFR-1, VEGFR-2, VEGFR-3, PDGFR-a/β, and c-Kit (Escudier et al., 2007; Motzer et al., 2007; Josep M. Llovet, 2008; Llovet et al., 2008; Ivy et al., 2009). However, these clinical successes have been accompanied

by some unexpected difficulties - the majority of patients are resistant to or do not respond at all to these anti-angiogenic therapies (Ebos and Kerbel, 2011).

Therefore, three crucial things must be emphasized as priorities, one is to understand multiple mechanisms of the therapeutic benefits associated with VEGF-targeted therapies, these will refine current knowledge and guide towards more effective use of these agents in the clinic. The second priority has to be to investigate drug resistance mechanisms resulting from VEGF-targeted therapies in appropriate pre-clinical animal models of all tumour progression stages. Finally, in order to use anti-angiogenic agents precisely and efficiently, it will be important to identify predictive biomarkers that indicate which patients are likely to have a good and stable response (Murukesh et al., 2010) and also to discover new combination regimens that improve their efficacy.

1.3 Prospective developments of anti-angiogenic therapy for cancer

1.3.1 Targeting tumour angiogenesis

Unexpectedly, it was recently reported that targeting VEGFA/VEGFR2 in mouse studies can lead to increased primary tumour invasion and metastasis (Ebos et al., 2009; Paez-Ribes et al., 2009). These pre-clinical studies have demonstrated that VEGF-targeted therapies may make cancer cells more aggressive and invasive, ultimately leading to increased metastasis. In addition, it has been reported that a rapid re-growth of tumour and associated vasculature occurs following withdrawal of VEGF-targeted treatment in pre-clinical studies (Mancuso et al., 2006). These findings, although interesting, have caused concern to clinicians and patients in consideration of anti-VEGF therapies' detrimental effects. It is absolutely necessary to look into the relevant data from collective recent clinical trials to determine whether these pre-clinical observations are likely to occur in the clinic. The answer from leading clinical investigators appears to be "No". The data from a number of phase III trials including 4205 patients with a variety of tumour types was reviewed and analysed using meta-analysis, which indicates there is no clinical evidence that

VEGF-targeted treatment lead to accelerated tumour aggressiveness and growth or increased death caused by enhanced metastasis. Also there was no evidence for earlier relapse occuring following cessation of bevacizumab treatment in patients (Ellis and Reardon, 2010). Further studies will help understand the mechanisms involved in generating increased tumour aggressiveness in the pre-clinical anti-VEGF models and these factors may yet be important in bevacizumab treated patients with longer survival times. Continuous and responsive pre-clinical and clinical research cycle – from bench to bedside and back to bench- are required to facilitate the best outcomes for patients in the longer term.

1.3.2 Effects of anti-angiogenic therapy in multistages of cancer progression

"Stage-dependent anti-angiogenic therapy" means that the efficiency of different anti-angiogenic therapies is dependent on specific stages of tumour progression. Transgenic mice (RIP1-Tag2) that develop pancreatic islet carcinoma in a multistage process were treated with four angiogenesis inhibitors AGM-1470, angiostatin, BB-94, and endostatin at three distinct stages of disease progression. This resulted in preventing the angiogenic switch in premalignant lesions, intervening in the rapid expansion of small tumours, or inducing the regression of large end-stage cancers, indicating that anti-angiogenic drugs may prove most efficacious when they are targeted to specific stages of cancer progression (Bergers et al., 1999). Furthermore, it was shown in this RIP1-Tag2 mouse model that Semaxinib (SU5416), targeting VEGFRs, effectively inhibits the formation of early-stage angiogenic islets rather than late-stage, intensely vascularized and invasive tumours (Bergers et al., 2003). In contrast, a PDGFR inhibitor (SU6668) prohibits advanced-stage tumour growth due to targeting more mature tumour vasculature. Application of SU5416 in combination with SU6668 were shown to be more efficacious against all stages of islet carcinogenesis than either single agent. Hence, it seems to be promising to apply combinatorial targeting of receptor tyrosine kinases in multiple stages of tumorigenesis (Bergers and Benjamin, 2003). Clinically, it should be informative to profile overexpression of pro-angiogenic

growth factors in distinct stages of cancer progression and explore specific biomarkers that can predict potential efficacy of certain anti-angiogenic agents.

1.3.3 Vascular 'normalisation' and combination therapies

Jain (2001) has proposed that some anti-angiogenic therapies can transiently 'normalize' tumour vasculature. This principle is based on the fact that tumour-associated blood vessels are leaky and dysfunctional and can result in inadequate delivery of chemotherapeutics from the bloodstream to the tumour cells. For example anti-VEGF therapies can promote 'Vascular Normalization' to reduce vascular leakiness and promote more uniform tumour vasculature that allows improved drug delivery (Jain, 2005b). This would synergise the effects of an anti-angiogenic therapy in combination with chemotherapy or radiation therapy over a defined time window. Anti-angiogenic therapy is supposed to be used in this transient defined time window when tumour vasculature are properly 'normalized'. In principle, tumour vascular 'normalization' improves the delivery of blood to the tumour which may underlie the synergistic benefit of both anti-angiogenic and cytotoxic therapies (Jain, 2005a). However, it remains to be established whether such a mechanism accounts for the long-term beneficial effects of combination treatment observed in some trials and also those benefits must be tested in randomized clinical trials.

'Metronomic Therapy' was proposed by Dr. Robert Kerbel and colleagues, which means chemotherapy delivered at close regular intervals using relatively low doses with no prolonged drug-free break periods and was thought to preferentially damage tumour associated ECs (Kerbel and Kamen, 2004; Emmenegger et al., 2010). Unlike conventional chemotherapy, which is designed to target proliferating cancer cells, the main targets of metronomic therapy are proliferating tumour associated ECs, so that this treatment strategy was also described as 'anti-angiogenic chemotherapy' (Browder et al., 2000). In addition, there is the possibility of combining metronomic therapy with anti-angiogenic agents, as well

as other types of targeted therapies. It was recently reported that metronomic delivery of irinotecan (CPT-11) combined with semaxinib (SU5416) to a human colon adenocarcinoma (HT-29) xenograft mouse tumour model significantly inhibits tumour growth which was coupled with reduced microvessels (Bocci et al., 2008). In addition, metronomic therapy may also inhibit circulating endothelial progenitor cells (cEPCs) that may support tumour regrowth (Daenen et al., 2009). Taken together, it will become increasingly critical to explore the more efficacious anti-angiogenic agents and design more effective ways of combining such drugs with metronomic chemotherapy (Hashimoto et al., 2010; Wong et al., 2010).

Basically, anti-vascular therapies in tumours can take place using two main approaches. One approach is that of vascular targeting using vascular disruptive agents (VDAs). This type of therapy aims to target endothelium of pre-existing tumour blood vessels leading to selective and rapid destruction of the tumour vasculature. This may be accompanied by extensive hemorrhagic necrosis due to tumour cell ischemia death (Tozer et al., 2005). A second approach is anti-angiogenic therapy that aims to prevent the formation of new vessels in the tumour. In principle, it will be more efficacious to combine these two types of agents targeting both existing and new intratumoural vasculature, particularly in advanced and late tumour diseases (Tozer et al., 2005; Siemann and Shi, 2008).

In fact, some critical questions must be considered in both pre-clinical and clinical studies, such as 1) the timing of anti-angiogenic therapy; 2) the optimal scheduling of chemotherapy in combination with anti-angiogenic therapy; 3) understanding reasons for unfavourable effects; 4) whether a combination of anti-angiogenic therapies has a synergistic anti-tumour effect; 5) tailored therapy depending on the different angiogenic phenotype and expression of endothelial growth factors at the distinct stages of tumour progression; 6) the optimal biological dose and minimal toxicity. Althought the question list is still extending,

we should continue to explore and identify novel anti-angiogenic agents and approaches. For example, Endoglin, a homodimeric transmembrane glycoprotein overexpressed on angiogenic tumour-associated endothelium (Burrows et al., 1995; F.J. Burrows, 1995; Seon et al., 1997; Miller et al., 1999; Fonsatti et al., 2001; Benetti et al., 2008; Clasper et al., 2008; Yoshitomi et al., 2008), seems to be a promising novel target for anti-angiogenic therapy.

1.4 Endoglin and its role in TGF-β signalling pathway

1.4.1 Endoglin structure and functional features

Endoglin, also known as CD105, is a disulphide-linked homodimeric transmembrane glycoprotein of 180 kDa that consists of an extracellular domain (561 amino acid residues) and a cytoplasmic region (serine/threonine-rich 47 amino acid residues) (Figure 1.4) (Gougos and Letarte, 1990; Bellon et al., 1993). The extracellular domain comprises a zona pellucida (ZP) domain, with an arginine-glycine-aspartic acid (RGD) binding motif (Gougos and Letarte, 1990; Jovine et al., 2005; Llorca et al., 2007), while several potential phosphorylation sites are located in the intracellular region (Lastres et al., 1994). The N terminus region of the ZP domain plays a role in protein-protein interactions (Jovine et al., 2002) (Figure 1.4) and is involved in ligand dependent or independent heteromeric interactions with receptors of the TGF-β family. Therefore, it seems that the ZP domain of endoglin may be responsible for its heteromeric association with TGF-β type I receptor (TGFBR1) and TGF-β type II receptor (TGFBR2), to transduce the signalling of the TGF-β receptor complex (Guerrero-Esteo et al., 2002). The RGD tripeptide is a critical recognition structure in cellular adhesion and has an interaction motif for integrins of cell surface (Gougos and Letarte, 1990; St-Jacques et al., 1994). Although endoglin lacks a signalling kinase domain, it has been shown to promote TGF-β signalling through the type I receptor, ALK1 (Lebrin et al., 2004).

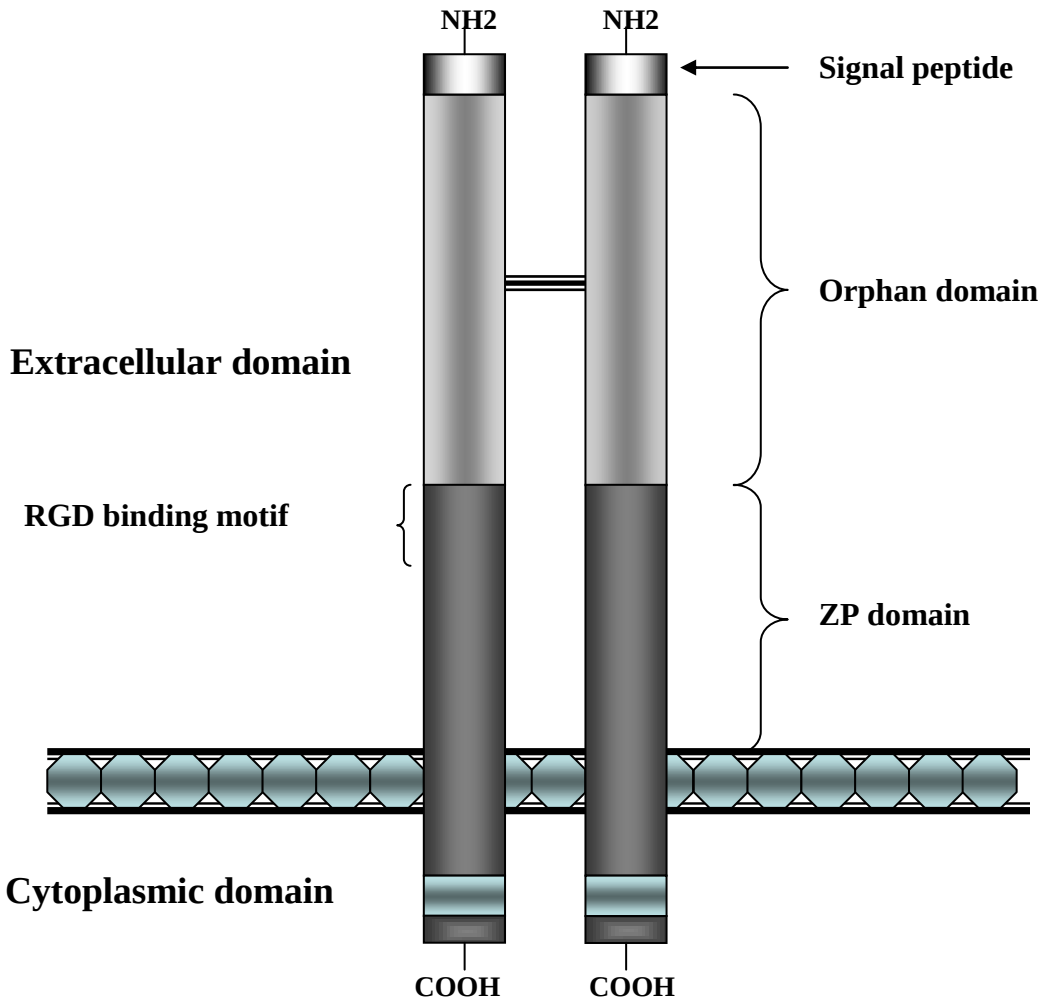

Figure 1.4 Schematic structure of the human TGF-β type III receptor endoglin.

Human endoglin protein consists of 625 amino acids and is present on the cell surface as a homodimeric transmembrane glycoprotein. The extracellular domain contains two long extracellular cysteine domains (orphan domain and ZP domain). A conserved RGD binding motif is found at the ZP domain. However, unlike its human counterpart, mouse endoglin does not itself contain an RGD tripeptide. Also endoglin has a short transmembrane region and a short C-terminal intracytoplasmic region and there is approximately 95% amino acid sequence identity between the transmembrane and cytoplasmic domains of human and mouse endoglin. Adapted from (Garcia-Pozo et al., 2008).

1.4.2 TGF- β superfamily

Transforming growth factor-beta (TGF-β) is the prototypical member of a large family of cytokines, which include the TGF-β isoforms (TGF-β1, TGF-β2 and TGF-β3), activins, bone morphogenetic proteins (BMP) and growth

differentiation factors (GDFs) (Isaac Yi Kim et al., 2005; Schmierer and Hill, 2007). The ligands of the TGF-β superfamily exert their signalling effects by binding to specific transmembrane Ser/Thr kinase receptors that are referred to as type I and type II receptor, some ligands can bind directly to their type II receptors while others can only interact with type II-type I receptor combinations (Lebrin et al., 2005). In addition, there are accessory TGF-β receptors, also known as type III receptors, endoglin and betaglycan (Gougos and Letarte, 1990; Lopez-Casillas et al., 1993). There is a possibility of crosstalk between different ligands and receptors in the different TGF-β signalling pathways, which modulate many aspects of cellular function, including cellular proliferation, differentiation, migration, apoptosis, adhesion, and immune surveillance. Consequently, TGF-β signalling can regulate a variety of important process such as embryonic development, wound healing, haematopoiesis, inflammation, fibrosis, carcinogenesis and angiogenesis (Gordon and Blobe, 2008).

1.4.3 Endoglin regulates angiogenesis through TGF-β signalling in endothelium

Endoglin, can be bound to TGF-β ligands in a complex with type I and type II TGF-β receptors. The type I receptors include activin-like receptor kinase (ALK)1 to ALK6. It has been reported that the type II TGF-β (TGFBRII), activin (ActRII) and BMP (BMPRII) receptors can interact with various type I receptors (Feng and Derynck, 2005; ten Dijke and Arthur, 2007; Gordon and Blobe, 2008). Moreover, it has been shown that endoglin interacts with TGF-β1, TGF-β3, activin-A, BMP-2 and BMP-7 ligands in combination with type I and type II receptors (Cheifetz et al., 1992; Yamashita et al., 1994; Letamendia et al., 1998; Barbara et al., 1999). More recently, Endoglin has been shown to bind BMP-9 to promote signalling through ALK1. This pathway inhibits bFGF-induced EC proliferation and VEGF-stimulated angiogenesis (Scharpfenecker et al., 2007). Furthermore, BMP10 may also act in a similar way to BMP9 (David et al., 2007). Therefore, it seems that the binding of endoglin to type I/II receptor ligand-complexes potentially plays a role

in the dynamic interactions of type I/II receptor of the TGF- β superfamily and their downstream signalling pathways.

How endoglin regulates TGF-β-dependent responses in vascular endothelial cells remains unclear. It has been proposed that endoglin influences TGF-β signals in ECs through two alternative pathways - the balance of which regulating the activation state of the endothelium and angiogenesis (Figure 1.5). Essentially TGF-beta binds the type II receptor (TGFBR2) which then recruits and activates the type I receptor (TGFBR1, also known as ALK5) by phosphorylation, subsequently ALK5 phosphorylates Smads 2 and 3 which then form a complex with Co-Smad 4 and translocate to the nucleus. Here, they regulate the transcription of target genes which, in ECs, lead to the inhibition of cell migration and proliferation-resolution phase of angiogenesis. In contrast, if the ALK1 type I receptor is activated, Smads 1, 5 and 8 bind Co-Smad 4 and are transported to the nucleus and regulate expression of specific downstream genes which conversely leads to promotion of cell proliferation and migration- processes associated with the activation phase of angiogenesis (Lebrin et al., 2004). ALK5 is the predominant mediator of TGF-β signalling in quiescent endothelial cells, but during angiogenesis, ALK1 is preferentially activated (Bertolino et al., 2005). In addition, the absence of ALK5 in cells results in a decrease in ALK1 signalling, demonstrating the presence of ALK5 is also required for signalling via ALK1 (Goumans et al., 2002; Goumans et al., 2003; Lebrin et al., 2004). Therefore, endoglin may exert "positive" or "negative" effects on endothelial cell growth and differentiation by regulating the balance between ALK1 and ALK5 receptor signalling. It seems to be well-recognized that endoglin functionally associated with ALK1 is critical for endothelial cell responses to TGF-β (Lebrin et al., 2004).

TGF-β1 exerts bifunctional effects on ECs *in vitro*, it can both stimulate and inhibit the proliferation of endothelial cells. Low concentrations (0.1-0.5 ng/ml) of extracellular TGF-β1 added in culture medium promotes the proliferation and

migration of ECs that leads to angiogenesis. In contrast, high levels (5-10 ng/ml) of TGFβ1 result in inhibition of cell proliferation, induction of apoptosis, cellular adhesion and synthesis of ECM proteins (Pepper et al., 1993; Lastres et al., 1996; Letamendia et al., 1998; Li et al., 2000; Li et al., 2003; Lebrin et al., 2004; Pardali and ten Dijke, 2009; Serrati et al., 2009). Endoglin can modulate these TGF-β-dependent responses in ECs but there have been a number of contradictory reports. For example, suppression of endoglin expression was shown to enhance the inhibition of endothelial cell proliferation associated with TGF-β1. This indicates endoglin expression has a pro-proliferative effect (Li et al., 2000). Similarly, it was shown that endoglin promotes endothelial cell proliferation through a TGFβ-ALK1 pathway in studies using $Eng^{-/-}$ and $Eng^{+/-}$ mouse embryonic endothelial cells (MEECs) (Lebrin et al., 2004). However, it was also reported that an $Eng^{-/-}$ mouse embryonic endothelial cell line can proliferate faster in response to TGF-β than control $Eng^{+/+}$ ECs, suggesting that endoglin is not required for EC proliferation (Pece-Barbara et al., 2005). Therefore, in order to clarify these endoglin-dependent effects on endothelial cell responses, future studies are required using appropriate primary endothelial cells.

Although important evidence of the TGF-β and BMP signalling pathways in vasculogenesis and angiogenesis were shown in several *in vitro* and *in vivo* studies, there are still some contradictions in the field. For instance, it was reported that BMP9 and ALK1 have pro- and anti-angiogenic effects on angiogenesis. ALK1 was reported to play an important role in either promoting the resolution phase of angiogenesis (Oh et al., 2000; Lamouille et al., 2002) or improving the activation phase of angiogenesis (Goumans et al., 2002; Goumans et al., 2003). This contradiction may be due to different cell types used in the studies or ALK1 could be alternatively implicated in both the resolution and activation phases of angiogenesis (Pardali et al., 2010). In addition, BMP9 appears to be an anti-angiogenic agent. It was reported that BMP9 inhibits proliferation and migration of ECs via binding with ALK1 and ALK2 and

phosphorylating Smad1 (David et al., 2007; Scharpfenecker et al., 2007) and also BMP9 signalling was shown to inhibit expression of VEGF through ALK1 (Shao et al., 2009). In contrast, BMP9 induced proliferation of a variety of ECs in in-vitro and in-vivo studies (Suzuki et al., 2010). Moreover, BMP9 in combination with TGF-β can promote VEGF induced EC proliferation and VEGF/bFGF induced angiogenesis in a matrigel *in vivo* assay (Cunha et al., 2010). The contradictions associated with the pro- and anti-angiogenic effects of TGF- β, ALK1 and BMP9 on EC function and angiogenesis remain to be elucidated.

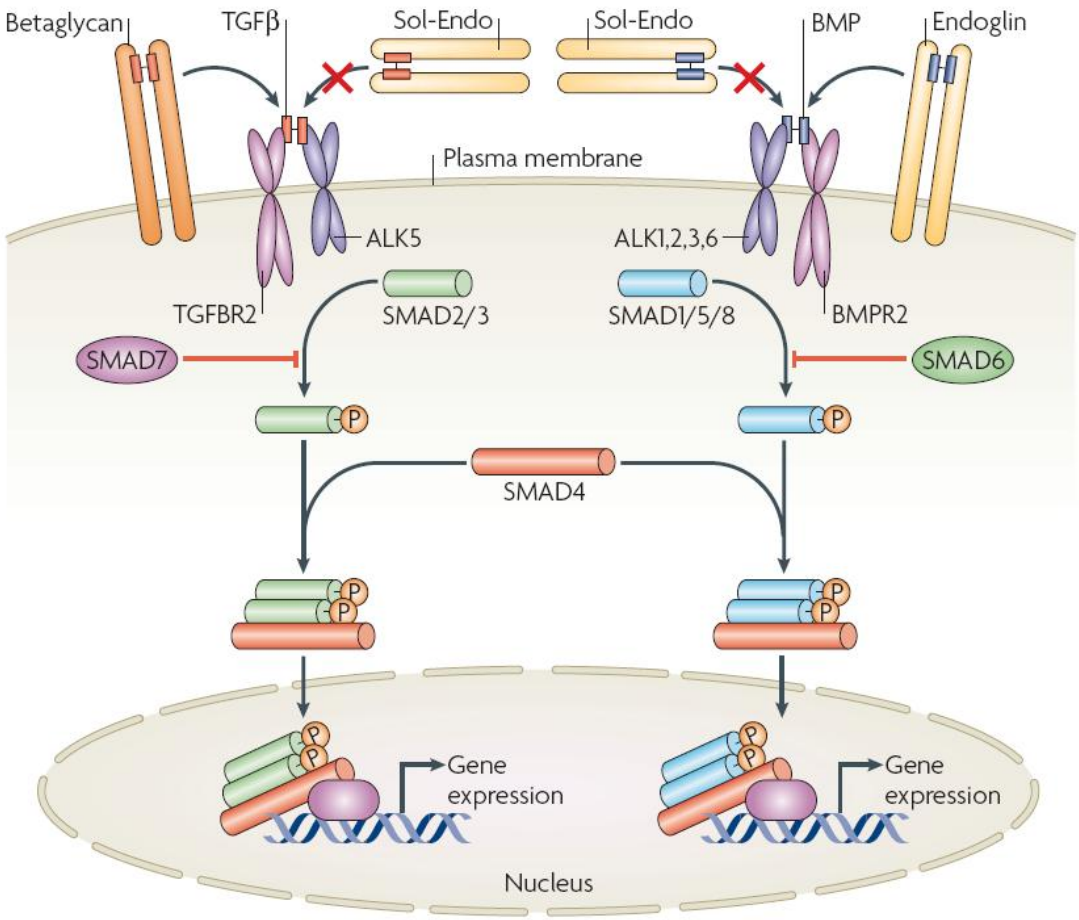

<u>Figure 1.5</u> TGF-β family members and its signal transduction in endothelium
TGF-β signals transduce through specific serine/threonine heterodimeric TGFBR1 and TGFBR2 receptor complexes. Binding of TGF-β to the extracellular domains of TGFBR2 leads to phosphorylation of TGFBR1, which can then specifically activate Receptor associated – Smads (R-Smads; either SMAD2/3 or SMAD1/5/8). Activated R-Smads form complexes with the Co-Smad, Smad4, and subsequently translocate and accumulate in the nucleus. Nuclear Smad complexes can bind to the DNA either directly or indirectly, in complex with other DNA-binding proteins, and regulate the transcription of specific target genes. The TGF-β signals can be

modulated by the accessory receptors betaglycan and endoglin. Endoglin may function to promote binding of members of TGF-β family to their receptors. Moreover, in most cells, TGF-β signals via TGFBR2 and ALK5, and bone morphogenetic proteins (BMPs) signal via the BMP type II receptor (BMPR2) and ALK1, -2, -3 and -6. Adapted from (ten Dijke and Arthur, 2007).

1.5 Endoglin and tumour angiogenesis

1.5.1 Endoglin overexpression as a marker of tumour angiogenesis

Endoglin is considered to be strongly overexpressed on tumour-associated vascular ECs, whereas variable levels of endoglin expression were shown in ECs of different normal tissues (Wang et al., 1993; Burrows et al., 1995; Seon et al., 1997; Miller et al., 1999; Fonsatti et al., 2000). Although it is considered that endoglin is a specific marker of proliferating ECs, it has also been shown to be expressed on several other cell types such as activated monocytes/macrophages, myofibroblasts (Lastres et al., 1992; O'Connell et al., 1992), vascular smooth muscle cells in atherosclerosis (Conley et al., 2000), neural crest stem cells during development (Mancini et al., 2007), adult bone marrow hematopoietic stem cells (HSCs) (Chen et al., 2002) and tumour associated lymphatic endothelium (Clasper et al., 2008; Yoshitomi et al., 2008).

In solid tumours, the expression of endoglin is almost exclusively restricted to ECs of tumour blood vessels (Fonsatti et al., 2001), while it is weakly expressed or absent on malignant cells (Gerhardt et al., 2003). In several solid malignancies of different histotypes, anti-endoglin mAb reacted almost exclusively with venous and arterial endothelium of both peritumoural and intratumoural vessels (Wang et al., 1993; Burrows et al., 1995; Seon et al., 1997; Bodey et al., 1998c; Bodey et al., 1998a; Bodey et al., 1998b; Seon et al., 2011). Occasionally, the antibody weakly stained the cytoplasm of neoplastic cells in sarcomas of different histotype, ovary carcinomas (Henriksen et al., 1995) and breast carcinomas (Fonsatti et al., 2000), or the tumour stromal components in ovarian endometrioid carcinomas (Fonsatti et al., 2001).

Endoglin is a marker of activated endothelium, and is associated with tumour associated proliferating ECs (Miller et al., 1999). Patterns of endoglin expression in primary colon adenocarcinomas and normal colon tissue have been compared with expression of the pan-endothelial marker, CD31. Whilst anti-CD31 antibodies stained blood vessels in both normal and malignant colon equally, endoglin expression was observed primarily in malignant lesions, with little to no expression in the vessels of normal colon tissue (Hawinkels et al., 2010). Furthermore, there were a number of studies that identified upregulation of endoglin expression in many other tumour associated ECs, including those of mammary gland (Li et al., 2001), prostate (Kassouf et al., 2004), cervix (Brewer et al., 2000), colon and rectum (Takahashi et al., 2001b; Akagi et al., 2002), lung (Tanaka et al., 2001), head and neck (Kyzas et al., 2006), kidney (Sandlund et al., 2006), esophagus (Saad et al., 2005) and uterus (Saad et al., 2003). In addition, a number of studies have reported endoglin expression in prostate cancer (Kassouf et al., 2004), squamous cell carcinomas (Wong et al., 2008), Ewing sarcoma and melanoma (Pardali et al.) and hematopoietic tumours including hairy cell leukemia (Pruneri et al., 2003) and multiple myeloma (Pruneri et al., 2002). In addition, it has been reported that endoglin may regulate proliferation, migration and invasion of cancer cells in carcinogenesis of human and experimental animal models (Perez-Gomez et al., 2010). This suggests anti-endoglin therapy may have effect on cancer cells but it is not yet clear that whether endoglin functions as a suppressor or promoter of tumour progression and metastasis (Perez-Gomez et al., 2010).

1.5.2 Endoglin as a diagnostic and prognostic marker

As discussed above, endoglin is predominantly expressed in the active and angiogenic tumour-associated vascular endothelium and this indicated that endoglin antibodies might be useful for tumour diagnosis. Therefore, the presence of increased endoglin expression in tumour angiogenic tissue might potentially be used to distinguish malignant neoplasm from benign tissue and help to select

patients who would be suitable for anti-angiogenic therapy. There were a number of promising early studies using radiolabelled antibodies against endoglin that indicated useful applications for immunoscintigraphy of tumours. For example, $^{99}Tc^{m}$-labeled anti-endoglin mAb E9 applied in renal carcinoma patients (Costello et al., 2004), ^{125}I-labeled anti-endoglin mAb MAEND3 used for a canine mammary carcinoma model (Fonsatti et al., 2000) and ^{111}In-labeled rat anti-mouse endoglin mAb MJ7/18 for imaging a mouse Bl6 melanoma xenograft model (Bredow et al., 2000) were all used to detect and monitor primary tumour growth and metastasis. These studies indicate tumour imaging might gain from taking advantage of endoglin labelled targets and may also benefit diagnosis of other angiogenic diseases. Furthermore, a similar approach using alternative reagents to label antibodies against endoglin could be used for other *in vivo* imaging systems such as MRI and PET scanning. In addition, these types of imaging methods may be valuable to monitor the response to anti-angiogenic therapies.

Microvessel density (MVD), a measure of tumour angiogenesis, has been examined as a potential and independent prognostic indicator of several human tumours, since increased MVD was significantly correlated with faster tumour progression, metastasis and shorter overall survival (Weidner et al., 1991; Horak et al., 1992; Weidner et al., 1992; Tanigawa et al., 1997; Choi et al., 2005). However, these findings were not replicated in other similar studies (Page and Jensen, 1995; Lindmark et al., 1996). Thus, it has been suggested that different methods used to define MVD and the use of different pan-endothelial antibodies may result in such discrepancies. The principal measuring approach is direct microscopic immuno-histochemisty/cytochemistry and vessel number counting. This approach has some limitations such as quantification, limited numbers of fields of view, selection of region of interest and subjective bias. Indeed, a number of vascular endothelium markers have been considered for routine use including CD31/PECAM-1, CD34 and von Willebrand factor (vWF). The measurement of MVD using these endothelial markers has been compared with MVD as

determined using anti-endoglin antibodies. In breast carcinoma, the MVD measured with antibodies directed against endoglin rather than anti-CD34 correlated with disease-free and overall survival and the MVD determined using anti-endoglin antibodies was also considered as an independent prognostic factor in a multivariate analysis (Wang et al., 1994). Also a high MVD measured by endoglin staining in a group of patients with head and neck squamous cell carcinomas (HNSCCs) showed endoglin, but not CD34, was an independent indicator of tumour recurrence or death in a multivariate analysis (Martone et al., 2005). Additionally, it was shown that the MVD score of endoglin expression is positively correlated with Gleason score of prostate cancer (Wikstrom et al., 2002) and with the tumour stages in oral squamous cell carcinomas (Schimming and Marme, 2002). These studies not only indicated that MVD determined using endoglin staining appears to be a more reliable prognostic indicator compared with other pan-endothelial markers, but also showed that levels of endoglin expression may be a useful marker of disease progression, recurrence and metastases.

1.5.3 Targeting endoglin as an anti-angiogenic therapy

A number of *in vitro* and *in vivo* studies have recently demonstrated that a variety of anti-endoglin monoclonal antibodies (naked, radiolabelled and immunotoxin conjugated) localized to the vicinity of major tumour neovascularization *in vivo* and inhibited proliferation of micro- and macro-vascular ECs *in vitro*. For example, anti-endoglin mAb significantly inhibits growth of human ECs *in vitro*, mainly in the presence of TGF-β1, indicating this anti-endoglin mAb synergistically interacts with TGF-β to inhibit EC proliferation (She et al., 2004). Moreover, a variety of engineered antibodies such as a bispecific antibody (Korn et al., 2004), single-chain Fv fragments (Volkel et al., 2004) and nanobodies (Ahmadvand et al., 2008) that target endoglin have also been developed and applied to ECs *in vitro*. These studies indicate that these engineered anti-endoglin mAb present additional promising tools for therapeutic applications. Furthermore, the immunotoxin conjugated (Seon et al.,

1997; Matsuno et al., 1999), radiolabelled (Tabata et al., 1999), or naked anti-endoglin mAb including SN6f, SN6j, and SN6k (Takahashi et al., 2001a; Shiozaki et al., 2006; Tsujie et al., 2006; Tsujie et al., 2008; Uneda et al., 2009; Seon et al., 2011) have been tested in pre-clinical studies using severe combined immunodeficiency (SCID) mice bearing human tumours, human skin/SCID mouse chimera. These studies demonstrated that tumour growth and metastasis can be suppressed with relatively long-lasting efficacy. For example, anti-endoglin mAbs were injected in mice with human breast or colon cancer xenografts and these anti-endoglin therapies significantly inhibited tumour growth and improved survival rates (Matsuno et al., 1999; Tsujie et al., 2006). Furthermore, to examine the effect of anti-endoglin therapy on metastatic activity, the metastasis models were generated by mammary fat pad injection of 4T1 murine mammary carcinoma cells and splenic injection of murine colorectal carcinoma cells. The anti-metastatic activity of endoglin specific antibodies was observed for both lung and liver metastases in this study (Uneda et al., 2009). All these positive responses are likely to be mediated by the inhibition of tumour-associated angiogenesis and/or by the destruction of tumour-associated vasculature.

Much of our understanding about the growth of new blood vessels has come from studies of angiogenesis and vasculogenesis during embryonic development. Many of the processes regulating vessel growth are recapitulated in disease. It was reported that endoglin is essential for angiogenesis in the mouse embryonic development and its expression is up-regulated on proliferating ECs during developmental angiogenesis (Arthur et al., 2000; Lebrin et al., 2004). It was thought that endoglin may also play an important role in tumour angiogenesis. Bernabeu and colleagues have investigated the role of endoglin in tumour angiogenesis and growth using endoglin heterozygous ($Eng^{+/-}$) and control mice ($Eng^{+/+}$ littermates) that were subcutaneously inoculated with 10^6 Lewis Lung carcinoma (LLC) cells and tumours harvested after 9 days. The results of these studies indicated that endoglin deficiency decreased tumour vascularization and growth (reduction of

tumour weight) in the short time frame used in this study (Duwel et al., 2007). However, this study did not investigate outcomes after longer time points nor the effect of reduced endoglin levels on metastasis.

Anti-endoglin therapy has now reached the clinic. A phase I study, aiming to assess tolerability and safety of the therapeutic anti-endoglin mAb, its pharmacokinetics and immunogenicity, as well as signs of clinical activity is in progress. Patients with advanced and/or metastatic cancer were given naked human/murine chimeric anti-endoglin mAb (TRC105) as a tumour vascular targeting agent (clinicaltrials-NCT00582985/ last update on 8th Sept 2010). Preliminary data from 50 patients with advanced refractory cancer in this clinical trial suggest clinical activity and good tolerability of the TRC105 antibody at doses up to 1 mg/kg every 2 weeks. In addition, a phase I/II study of TRC-105 in metastatic castrate resistant prostate cancer (CRPC) is now active. This study aims to define the maximum tolerable dose (MTD) and safety of TRC105 in treating CRPC, but also to determine the effects of TRC105 as a treatment for CRPC, in particular to determine whether single-agent TRC105 is associated with a 6-month progression-free survival probability of 30%, when administrated at the MTD to patients with CRPC (clinicaltrials-NCT01090765/ last update on 28th Jan 2011).

Altogether, in light of its tissue distribution pattern (e.g., predominantly restricted to tumour-associated vacular ECs), molecular nature (e.g., a transmembrane glycoprotein) and functional properties (e.g., actions in TGF- signalling pathway), it seems that endoglin can be used as a tumour-associated vascular target for cancer diagnosis and therapeutic anti-angiogenic strategies (Dallas et al., 2008; ten Dijke et al., 2008; Bernabeu et al., 2009; Fonsatti et al., 2010; Seon et al., 2011). However, the potential adverse effects of pre-clinical and clinical applications and the most appropriate therapeutic applications in the clinical setting still need to be investigated.

1.6 Adverse effects of anti-angiogenic therapy

It is generally considered that anti-angiogenic therapies are safer and more tolerable than conventional chemotherapy agents, mainly because anti-angiogenic agents are more likely to be exclusively selective in their cellular effects. Nonetheless, a variety of distinct side effects caused by the validated agents such as Bevacizumab (Avastin), Sorafenib (Nexavar), Sunitinib (Sutent) and Pazopanib (Votrient) are strictly required to be monitored and managed in clinic. Bevacizumab is the first approved anti-angiogenic drug and most of its side effects are associated with hypertension, proteinuria, thrombosis and bleeding events. Less frequent side effects from Bevacizumab therapy include wound healing complications, gastrointestinal perforation and renal damage (Gressett and Shah, 2009). In addition, the TKI inhibitors, sorafenib (Nexavar) and sunitinib (Sutent) generated a wider range of adverse effects than anti-VEGF antibody therapy. The toxicities most often reported include diarrhea, hypertension, fatigue, and nausea in clinical trials of sunitinib, while for sorafenib they were diarrhea, skin toxicities, and alopecia (Porta et al., 2007).

In principle, anti-endoglin therapy may potentially develop some similar adverse effects to those caused by other anti-angiogenic agents. Anti-endoglin therapy related side effects are currently being tested in the two ongoing phase I clinical trials (NCT00582985/NCT01090765). Unexpectedly, there has been a Grade 3 severe allergy and a Grade 4 hemorrhage (gastric ulcer bleeding in one out of 50 patients) observed to date. Although only one case has been reported so far it seems that anti-endoglin treatment may result in haemorrhage similar to anti-VEGF mAb therapy (Rosen et al., 2008; Rosen et al., 2009; Goldman et al., 2011). This side effect could also be in line with concerns that anti-endoglin therapy may lead to vascular defects similar to those present in Hereditary Haemorrhagic Telangiectasia (HHT) patients. HHT type I is caused by a heterozygous mutation of endoglin (McAllister et al., 1994) and this vascular disorder is characterized by bleeding from small vascular malformations

(telangiectases) in the nose and gastrointestinal tract, and by larger arteriovenous malformations (AVMs) that have most frequently been reported in the lung, brain or liver, but may also occur in the retina (Guttmacher et al., 1995). In addition, endoglin heterogyzous mutation mice in Ola/129 gene background spontaneously developed phenotypes such as telangiectases on the ears, bleeding from nose/mouth and gastrointestinal surface and some AVMs occurred in the lung brain and liver, which are similar to clinical symptoms of HHT type I patients (Bourdeau et al., 2001). This possibility of side effects caused by anti-endoglin therapy therefore remains to be more fully determined in patients and will also be addressed in part using mouse models in C57BL/6 gene blackground in this thesis.

1.7 Justification for the project and a list of the aims

As mentioned above, endoglin is predominantly overexpressed in the tumour-associated vascular endothelium, where it modulates tumour angiogenesis. Although some investigations showed an effect of endoglin reduction or anti-endoglin therapy on primary tumour growth, when this project commenced no studies had been performed on the effect of endoglin depletion on metastasis. Therefore, I used a floxed endoglin mouse that had been generated in my host laboratory (Allinson et al., 2007) to determine the effect of endoglin depletion on angiogenesis, tumour growth and metastases. The LLC-RFP subcutaneous primary tumour model was used taking advantage of RFP expressing LLC cells for the detection of lung metastases.

The main hypothesis to be addressed in this thesis is that loss of endoglin in ECs can delay or reduce angiogenesis and primary tumour growth, and also reduce the frequency and severity of metastases.

To address this hypothesis the aims of the work described in this thesis are as follows:

1. Optimize endoglin depletion in ECs using adult mice with a conditional knockout allele (Eng-iKO^{e});
2. Test the effect of endoglin loss in ECs on *in vivo* angiogenesis;
3. Optimize and characterize the LLC subcutaneous primary and 'spontaneous' secondary tumour model;
4. Investigate the effect of endoglin depletion on LLC primary tumour growth and lung metastases;
5. Examine potential side effects of targeting endoglin using the Eng-iKO^{e} mouse model;
6. Investigate the effect of endoglin loss on mouse lung endothelial cells (MLECs) *in vitro*.

Chapter 2. Materials & Methods

2.1 Materials

2.1.1 Suppliers

In general, most chemicals and reagents were provided by Sigma Aldrich, Invitrogen, BD Biosciences, PeproTech, eBioScience Technology.

All plasticware for cell culture and general laboratory consumption was obtained from Greiner, Iwaki, or Corning. The medium for primary endothelial cells and cancer cells was purchased from PromoCell and Invitrogen respectively.

Magnetic separator was obtained from Invitrogen.

2.1.2 General Solutions

PBS, Tris, citrate buffer and 0.1% gelatin solutions were sterilised by auotoclaving at 121°C for 30 mins. The constituents of the solutions are listed below:

PBS

80g of NaCl
2g of KCl
14.4g of Na_2HPO_4
2.4g of KH_2PO_4

in 800ml of distilled H_2O. Adjust the pH to 7.4 with HCl. Add H_2O to make 1 litre.

4% Paraformaldehyde Solution (PFA)

Add 4g Para-Formaldehyde (PFA) powder to 100ml PBS and dissolve at 60°C. Store in 10 ml aliquots at -20°C until required.

1M Tris-HCL

TRIZMA base dissolved in Milli-Q H_2O and adjusted to the appropriate pH using HCl.

TE Buffer

Add 10mM Tris.Cl at pH 7.4 to 1mM EDTA at pH 8.0 then make up to a final pH of 7.4

Citrate Buffer (pH 6.0)

Add 0.1M citric acid, 0.1M Trisodium citrate in deionised water and adjust the pH to 6.0 with 0.1M NaOH.

PBST

0.1% Tween 20, 1x PBS

β-galactosidase (β-gal) Staining

Components	Volume	Stock concentration
0.2% Gluteraldehyde	160µl	25% (stored at -20°C)
0.02% NP40	40µl	10%
0.005M EGTA	200µl	0.5M
0.002M $MgCl_2$	40µl	1.0M
0.1M Phosphate buffer at pH 7.6	4ml	0.5M
DDH_2O	Make up to 20ml	

Table 2.1 Glutaraldehyde Fixative Solution

Notes: just before use add Glutaraldehyde to a final concentration of 0.2%.

0.5M Sodium Phosphate Buffer (pH 7.4)

Add 34.2ml 1M Na_2HPO_4 , 15.8ml 1M NaH_2PO_4 and DH_2O to make up to 100ml buffer.

Components	Volume	Stock concentration
0.005M K3 Ferricyanide	1ml	0.5M
0.005M K4 Ferrocyanide	1ml	0.5M
0.1M Sodium-Phosphate buffer (pH 7.4)	20ml	0.5M
2mM $MgCl_2$	200µl	1M
0.01% Sodium Deoxycholate	1ml	1%
0.02% NP40	200µl	10%
DDH_2O	Make up to 100ml	

Tabel 2.2 X-gal Staining Solution

Notes: Staining solution stored in dark without X-Gal at 4°C.

X-gal

X-gal powder dissolved in 99% dimethylformamide to a concentration of 25 mg/ml in glass container stored at -20°C and was added to staining solution at a final concentration of 1mg/ml just before use.

Wash Buffer

0.02% NP40 in PBS

DNA Preparation

Tris-Acetate (TAE) Buffer

0.04M Tris-acetate, 0.001M EDTA

Gel Loading Buffer

0.25% bromophenol blue, 0.25% xylene cyanol FF and 40% sucrose in water.

Lysis Buffer A

0.5M NaOH, 0.5M EDTA, Milli-Q H_20, adjust to pH 12

Lysis Buffer B

0.5M Tris-HCL, Milli-Q H_20, adjust to pH 5.

Counterstains

Triple Eosin Counterstain

9g of Eosin (water soluble) powder, 1g of erythrosin B, and 0.5g of Phloxine. Dissolve in 160ml of 20% ethanol then add 640ml of tap water. A 1/30 dilution was used to counterstain x-gal stained sections (see below).

Carazzi's Haematoxylin

Add 2g of Haematoxylin to 200ml glycerol, leave overnight to dissolve. Dissolve 50g Potassium Alum (Potassium aluminium sulphate) in 600ml ddH_2O then add 0.2g potassium iodate. Mix and add to the haematoxylin and glycerol mixture. Make up to a final volume of 1 litre with ddH_2O.

1% Acid Alcohol

1% HCl in 70% Ethanol.

Ammonia Water

2.5 ml Ammonium Hydroxide in 1000ml Tap Water.

2.1.3 Mice

All of the mouse models were bred in ventilated rooms, in a germ-free facility, under controlled conditions of light, temperature and humidity (FGU, IGM, the

Centre for Life, Newcastle University, UK) and fed a standard chow for laboratory mice with water *ad libitum*.

All experiments using experimental animal models should incorporate the 3Rs: replacement (avoids the use of animals or use alternative approaches to animals), reduction (minimises the number of animals used) and refinement (improves experimental design and techniques to minimise animal suffering). The 3Rs must be considered as an integral part of designing experiments using animals and also the 3Rs need to be followed throughout studies. However, in all cases, experimental designs and procedures should be tailored to the requirements and purposes of the specific studies.

Studies were performed in accordance with international and national institution guidelines for the care and use of laboratory animals under home office licence PPL60/3622.

Inducible *Cdh5*(PAC)Cre-ER^{T2} *Endoglin*$^{fl/fl}$ mice

Cdh5(PAC)Cre-ER^{T2} mice were obtained from Dr Ralf Adams (CRUK, London). This mouse expresses the tamoxifen activated Cre-ER^{T2} sequence that was inserted into a PAC (P1 artificial chromosome) containing the vascular endothelial Cadherin -VE-Cadherin (Cdh5)- promoter gene to generate the transgene construct (Source: http://www.informatics.jax.org/searches/accession_report.cgi?id=MGI:3848980). To activate Cre-ER^{T2}, mice were injected intraperitoneally with 2mg tamoxifen (specific binding to estrogen receptor (ER)) for 5 consecutive days and two additional injections on subsequent alternative days. *Eng* $^{fl/fl}$ *Cdh5*(PAC)Cre-ER^{T2} mice were backcrossed for 5 generations with C57BL/6 to generate an approximately syngeneic line.

Inducible Rosa-Cre *Endoglin*$^{fl/fl}$ mice

Inducible Rosa-Cre-ER^{T2} mice were generated in Dr. Alex Joyner's Lab, New York and obtained from Dr Li, Connecticut, USA. This mouse expresses tamoxifen-activated Cre recombinase (Cre-ER^{T2}) under the regulation of the ubiquitously expressed Rosa26 promoter. Adult *Eng*$^{fl/fl}$ Rosa26-Cre-ER^{T2} mice were injected intraperitoneally with 2mg tamoxifen (10mg/ml) for 5 consecutive to activate Cre-ER^{T2}.

Rosa26R mice

A stock colony of Rosa26R mice were obtained from Prof D. Henderson (Newcastle University). This gene trap strain contains a loxP flanked neo expression cassette ("floxed stop cassette'') upstream of a lacZ gene. LacZ expression driven by the ubiquitous Rosa26 promoter is conditional on the removal of this intervening floxed stop cassette by Cre recombinase (Soriano, 1999). These mice were crossed with *Cdh5*(PAC)Cre-ER^{T2} and Rosa26-Cre-ER^{T2} mice to map the expression of these respective Cre recombinases by X-gal staining in adult tissue or primary ECs.

Immortomouse

H-2K^{b}-tsA58 transgenic mice (Immortomice) were obtained from Dr. Peter Hohenstein (Edinburgh University), and express a thermolabile form of the SV40 T antigen (Jat et al., 1991). The mouse major histocompatibility complex H-2K^{b} promoter directs expression of tsA58 to a broad range of tissues including ECs (Lidington et al., 2002). Immorto- *Eng*$^{fl/fl}$ RosaCre-ER^{T2} mice, were used for isolation of conditionally immortalized EC lines.

2.1.4 Cell lines

Endothelial cell lines

The sEND-1 cell line was originally derived from mouse skin microvasculature from a transgenic mouse line expressing expressing polyoma middle T antigen

(Williams et al., 1988). sEND-1 cells were obtained from Prof. Roy Bicknell (University of Oxford) and were grown in Dulbecco's modified Eagle medium (DMEM, Invitrogen) supplemented with 10% fetal calf serum (FCS, Invitrogen).

The conditionally immortalized EC line was initially isolated and purified from mouse lung microvasculature of Immorto-Eng$^{fl/fl}$ RosaCre-ER^{T2} mice and Immorto-Eng$^{fl/fl}$ mice. To passage this cell line, microvascular ECs growth medium (PromoCell) was used, and 'pure' primary ECs were seeded into 0.1% gelatin pre-coated 12-well plates under permissive temperature conditions (33°C, 5% CO_2) and presence of interferon (IFN)-γ (20U/ml). Normally, medium was refreshed every other day and cells were maintained at high confluence (passaging using a twofold dilution on reaching 85–90% confluence). The protocol to prepare conditionally immortalised ECs from mouse lungs is described below (2.2.13)

Cancer cell lines

A lewis lung carcinoma cell line that constitutively expresses m-cherry red fluorescent protein (LLC-RFP) was provided courtesy of Dr. Vivek Mittal (Cold Spring Harbor Lab, USA) (Gao et al., 2008). LLC cells were originally derived from the lung of a C57BL/6 mouse implanted with a primary lewis lung carcinoma (Bertram and Janik, 1980). LLC-RFP was grown in DMEM + 2mM Glutamine + 10% Fetal Bovine Serum (FBS). Confluent cultures were passaged at a 1:10 to 1:20 dilution and were grown in standard conditions (5% CO_2 and 37°C). Once every 50-60 passages Puromycin (2µg/ml) was added to enrich for cells carrying the RFP construct.

2.2 Methods

2.2.1 Genotyping of mouse models

To genotype the offspring from each mouse line, normally, an earclip from each mouse was used for DNA extraction. 100µl of 25mM NaOH/0.2mM EDTA (pH~12) was added to each clip and samples incubated at 95°C with constant shaking (350rpm) for ~1 hour. After vortexing, the addition of 100µl of 40mM Tris-HCl ~pH5 to neutralise pH, and centrifugation at 13000g for 5 mins to remove the cell debris, 2µl of the supernatant was used in a 25µl polymerase chain reaction (PCR) reaction using RedHot DNA Polymerase (Thermoscientific) or stored at -20°C until required.

Genotyping was performed using PCR technique. In one reaction, two primer pairs were used to amplify regions of the target genes. The standard PCR protocol was used (see section 2.2.2) with an annealing temperature of 58°C and 35 cycles.

Primers are listed in Table 2.3 Positive (DNA of known genotype) and negative (no DNA) control samples were also used. PCR products were separated by electrophoresis on a 2% agarose gel, and visualised under UV light followed ethidium bromide staining.

Primers	Sequences (5' to 3')	Size of Products
LacZ Forward LacZ Reverse	AGATGATCACACTCGGGTG AATCTCTATCGTGCGGTGG	250bp
m-Eng-NewF4	GGTCAGCCAGTCTAGCCAAG	602bp (for Eng Δ allele in PCR with m-Eng-R7)
m-Eng-R7 m-Eng-F6	CCACGCCTTTGTCCTTGC GACGCCATTCTCATCCTGC	420bp (for WT allele) 500bp (for Eng^{fl} allele)
m-Eng-F9b m-Eng-R10	TCAGTTTTCCCGTCAGGCTC GTTCGATGGTGGTGGATGC	600bp
m-Eng-F12 m-Eng-R13	ATGCGCCTGAACATCGTC AATCAGGAAGGCACCAAAGG	900bp
CreF CreR	GATCGCTGCCAGGATATACG AATCGCCATCTTCCAGCAG	574bp
WT-R26 R26 R26Gtrgeo	GCGAAGAGTTTGTCCTCAACC GGAGCGGGAGAAATGGATATG AAAGTCGCTCTGAGTTGTTAT	600bp (for WT allele) 310bp (for Rosa allele)
Immorto-F Immorto-R	AGCGCTTGTGTCGCCATTGTATTC GTCACACCACAGAAGTAAGGTTCC	1000bp

Table 2.3 Primers used in genotyping PCR and cell PCR reaction.

To distinguish between wild type, heterozygous, and knockout genotypes, primer pairs for the endoglin gene and the other genes were used in the PCR reaction. The size of the PCR product is shown in the right column.

Note: The size of the PCR product is shown in the right column, bp = base pairs and wt = wild type. Figure7.9 shows the position of endoglin primers relative to the floxed endoglin allele.

2.2.2 Standard PCR amplification

PCR was carried out in 200µl thin walled PCR tubes using 2µl of DNA, 0.5µl of 10mM of dNTPs consisting of dATP, dTTP, dGTP and dCTP (Invitrogen), 0.2µl 1x Taq polymerase, 2.5µl, 25mM $MgCl_2$, 2.5µl 10x Buffer IV (all from Thermo

Scientific), 0.25 µl of 20µM forward primer, 0.25µl of 20µM reverse primer and 17.8µl of sterile filtered distilled water. A negative control containing sterile filtered water was included to make sure the reaction mixture was not contaminated with another source of DNA. In addition to this, a positive control was used to make sure all the reagents were still working appropriately. A Perkin Elkin thermal cycler was used and the cycling parameters are shown in the following table (Table 2.4).

Reaction Step	**Reaction Conditions**
1	95^{o}C (1 minute)
2	95^{o}C (15 seconds)
3	58^{o}C (30 seconds)
4	74^{o}C (1 minute)
5	74^{o}C (7 minutes)
6	4^{o}C (infinite)
Cycles (Steps 2-4)	35

Table 2.4 The conditions required for PCR reactions to genotype *Eng*$^{fl/fl}$, *Eng*$^{fl/\Delta}$, *Cdh5*(PAC)Cre-ER^{T2}, Rosa26R and Immorto-mice.

2.2.3 Agarose gel electrophoresis

The standard concentration of agarose was 2% in 100ml 1x TAE buffer. The agarose was boiled in a microwave for 3 minutes to make sure the agarose was fully dissolved. The solution was cooled with cold running tap water for around two minutes to allow the temperature to cool to about 55-65°C. When cooled the solution was slowly poured into a gel tank containing a 14 well comb (which allowed 13 samples including the 1Kb ladder to be run) and this was left to set for approximately 40 minutes. When solidified the comb was carefully removed and the gel was fully immersed in 1x TAE buffer. The samples were prepared by adding 4µl of DNA sample to 1 µl of 5 x DNA loading buffer and loading 4 µl into the wells of the gel. A 1kb DNA ladder (Invitrogen) was also loaded onto the

gel to permit size analysis of PCR products. Electrophoresis was performed at 65-75 v for approximately 45 minutes allowing the fragments to completely separate. On completion, the agarose gel was immersed in Ethidium Bromide (1µg/ml) diluted in H_2O for 20 minutes. The DNA bands were visualised by placing the gel into a UV transluminator and the image was captured with using Genesnap software (Syngene Bio Imaging).

2.2.4Tamoxifen administration

To activate Cre-ER^{T2}, tamoxifen was prepared at 10mg/ml, by dissolving 1mg tamoxifen powder in 10 µl 100% ethanol and then mixing with 90µl peanut oil. This method was used to prepare tamoxifen for activating Cre enzyme in adult mice, such as topical tamoxifen application and tamoxifen intraperitoneal (i.p.) injection. Following tamoxifen application, the health of the mouse models were carefully monitored.

Topical application of Tamoxifen on ears

100 µl tamoxifen (10mg/ml) was applied to the right ear using a gilson pipette whilst the left ear was used as an internal control and 100µl peanut oil was applied. The treatments were repeated 3 times per week (Monday, Wednesday and Friday) for 6 weeks.

Subcutaneous implantation of 21-day slowly resealing tamoxifen pellet

Slow-release pellet containing 25mg Tamoxifen citrate (Innovative Research of America) was implanted subcutanously into the scruff by making a 1cm incision in the dorsal skin and inserting the pellet away from the wound towards the tail of the mouse. The wound was closed using stitches of absorbable thread. The mouse was anaesthetised by isoflurane (oxygen flow rate: 500ml/min, isoflurane induction rate: 5% and isoflurane sustained rate: 2-3%) throughout the procedure.

Intraperitoneal injection of tamoxifen

Mice were injected intraperitoneally once daily with 2 mg tamoxifen (10mg/ml) per mouse for 5 consecutive days followed by a further injection at day 7 and one more at day 9 (total dose of tamoxifen for per mouse is 14mg over 9 days). Care was taken during the injection to avoid any damage to internal organs.

2.2.5 Histological procedures

Tissue dissection

Mouse skin, matrigel plugs, LLC primary tumour and heart & lungs were dissected for tissue analysis. Fixatives (0.2% PFA, 4% PFA or Formalin) and dissecting instruments (a fine/round tipped pair of scissors, old scissors for cutting bone, and forceps) were assembled prior to culling mice. Mice for isolation of mouse lung primary endothelial cells were killed by cervical dislocation and all other mice were sacrificed using CO_2.

To harvest matrigel skin or primary tumour, mice cadavers were pinned to a dissecting board with dorsum/back of mouse facing up under a light source. The hair surrounding matrigel plugs or primary tumour was shaved off, and the skin was moistened using 70% ethanol. Skin close to matrigel plug or primary tumour was tightly held up using a fine tipped forceps and an incision made with fine tipped scissors underneath the deep muscle layer. The integrated tissue block including skin, matrigel plugs or primary tumour and deeper muscle layer was dissected.

To remove lungs for preparing ECs, mice cadavers were pinned out on the dissecting board with the peritoneal wall facing up under a light source. The mouse body was moistened using 70% ethanol and a longitudinal incision through the skin was made from the abdomen to the top of the thorax. The abdominal wall was opened below the ribcage, the sternum raised with tweezers and the diaphragm cut. Then the main part of the ribcage was cut away to partially expose the heart and lungs. A small incision in the left atrium was made under a

dissecting microscope for drainage. A 10 ml syringe with 10ml cold PBS was inserted into the apex of the right ventricle and used to flush the blood from the mouse. Fat and connective tissue was trimmed away around the heart and lungs which were then removed from the thoracic cavity and processed as described in 2.2.13 below.

Processing tissue to paraffin wax blocks

To prepare paraffin sections for histological analysis, tissue was briefly washed in PBS and then fixed in 4% formaldehyde/PBS for at least 3 hours at room temperature. Tissues were washed well in 3 changes of PBS for 3 hours (= 3 x 1 hour) at room temperature. Tissue was dehydrated by transferring to 50% Ethanol/H_2O for a minimum of 2 hours at room temperature on the shaker, and then overnight in 70% Ethanol/H_2O. Dehydration was completed in 100% Ethanol in 3 changes for 6 hours (=3 x 2hours) at room temperature. Tissue was cleared in a glass container in Histoclear (National Diagnostics) overnight in fume cupboard, and then equilibrated in 3 changes of paraffin over 6 hours (= 3 x 2 hours) at 60°C with occasional swirling of the glass tubes to ensure adequate penetration of the wax. Finally, tissue was orientated in plastic moulds (Lamb) such that the cut surface accurately represents the tissue and left to set at room temperature for at least 1 hour and cooled on ice or in fridge before removing paraffin block from mould.

Processing tissue to frozen blocks

Tissues were removed from mice quickly and carefully, rinsed in cold PBS and then washed in 2 changes of PBS. Tissues were subsequently fixed in 0.2 % or 4 % PFA/PBS (fixative concentration depends on tissue and antibody requirements) overnight on the shaker at 4°C. Next morning tissues were rinsed with cold PBS and left overnight at 4°C in 30% sucrose/PBS. Tissues were briefly washed with cold PBS, covered in OCT (Lamb), orientated in the plastic moulds, rapidly

transferred to the dry ice box and left for at least 15 minutes. When tissues were frozen, blocks were put in the -80°C freezer for storage until required.

Microtome sectioning

Paraffin blocks of skin and matrigel plugs were sectioned at a thickness of 5μm - 10 μm using a Leica RM2135 rotary microtome with disposable microtome blades (Lamb). Transverse or sagittal serial sections were cut into small ribbons. Sections were floated into a water bath at 37°C for the sections to expand and creases removed. The sections were carefully floated onto Histobond slides (Marienfeld, Germany) and drained. To remove the remaining water, the slides were dried for a couple of hours at 39°C on a heating plate, this also promoted adhesion of the sections to the glass slides. The slides were stored in the plastic slides box at room temperature until required. At least one hour before staining, slides were left in the 60 ^{o}C oven, and then paraffin sections were dewaxed in two changes of histoclear for 10 minutes (2 x 5 minutes) and hydrated in graded concentrations of ethanol from 100% ethanol (2 minutes) through 70% ethanol (2 minutes), 50% ethanol (2 minutes), to water.

2.2.6 Cryostat sectioning

The tissue blocks taken from -80°C freezer were left to equilibrate at -20^{o}C for at least 30min in the chamber of cryostat (Microm HM 560 cryostat, Germany). Serial horizontal cryostat sections (thickness: 10μm - 20μm) were cut at -20^{o}C to -22^{o}C and mounted on polylysine glass slides (VWR). Sections were left to air dry for 60 minutes at room temperature before being stored in labeled slide mailers in the -80°C freezer. Before use, slide mailers were taken out of -80°C freezer and left at room temperature for 30 minutes. Subsequently, slides taken out from mailer were left at room temperature for another 30minutes. Sections were fixed in cold acetone on ice for 10 minutes and taken out of acetone to air dry for 15minutes, before washing in PBS for 5 minutes.

2.2.7 H&E staining

Paraffin sections were stained in Carazzis Haematoxylin (H) for 5 minutes followed by a 2 minutes rinse in H_2O. The sections were then differentiated in 1% acid alcohol for 5-10 seconds. After a quick water rinse the sections were then immersed in ammonia water for 10 seconds or until the sections turned blue. Sections were then washed in running tap H_2O for 10 minutes then stained with eosin (E) for 45 seconds. For even staining results, slides were dipped several times before leaving them in the solutions for the desired time. The sections were dehydrated through a separate series of increasing ethanol solutions. Finally stained sections were mounted on slides using Histomount mounting medium (National Diagnostics). In H&E stained sections the nuclei are stained blue, cytoplasm pink and muscle fibres, fibrin and connective tissues are shades of red to pink.

To stain nuclei, cryosections were stained for 2 minutes in Mayers Haematoxylin (Lamb), quickly rinsed in tap water, before dipping into eosin counterstain for 1-2 seconds. Sections were dehydrated rapidly through graded ethanol solutions by dipping slides 3 times in each of 50 %, 70 %, 100 % and a second 100 % ethanol. Sections were left in histoclear solutions (2 x 10 minutes) to clear. Finally, slides were mounted with coverslips using histomount.

2.2.8 X-gal staining

The bacterial beta-galactosidase gene lacZ is frequently used as a reporter gene and was monitored by histochemistry with the chromogenic substrate X-gal.

<u>Whole Mount X-gal Staining</u>

Tissue was dissected into cold PBS (4°C) on ice, and then washed in enough cold PBS (4°C) to remove excess serum completely. Next, tissue was fixed by immersion in pre-cooled glutaraldehyde fixative solution (Table 2.1) at 4°C for 30 minutes, using the shaker in cold room to ensure even fixation. Subsequently, tissue was rinsed with PBS to remove excess fixative, then thoroughly washed 3

times (for 30 minutes each wash) at room temperature in plenty of washing solution (PBS/0.02% NP40) using a rocker. Finally, the tissue was stained in the dark in X-gal staining solution (Table 2.2) at 33°C overnight in a water bath with gentle agitation. (Note: background beta galactosidase activity, which may be a problem in adult tissues, was minimized by using 33°C incubation temperature).

X-gal staining on frozen sections

Tissue cryosections from freezer (-80ºC) were brought to room temperature inside slide mailers to minimize condensation (30 minutes) then air dried for an additional 30 minutes. Sections were encircled with a hydrophobic barrier pen (ImmEdge,Vector), whilst drying. Frozen sections were postfixed in 0.2% PFA on ice for 10 min and then washed twice in PBS containing 2mM $MgCl_2$ on ice (= 2 x 10 minutes wash), (Placing slides in detergent rinse – 0.02% NP40 in 1x PBS is an option to improve penetration of stain into tissues in the next step). The X-gal staining solution (X gal was used at a final concentration of 1.25mg/ml) was gently placed on the sections and incubated at 32°C overnight in the dark. Slides were washed twice in PBS with 2mM $MgCl_2$ and rinsed in distilled water, before counterstaining with light eosin (1/30) for 8 minutes. Slides were then washed three times in distilled water for 5 min each and dehydrated through the graded ethanol series (50%, 70% and 100%). Finally, sections were cleared by placing in Histoclear (= 2 x 5 minutes) and mounted in histomount.

X-gal staining on cells

Cells were seeded onto 8-well glass slides (Lab-Tek, USA), and it was not necessary to pre-coat wells with gelatin for adherence of endothelial cells. To promote endoglin deletion in *Eng*$^{fl/fl}$ Cre-ER^{T2} lines, cells were allowed to grow for 24 – 48 hours before adding 1µM 4-Hydroxy Tamoxifen (4-OHT) (Sigma Aldrich) for 48 hours. The media was replaced and cells left for another 24 to 48 hours to allow time for lacZ expression. Cells were washed twice with 200µl PBS and then fixed for 10 minutes at room temperature in 2ml of 0.5% glutaraldehyde

diluted in PBS. The fixative was removed by washing cells 3 times with 2 ml PBS containing 1 mM $MgCl_2$ and then X-gal staining solution (Table 2.2) was added to wells before incubating at 37°C until the desired staining was achieved (overnight incubation gives the most intense staining). The cells were then washed with PBS and counterstained with a light eosin counterstain (achieved by staining slides for 1min in 1/30 eosin, followed by brief wash in tap water). Finally, slides were rapidly dehydrated through 50% and 100% ethanol and cleared in histoclear before being mounted with Histomount (National Diagnostic) and coverslipped prior to examination under the microscope.

2.2.9 Immunohistochemistry (IHC)

Anti-CD31(Clone MEC13.3, provided as 15.625 µg/ml stock solution, BD Biosciences, Pharmingen) and anti-endoglin (Clone MJ7/18, provided as 0.5 mg/ml stock solution, eBioscience) are both monoclonal rat anti-mouse antibodies and used on mouse tissue cryosections. Preliminary experiments were carried out to determine the optimum dilutions of each primary antibody that resulted in clear staining with low background. This was determined to be a 1:25 dilution and 1:100-200 dilution in 5% rabbit serum (Vector Laboratories) for CD31 and endoglin antibody respectively.

Prior to commencement of staining, the tissue cryosections were removed from the freezer and allowed to reach room temperature. All subsequent staining steps were done at room temperature and all incubations were done in a humidified chamber. For immunostaining with anti-CD31 or anti-endoglin, the sections were blocked by 5% rabbit serum (Vector Laboratories) in PBS for 20 minutes, washed in PBS for 5 minutes, then incubated with the primary antibody in cold room (4ºC) overnight. Sections were washed in 3 changes of PBS (5 minutes each) before application of the biotinylated secondary rabbit anti-rat antibody (Vector Laboratories) at 1:200 dilution in 5% rabbit serum in PBS for 30 minutes. Following the secondary antibody incubation, sections were washed in 3 changes

of PBS (5 minutes each) then incubated with the Vectastain ® Elite ABC Reagent (Vector Laboratories) for 30 minutes. After further washing in PBS (3 changes, 5 minutes each), antibody binding was visualized using the liquid DAB substrate kit (BioGenex). Sections were counterstained with Mayer's haematoxylin (Sigma-Aldrich®), washed in PBS, and then dehydrated in a graded alcohol series of 70%, 90% and 100% ethanol. Following dehydration of the sections, the slides were cleared in Histoclear (National Diagnostics) and coverslipped with a mountant (HistoMount). Negative controls for the immunostaining were carried out as above, except that the primary antibodies were replaced with PBS.

2.2.10 Isolection B4 staining

Cryosections were removed from freezer (-80ºC), and allowed to air dry as before. The tissue area was marked using a hydrophobic barrier pen (ImmEdge,Vector). Sections were gently washed once in PBS and incubated with 1% bovine serum albumin (BSA, ≥ 98%, Sigma-Aldrich) blocking solution for 1 hour. Then, sections were washed twice in PBS (5 minutes each wash), and incubated with Isolectin B4 conjugated Alexas 488 IgG (Invitrogen, stock concentration: 500µg/ml, diluted in PBS + 0.1mM $CaCl_2$ to a working concentration of 20µg/ml) at RT in a dark humidified chamber for 1 hour. Surplus isolectin was removed by washing slides 3 times with PBS (2 minutes for each wash). Slides were mounted using Vectashield Mounting Medium Hard set with DAPI (Vector) and stored in the dark at 4 ºC until inspection under the microscope. (Note: Staining of Isolection B4 and DAPI was stable for at least 10 -15 days and 4-5 days, respectively, when slides were stored in this way).

2.2.11 Immunofluorescent staining

There were two types of immunofluorescence staining methods used in this thesis. One was to do direct immunofluorescence staining in which the primary antibody labeled with fluorescence dye (e.g. αSMA- fluorescein isothiocyanate (FITC) (1:200)), and the other one was to do indirect immunofluorescence staining in

which a secondary antibody labeled with fluorochrome (e.g. Alexas488 (1:200), Alexas594 (1:200) and Alexas647 (1:10); incubation for 1hour at RT) was used to recognize primary antibodies (working concentrations and conditions of a number of primary antibody used in my experiments as follow, CD31 (PECAM-1, 1:25-50), endoglin (CD105, 1:100-200), Collagen IV (1:200), lymphatic vessel endothelial HA (hyaluronic acid) receptor (LYVE-1) (1:200), HIF-1α (1:100), fibroblast specific protein (FSP)1 (1:100); incubation at 4^{o}C, O/N). The same approach was performed prior to commencement of staining as described in the section 2.2.9. In addition, the blocking solution (5% blocking serum and 1% BSA incubation for 1hour at RT) were used before adding primary antibodies. Immunofluorescence stained samples are examined under a fluorescence microscope.

2.2.12 In vivo matrigel angiogenesis assay

Matrigel implantation

High concentration Matrigel (BD Biosciences) was thawed at 4ºC and kept on ice to maintain a liquid consistency. Growth factors: 600ng/ml bFGF and 300ng/ml VEGF (Peprotech) were added on ice and the mixture left on the rotator overnight at 4^{o}C to ensure good mixing prior to injection.

A small volume of Matrigel and growth factor mixture (400µl) was injected subcutaneously into the right flank region of mice under anesthesia with Isoflurane. Staring the same day, 200µl (10mg/ml) liquid tamoxifen was injected intraperitoneally, and i.p. injections continued over 7 days as described above (Section 2.1.3.1). Animals were humanely culled on day 15 after matrigel injection. Each matrigel plug was harvested and processed by fixing overnight in 4% PFA and processed to paraffin for H&E staining, or by directly freezing in liquid nitrogen-cooled isopentane for immunohistochemistry.

Immunohistochemistry of matrigel plugs

Frozen matrigel plugs were sectioned and immunostained for CD31 and endoglin as before (Section 2.2.9) except that sections were briefly fixed for 10 minutes with cold 100% acetone before immunostaining.

Vessel quantification in matrigel plugs

For vessel quantification, cryosections of the whole matrigel tissue block taken from each mouse were prepared and every fifth slide was chosen for CD31 immunostaining and vessels were counted for the images taken. The section with maximum number of blood vessels in each matrigel plug was selected for statistical analysis.

2.2.13 Isolation of primary mouse lung endothelial cells (MLECs)

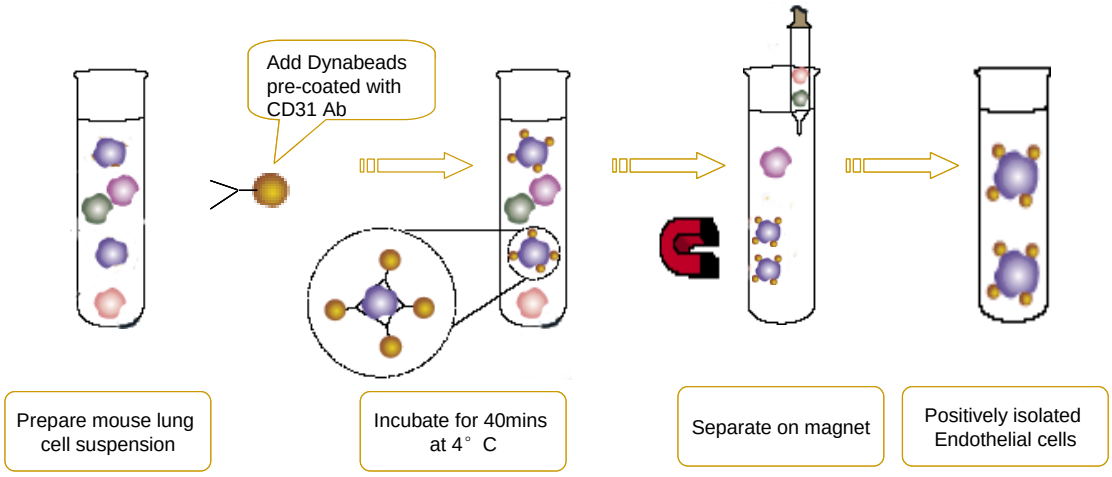

Figure 2.1 summary of optimized MLECs isolation using antibody-Dynabeads conjugates by magnetic separator.

Finely minced mouse lungs from 3-4 mice (8-10 weeks) were digested by collagenase (2mg/ml) for 1 hour at 37^{o}C. All the following procedures were carried out under sterile conditions in a tissue culture hood. The cell suspension was incubated with CD31-Dynabeads conjugates in endothelial cell growth medium for 40 minutes at 4^{o}C. The tube containing MLECs bound with CD31-magnetic Dynabeads conjugates and non-MLECs were placed on the magnetic separator for 1 minute before pipetting off the non-MLECs. This step was repeated three times in the exactly same way, to obtain the 'pure' MLECs which were then cultured in complete endothelial cell growth medium MV_2 (Table 2.5). As any contaminating fibroblasts tended to grow more rapidly than ECs, then after about 1-2 weeks in culture, a second sorting step used

CD102 (ICAM-2) antibody pre-coated Dynabeads (see below). After these two rounds of cell sorting and subsequent cell passaging, there was a relatively good yield of almost pure endothelial cells for the subsequent functional assays.

Prior to Cell Isolation

Mouse lung endothelial cell media were prepared as follows:

Isolation Medium was MV_2 endothelial cell growth medium (Promocell) without supplement mix + 20% FCS + 1% Penicillin/Streptomycin

Growth Medium was MV_2 Endothelial cell growth medium (Promocell) with supplement mix + 1% Penicillin /streptomycin

Components	Concentration
Fetal calf serum	5%
Epidermal Growth Factor (EGF)	5.0ng/ml
Vascular Endothelial Growth. Factor (VEGF)	0.2µg/ml
Hydrocortisone	0.5ng/ml
basic Fibroblast Growth Factor (bFGF)	10ng/ml
R3 IGF-1	20ng/ml
Ascorbic Acid	1µg/ml

Table 2.5 Components of complete MV2 endothelial cell growth medium

Preparation of Anti-mouse CD31 (PECAM-1, BD) Dynabeads:

Prior to use, 75µl sheep anti-rat Dynabeads (Invitrogen) were resuspended in 5 ml of 0.1% BSA/PBS in a 15ml falcon tube and then placed on a magnetic separator (DynaMag-15, Invitrogen) for 1 minute. The supernatant was removed and the washing step repeated 3 times. Beads were resuspended in original volume (75µl) of 0.1% BSA/PBS. Afterwards, 15µl of CD31-Ab (MEC13.3, BD Pharmingen, Cat.553369) was added to 75µl of beads and the volume made up to 0.5 ml with 0.1% BSA/PBS. The beads and CD31-Ab mixture was mixed overnight on rotator at 4°C (or for 2 hour at RT). Excess antibody was removed by washing beads with 0.1% BSA/PBS 4 times as before. Finally, beads were resuspended in original volume (75µl) with 0.1% BSA/PBS to maintain beads at 4×10^8 beads/ml. (Beads were stored at 4°C and used within 1-2 weeks).

On The Day of The Isolation

Collagenase Preparation:

Type I Collagenase (Sigma-Aldrich) was dissolved at 2mg/ml (150-170 U/mg) in 15 ml of DPBS + Ca^{2+}/Mg^{2+} (Invitrogen) by gentle shaking (50 – 60 times per minute) at 37°C for 1 hour then filter sterilized using a 0.22 μm filter (Life Science).

Dissection:

A young adult mouse (age 8-10 weeks) was sacrificed by cervical dislocation and was thoroughly wetted with 70% ethanol. The skin was nicked above the pubis with scissors and removed to above the chest. The mouse cadaver was pinned out supine on a Styrofoam board on bench top and any loose fur from gloves was carefully removed. The anterior abdomen was cut open, and the anterior diaphragm was taken down with sterile scissors. Using a fresh sterile set of scissors and tweezers for within the thorax, the lung lobes and heart were dissected out from the mediastinum. Lung lobes and heart were placed in 50 ml falcon tube containing 20ml cold Isolation Medium and kept on ice until beginning the cell isolation procedure. (Note: it is possible to store the lungs for up to 6 hours on ice before beginning the cell isolation procedure, but longer storage may result in a lower yield and reduced viability of cells). These steps were repeated for a second mouse and lobes from different mice were pooled. At least 3 mice were found to be required for a good yield of ECs.

Tissue Dissociation:

The Falcon tube with lung lobes was transferred to a sterile laminar flow hood for subsequent work. To clean and dissect the lungs, three 5-cm diametre Petri dishes, each containing 10 ml growth medium were prepared. Using new sterile scissors, the heart was cut off (taking care to avoid as much of the aorta as possible) and

any visible bronchi and mediastinal connective tissue was carefully removed from the lung lobes. The lungs were placed in a dry 5cm dish and minced finely with scissors for 5 -10 minutes (This step is important because the smaller the tissue pieces are the better will be the final cell yield).

To separate the cells, all lung pieces (including all bits off the plate) were placed in 15 - 20 ml (this volume depending on how many lung lobes were used, usually 15ml for lung lobes of 3 mice) of pre-warmed (37°C) collagenase (2 mg/ml, dissolved in DPBS with Ca^{2+} and Mg^{2+}) and incubated in a shaking water bath (shaking speed at 80 – 90 times per minute) for 1 hour at 37°C. The timing is critical because longer or shorter incubations will compromise the final cell yield. The cell suspension was removed from the waterbath and 10 ml of growth medium was added. Then a 20 ml syringe attached firmly to the cannula, was used to triturate (bring up and down through the syringe) the suspension 4 times, taking care to avoid frothing (bubbles in the tube can dislodge beads that are attached to the magnet in the next step; also oversyringing can cause whitish strands of DNA to precipitate out of the cells which may compromise the culture).

The cell suspension was filtered through a 70µm cell strainer (Falcon) into a 50 ml tube (optional: containing 20 ml of growth medium) and centrifuged for 5 min at 1000g (1029rcf =2300rpm). Most of the supernatant was carefully removed leaving approximately 0.5 ml of liquid and the cell pellet in the bottom of the 50 ml tube. (It was important to avoid creating bubbles in the tube, as before.) The cell pellet was carefully resuspended in an additional 1ml growth medium by gentle pipetting. This cell suspension was incubated with anti-CD31 pre-coated Dynabeads for cell sorting.

Cell Sorting:

Approximately 1.5ml cell suspension was transferred to a cryotube containing 7.5µl anti-mouse CD31- Dynabeads. The cryotube was incubated on a rotator at 4°C for 40 minutes (Note: when incubating Dynabeads and cells, the incubation temperature must be 2-8°C to reduce phagocytic activity and other metabolic processes). Bead and cell suspension mixture was transferred to a 15ml falcon tube in a magnetic separator and left for 1 minute. The supernatant was removed. (Note: the beads & cells should look somewhat foamy if there is good yield of positive selection.) The falcon tube was removed from magnetic separator and beads & cells resuspended in 5 ml growth medium by vigorous trituration. (Note: This step needs to be vigorous to avoid overgrowth of contaminating non-endothelial mesenchymal cells.) The beads & cells were transferred to the magnetic separator for 1min and this washing step was repeated until the supernatant was clear (usually 4-5 washes). The cells were resuspended in Growth Medium and plated in one 0.1% gelatin-coated T25 flask or 6 wells of 0.1% gelatin-coated 12-well plate. The next day, the cells were washed three times with growth medium to remove any loosely adherent cells and surplus beads.

Second Sort (optional):

Cells were fed with Growth Medium every other day until approaching confluence (approx. 80%) at 5-9 days after plating (Note: Nests of 'cobblestone' endothelial cells should be seen and other mesenchymal cells are notable for the way they pile up and don't form monolayers). Cells were rinsed once with Ca^{2+} /Mg^{2+} -free PBS and then Trypsin-EDTA (0.05%:0.5M, Invitrogen) was added for the minimum time necessary to detach the cells. Approximately 2-10ml of isolation media was then added to inactivate Trypsin. The cell suspension was transferred to a 15 ml falcon tube and centrifuged at 1000g for 5 minutes. The supernatant was carefully removed and cells resuspended in 2 ml of DPBS. CD102 (ICAM-2, BD) coated sheep anti-rat Dynabeads were prepared in a similar way to the CD31 beads and added to the cell suspension (15 µl/ml) for 40 minutes at 4°C. The dynabead- bound cells were washed gently three times in 5 ml growth

media using the magnetic seperator as before. After the final wash the cell pellet was resuspended in 10 ml growth media and plated onto gelatin-coated flasks or multiwell plates.

NOTES:

Anti-CD31 antibody-coated Dynabeads are used in the first cell sorting, but their use in later sorts is hindered by CD31 sensitivity to trypsin digestion. The washes of the initial plating of cells can also be done as early as two hours after plating, but yield may suffer. Additionally, the first rinse (containing non-adherent cells) can be plated on a second flask to increase yield, while still maintaining a fairly high purity of ECs.

2.2.14 Cryopreservation and cells recovery culture

Recovery Cell Culture Freezing Medium (Invitrogen) was prepared on ice and cryotubes fully labelled with details about cells to be frozen. Subconfluent cells were detached with Trypsin-EDTA as before and cells were washed with cold medium in cold centrifuge and a pellet of cells was obtained. The cells were resuspended in 1 ml ice-cold freezing medium (1ml for per T75 flask of cells) on ice and 0.5 ml was dispensed into one cryovial on ice. Cells were slowly cooled down to -80°C using a cell freezing container containing Isopropanol, ensuring a steady freezing process. After 1 – 3 days, the tubes were then transferred into liquid nitrogen for prolonged storage.

To recover frozen cells, the cryovial was removed from liquid Nitrogen into an ice bucket for transfer to cell culture room. The cells were then thawed rapidly in 37^{o}C waterbath or rolled between hands. When just liquid, a pipette was used to gently drip cells into 10ml pre-chilled complete medium on ice. After centrifugation, the supernatant was removed and cells were resuspended in pre-warmed medium and were pipetted gently up and down. Cells from each cryovial were seeded into one T25 flask. When seeding density was critical, a dilution

series (1:2, 1:4; 1:8 etc) can be prepared using a 12 well plate as one of these is likely to generate the correct cell density.

2.2.15 Immunocytochemistry

Major optimized steps	Original two-step method	Test of three-step method	Optimized two-step method
Fixation	2.5% PFA @ RT 10 minutes	Cold acetone @ 4oC 10 minutes	Acetone @ RT 5 minutes
Washing post-fixation	1x PBS wash 0.3% Triton X-100/ PBS	1x PBS wash	1x PBS wash
Blocking solution	10% FCS, 0.3% Triton X-100, 2% BSA, 5% Marvel milk powder 30 minutes	10% rabbit serum, 30 minutes; Strepavidin/biotin blocking kit	5% Goat serum 1% BSA @RT, 20 minutes
1^{o}Ab titration	1/25, 1/15, 1/10	1/25, 1/15, 1/10	1/25
1^{o}Ab incubation	Diluted in blocking solution, @ RT, 2 hours	Diluted in 1.5% rabbit serum, @ 4^{o}C, O/N	Diluted in blocking solution, @ 4^{o}C, O/N
Washing post-1^{o}Ab incubation	0.1% Triton X-100/PBS, 3 times	0.1% Triton X-100/PBS, 3 times	1x PBS wash, 3 times
2^{o}Ab incubation	Diluted in blocking solution, @ RT, 1 hour	Diluted in 1.5% rabbit serum+0.1% Triton X-100/PBS, @ RT, 45 minutes	Diluted in blocking solution, @ RT, 1 hour
Washing post-2^{o}Ab incubation	0.1% Triton X-100/PBS, 3 times; dH_2O, twice	0.1% Triton X-100/PBS, 3 times	1x PBS wash, 3 times
Mounting medium	Vectorshield Mounting Medium with DAPI	Vectorshield Hardset Mounting Medium with DAPI	Vectorshield Hardset Mounting Medium with DAPI

Table 2.6 The details of optimization for immunocytochemistry on MLECs.

Cells were grown for 24 to 48 hours on multiwell slides (Lab Tek II, Nunc) in the presence or absence of cytokine at 37°C in humidified chambers and 5% CO_2 atmosphere. All subsequent incubations were carried out at room temperature. Cells were washed in PBS, and fixed with 2.5% paraformaldehyde in PBS for 20

minutes. Alternatively, when staining for CD31 protein, cells were fixed in 100% methanol for 2 minutes. Fixative was removed and followed by 2 washes in PBS. To diminish background fluorescent signal, the cells were incubated with blocking solution (5% goat serum, 1% BSA) for 20 minutes. The blocking solution was removed and the primary antibody, diluted in blocking solution, was applied. After the time indicated for the particular antibody in Table 2.7, the slides were rinsed three times in PBS. The appropriate fluorescein conjugated secondary antibody (1.5 mg/ml, Vector Laboratories) was applied for 1 hour at 1/200 dilution in blocking solution. Cells were washed three times in PBS, and slides were mounted with anti-fade water-based mountant hard set with DAPI (Vector Laboratories) and coverslips.

Primary antibody	**Source**	**Dilution**	**Incubation**
PECAM1(CD31)	BD Pharmingen (cloneMEC13.3)	1/25	o/n, 4°C
Endoglin (CD105)	eBioscience	1/100	o/n, 4°C
Secondary antibody	**Source**	**Dilution**	**Incubation**
Fluorescein goat anti-rat Alexa488 IgG	Invitrogen	1/200	1 hr, RT
Fluorescein goat anti-rat Alexa594 IgG	Invitrogen	1/200	1 hr, RT

Table 2.7 Antibodies used for immunofluorescence.

2.2.16 PCR to genotype cultured cells

PCR was performed following the protocol for genotyping in section 2.2.1. The minimal cell number required for genotyping by PCR was optimized using the sEND-1 cell line.

2.2.17 MTT assay

To measure cell viability, the MTT assay was performed following the approaches shown in Figure 2.2.

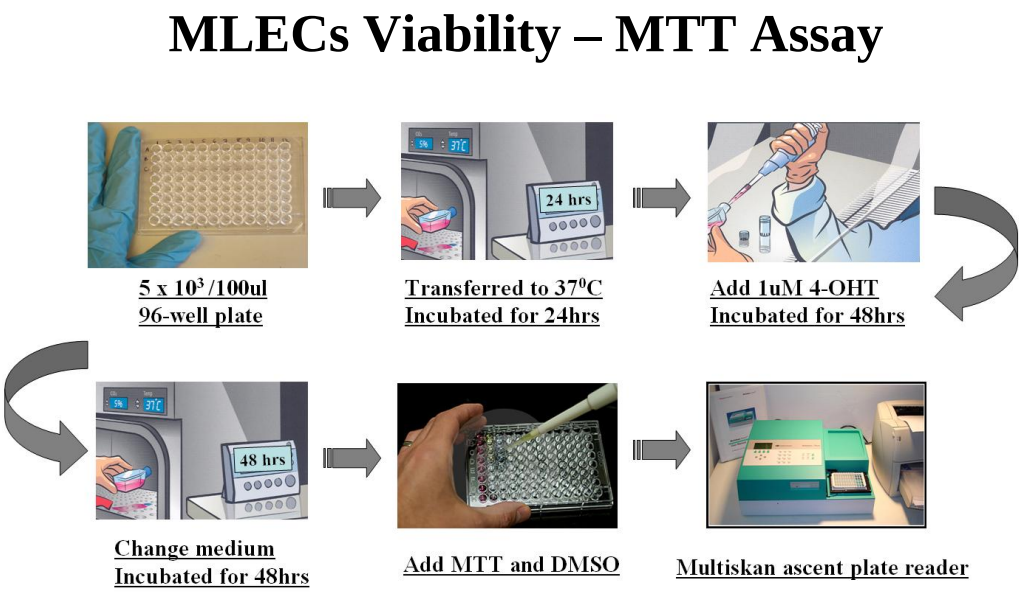

Figure 2.2 MLECs Viability –MTT Assay

For the viability assay, MLECs were incubated in 100µl microvascular endothelial cell medium (MV_2) with 5 % FBS at an initial density of $5x10^3$ per well in 96-well microplates (coated with 0.1% gelatine). After 24 hours, the media were replaced by MV_2 medium with 1µM 4-OHT, and the control wells with MV_2 medium only. After 48 hours of incubation, the medium in all the wells were changed to MV_2 medium, after another 48 hours, 10 µl MTT (5 mg/ml in PBS) was added to each well. After 4 hours of MTT incubation, the media were discarded, and 100µl dimethylsulfoxide (DMSO) was added to each well. The plate was shaken for 30 seconds and the absorbance was measured at 570 nm using a Multiskan microplate reader (MultiScan Ascent, Thermo Labsystems).

2.2.18 Scratch assay

Prior to the assay, a line was drawn with a marker on the bottom of the well and $5x10^4$ cells/ml (sEND-1) were seeded per well of a 12-well plate. Cells were cultured for 24 – 48 hours until confluent (90% confluence is best). On the day of the assay, a sterile trimmed cell scraper (approx. 1.5-2 mm) was used to scratch one 'wound' through the cells moving perpendicular to the line drawn on the base of the well. (Note: it was important to keep the same angle of the pipet tip at 90^o to well surface and to maintain constant pressure of the tip). A picture of the 'wound' was taken using phase contrast and 5 x objective (Note: If this is done

just above and/or just below each line, this will help orientate the measurements). The distance between the two migrating fronts of the cells was measured using 'measure' tool in Axiovision software. Further images were taken at 6, 12 and 24 hours and so on until confluence was reached (the final selection of different timepoints depends on the rate of cell growth and cell type). Based on the sEND-1 cell line wound healing study, MLECs scratch healing assay was optimized and performed following the approaches shown in Figure 2.3.

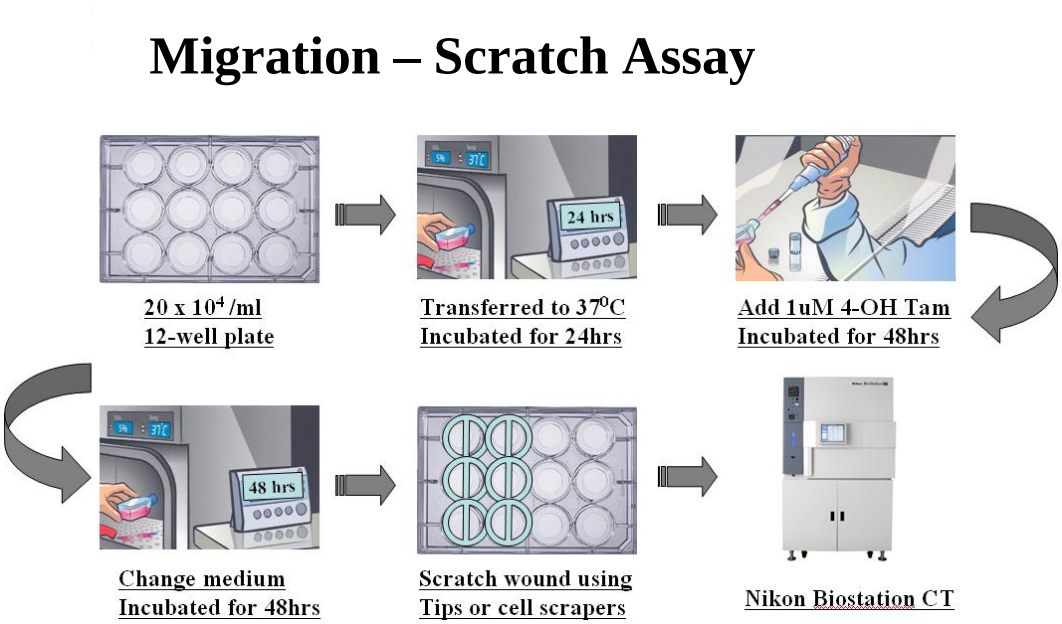

Figure 2.3 ***In Vitro*** **MLECs Monolayer Scratch 'Wound' Healing Model**

For the in vitro monolayer scratch-healing model, MLECs were incubated in 1ml microvascular endothelial cell medium(MV_2) with 5 % FBS at an initial density of 20 x 10^4 cells/well in 12-well plates coated with 0.1% gelatin. After 24 hours, the media was replaced by MV_2 medium with 1µM 4-OH tamoxifen, and the control wells with MV_2 medium only. After 48 hours of incubation, an approx. 2-mm-wide incision in the cell monolayer was created using a sterilized trimmed cell scraper (it was optimized in this experiment since it was easier to make uniform scratch compared with using a pipet tip). Subsequent to wounding, the media were removed, and the plates were washed with PBS and were added endothelial cells growth medium MV_2. The absence of cellular materials in the 'wounded' area was monitored under a microscope using the Nikon Biostation. Subsequently, endothelial cells migrated from both leading edges to close the 'wound' and digital images were taken using a x4 objective every 2 hours over a 28-hour period (starting 90 minutes after the wounding to minimize condensation) for subsequent measurements of 'wound' areas. Throughout this period, the cells were incubated at

37°C in a humidified atmosphere of 5% CO_2 and 95% air. This experiment was performed three times.

2.2.19 MLECs proliferation study – cell counting

MLECs proliferation study was simply performed by cell counting following the procedures shown in Figure 2.4.

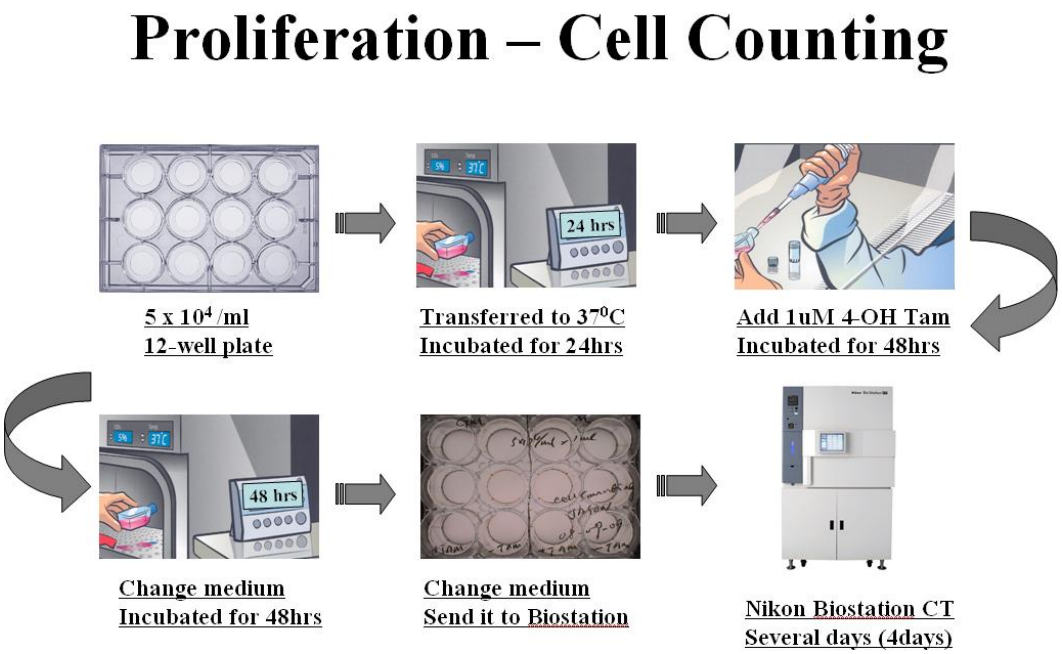

Figure 2.4 Cell number counting – MLECs proliferation assay.

For the cell counting proliferation assay, MLECs were incubated in 1ml microvascular endothelial cell medium (MV_2) with 5 % FBS at an initial density of $5x10^4$ cells/well in 12-well plates (coated with 0.1% gelatine). After 24 hours, the media were replaced by MV_2 medium with 1µM 4-OH tamoxifen, and the control wells with MV_2 medium only. After 48 hours of incubation, the medium in all the wells were changed to MV_2 medium, afterwards, endothelial cells proliferating measurement areas were set up for every 4 hrs images taken within 80 hours using Nikon BioStation. During the observation and images taken, the cells were incubated at 37°C in a humidified atmosphere of 5% CO2 and 95% air. Digital images were taken every 4 hours using a x10 objective, starting 90 minutes after the wounding (to minimize condensation). This experiment was performed three times (truly include pilot study).

2.2.20 Microscopy and image analysis

Apart from work using the Nikon Biostation, cells grown in tissue culture dishes or flasks were viewed and photographed with a Zeiss Axiovert 200 inverted microscope. Slides with fixed tissue sections or cells were viewed using a Zeiss

Axioplan 2 microscope, a Zeiss Axio Imager II or a Zeiss Axiovert 200 inverted scanning confocal microscope. Whole mount stained or lungs with metastatic lesions were visualized using a Zeiss Axioplan stemimicroscope.

Images of primary tumour were obtained with Axiovision software and vascularity of primary tumour was quantitatively analysed using ImageJ software (NIH, USA). The other images were obtained and analysed with Axiovision software.

2.2.21 Statistical analysis

Statistical analysis was performed using Minitab 15 statistical software (Minitab Ltd. USA). In order to promote valid data collection, I designed a database on the platform of Microsoft Access 2000. This has the advantage of promoting validation and security of data and was also equally important to input data to statistical software rapidly and automatically for analysis. The basic statistical description includes whether the data set is normally distributed. Generally, normally distributed data sets were analysed using parametric statistics whilst non-normally distributed data sets were analysed using non-parametric statistics.

Parametric statistical tests used were Fisher's exact test, student's t-test and the Chi-square test. The nonparametric data were analyzed by using the Mann Whitney test. A linear regression analysis and power analysis were also used. Multiple testing was corrected using slopes analysis. Differences at the $P < 0.05$ level were defined as being statistically significant.

Chapter 3. Establishing the Endoglin Conditional Knockout Adult Mouse Model

3.1 Introduction

To investigate the role of endoglin, three different laboratories have generated endoglin homozygous null mice. All mice with null endoglin alleles showed early embryonic lethality at E10.5–11.5 and were characterized by defective angiogenesis of the yolk sac and aberrant cardiac development (Bourdeau et al., 1999; Li et al., 1999; Arthur et al., 2000). This early embryonic lethality does not give any opportunity to look into the function of endoglin at later developmental stages in adult life. In order to investigate whether endoglin is required for the formation and stabilization of neovasculature in neonatal development and adult life and whether it plays a major role in tumour angiogenesis, growth and metastasis, an endoglin floxed mouse (*Eng*$^{fl/fl}$), having two loxP sites flanking exons 5 and 6 of the endoglin alleles (Figure 3.1) was generated in my host laboratory for conditional knockout studies (Allinson et al., 2007).

To allow time-specific activation of Cre-recombinase function and tissue-specific depletion of target gene, a tamoxifen inducible *Cdh5*(PAC)Cre-ER^{T2} transgenic mouse (Mahmoud et al., 2010; Wang et al., 2010b) was crossed with the *Eng*$^{fl/fl}$ mouse to generate *Eng*$^{fl/fl}$ *Cdh5*(PAC)Cre-ER^{T2} mice (Figure3.1). Homozygous endoglin floxed mice (*Eng* $^{fl/fl}$) are viable and fertile, with no obvious phenotype. However, in the presence of active Cre recombinase a recombination event occurs between the two loxP sites to generate specific deletion of endoglin exons 5 and 6. This also leads to a frameshift mutation in exon 7 and generates a null allele. The tamoxifen-inducible Cre-recombinase (Cre-ER^{T2}) under the regulation of the vascular endothelial cadherin promoter (*Cdh5*) was used to achieve temporal control of endoglin expression in the endothelium (Figure 3.1). In the *Cdh5*(PAC)Cre-ER^{T2} line, Cre recombinase is expressed as a fusion protein with part of the estrogen receptor which can in turn bind to tamoxifen, leading to the activation of Cre enzyme. Therefore, *Eng*$^{fl/fl}$ *Cdh5*(PAC)Cre-ER^{T2} mice were used

to conditionally knockout endoglin expression specifically in vascular ECs at specific time-points during adult life.

In order to monitor Cre activity, the Rosa26R reporter line was used. Here, the lacZ gene is inserted into the ubiquitously expressed Rosa locus in front of which a transcriptional stop cassette flanked by loxP sites is located (Mao et al., 1999; Soriano, 1999). In the presence of Cre recombinase the stop cassette is removed by recombination between the loxP sites (Figure 3.2) and lacZ is expressed and can be monitored using X-gal staining of whole mount and tissue cryosections. As the *Cdh5*(PAC)Cre-ER^{T2} line was not fully characterised at the start of my project, an early goal was to optimise Cre activation prior to using this line to deplete endoglin.

To investigate how endoglin depletion in *Eng*$^{fl/fl}$ *Cdh5*(PAC)Cre-ER^{T2} mice affected new blood vessel formation, *in vivo* matrigel implantation angiogenesis assays were performed. Tissues were analyzed using immunostaining with antibodies to CD31 (also known as PECAM-1, a pan-endothelial cell marker) and CD105 (endoglin). Importantly, i.p. injection of tamoxifen in adult control animals was tested for any impact on general health or on new blood vessel formation in the matrigel plugs. The work described in this section aims to establish whether the *Eng*$^{fl/fl}$ *Cdh5*(PAC)Cre-ER^{T2} mouse is a valuable tool to study the function of endoglin in tumour angiogenesis, growth and metastases.

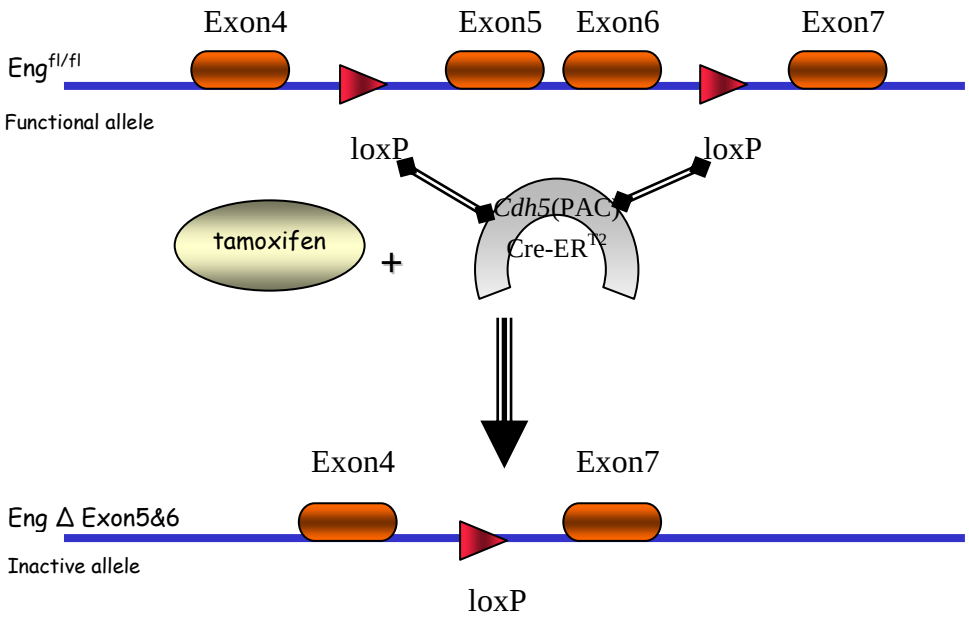

Figure 3.1 The temporal & spatial inactivation of endoglin bifloxed allele by Cre-loxP technology.

The activation of the *Cdh5*(PAC)Cre-ER^{T2} recombinase following tamoxifen administration, leads to EC specific recombination between loxP sites and excision of exons 5 and 6 of the endoglin gene. This also leads to a frameshift mutation in exon 7, giving rise to a null endoglin allele encoding a truncated protein.

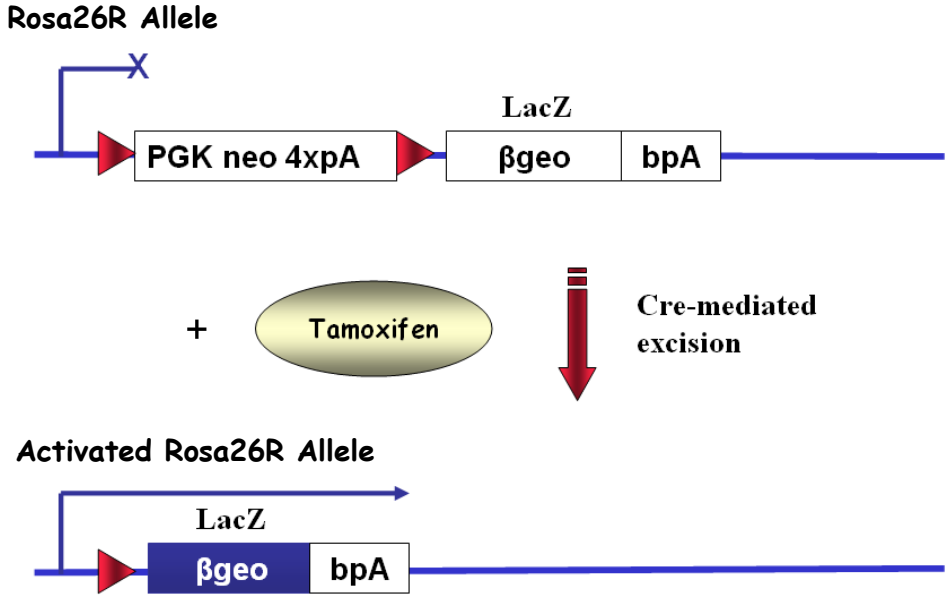

Figure 3.2 Cre mediated recombination of the Rosa26R allele

The Rosa26R gene trap strain contains a loxP flanked neo expression cassette ('floxed stop cassette') upstream of a lacZ gene. LacZ expression driven by the ubiquitous Rosa26 promoter is conditional on the removal of this intervening floxed stop cassette by Cre recombinase.

3.2 Results

3.2.1 Cdh5(PAC)Cre-ER^{T2} expression

In order to assess activation and cell specifity of the *Cdh5*(PAC)Cre-ER^{T2} line, I first crossed with the Rosa26R Cre reporter line and used X-gal staining to detect Cre activity following intraperitoneal (i.p.) injection of tamoxifen. Wholemount stained skin tissues clearly showed Cre activity in the blood vessels of the ear and dorsal skin (Figure 3.3). For a more detailed examination of vessels where Cre recombinase had been activated, light eosin counterstained paraffin sections of X-gal stained wholemount ear and dorsal skin tissues were prepared (Figure 3.4). The blue staining was mainly localized within the ECs of blood vessels, confirming that *Cdh5*(PAC)Cre-ER^{T2} is located in vascular ECs (Figure 3.4). In contrast, no detectable lacZ enzyme was detected in control sections from ROSA26R animals that had been treated with tamoxifen. Although the X-gal staining of sections from the skin stained in whole mount preparations clearly showed endothelial X-gal staining the intensity was weak and incomplete (Figure 3.4 A). This may be because of inefficient perfusion of the X-gal staining solution. To address this possibility, I therefore performed X-gal staining directly on dermal cryosections. It can be seen in Figure 3.5 A that almost all the dermal vasculature was stained with X-gal indicating efficient Cre activation in adult dermal blood vessels following i.p. tamoxifen treatment of *Cdh5*(PAC)Cre-ER^{T2} Rosa26R mice. Due to technical reasons I was unable to stain using the vascular endothelial marker CD31 on cryosections stained with X-gal, to confirm 100% activation in all blood vessels. However, the X-gal staining specificity and efficiency appeared to be at a high enough level to confirm suitability of the *Cdh5*(PAC)Cre-ER^{T2} line for further experiments.

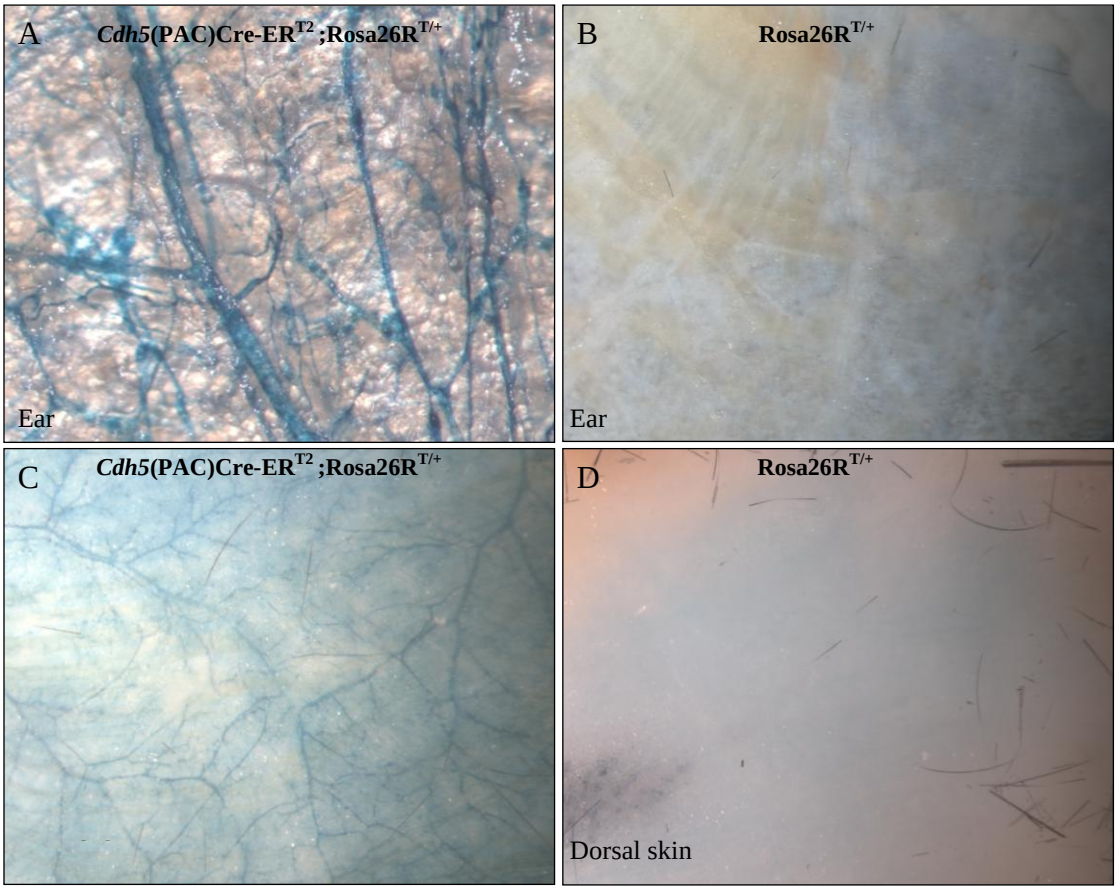

Figure 3.3 Characterizing expression patterns of activated *Cdh5*(PAC)Cre-ER^{T2} recombinase by wholemount X-gal staining.

A&C, The expression of Cre enzyme on the ear (A) and dorsal skin (C) of *Cdh5*(PAC)Cre-ER^{T2}; Rosa26R$^{T/+}$ adult mice; a network of blue stained blood vessels was detected by X-gal whole mount staining.

B&D, Ear (B) and dorsal skin (D) of Rosa26R$^{T/+}$ adult mice revealed no blue blood vessels following X-gal whole mount staining. Note small amount of background staining likely due to endogenous galactosidase activity (see section 3.3 for discussion of this problem).

Note mice used in this experiment were treated with tamoxifen i.p. injection.

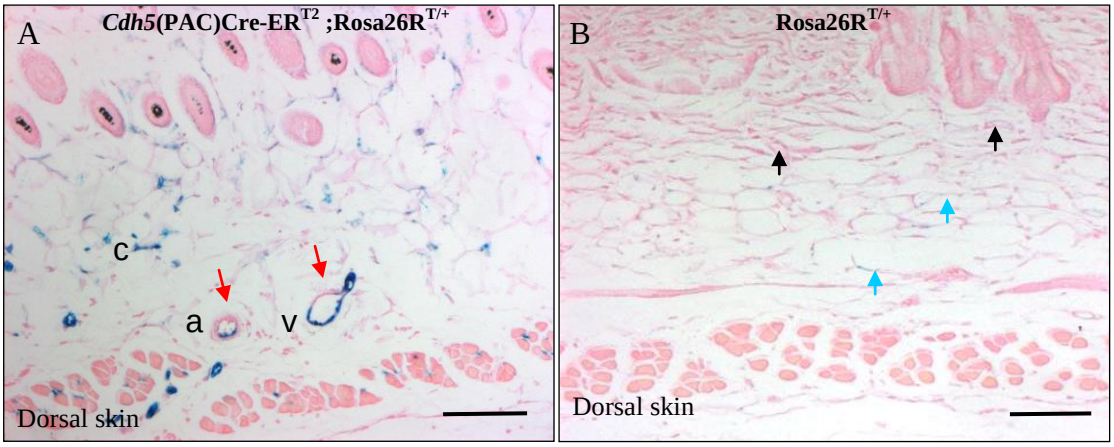

Figure 3.4 Skin sections following whole-mount staining in X-gal.

A, Light eosin counterstained paraffin skin sections show that X-gal positive staining is associated with the capillary network in *Cdh5*(PAC)Cre-ER^{T2}; Rosa26R$^{T/+}$ mice. Red arrows show the unstained region of an arteriole and a venule (The possible reasons for incomplete activity are discussed in section 3.3.1);

B, No lacZ expression was detected in the control (Rosa26R$^{T/+}$) skin, but there are some small blue crystals likely due to non specific background staining (blue arrow; discussed in section 3.3.1), black arrows indicate unstained blood vessels.

Scale bar = 100µm. Abbreviations: a, arteriole; v, venule; c, capillaries.

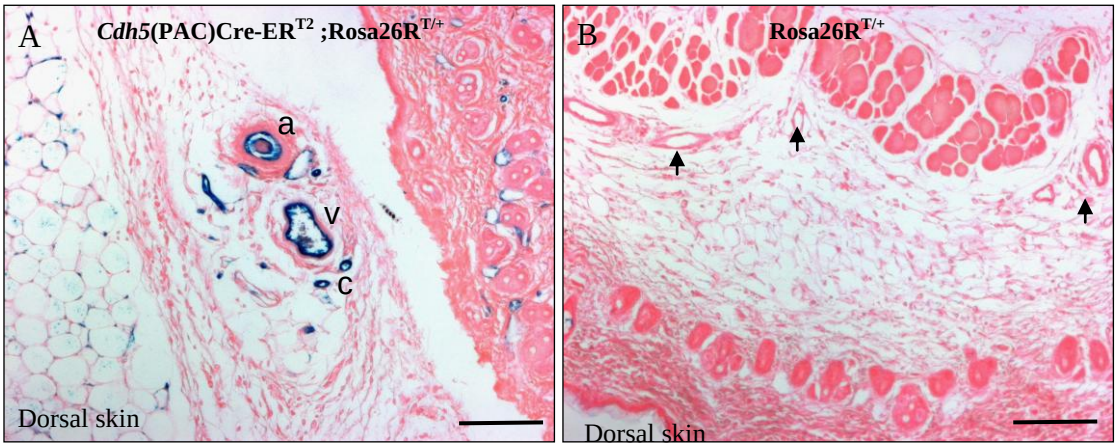

Figure 3.5 Direct X-gal staining of dermal cryosections

A, X-gal staining shows efficient Cre activation in adult dermal blood vessels following tamoxifen treatment of *Cdh5*(PAC)Cre-ER^{T2} Rosa26R mice. Blue colour represents endothelial expression of lacZ resulting from Cre activation of the Rosa26R Cre reporter allele. Sections were lightly counterstained with eosin to show tissue morphology.

B, No blue staining detected in the skin of control Rosa26R mice without Cre. Black arrows indicate non-stained blood vessels.

Scale bar = 100 µm. Abbreviations: a, arteriole; v, venule; c, capillaries.

3.2.2 Endoglin expression is reduced following topical tamoxifen application to ears

Although the work described above showed activation of Cre-ER^{T2} by i.p. injection of tamoxifen in the *Cdh5*(PAC)Cre-ER^{T2} line, I also wished to explore the efficiency of other protocols for tamoxifen delivery to determine which was the most efficient and the most convenient for regular use in the remainder of the project. I therefore tried three means of tamoxifen application: 28-day continuously released tomoxifen pellets, topical application and compared these with i.p. injection (following similar published protocols (Alva et al., 2006; Monvoisin et al., 2006) and also personal communication with Dr. Ralf Adams). I also focussed on the outcomes in terms of efficient knockdown of endoglin protein expression (rather than induction of LacZ expression) as this was the primary objective for the remainder of the study. To do this I used immunostaining with CD31 and endoglin antibodies on ears and skin of *Eng*$^{fl/\Delta}$*Cdh5*(PAC)Cre-ER^{T2} mice and control mice following tamoxifen topical application, tamoxifen pellets and i.p. injection of tamoxifen. Eng$^{fl/\Delta}$ indicates heterozygosity for the floxed endoglin allele and an endoglin deficient (Δ) allele, generated in a previous cross of the endoglin floxed line with the PGK-Cre line. The aim was to reduce the starting level of endoglin protein to maximise knockdown efficiency.

Firstly, I investigated whether endoglin expression is reduced following topical application of tamoxifen. In this case it is important to consider that tamoxifen is converted to the active hydroxytamoxifen after being absorbed through the skin and passing through the liver. Left ears of mutant and control mice were treated with peanut oil and right ears were treated with tamoxifen three times per week for 6 weeks. Tissues were then examined by immunostaining with CD31 and endoglin antibodies. The results showed similar CD31 expression in ears of *Eng*$^{fl/\Delta}$ *Cdh5*(PAC)Cre-ER^{T2} mice and control mice (Figure 3.6). However, there

was some loss of endoglin expression in the right ear of *Eng*$^{fl/\Delta}$ *Cdh5*(PAC)Cre-ER^{T2} mice compared with that of control mice (Figure 3.7). This demonstrates that Cre-ER^{T2} recombinase can be activated by topically applied tamoxifen and also that there was partial deletion of the endoglin. Some reduction of endoglin expression in the left ear of *Eng*$^{fl/\Delta}$ *Cdh5*(PAC)Cre-ER^{T2} mice compared with that of control mice, indicated systemic reduction of endoglin expression. However, there was significant background staining, which may have been due to endogenous pseudoperoxidase activity within tissues (Figure 3.8). Tissue elements most commonly responsible for pseudoperoxidase activity are hemoproteins such as hemoglobin in red blood cells, myoglobin in muscle cell, cytochrome in granulocytes, and monocytes. Further optimisation of the endoglin immunostaining protocol was required to reduce the background staining. Despite the problem of background staining caused by possible endogenous pseudoperoxidase this data suggested that endoglin expression was partially reduced in both ears following topical tamoxifen application.

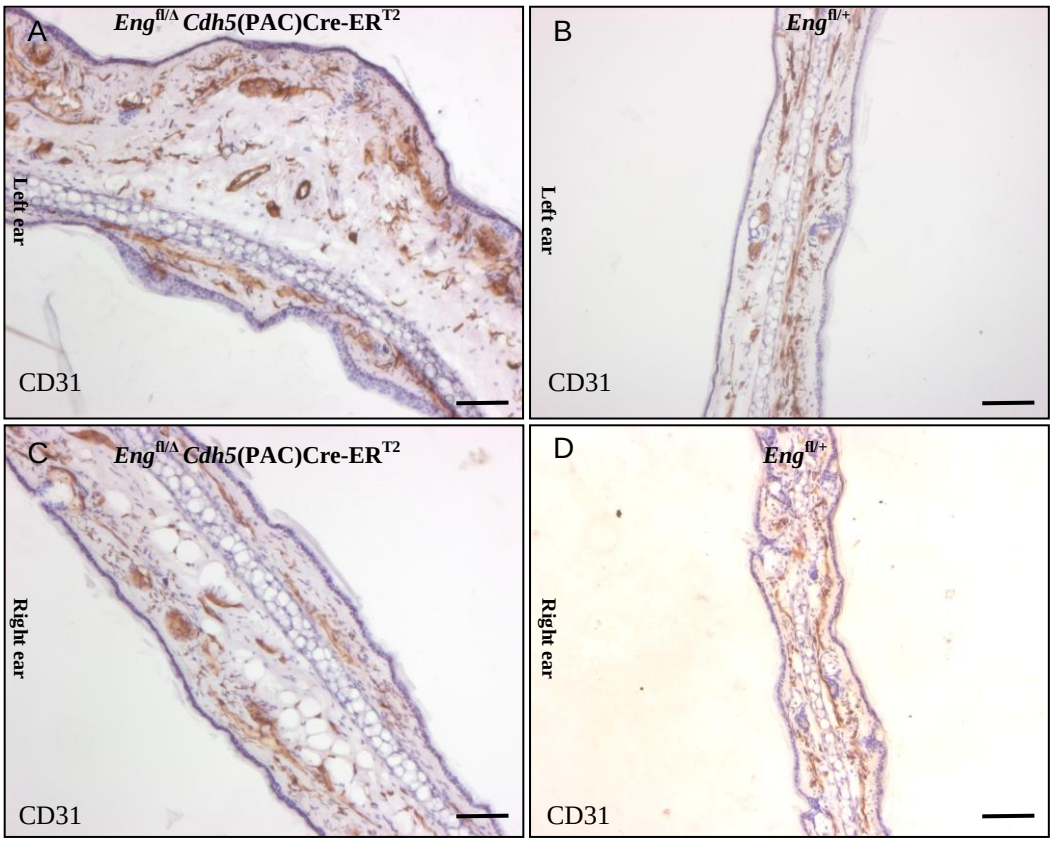

Figure 3.6 Vasculature of the ears from *Eng*$^{fl/\Delta}$ *Cdh5*(PAC)Cre-ER^{T2} and *Eng*$^{fl/+}$ mice show similar CD31 expression.

A, CD31 immunostaining of left ear of *Eng* $^{fl/\Delta}$ *Cdh5*(PAC)Cre-ER^{T2} transgenic mouse model (topical peanut oil treatment only); haematoxylin used as nuclear counterstain.

B, CD31 immunostaining of left ear of *Eng* $^{fl/+}$ mouse model (topical peanut oil treatment only);

C, CD31 immunostaining of right ear of *Eng* $^{fl/\Delta}$ *Cdh5*(PAC)Cre-ER^{T2} transgenic mouse following topical tamoxifen treatment;

D, CD31 immunostaining of right ear of *Eng* $^{fl/+}$ mouse following topical tamoxifen treatment.

Note that some sections appear thicker than others because they had been cut at slightly different angles. Scale bar = 100µm.

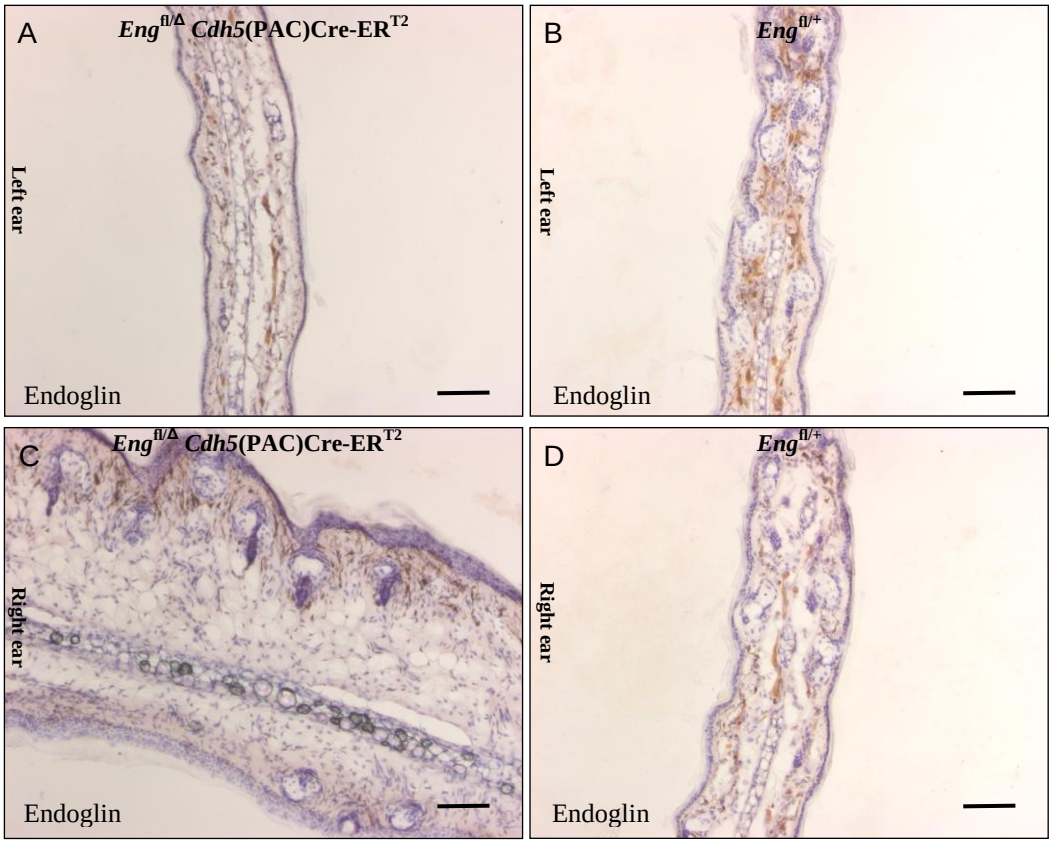

Figure 3.7 Endoglin expression appears to be reduced in ears from *Eng* $^{fl/\Delta}$ *Cdh5*(PAC)Cre-ER^{T2} mouse following topical tamoxifen application

A, Endoglin immunostaining of left ear of *Eng* $^{fl/\Delta}$ *Cdh5*(PAC)Cre-ER^{T2} transgenic mouse model (topical peanut oil treatment only);

B, Endoglin immunostaining of left ear of *Eng* $^{fl/+}$ mouse model (topical peanut oil treatment only);

C, Endoglin immunostaining of right ear of *Eng* $^{fl/\Delta}$ *Cdh5*(PAC)Cre-ER^{T2} transgenic mouse following topical tamoxifen treatment;

D, Endoglin immunostaining of right ear of *Eng* $^{fl/+}$ mouse following topical

tamoxifen treatment.

Note: To allow direct comparison, these tissue sections were stained in parallel and images were taken using the same exposure time. Scale bar = 100µm.

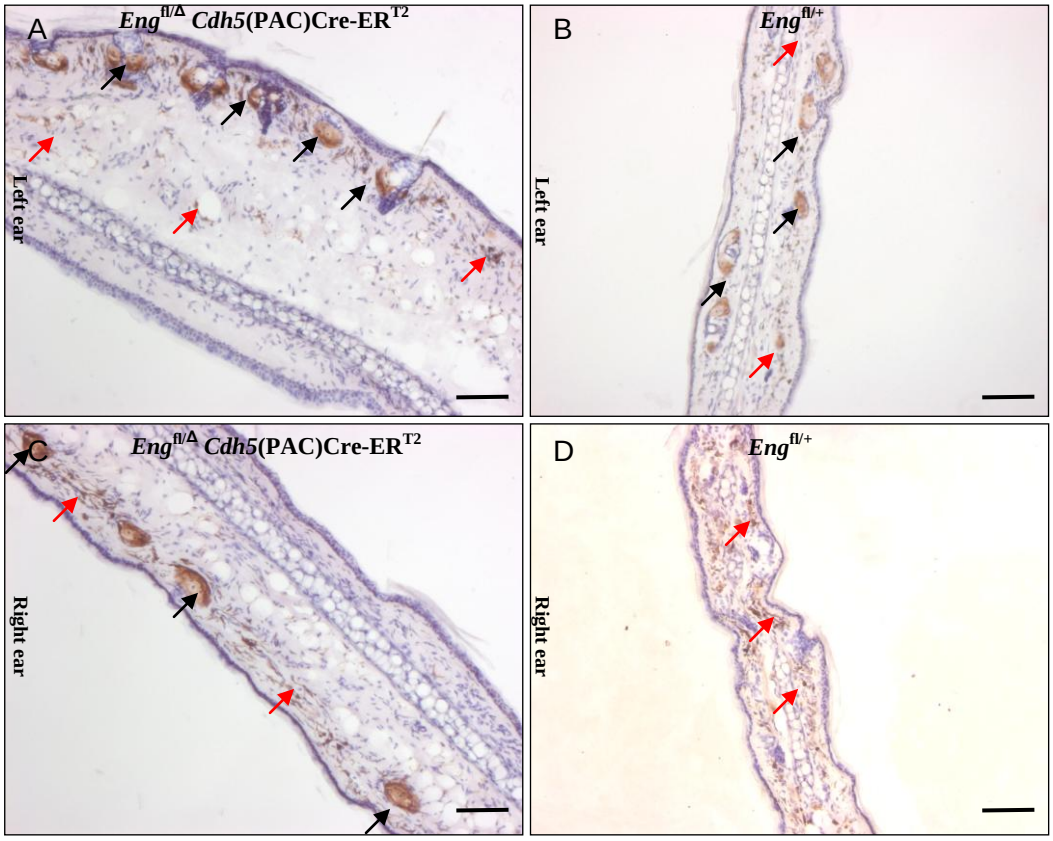

Figure 3.8 No primary antibody controls using ears from control and mutant mice to show level of background staining

A, Left ear of *Eng* $^{fl/\Delta}$ *Cdh5*(PAC)Cre-ER^{T2} transgenic mouse model (topical Peanut oil treatment only);

B, Left ear of *Eng* $^{fl/+}$ mouse model (topical peanut oil treatment only);

C, Right ear of *Eng* $^{fl/\Delta}$ *Cdh5*(PAC)Cre-ER^{T2} transgenic mouse following topical tamoxifen treatment;

D, Right ear of *Eng* $^{fl/+}$ mouse following topical tamoxifen treatment.

Note: red arrows indicate background staining, black arrows indicate non-specific staining of hair follicles. Scale bar = 100µm.

3.2.3 Endoglin expression is reduced following tamoxifen pellet implantation

Slow release (over 21days) tamoxifen pellets were implanted subcutaneously. In principle, this is a very convenient method for tamoxifen treatment as the pellets once in place, can be left to release tamoxifen over a 3-week period. Tissue was harvested at 3 and 5 weeks and cryosections were immunostained with CD31 and

endoglin antibodies (Figure 3.9). The results showed partial loss of endoglin expression in the skin of *Eng*$^{fl/\Delta}$ *Cdh5*(PAC)Cre-ER^{T2} mice compared with that of control mice, demonstrating that the slow release pellets did lead to some recombination of the target loxP sites in the floxed endoglin allele. However, due to persistent problems with background staining (Figure 3.10 shows no primary control images), it was difficult to know how efficiently endoglin was deleted. In addition, conspicuous side effects of this method of tamoxifen delivery were observed. For example, local ulceration of the skin lying over the pellet occured in 4/6 animals. And more seriously, stomach haemorrhage was observed in 1/4 *Eng*$^{fl/\Delta}$ *Cdh5*(PAC)Cre-ER^{T2} mice when animals were observed post mortem. For this reason the pellets were not used in further experiments.

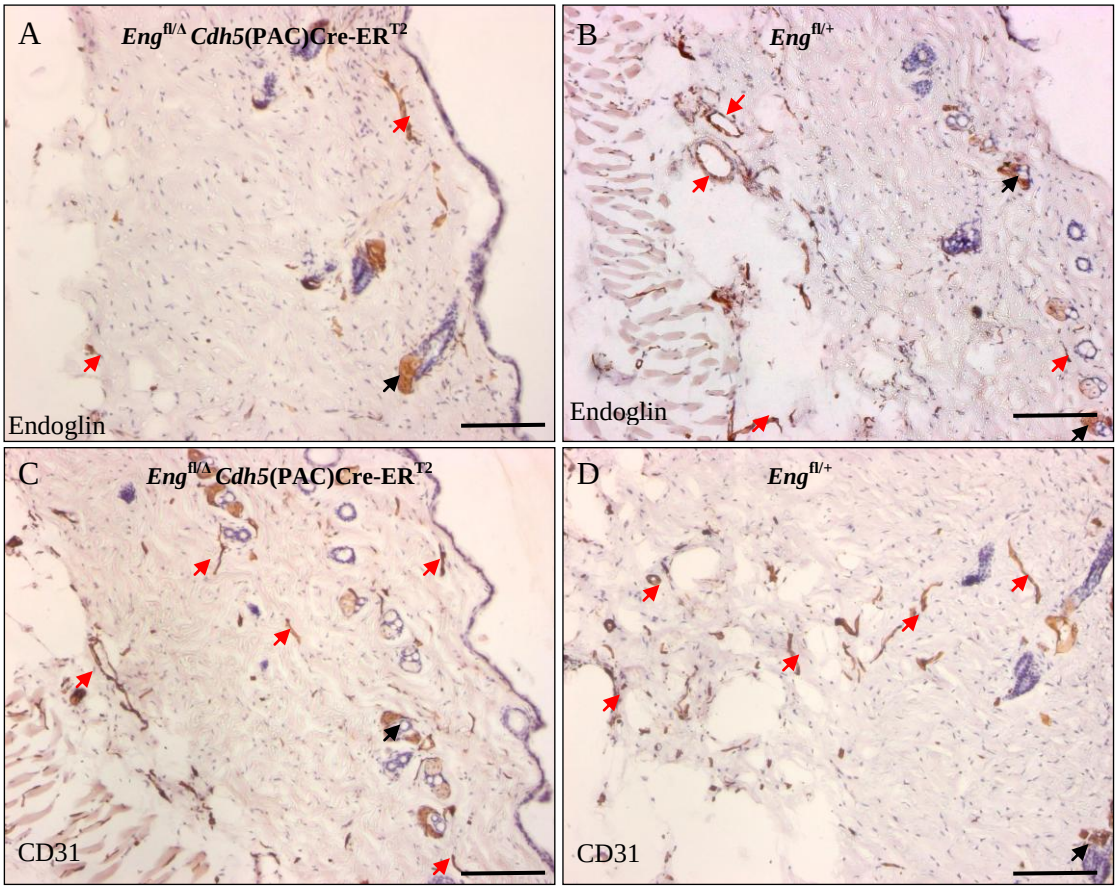

Figure 3.9 CD31 and endoglin expression in the skin following 21 day slow-release tamoxifen pellet application

A, There is less endoglin expression in the skin of *Eng*$^{fl/\Delta}$ *Cdh5*(PAC)Cre-ER^{T2} mice compared with **B,** which shows many endoglin-positive microvessels in the skin of *Eng*$^{fl/+}$ mice. Scale bar = 100μm.

C & D, CD31 expression in the skin of *Eng*$^{fl/\Delta}$ *Cdh5*(PAC)Cre-ER^{T2} (C) and

Eng$^{fl/+}$ mice (D). Black arrows indicate hair follicles, red arrows indicate microvessels.

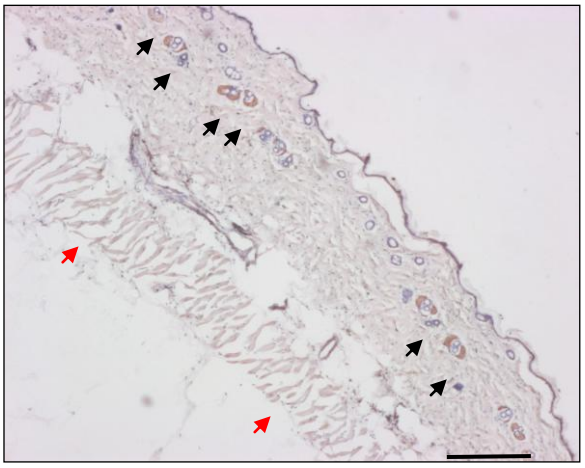

Figure 3.10 No primary antibody control using ears from an *Eng*$^{fl/\Delta}$ *Cdh5*(PAC)Cre-ER^{T2} mouse to show level of background staining
Black arrows indicate hair follicles and red arrows indicate background staining in muscle fibres. Scale bar = 100µm.

3.2.4 Endoglin expression is absent following tamoxifen intraperitoneal injection

Adult mice received tamoxifen i.p. injections 2 mg once a day for 5 consecutive days. On day 10 after the first injection, the skin and ears were removed and cryosections were immunostained with CD31 and endoglin antibodies (Figure 3.11&12). Significant differences in endoglin expression between the skin of mutant mice and that of control mice can be seen. Endoglin protein expression appears to be completely lost from the skin of *Eng*$^{fl/fl}$ *Cdh5*(PAC)Cre-ER^{T2} mice and also from the heart and lung (personal communication, Dr. Marwa Mahmoud and Rachael Redgrave). In addition, the immunostaining protocol was optimized by using avidin/biotin blocking solution and prolonging washing times to remove background staining. Therefore from this immunostaining evidence, I was able to conclude endoglin was efficiently reduced in *Eng*$^{fl/fl}$ *Cdh5*(PAC)Cre-ER^{T2} mice following i.p. injection of tamoxifen.

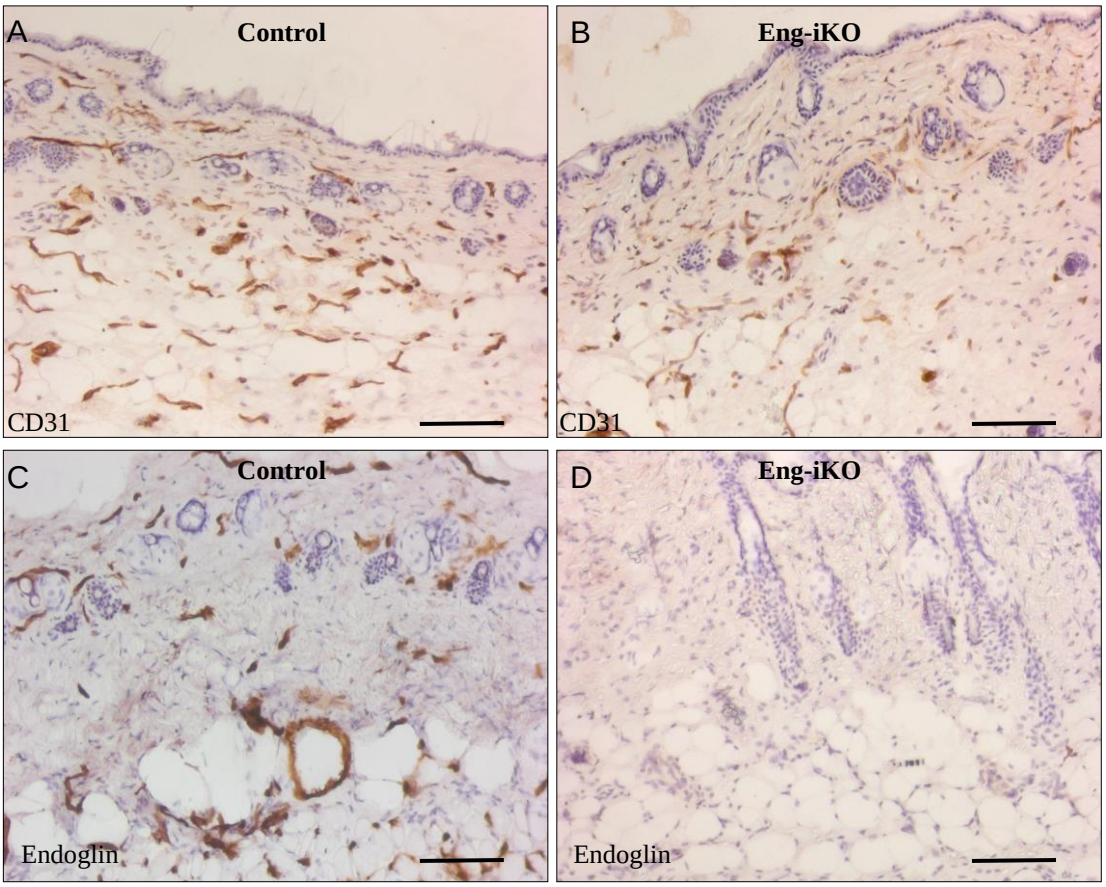

Figure 3.11 Endoglin is efficiently reduced in skin of *Eng*$^{fl/fl}$ *Cdh5*(PAC)Cre-ER^{T2} (Eng-iKO) **mice compared with that of control mice**

A&C, Left panel shows cryosections of skin taken from control mice (*Eng* $^{fl/fl}$ *Cdh5*(PAC)Cre-ER^{T2} mice in the absence of tamoxifen treatment). Immunohistochemistry on adult skin sections shows normal expression of CD31 (A) and endoglin (C) on dermal blood vessels.

B&D, Right panel shows CD31 is expressed in skin in the endoglin inducible knockout (iKO) mouse (B) but endoglin expression is efficiently lost in the *Eng*$^{fl/fl}$*Cdh5*(PAC)Cre-ER^{T2} mouse (D) following tamoxifen treatment (i.p.). Scale bar = 100µm.

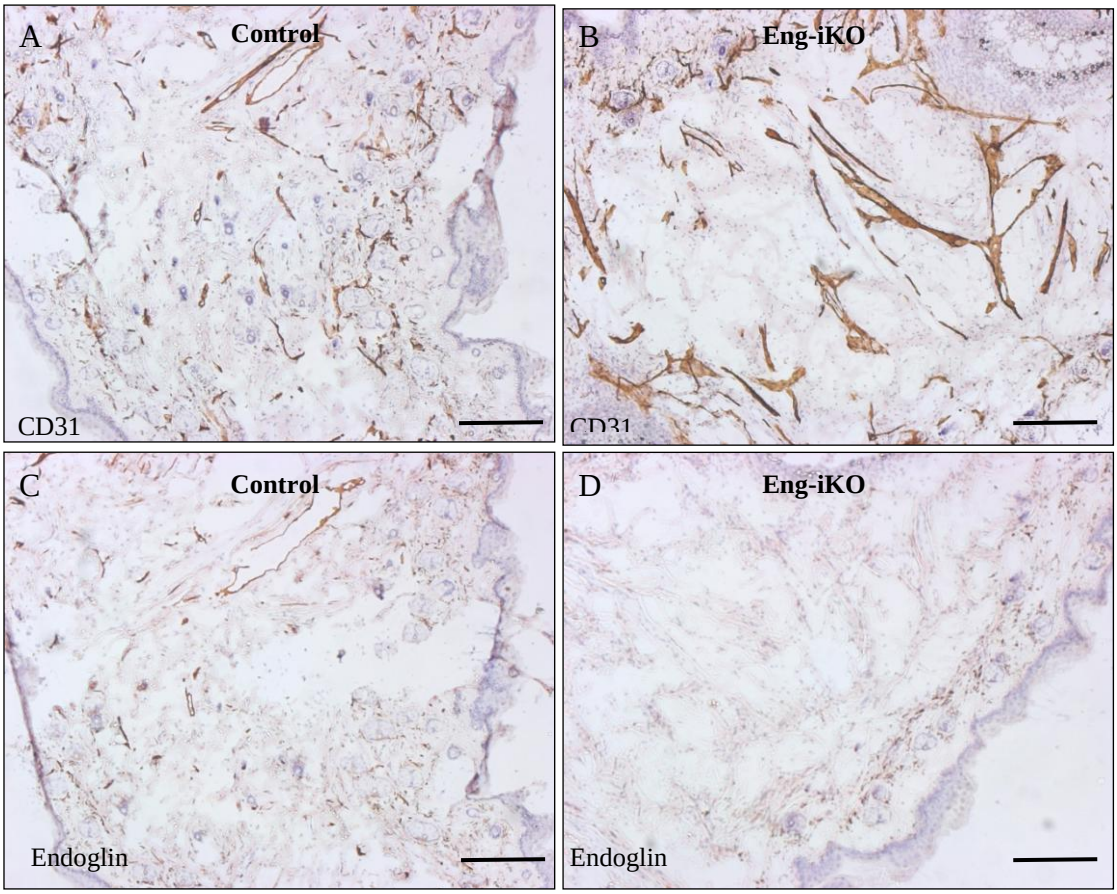

<u>Figure 3.12</u> Endoglin is efficiently reduced in ears of *Eng*$^{fl/fl}$ *Cdh5*(PAC)Cre-ER^{T2} (Eng-iKO) mice compared with that of control mice

A&C, Left panel shows cryosections of ear taken from control mice (*Eng* $^{fl/fl}$ *Cdh5*(PAC)Cre-ER^{T2} mice in the absence of tamoxifen treatment). Immunohistochemistry on adult ear sections shows normal expression of CD31 (A) and endoglin (C) on ear blood vessels.

B&D, Right panel shows CD31 is expressed in ear in the endoglin iKO mouse (B) but endoglin expression is efficiently lost in the *Eng* $^{fl/fl}$ *Cdh5*(PAC)Cre-ER^{T2} mouse (D) following tamoxifen treatment (i.p.).

Scale bar = 100µm.

3.2.5 Tamoxifen i.p. injection is the most appropriate method to activate Cre-ER^{T2} recombinase in vivo

Compared with the other two methods of tamoxifen administration, topical application on ears and pellet implantation, it seems that tamoxifen i.p.injection is the most appropriate and efficient method to activate Cre-ER^{T2} recombinase in vivo in adult mice. Endoglin expression was approximately 100% lost in skin and ears following tamoxifen i.p. injections (Figure 3.11&12). This appeared to be more efficient than endoglin knockdown using topical tamoxifen even when the previous background staining problems were taken into account. In addition, lacZ expression was activated efficiently by Cre-ER^{T2} recombinase following tamoxifen i.p. injections (Figure 3.5). Furthermore, during the course of these studies, we did not observe any deleterious effects of tamoxifen treatment delivered by i.p. injection in either control or *Eng*$^{fl/fl}$*Cdh5*(PAC)Cre-ER^{T2} mice. Therefore, the i.p. injection method appears to be the most appropriate method of delivering tamoxifen to activate Cre-ER^{T2} recombinase to generate a satisfactory adult EC-specific endoglin inducible knockout (*Eng*-iKO^{e}) mouse model for subsequent experiments.

3.2.6 In vivo angiogenesis is significantly reduced in Eng-iKO^{e} mice compared with control mice

To identify the effect of endoglin loss on angiogenesis *in vivo*, the matrigel implantation assay was performed. Endoglin was depleted in the Eng-iKO^{e} mice using i.p. tamoxifen, and two control groups of mice were tamoxifen treated and untreated, respectively. The efficiency of endoglin gene deletion in the Eng-iKO^{e} mouse and the formation of new vessels in the matrigel implant were monitored using immunohistochemistry (Figure 3.13).

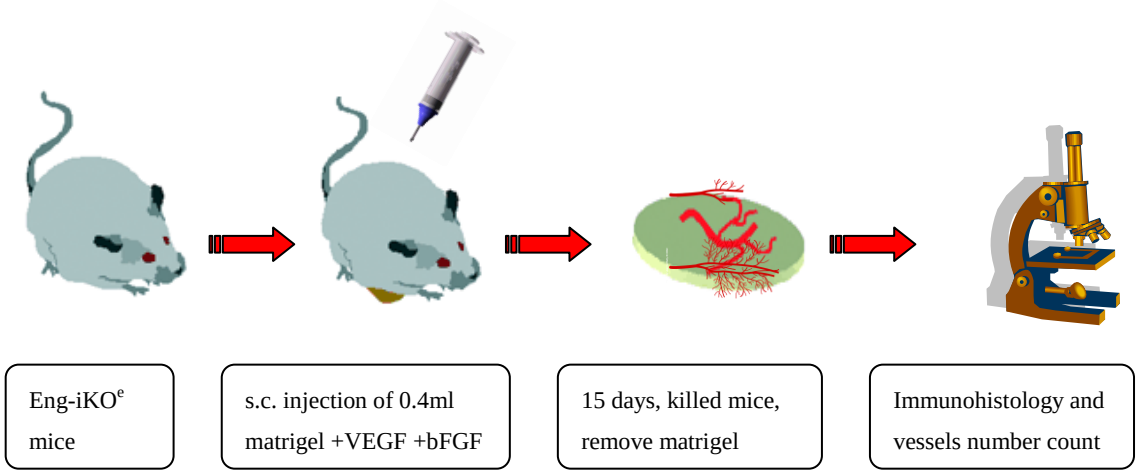

Figure 3.13 Summarized schematic picture of *in vivo* angiogenesis study using matrigel plugs
Eng$^{fl/fl}$*Cdh5*(PAC)Cre-ER^{T2} mice were intraperitoneally injected with tamoxifen to deplete endoglin. At the same time, 0.4 ml matrigel mixed with VEGF and bFGF was subcutaneously implanted into the right flank of mutant and control mice. After 15 days, mice were humanely killed and matrigel plugs together with surrounding skin tissues as well as skin from the contra-lateral (left) flank were removed from mice and tissue was processed for immunohistology and vessel counts.

Cryosections from the matrigel plugs were evaluated for neovascular formation by immunostaining with CD31 and endoglin antibodies (Figure 3.14) and by counting the number of vessels as described in the vessel quantification in matrigel plugs in Chapter 2. Vessel quantitation was performed blind to the genotype of mice. In the control mice, new microvessels formed in the plugs, not only in the area close to the surface, but also in the central region of the matrigel plugs. In contrast, there was

either no neovasculature or few neovessels in the matrigel plugs from the Eng-iKO^{e} mice. For statistical analysis, the number of neovessels in matrigel plugs from control mice with tamoxifen treatment was not normally distributed and therefore, the non-parametric Mann-Whitney test was used to compare results from Eng-iKO^{e} mice with this control group (n = 6 in each group). There was a significant reduction in the number of microvessels in the plugs of the Eng-iKO^{e} mice compared with that of the control mice (P = 0.02, Figure 3.15). This result supports the idea that endoglin contributes to ECs migration as well as to neovessel formation. In some cases enlarged vessels occurred in the veins close to the matrigel plugs of the Eng-iKO^{e} mice. This was noted but the experiment was not designed to investigate whether this was a matrigel specific response. Further investigations of this phenotype are discussed in chapter 6.

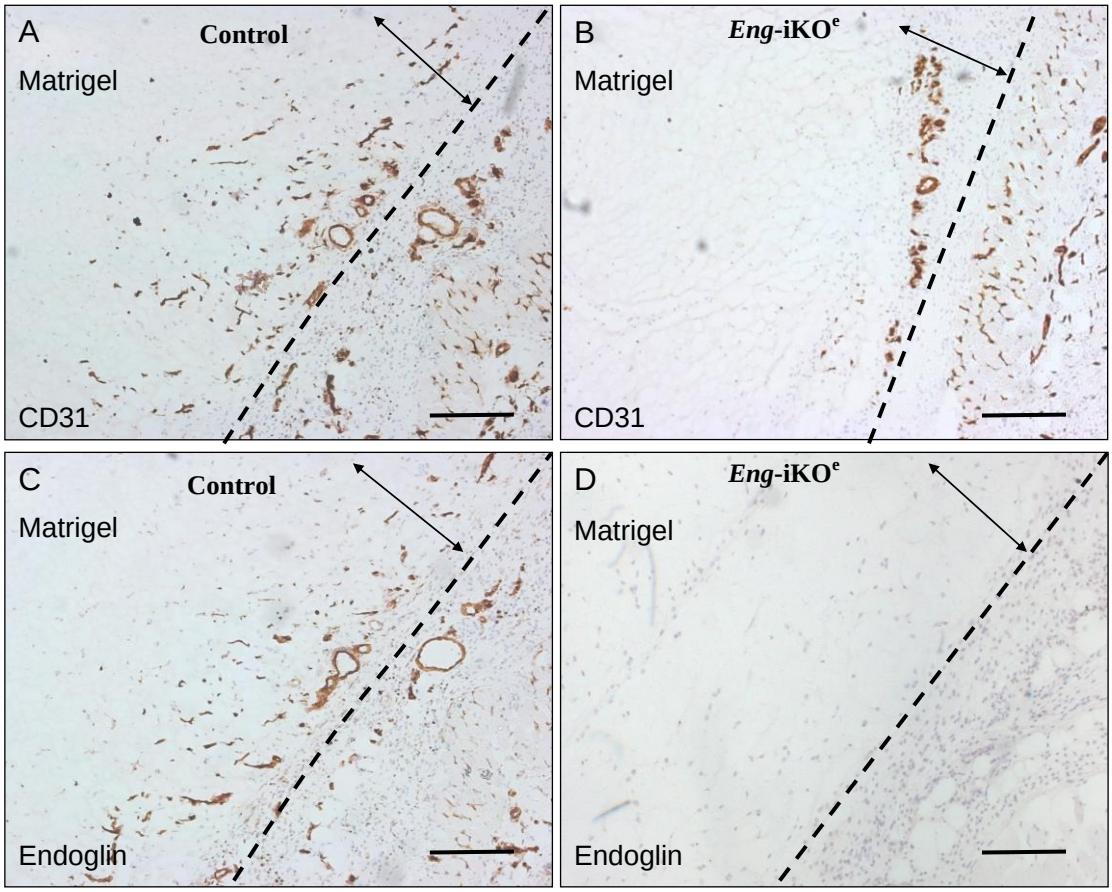

Figure 3.14 New blood vessel formation is reduced in Eng- iKO^{e} mice compared with control mice

Left panels show cryosections of matrigel implants taken from control mice. CD31 (A) and endoglin (C) positive neo-vessels, in which brown staining can be seen

invading matrigel in the control mouse. In contrast, right panels show few new CD31 positive vessels in the matrigel in Eng-iKO^{e} mice (B). Also endoglin expression is not detected in the Eng-iKO^{e} skin and was therefore efficiently knocked down by tamoxifen treatment (D). Dotted lines separated matrigel and skin, arrows indicated the matrigel area close to skin. Scale bar = 100µm.

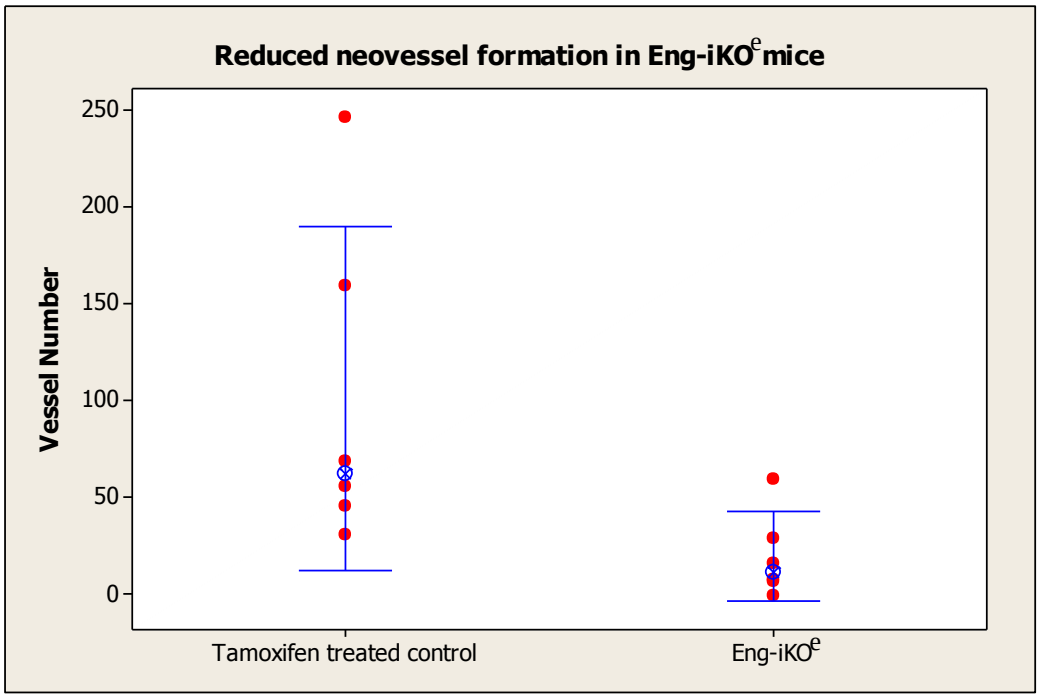

Figure 3.15 The statistical analysis of vessel number whithin matrigel plugs in Eng-iKO^{e} mice and control mice.
The figure shows reduced neovessel formation in Eng-iKO^{e} mice (Median = 62.5, n = 6) compared with tamoxifen treated control mice (Median = 12, n = 6). (W = 24.0, P = 0.02, non-parametric Mann-Whitney test used). The interval bar (green bar) indicates the confidence interval for the median (the blue circle with inside cross). Each individual red dot represents the vessel number from a matrigel plug in each individual mouse model.

3.2.7 Tamoxifen treatment alone does not significantly affect angiogenesis in vivo

It was important to use an additional control in this study because the tamoxifen used to activate Cre-ER^{T2} also has the ability to induce TGF-β in vascular tissues (Grainger et al., 1993), and may therefore affect angiogenesis in the matrigel experiment. To test this, angiogenesis in matrigel plugs was compared in control mice with and without tamoxifen treatment and neovessel counting was performed and analysed as described above. There were no significant differences

in the number of new blood vessels formed between the mice with and without tamoxifen treatment (Figure 3.16, P = 0.3613). According to this evidence, it was therefore concluded that tamoxifen does not significantly affect endothelial cell migration or new blood vessel formation in our matrigel angiogenesis in vivo study. Therefore, the tamoxifen treatment of mice for the induction of the Cre enzyme did not confound our results.

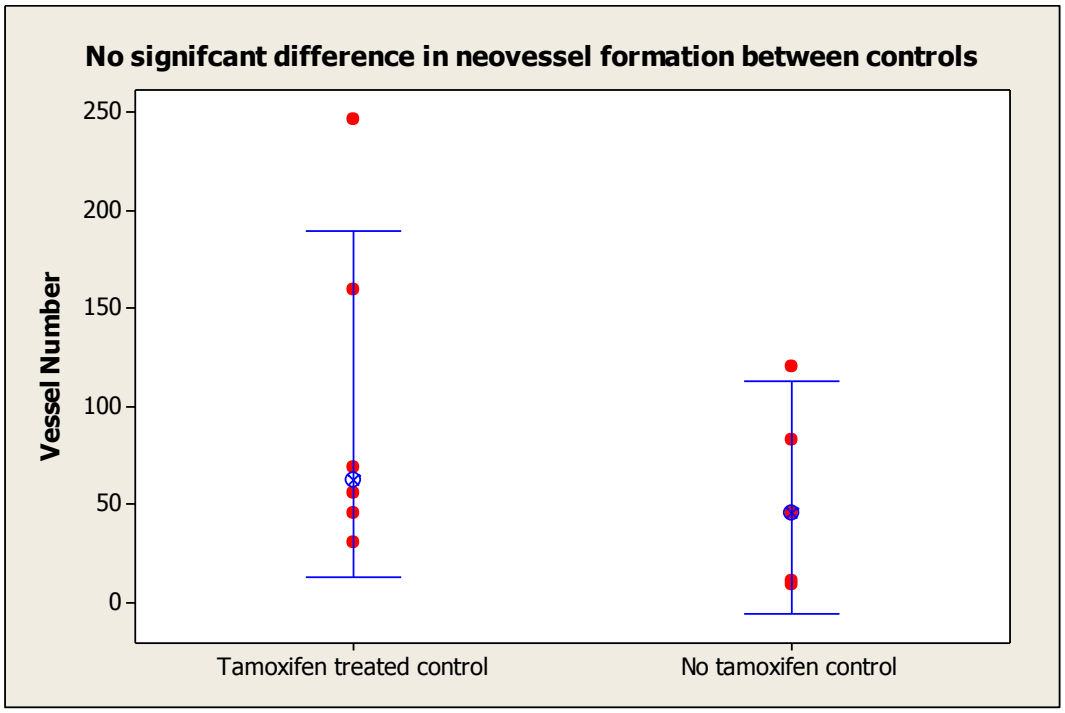

Figure 3.16 No significant difference in neovessel formation in tamoxifen treated control mice compared with no tamoxifen treated control mice.
The figure shows there is no significant difference in neovessel formation between tamoxifen treated control mice (Median = 62.5, n = 6) and no tamoxifen control mice (Median = 46, n = 5). (W = 41.5, P = 0.3613, non-parametric Mann-Whitney test used). The interval bar (green bar) indicates the confidence interval for the median. The power of this statistical analysis was automatically set up at default value of 0.80 in Minitab 15 statistical analysis software.

3.3 Discussion

3.3.1 Cdh5(PAC)Cre-ER^{T2} expression

The endothelial junction protein vascular endothelial (VE)-cadherin, originally termed cadherin-5 (Suzuki et al., 1991), also known as CD-144 and Cdh5, is located on the transmembrane part of the endothelial adherence junction and contributes to endothelium integrity and regulate vascular permeability as well (Breviario et al., 1995). At the start of the work described in this chapter, this endothelial specific and tamoxifen inducible Cre line was novel and unpublished and it was therefore extremely important to establish the Cre-ER^{T2} expression pattern and activation efficiency.

In this chapter I have shown that the expression of *Cdh5*(PAC)Cre-ER^{T2} was in the vasculature of adult skin/ears and was efficiently activated by i.p. tamoxifen injections. LacZ is a widely applied reporter gene, encoding the bacterial escherichia coli enzyme β-gal. β-gal activity is visualized by the standard substrate X-gal in an intense blue colour. There was no significant background X-gal staining found in either Rosa26R positive tissue or control tissue. LacZ expression is efficiently and specifically induced in vascular endothelial cells of arteries, veins and capillaries in adult skin (Figure 3.5), as well as in all other tissues tested to date including adult heart and lung (investigated in other projects in my host laboratory). Both X-gal whole mount staining and X-gal staining on cryosections were used. There are a number of ECs where LacZ is not expressed as the limitation of whole mount staining is mainly due to substrate penetration into the tissue, which can be a problem particularly in skin and very thick tissue, (even though tissue was left in staining solution in the shaking water bath overnight). The prolonged incubation time required for maximal tissue penetration might be responsible for the small amount of background staining. Where it was necessary to bypass the minor background X-gal staining difficulties and substrate penetration problems caused by whole mount staining, X-gal staining on

cryosections was performed. This showed that LacZ is expressed on almost all the ECs in skin tissue.

Therefore *Cdh5*(PAC)Cre-ER^{T2} was efficiently induced following i.p. tamoxifen treatment, and specifically expressed in the vasculature. The dermal vasculature was the focus of the work in this chapter. In parallel, the Eng-floxed allele was converted to a null allele in the presence of activated Cre-ER^{T2}, leading to loss of endoglin protein in the dermal blood vessels in Eng-iKO^{e} mice (Section 3.2.4).

3.3.2 Efficacy of endoglin depletion in the skin and lung of adult mice

To investigate the efficency of endoglin depletion, immunostaining with CD31 and endoglin antibodies was performed. The data show that deletion of endoglin in the skin of Eng-iKO^{e} adult mice was very efficient. This indicates that the Eng-iKO^{e} mouse is likely to be suitable to study the function of endoglin gene in tumour growth and metastases as will be described in chapter 5.

Some variabilities in the efficiency of depletion of endoglin protein did occur in lung tissue (Rachael Redgrave, personal communication). The range of endoglin deletion efficiency in the lung was approximately 70-80% even in mice where there appeared to be 100% loss of endoglin protein in the skin. The specific mechanism for this finding is unclear, however, several possibilities could explain these results: (1) the *Cdh5*(PAC)Cre-ER^{T2} used to drive the specific gene deletion may not be efficiently expressed in certain ECs of lungs; (2) activity of Cre or the Cre-ER^{T2} fusion is suppressed in some ECs in lungs; (3) Cre recombination was induced in a dose-dependent manner (Monvoisin et al., 2006), sufficient dose for gene deletion in skin might be insufficient for Cre recombination in lungs, or (4) the patterns of blood flow through the lungs might be variable in different lobes. Cre-ER^{T2} can not be activated if the hydroxytamoxifen in the blood does not reach the tissue. Since the efficacy of endoglin gene depletion in lung might be important for the growth potential of lung metastases, additional experiments would be needed to discriminate between these possibilities. Nonetheless, these

analyses highlighted the relatively high efficacy of endoglin depletion in the skin and lung of Eng-iKO^{e} mice.

3.3.3 Effect of tamoxifen on angiogenesis in vivo

Tamoxifen is an important oestrogen partial antagonist and most of its clinical effects are mediated via oestrogen receptors. It also has a number of oestrogen-independent effects (Grainger and Metcalfe, 1996), including possible anti-angiogenic effects (Gagliardi et al., 1996). Tamoxifen influences the expression level of a number of cytokines involved in the regulation of angiogenesis, including insulin-like growth factor (IGF) (Huynh et al., 1993), basic fibroblast growth factor (bFGF) (Fujimoto et al., 1997) and VEGF (McNamara et al., 2001).

Previous studies have also demonstrated that tamoxifen has additional effects on the potent pro-angiogenic cytokine TGF-β. Tamoxifen has the ability to induce vascular smooth muscle cells to induce TGF-β *in vitro* (Grainger et al., 1993). Also, tamoxifen elevates TGF-β expression in breast tumours *in vivo* (Butta et al., 1992). The data *in vivo* show that a major effect of tamoxifen in the C57BL/6 mice is to elevate TGF-β in the aortic wall and in the circulation. Active TGF-β reached a maximum at 7 days after a tamoxifen diet (equivalent to a dose of approximately 1mg tamoxifen per kg body weight per day) of 28 days (approx. 1mg tamoxifen in total delivered by a diet over 28 days as an average body weight of adult C57BL/6 mice was assumed to be about 30g) and reduced after 28 days, active TGF-β was only elevated by 1.5-fold in serum and 2.2-fold in the aortic wall (Grainger et al., 1995). All this evidence seems to indicate tamoxifen affects TGF-β levels and may therefore indirectly affect angiogenesis. Although more tamoxifen was used in my project (14 mg tamoxifen in total delivered by i.p. over 9 days), to evaluate any confounding effects of tamoxifen on *in vivo* matrigel angiogenesis study, I included two control groups, one with and one without tamoxifen treatment. However, there was no significant difference in the degree of matrigel vascularisation between these two control groups. This indicates that

tamoxifen i.p. injection protocol used in this project did not affect *in vivo* angiogenesis in matrigel plugs. It appears that our results are not in line with the previous data published, possibly because the dose of tamoxifen used in this project is just sufficient to activate Cre recombinase, but is not enough to lead to other detectable effects. On the other hand, the previous publications mostly focused on the effect of tamoxifen on growth factor levels rather than angiogenesis.

Tamoxifen also has a role in modulation of another important angiogenic molecule, VEGF. Tamoxifen inhibits EC proliferation and attenuates VEGF-mediated angiogenesis and migration *in vivo* (McNamara et al., 2001). Tamoxifen treatment alone has been shown to have anti-angiogenetic effects in cancer animal models which appear to be, at least in part, independent of tamoxifen's estrogen receptor antagonist properties (Blackwell et al., 2000). Therefore in each experiment in this thesis, any effects of tamoxifen were carefully tested.

3.3.4 Limitations of methods used to quantify angiogenesis in vivo

Analysis of the subdermal matrigel plug method used for evaluation of vascularization in this chapter requires antibodies that differentiate ECs from other cells within the matrigel. For this purpose, the pan endothelial marker CD31 was used for immunohistochemical staining. However, the much more difficult step is the evaluation and appropriate interpretation of stained matrigel sections. One of the most common parameters for evaluating angiogeneis is calculation of microvessel density (MVD), which was considered to be the 'gold standard'. Various methods and guidelines for determining MVD in angiogenic area/tumours have been described, based on the initial method reported by Weidner et al. (Weidner et al., 1991; Takahashi et al., 1996). For example, vessels may be counted by choosing the five most vascularized areas in a tumour/matrigel plug and counting the vessels in these areas under higher magnification. Vessels

can also be quantified using image analysis software or vessel density can be graded on a scale 0+ to 3+, with being 3+ the most vascular. In addition, the degree of angiogenesis can be assessed by counting numbers of branch-points or by measuring inter-capillary distance.

Visualization and quantification of the *in vivo* angiogenic response is problematic. The fractal nature of the vasculature may lead, under some circumstances, to false identification of nonangiogenic supporting macrovessels of the pre-existing venous bed as angiogenic capillaries (Rendell et al., 1998). It is also technically difficult to simultaneously follow the changes of the functional vasculature of the whole matrigel plug (or tumour) and in its capillary compartment over time (e.g. vessel proliferation). The direct observation or quantification of vessel remodeling is impeded by the fact that visibility of vascular system is dependent on the presence of markers such as CD31 staining, infused fluorescent dextran or IsolectinB4 and in situ erythrocytes and so on. However, vessel localization based on erythrocyte content can lead to misidentification, as they may not always be present in the lumen of small capillaries or may appear in haemorrhagic areas of tumour masses. Vascular perfusion analysis is necessary for identification of functional neovasculature (e.g. using fluorescent stains such as FITC-isolectin). Counting vessels on histological sections is prone to high variation as the vasculature of solid tumours is unevenly distributed and routine histological analysis can not distinguish between active and non-functional circulation. Although there is no ideal quantitative routine technique, I believe the analysis of matrigel vascularity used in the work described in this chapter was careful, thorough and objective. The whole matrigel region was sectioned generating 300 sections per block per mouse; every 5th slide was stained with CD31 and vessel counting was blinded to the study groups for each sample. The maximum number of CD31 positive capillaries in an entire section were counted was selected for statistical analysis and was not limited to a few fields of view as normally used in these types of studies.

Taken together, the work described in this chapter shows the establishment of the Eng-iKO^{e} mouse in which endoglin is specifically deleted from ECs, and also that endoglin is important for new blood vessel formation in an *in vivo* matrigel plug angiogenesis assay. This work is now published as part of a study on the role of endoglin in angiogenesis (Mahmoud et al., 2010). The next major task required, in order to investigate the role of endoglin in tumour angiogenesis and metastasis, was to establish and characterize an appropriate tumour model.

Chapter4. Primary and Secondary Lewis Lung Carcinoma Mouse Model

4.1 Introduction

For the work described in this thesis, the choice of tumour model is based on a clinically relevant tumour type (Lewis lung carcinoma), previous successful use in an endoglin heterozygote mouse study (Duwel et al., 2007) and labelled with an integral fluorescent protein label to track metastases. Using this model, I aimed to test whether loss of endoglin has an anti-angiogenic effect. To do this red fluorescent protein (RFP) labelled lewis lung carcinoma (LLC) cells were injected subcutaneously, primary tumour growth was measured over time and lung metastases were evaluated at the end of the study. Therefore, this chapter characterises the subcutaneous LLC-RFP primary tumour and 'spontaneous' lung metastases to set an accurate framework for using this model in the work described in chapter 5. A further aim was to establish reliable methods for monitoring metastasis frequency and primary tumour vascularity. This part of the project was important as my host laboratory had no previous experience in using tumour models.

4.2 Results

4.2.1 Characterization of LLC-RFP cells

Red fluorescent protein (RFP) expressing LLC cells were a kind gift from Dr. Vivek Mittal's lab (Cold Spring Harbor Laboratory) (Gao et al., 2008). The RFP is mcherry-RFP, which is an excellent general-purpose red monomer owing to its superior photostability and easy tractability using m-cherry red fluorescence detection (Shaner et al., 2005). The maximum excitation is at 584nm and the maximum emission is at 607nm (personal communication with Dr. Dingcheng Gao from Dr. Mittal's lab), and was confirmed using the confocal microscope in house (Carl Zeiss LSM 510). The recommended filter sets for mcherry are similar to TexasRed (Table 4.1). To visualize the red cancer cells, LLC-RFP cells were placed on a slide and observed via the TexasRed channel (Zeiss filter set 00) using the inverted fluorescent microscope (Carl Zeiss). Expression of RFP in these cancer cells was strong and stable over 50 passages (Figure 4.1). As a precaution, a selection step for the RFP expressing cassette was performed every 60 passages using puromycin (2μg/ml) for 24 hours.

Fluorescent proteins	**mcherry**		**TexasRed**
Maximum excitation(nm)	584		596
Maximum emission (nm)	607		613
Excitation*	585/20	575/50	585/20
Emission*	675/130	640/50	620/20
Filter sets from Carl Zeiss	Filter set 00	M-Cherry Cube	Filter set 00

Table 4.1 Recommended filter sets for visualizing LLC-RFP.

* Values are given as center/bandpass (nm). Bandpass filters with the steepest possible cutoff are strongly preferred.

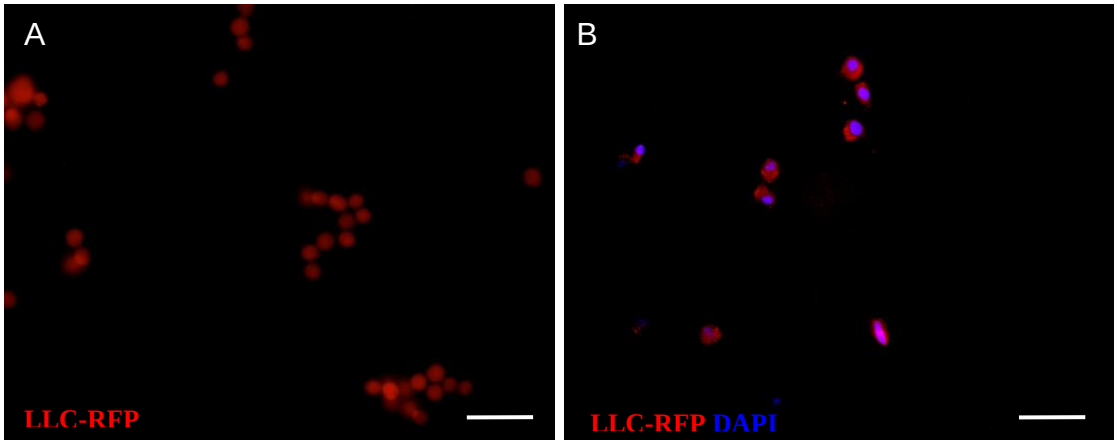

Figure 4.1 The visualization of red fluorescent protein (m-cherry) in LLC-RFP cancer cells.

A, Red fluorescent protein was visualized via TexasRed channel of a Zeiss Axiovert fluorescent microscope after 11 passages.

B, After over 50 passages, the expression of red fluorescent protein was visualized via Alexa594 channel of a Zeiss Axioplan fluorescent microscope, showing that RFP was expressed in a strong and stable manner in the vast majority of cells.

Scale bars = 100µm.

4.2.2 Effects of inoculum cell number on tumour growth and tumour takes

Tumour implantation was performed by subdermally injecting LLC-RFP cells into C57BL/6 female mice (female mice were used because LLC-RFP cells were derived from C57BL/6 female mice). Subsequent development of the implant depends on the age and nutrition of the host animal, the site of inoculation and the character and quantity of the inoculum. In order to optimize the appropriate initial injection dose, different numbers of cells were used in the inoculum. The aim was to generate a tumour which had a reproducible and rapid growth rate. An inoculum less than 10^6 cells led to unsuccessful tumour 'take' (Table 4.2). Cell doses greater than 10^6 cells indicated the probability of successful 'tumour take' is high (100%) (Table 4.2). Therefore, the quantity of the cell inoculum is a very important factor which affects growth of the tumour. Finally, the dose of cells for injection was optimized at 2.5 x10^6 in a volume of 50µl. The protocol for the main experiment is summarised below in figure 4.2.

No. of mice	Volume of cells	Cell number	Primary tumour	Lung metastasis
1	50 µl	1 x 10^4	absent	none
1	50 µl	5 x 10^4	absent	none
1	50 µl	5 x 10^4	absent	none
1	100 µl	5 x 10^4	absent	none
1	100 µl	1 x 10^5	present (1/1)	present (1/1)
1	100µl	2 x10^5	present (1/1)	none
7	50 µl	5 x 10^6	present (7/7)	present (4/7)
11	50 µl	2.5 x 10^6	present (11/11)	present (8/11)

Table 4.2 Summary of pilot experiments to compare tumour 'take' and frequency of metastases following subdermal injection of different LLC-RFP cell doses. Note: The 11 mice given the optimised tumour cell dose (50ul of 2.5 X 10^6 LLC-RFP cells were added to the main study below for the final analysis.

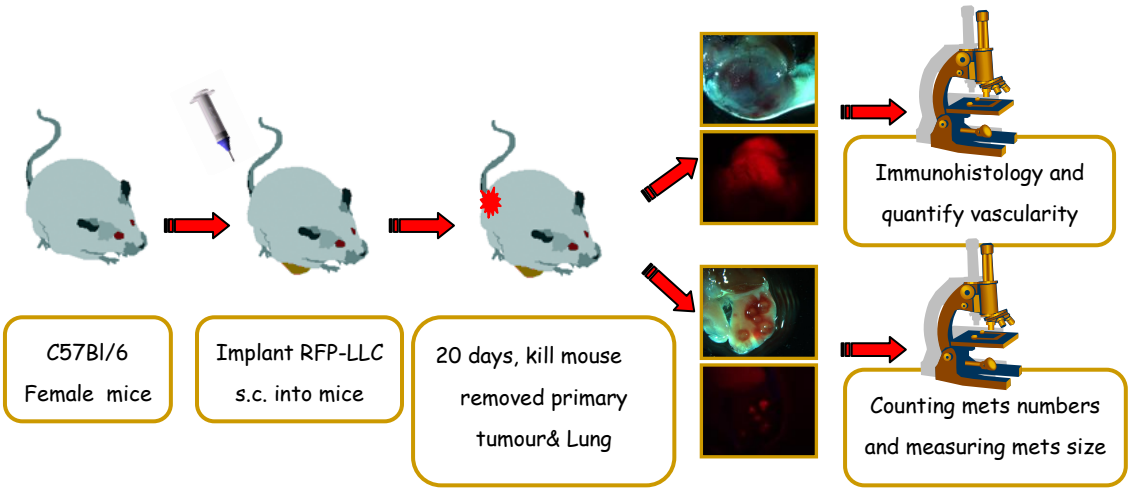

Figure 4.2 Sumary of LLC-RFP tumour model.
C57BL/6 female mice (age ~8 weeks) were implanted subcutaneously into the right flank with 2.5 x 10^6 (50µl) LLC cancer cells and monitored over approximately 3 weeks. Mice were then sacrificed and primary tumour masses and lung lobes were removed for analysis. Tissue sections of the primary tumour were stained with IsolectinB4 to examine vascularity which was quantified using ImageJ software. Lungs were visualized using a stereomicroscope in white light phase and fluorescent phase and the number of metastases was counted. In a small group of mice, MRI was also used for lung metastasis detection *in vivo*.

4.2.3 Features of primary tumours

To investigate the properties of tumour growth, vascularity and metastases using this model, 22 female C57BL/6 mice were injected subcutaneously with the optimal dose of LLC-RFP cells. To investigate the growth rate of the primary tumour, a digital calliper was applied every other day to measure tumour width and length (Figure 4.3). Tumour diameter data were converted to tumour volume by the following formula (size = width x length^2 x π /6) (Gao et al., 2008). In this way, the growth rate of the implanted tumour and its metastases (seen post mortem) were observed in the same mouse.

The primary tumour growth appeared to have 3 phases mathematically determined within the observing duration period of 20 days, up to day8, day8-day14 and day14-day20 (Figure 4.4). The average change of 3 phases in tumour size is 113 mm^3 (16.10mm^3/day), 363 mm^3 (72.60mm^3/day) and 902 mm^3 (150.30mm^3/day) respectively. This indicates the tumour size increased dramatically over these 3 periods. This indicates that LLC primary tumour has differential progression stage based on the tumour size.

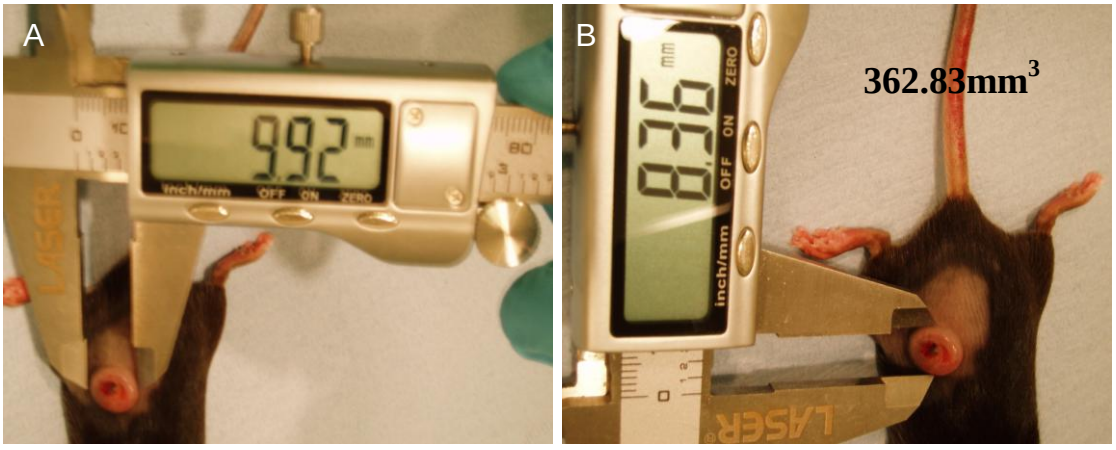

Figure 4.3 The width and length of primary tumour was measured using a calliper with digital indication screen.
A, shows the width of tumour is 9.92mm;
B, shows the length of tumour is 8.36mm, therefore the tumour size is 362.83mm^3.

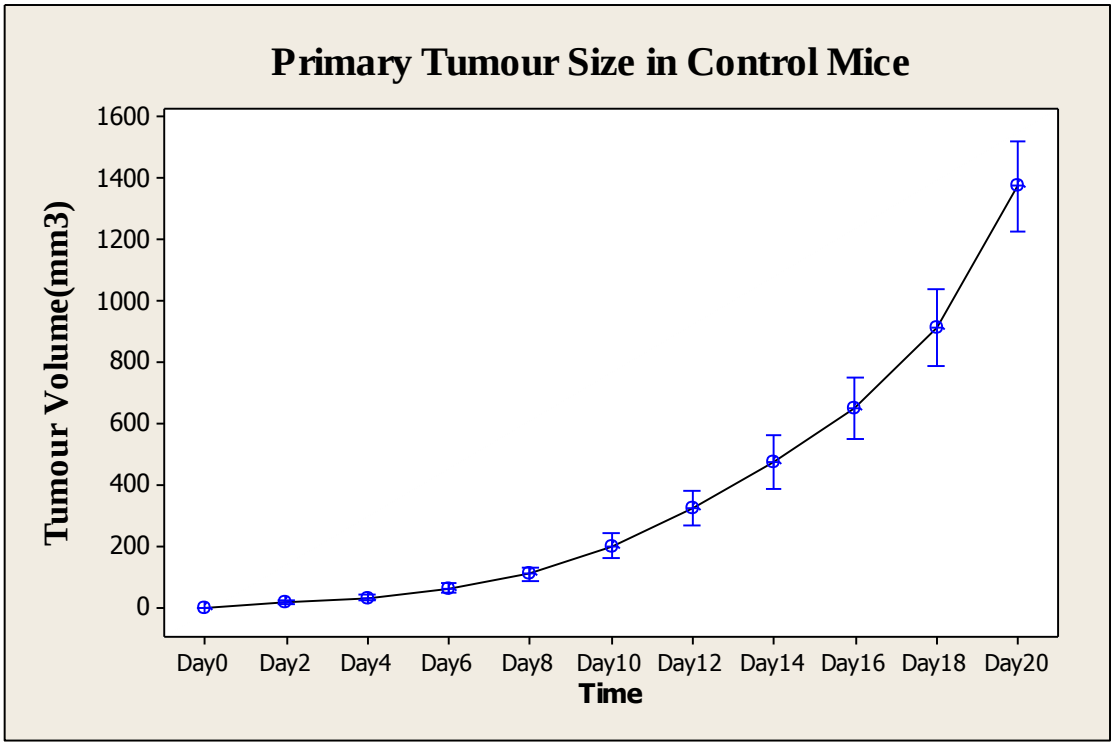

Figure 4.4 The LLC-RFP primary tumour size dramatically increases in C57BL/6 control mice over 20 days following an initial subdermal injection of 2.5 x 10^6 cells/50µl.

Each data point corresponds to the mean and 95% confidence intervals of the mean, n = 22. Mean of final primary tumour size = 1352.83 mm^3; standard deviation of final primary tumour size = 339.61 mm^3.

One of the most significant properties and capabilities of tumour is invasiveness, which is a key step for cancer cell spread and metastasis. The figure 4.5 shows the histological anatomy of mouse skin and the position of cancer cell injection. In fact, the LLC-RFP tumour is aggressively invasive and can invade into the surrounding tissue sub-dermis or deeper muscle. Severe invasiveness can even destroy the original histological structure of the skin (Figure 4.6). Using H&E stained sections to monitor the extent of invasiveness, I established a classification for this property of the primary tumour as 0, 1, 2, etc. that corresponded to the different level of invasiveness (Table 4.3) and was used to characterise all the dermal tumours.

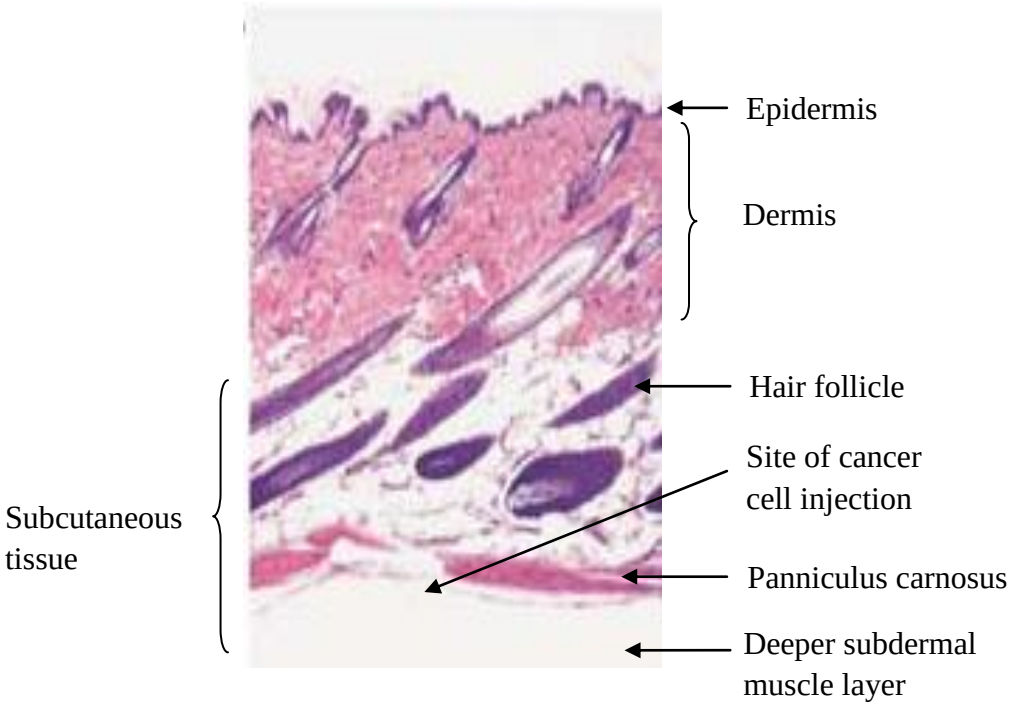

Figure 4.5 Anatomy of mouse skin and position of cancer cell injection.
Mouse skin generally comprises only three layers including epidermis, dermis and subcutaneous tissue. Cancer cells were injected underneath the panniculus carnosus (a subcutaneous muscle layer present in mouse skin) but above the deeper subdermal muscle layer. Adapted from (Gudjonsson et al., 2007).

Invasion Scores	
0	NO
1	Partial invasion of either dermis or subdermal muscle layer
2	Partial invasion of dermis and subdermal muscle layer
3	Complete invasion of either dermis or subdermal muscle layer
4	Complete invasion of dermis and subdermal muscle layer
5	Complete invasion of dermis or subdermal muscle layer and loss of the original structure

Table 4.3 LLC primary tumour invasion scores

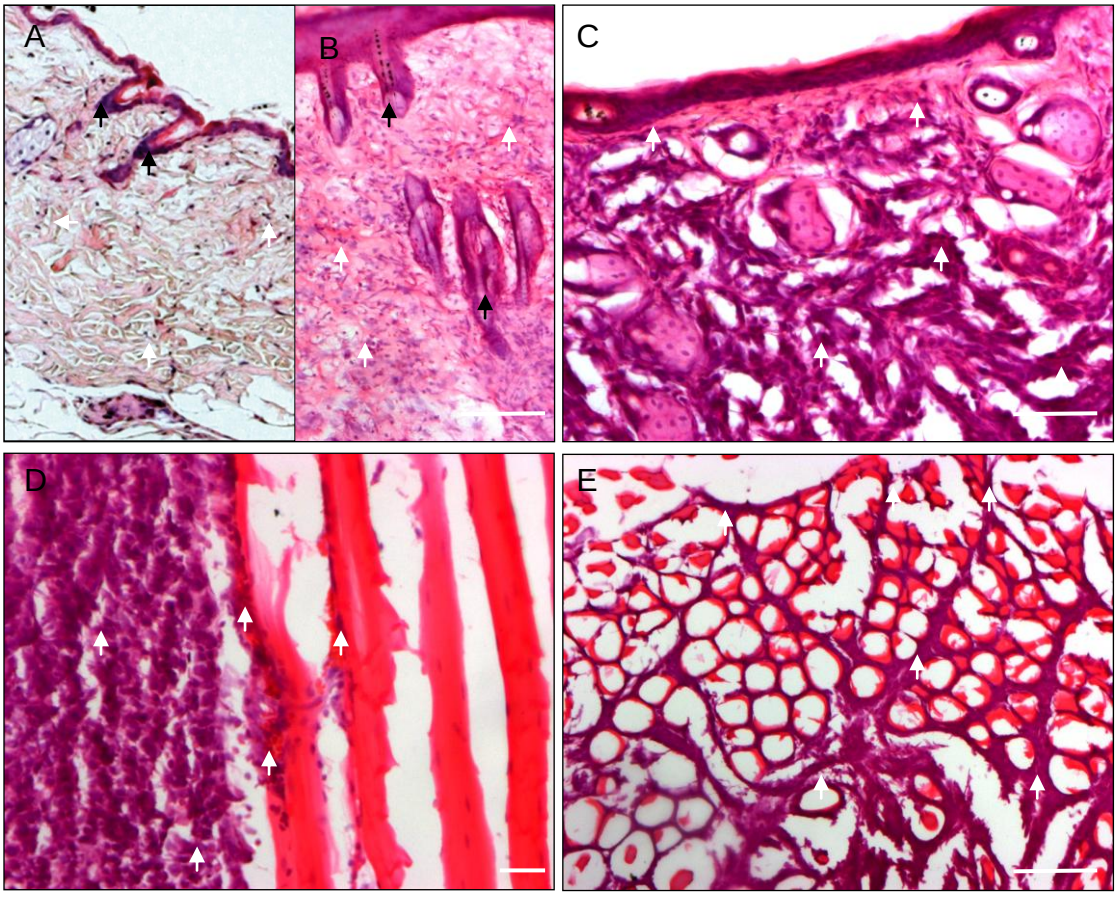

<u>Figure 4.6</u> Figure to show the different degrees of invasiveness of implanted LLC-RFP cancer cells into surrounding tissue.

A, H&E stained section showing normal appearance of dermal and epidermal layers of mouse skin. Black arrows indicate hair follicles.

B, Many LLC-RFP cancer cells invade into the dermal and epidermal layers of skin (white arrows) although the fundamental architecture of the skin was maintained.

C, LLC-RFP cancer cells invade into the whole skin and destroy its normal structure.

D, The deeper muscle layer (which stains strongly with eosin) was invaded with LLC-RFP cancer cells;

E, Major cancer cell invasion into deeper muscle layer destroyed the normal structure of muscle. The cancer cells grow around the muscle fibres to form a lattice.

White arrows indicate invasive cancer cells (likely also to be associated with an inflammatory infiltrate) and black arrows show hair follicles. Scale bar = 100µm.

Two features of primary tumour - tumour size and invasiveness- are used in the TNM staging system used clinically. Therefore, for this study I created a similar classification for the LLC stage based on the size and invasiveness of primary tumour and classified into 5 levels as described in table 4.4. In this way, the final tumour size, vascularity, invasion, primary tumour stage and number of lung metastases were summarized in table 4.5. In addition, I also found all primary tumours (at day20) had some haemorrhagic areas (Figure 4.7).

Stage	Criteria
T1	final tumour size 700mm^3 or less with/without invasion
T2	final tumour size larger than 700mm^3 but smaller than 1000mm^3, with invasion
T3	final tumour size larger than 1000mm^3 but smaller than 1400mm^3, with invasion
T4	final tumour size larger than 1400mm^3, with invasion
T5	final tumour size larger than 1400mm^3 with deep invasion causing a change in normal structure

Table 4.4 LLC primary tumour stage

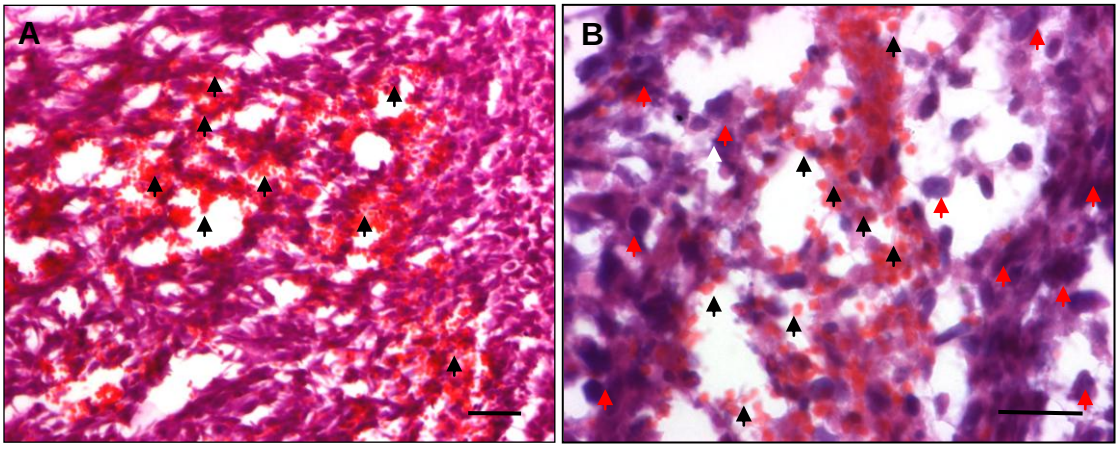

Figure 4.7 An example of haemorrhage in LLC-RFP primary tumours.

A, Left panel shows the obvious haemorrhage (indicated by black arrows) in the central part of a tumour;

B, Right panel shows haemorrhage (indicated by black arrows) in a different tumour at higher magnification and some cancer cells (indicated by red arrows and although likely also to be associated with an inflammatory infiltrate, a vast majority of cancer cells were identified based on histopathologic characteristics of cancer cells that differ from normal cells including nuclear size (large), shape (nonuniform), and haematoxylin staining intensity (high)).

Scale bar = 100µm.

Final tumour size	Vascularity	Invasion	Tumour stage	Number of lung metastasis
635.491	11.680	4	1	0
786.533	12.670	5	2	0
842.971	11.503	5	2	3
1071.866	4.321	3	3	0
1110.984	6.665	3	3	2
1128.368	9.465	3	3	0
1138.101	17.422	5	3	2
1180.418	3.852	2	3	0
1229.743	11.128	3	3	0
1315.795	8.985	5	3	4
1369.326	12.752	3	3	5
1390.030	11.882	5	3	3
1484.417	19.752	5	5	12
1531.273	13.733	3	4	6
1549.320	6.458	4	4	0
1622.823	14.980	4	4	2
1636.377	14.062	5	5	3
1655.417	8.431	3	4	2
1691.748	20.079	4	4	2
1767.146	12.300	2	4	0
1767.146	15.868	4	4	3
1856.924	10.981	4	4	1

Table 4.5 Data summary: final tumour size, vascularity index, invasion score, primary tumour stage and number of metastases (n = 22).
Note the data were ordered based on the ascending final tumour size.

To identify the vascularity of primary tumour, adjacent cryosections were taken from the central part of each tumour block and subjected to Isolectin B4 staining. To determine the vascularity index of the primary tumour, the percentage isolectin positive stained area on tissue sections was determined using ImageJ software (NIH) and averaged from 3 random fields of view (n = 22) (Figure 4.8), in a similar way to a previously published method (Tammela et al., 2008). As Isolectin B4 staining can pick up some inflammatory cells and it seems to be difficult to indentify Isolectin B4 positive inflammatory cells from ECs, I therefore decided to use CD31 staining for vascularity quantification instead of Isolectin B4 in the subsequent experiments.

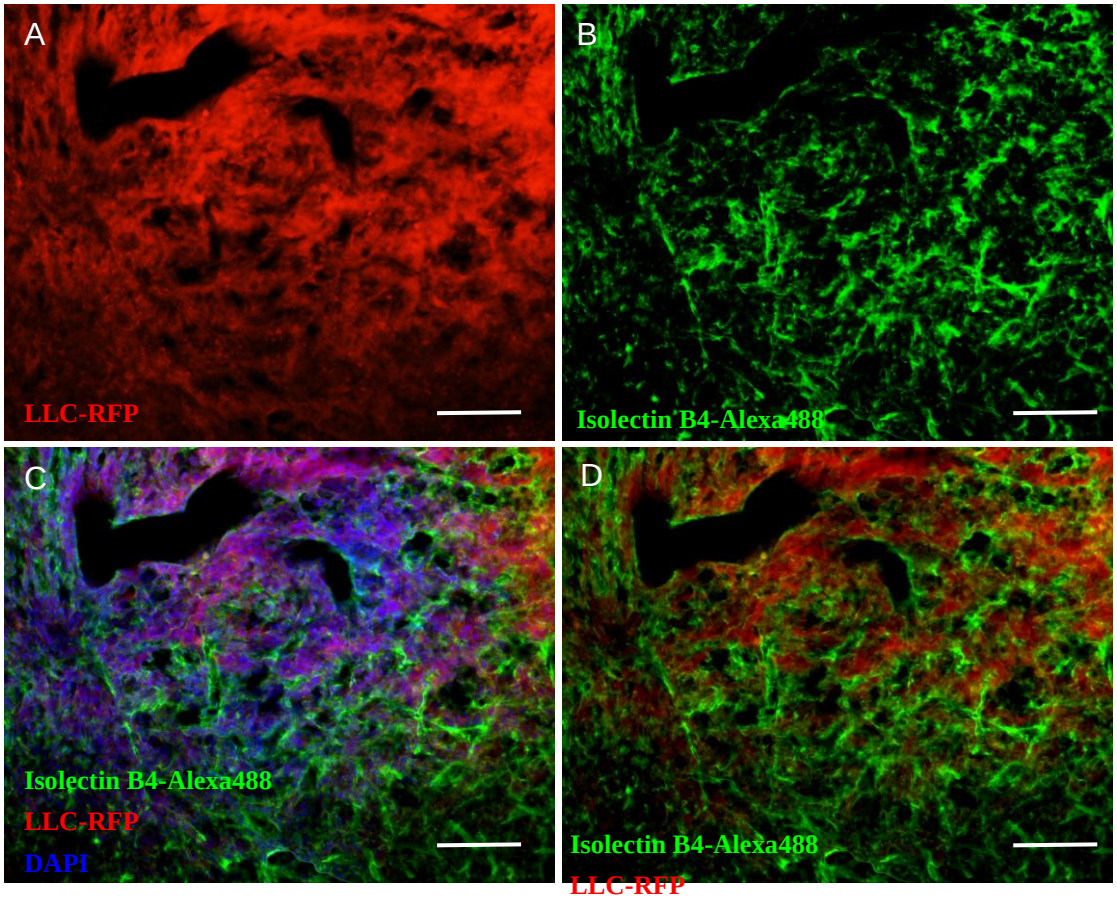

Figure 4.8 Vascularity of LLC-RFP primary tumours; an example of images used to determine the vascularity index.

A, RFP-LLC primary tumour cells (red);

B, Blood vessels identified by isolectin B4-Alexa488 staining (green) on a cryosection of a LLC-RFP primary tumour; the percentage isolectin positive area of this field of view was 17.42%.

C & D, Overlay with and without DAPI nuclear staining (blue).

Scale bar = 100µm.

4.2.4 Frequency and Size of Lung Metastases

The number of lung metastases was counted directly after the lungs were dissected (Table 4.5). Metastases (≥1 mm in diameter) were visualised under the stereomicroscope using white light and confirmed as originating from the LLC-RFP primary tumour using fluorescence to detect m-cherry (Figure 4.9).

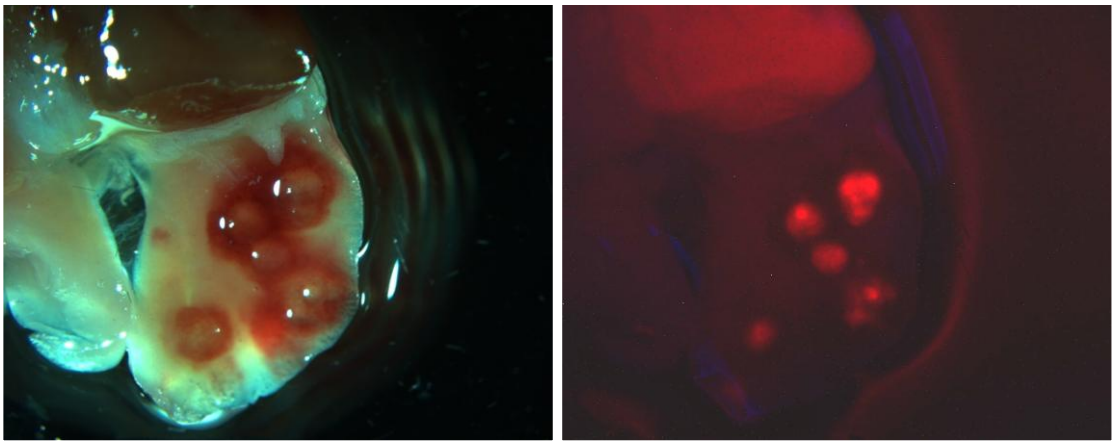

Figure 4.9 LLC-RFP metastatic lesions in lung lobes visualised using white light (left) and fluorescent light (right). Metastases are clearly seen in both views.

4.2.5 Variability of Model

The variability of the LLC tumour model was minimised as far as possible by controlling age and weight of mouse and size and position of inoculum. However, variability of primary tumour size, vascularity and frequency of lung metastases was present and evaluated by calculating range, interquartile range (IQR), variance and standard deviation (SD) and coefficient of variation (CV) (Table 4.6).

To choose appropriate measure of variability, the shape of data's distribution is the most critical element to consider. If data are symmetric, with no serious outliers, range and standard deviation are used to evaluate variability. The primary tumour size and vascularity index of primary tumour showed a normal distribution of the data (analysed using Kolmogorov Smirnov test) and there were no serious outliers, therefore, the range and standard deviation reflect their variability (Table 4.6). However, the frequency of metastases data was not normally distributed and had serious outliers, therefore, the variability of frequency of metastases was presented

by interquartile range (IQR) (Table 4.6). Also variation across two data sets, for example, amongst primary tumour size, vascularity index of primary tumour and frequency of metastases, was compared using coefficient of variation (Table 4.6). Therefore, if we just consider coefficient of variation of primary tumour size, vascularity index of primary tumour and frequency of metastases to compare the variability, the variability of frequency of metastases was the maximal one.

Items / Measures	Primary tumour size (mm^3)	Vascularity index of primary tumour	Number of metastases
Median	1379.68	11.781	2
Range	1221.4	16.227	12.000
Interquartile range	517.1	5.445	3.000
Variance and standard deviation	115331.5 339.6	19.084 4.369	7.827 2.798
Coefficient of variation	25.10	37.11	123.10

Table 4.6 Variability of primary and secondary tumour model

4.2.6 Vascularity of primary tumour correlates with frequency of lung metastases

Tumour vascularity is clinically associated with probability of metastases (Davies et al., 2002) . One of most reasonable explanations is that increased primary tumour vascularity enhances haematogenous dissemination by offering greater opportunity for tumour cell invasion into the circulation (intravasation).

The vascularity index of the primary tumours ranged from 3.852 to 20.0792 and frequency of lung metastasis ranged from 0 to 12, (Figure 4.10). A correlation analysis was performed using linear regression and correlation using Minitab15 software, which indicates that there is a statistically significant correlation of metastases frequency with primary tumour vascularity index (Figure 4.11, Pearson correlation coefficient = 0.532; p = 0.011). These data strongly support our hypothesis that reducing primary tumour vascularity by targeting endoglin will reduce the frequency of metastases.

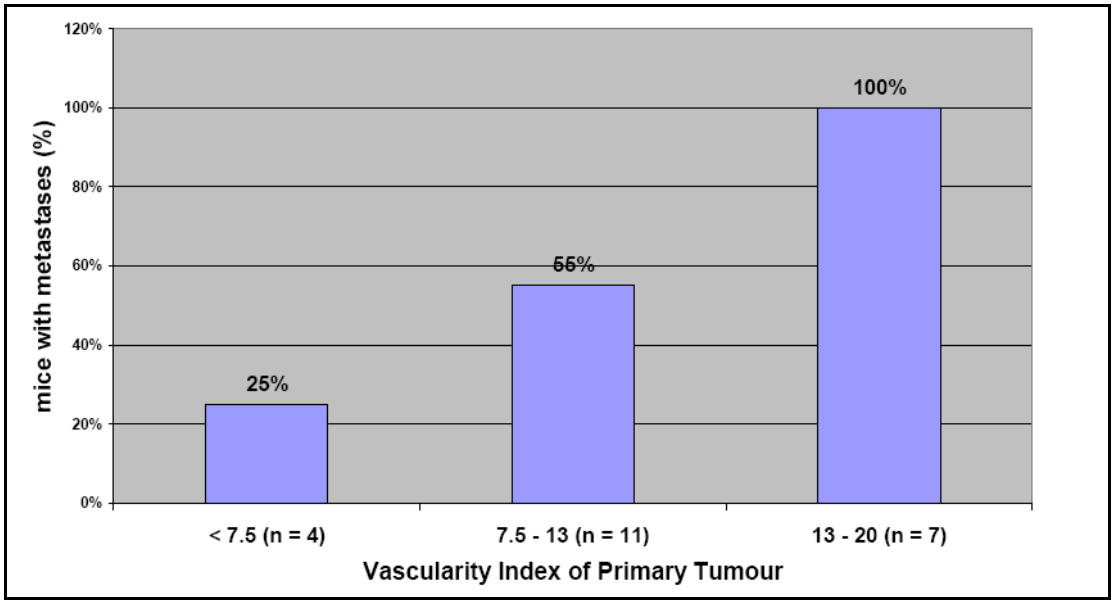

Figure 4.10 Metastases occur at higher frequencies in mice with more vascular primary tumours.

When primary tumour vascularity index increases from less than 7.5 to between 13 and 20, the percentage of mice with one or more metastatic lesions goes up from 25% to 100%.

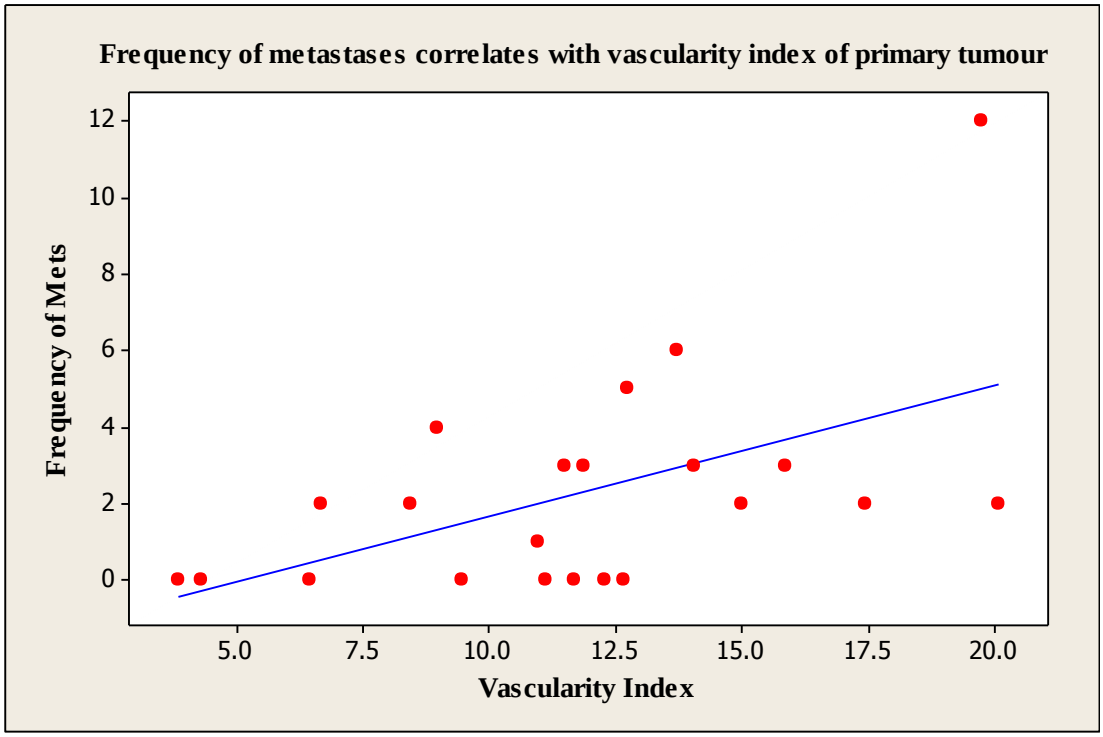

Figure 4.11 Frequency of metastases correlates with vascularity index of primary tumour.

This analysis not only indicates that there is a linear regression (shown by blue line) between probability of metastases and vascularity index of primary tumour, but also shows that frequency of metastases will increase accordingly with vascularity of primary tumour (Pearson correlation coefficient = 0.532; p = 0.011).

4.2.7 Stage of primary tumour correlates with frequency of lung metastases

Clinical evidence had demonstrated that there was an interrelationship between primary tumour size and invasion and the frequency of metastases in certain types of solid tumour (Valdevenito et al., 2007). This may be simply because the bigger and more invasive tumour has the greater opportunity to allow cancer cells to intravasate into the nearest blood and/or lymphatic vessels and subsequently migrate to a distant tissue or organ.

The primary tumour stage was classified into 5 levels (T1 - T5, see Table 4.4) in terms of primary tumour size and invasion and then converted to numerical values (1- 5), for statistical analysis. The number of lung metastases per mouse ranged from 0 to 12. A correlation analysis was performed using linear regression and correlation using Minitab15 software. This showed that there is a statistically significant correlation of metastases frequency with primary tumour stage (Figure 4.12), Pearson correlation coefficient = 0.443; p = 0.039), which indicated that higher the primary tumour stage is, the higher the frequency of metastases is.

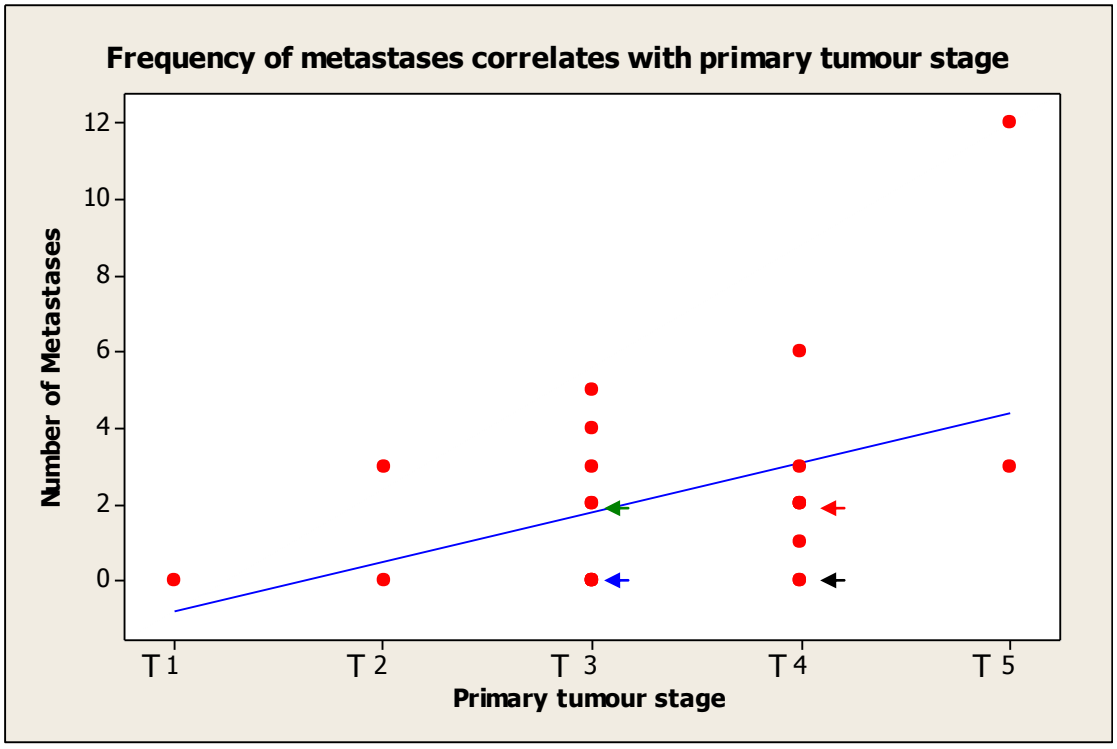

Figure 4.12 Frequency of lung metastasis correlates with primary tumour stage

The linear regression line (blue line) represents interrelationship between primary tumour stage and frequency of metastases, and indicates there is a positive correlation. Red dots represent the number of metastases matched to corresponding primary tumour stage and show the vertical distance from each individual red dot to the linear regression line.

Note: The red dot indicated by blue arrow represents 4 mice, the red dot indicated by red arrow represents 3 mice and the red dot indicated by black and green arrow demonstrates 2 mice respectively. Each of remaining red dots indicates one mouse.

4.2.8 Detection of lung metastases in vivo with magnetic resonance imaging (MRI)

The aim of this part of the study was to develop an MRI protocol to detect lung metastases of implanted LLC C57BL/6 mouse on a 7 Tesla horizontal bore magnetic resonance research system (Varian Inc., Palo Alto, CA). Both conventional T1- and T2-weighted imaging and dynamic, contrast-enhanced T2-weighted imaging with the MR contrast agent Gadodiamide (a gadolinium-based contrast agent) were performed on an additional group of 10 C57BL/6 female mice at late stage of primary tumour progression (day19). Lung metastases were detected in different lung lobes (Figure 4.13 & 4.14). However, when lungs were checked

after dissection it was clear that MRI was not able to detect all metastases (Table 4.7). In particular, the smaller lung metastases (less than 0.5-1mm in diameter) were not detected by MRI but can be visualized using fluorescent stereomicroscope. Therefore, in order to overcome the resolution limitation of MRI, we determined to take advantage of endogenous RFP in combination with fluorescent stereomicroscope for the detection of RFP-LLC lung metastasis for the remainder of the study.

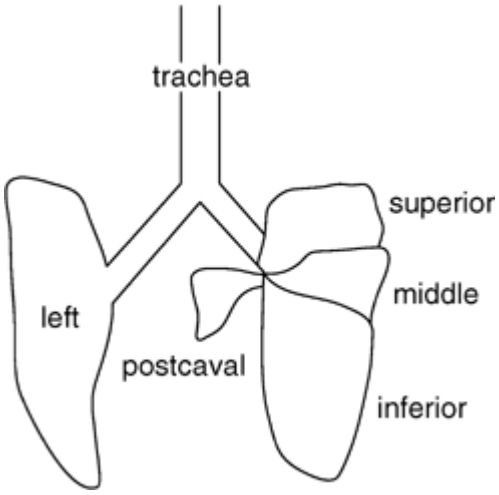

Figure 4.13 A schematic picture of mouse lung
This picture shows the name and position of mouse lung lobes.
Note that postcaval lobe, superior lobe and inferior lobe are also known as accessory lobe, cranial lobe and caudal lobe, respectively. Adapted from (Regal, 2004)

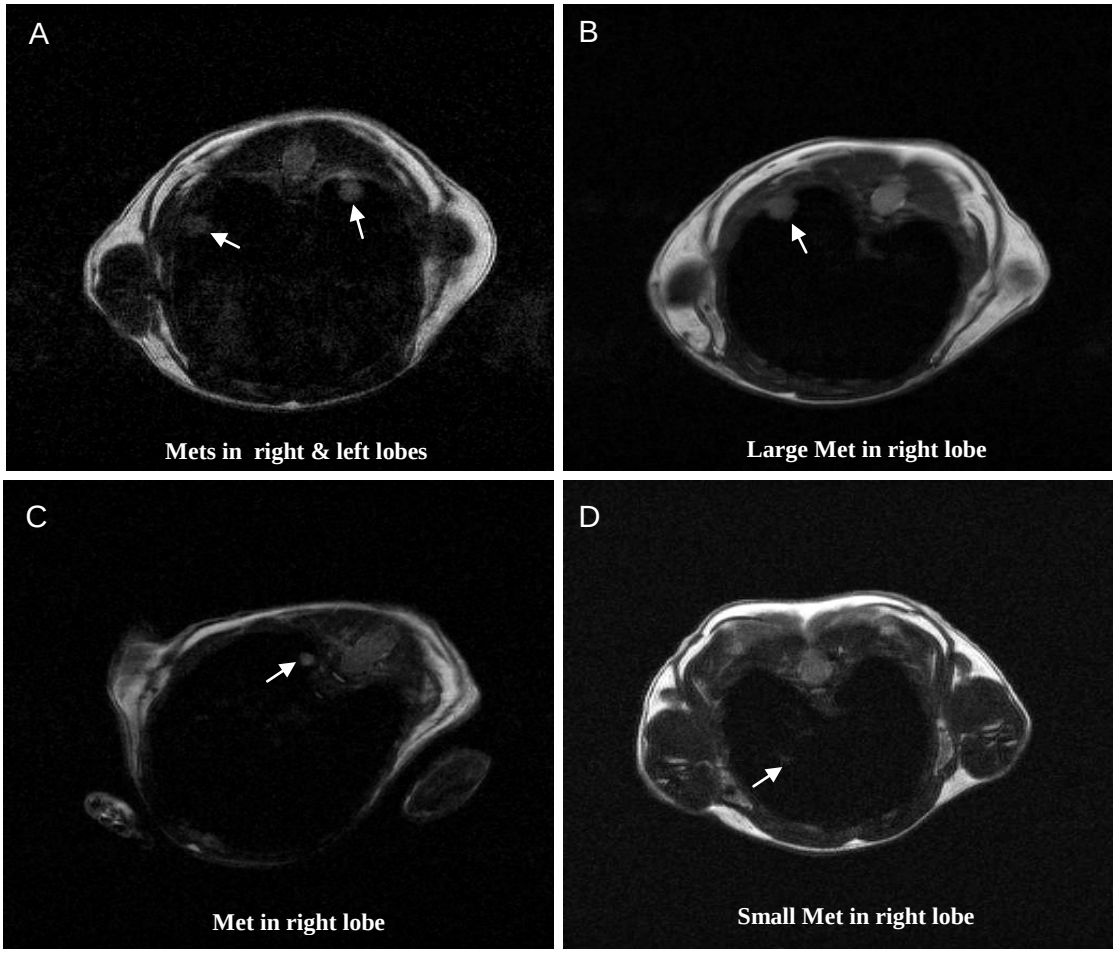

<u>Figure 4.14</u> Transverse views of thoracic cavity showing detection of lung metastases using MRI

The arrows indicate large and relatively small lung metastases were detected in either left or right lung lobes of C57BL/6 mice that had been innoculated with LLC-RFP subdermally, 19 days earlier. Tumour sizes were measured in dorsal-ventral direction and left-right dimension using MRI software and are listed below:

A, 1.3 x 1.3 mm and 1.3 x 1.1 mm

B, 1.6 x 1.5 mm

C, 0.8 x 0.7 mm

D, 0.7 x 0.6 mm

Note: All MRI image data was obtained with fast-spin echo (multi-slice) imaging sequence, including respiratory gating; Notional TR = 1500ms (reality depends on respiration rate and how the gating works). Effective echo time (TE) = 48ms. Therefore best images are T2-weighted. Spatial resolution = 0.12mm in-plane and 1mm slice thickness from 4 averages.

Mouse	Lung metastases visible post mortem using stemi-microscope		Lung metastases visible or suspected using MRI	
	No.	Position	No.	Position&sizes
YF1	0	None	1	One suspect micrometastasis(slice 9) right lobe 0.8mm
YF2	0	None	0	None
YF3	1	accessory lobe	0	None
YG1	1	left lobe	0	None
YG2	0	None	0	None
YG3	0	None	0	None
YG4	1	accessory lobe	0	None
YI1	11	4 on left lobe & 4 on superior lobe, 2 on middle lobe, 1 on inferior lobe	4	Largest in left lobe near spinal column; Sizes: 4.5mm, 2.5mm, 1.4mm & 1.2mm * Note that no averages were used for the slices in these images
YI2	7	3 on left lobe & 2 on accessory lobe, 6 on superior lobe	4	Left lobe 7.6mm, 6.4mm & 1.08mm. Right lobe 1.4mm.
YI3	2	1 on left lobe & 1 on superior lobe	2	One suspect metastasis (slice7) 0.7mm right lobe near spinal column; possibly one in (slice 9) too.

Table 4.7 The comparison of detection difference between stemi-microscope and MRI

Note that lung metastases were observed using stemi-microscope in both white light and fluoresecence field; The detection of lung metastases were performed using MRI by Dr. Ross Maxwell and Mr. Ian Wilson and the analysis was carried out by an experienced observer (Dr. Maxwell) blinded to results from the stemi-microscope.

4.2.9 Detection of lung metastases in vivo with positron emission tomography – computed tomography (PET- CT)

To develop a PET-CT protocol to detect lung metastases of implanted LLC C57BL/6 mouse on an X-ray NanoCT scanner (Bioscan) and PET imaging system (Philips). Mice at late stage of primary tumour progression (day19) were anaesthetised by isofluorane, and fludeoxygluose (FDG) (fluorine-18 labelled, total activity approx. 10 MBq, volume 100-200 microlitres) was injected via tail vein and mouse was imaged 1 hour post injection. A homogeneous primary tumour was detected on the right flank of mouse (Figure 4.15), but high FDG uptake of the heart challenges visualisation of any lung metastases. From the preliminary data, PET imaging of the primary Lewis lung tumour was clear. The use of isofluorane inhalation affected the intensity of heart signal which was higher with isofluorane compared with i.p. injected anaesthetic Hypnorm/Hypnovel (personal communication, Dr. Ross Maxwell). In order to reduce the effect of higher heart signal intensity on the detection of lung metastases, 4 mice were anaesthetised by i.p. injection of fentanyl citrate (0.32 mg/kg), fluanisone (10 mg/kg, both from Hypnorm, Janssen Animal Health, High Wycombe, United Kingdom) and midazolam (5 mg/kg, Hypnovel, Roche, United Kingdom). Although PET scanning might suggest that one mouse possibly had a metastasis in the left lobe, it is also possible this reflected a leftward portion of the heart. As there were lung metastases in all 4 mice detected post mortem, this suggests PET is probably not sufficiently sensitive for lung metastases detection.

Figure 4.15 Detection of LLC primary tumour using X-ray CT and PET
The primary LLC tumour was detected on the right flank (white arrow). High uptake of FDG in heart (cross) was particularly evident using isofluorane anaesthesia (as in this case). Mouse skeletal anatomical structure was visualized by X-ray CT. Acquisition time: 15 minute; Image resolution: 2-3mm; Field of view diameter: 128mm.

4.3 Discussion

4.3.1 Efficacy of LLC-RFP subcutaneous tumour model for investigating tumour angiogenesis and metastases

The LLC-RFP subcutaneous cancer model generated a very useful tumour model with which to investigate the effect of angiogenesis on tumour growth and metastases. In this chapter I showed that the model was reproducible and the vascularity of the primary tumour correlated with frequency of metastases to the lungs. This suggests it would be a useful model to test the anti-angiogenic effects of reducing endoglin expression in the next chapter. The incidence of metastases in the main study group was approximately 65% (15 mice had lung metastases including one mouse that died early (just only for roughly predicting possible incidence of metastases in control mice for later power and sample size analysis), whilst 8 mice did not). These data show that the LLC-RFP grafted primary tumour can disseminate to the lung, and is occuring at sufficient frequency that the model could be used to test the hypothesis that reducing primary tumour vascularity by targeting endoglin would reduce the frequency of metastases.

4.3.2 Results inform power and sample size calculation for main study

The data obtained from the work described in this study was used to inform the experimental design for the main study to test the effect of reducing endoglin on tumour growth and metastases. This was done using a statistical power analysis and sample size calculation. These analyses will inform not only sample number, but also how likely the potential statistical test will detect effects of a given size in a particular situation. If sample size is too low, the experiment will lack the power to provide reliable answers to the questions it is investigating. If sample size is too large, time and resources will be wasted.

Basically, the parameters required are: 1) inherent variability of the study material (coefficient of variation, CV); 2) how big a difference is expected; 3) the confidence required for any conclusion drawn. Therefore, based on the frequency of

metastases in the study described in this chapter, we can calculate how many mice are needed to compare the effects of endoglin loss on tumour growth and metastases. We plan to use single factor design with one treatment (endoglin depletion using the Eng-iKO^{e} mouse) and will choose $P < 0.05$ to be statistically significant and require power of 80% (0.8) for study. Consequently, we required the sample size to detect a difference between 68% (0.68) metastases in the control group and a range of metastases frequencies (0.2, 0.3, 0.4 &0.5) in the Eng-iKO^{e} group.

The analysis was performed using the power and sample size test for two proportions in Minitab15 statistical package (Figure 4.16 & Table 4.8), if there is a big difference between frequency of metastases (70%) in control group and that (20%) in mutant group, that means that 15 mice would be needed in each group to have 80% power to detect a 20% - 70% difference.

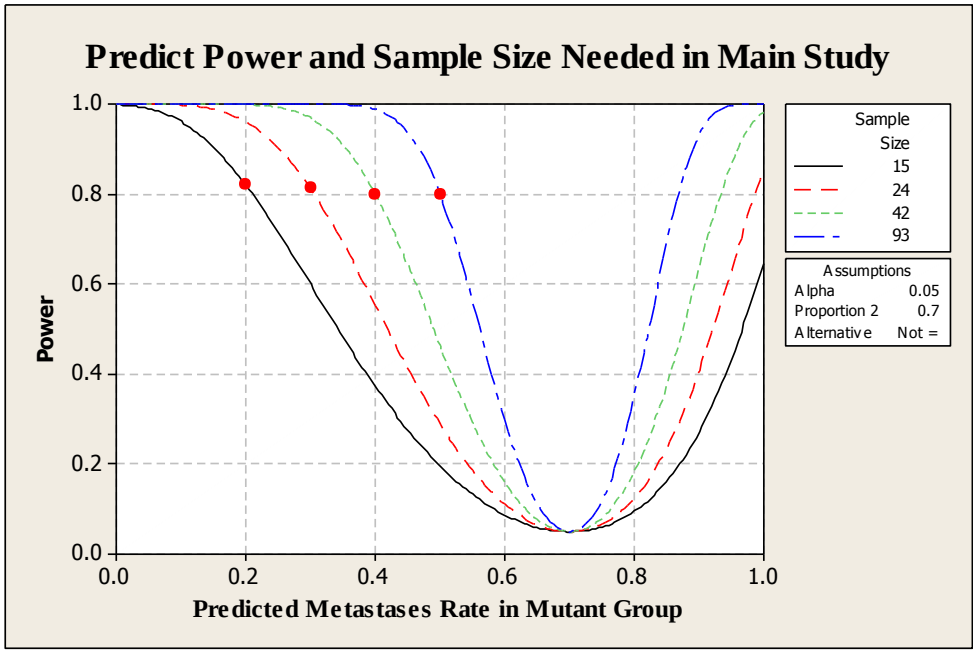

Figure 4.16 Power and sample size needed in main study calculated based on frequency of metastases in C57BL/6 control mice.
Different types and colours of bell-shaped curve represent different predictions for sample size, all the calculations are based on the frequency of metastases (0.7) seen in the mice analysed in this chapter.

Predicted incidence of metastases in Eng-iKO^{e} group	Sample size	Target power	Actual power
0.2	15	0.8	0.820319
0.3	24	0.8	0.811981
0.4	42	0.8	0.800288
0.5	93	0.8	0.800006

Table 4.8 Power and sample size calculation

It can be seen from the results of the power analysis in Table 4.7 that if the true frequency of metastases is 0.2 in the Eng-iKO^{e} group, the sample size required to detect this change compared with a frequency of 0.68 in the control group will be 15 mice per group. In contrast, 93 mice per group would be required to detect a significant difference if the true frequency of metastases in the Eng-iKO^{e} group is 0.5. On the basis of this analysis combined with the goal of designing a reasonably costed study, I decided that I would use 15 mice per group and that this study design would be powered to detect a change if the frequency of metastases in the Eng-iKO^{e} group was reduced to 0.2. If the true metastases frequency was not reduced to this level in the Eng-iKO^{e} group, then the effect of endoglin on metastases would not be detected in the study. However, it could be concluded to have either no effect, or a relatively small effect with limits that could be statistically defined..

4.3.3 Tumour imaging in vivo

Imaging has become an indispensable tool in cancer research, clinical trials and medical practice. In the past three decades, there has been a huge increase in the number of imaging technologies and their applications, particularly in the field of imaging of tumour angiogenesis and anti-angiogenesis.

In the work described in this chapter, imaging tumour angiogenesis and metastases was performed at the end point of the study. The investigation of tumour angiogenesis was performed by applying immunofluorescent staining to cryosections of primary tumour tissue. Lung metastases were detected by examining dissected lungs, also at the end of the study. However, MRI and PET-CT were tested in a pilot group of animals to evaluate their potential for monitoring metastases *in vivo*. The weakness of MRI is the limitation of resolution as small metastases (<1mm) cannot be seen and even some larger metastases (>1mm) were not always visible (table 4.7). The reasons for missing some metastases are unclear, although it probably depends on the size and location of tumours as well as how successful the respiratory gating method was in each individual mouse. Overall I found that MRI analysis did offer some potential for useful imaging of lung metastases that could be used in future experiments.

In contrast, PET-CT scans were not very successful for detecting lung metastases using FDG in this model. There were three main factors that could affect the result of FDG-PET scan. 1) In general we have not found consistent and very high FDG uptake in primary tumours in mice. This is different to most cases in human patients. 2) The large and high uptake of FDG by heart is not helpful in trying to identify lung metastases. 3) The spatial resolution is limited to 1-2 mm. In principle, the read-outs from imaging systems should be ideally quantitative, high resolution, longitudinal (i.e. allow imaging over time), comprehensive, standardized and digital (Weissleder and Pittet, 2008). However, it is really difficult to get this type of ideal imaging system that has all these merits. Therefore, for the next part of my project I used the combination of histological analysis of the primary tumour and examination of dissected lungs at the end of the study for accurate evaluation of tumour angiogenesis and lung metastases, respectively.

4.3.4 Variability of experimental mouse model

Laboratory mice are widely and successfully used model system for studying human disease, but the variations of experimental mouse models cannot be eliminated. Basically, there are two types of variations in the experimental mouse model system - inherent variations (biological stochastic variations) and technical or human error (eg. slight differences in subdermal injection sites for tumour cells).

Indeed, there were both sorts of variations (Section 4.2.5) in my experimental tumour model. As for the quantification of vascularity index of primary tumour, the repeated measurements of vascularity on a section were performed and then some variations (intra- or within-subject variability) were observed. This may be because a mouse does not respond in exactly same way and/or because of measurement error. However, the variation within an individual is usually less than the variation obtained when we take a single measurement on every individual in a group (inter- or between-subject variability). For example, I counted the number of lung metastases in every mouse in a control group (n = 22) of C57BL/6 females, and obtained relatively variable data. In theory, this variation in data may be caused by known factors (such as mouse individual differences and slight variation in implantation site or cancer cell number), or may be unexplainable random variations. Clearly, it is desirable to reduce the impact of variation as far as possible, and thereby increase the precision of the analysis. To address these issues it may be benefitial to reproduce more carefully the exact position of cancer cell injection on the flank of each mouse. I also decided to change the way I injected the cells to generate a more uniform "round" shape of implanted cell volume. The vascularity of the tumour sections would be more accurately measured using immunostaining with anti-CD31 instead of isolectin, because isolectin also detects inflammatory cells in addition to vascular endothelium. In addition, data values will be more precise if additional replicates are used. For this reason I planned to use anti-CD31 and to increase the number of fields of view (from 3 to 5) for calculating the vascularity index in future experiments.

In summary, the results described above demonstrate that the subdermal LLC model produces a vascularised primary tumour that can metastasize to lungs. Through my optimizations such as the number of LLC cells for injections, the position and approaches of injections, an appropriate time of LLC cells inoculation and colonization of lung metastases, I felt that I had been able to establish the subcutaneously primary LLC-RFP and spontaneously metastatic model in my host lab. In addition, it seemed that RFP did not affect cancer cells' ability to grow and disseminate to the lungs as previously shown for RFP and other fluorescent proteins (DsRed-2 and GFP) (Jiang et al., 2006; Gao et al., 2008; Zhou et al., 2009). Moreover, there was also a correlation between the vascularity index of the primary tumour and the frequency of metastases in lungs. I therefore used the subcutaneously implanted primary and spontaneously metastatic tumour LLC-RFP model to investigate the role of endoglin in tumour vascularisation and metastases which is described in the next chapter.

Chapter 5. Effect of Endoglin Depletion on Tumour Vascularisation, Tumour Growth and Metastases

5.1 Introduction

During tumour angiogenesis, malignant cells secrete the growth factor TGF-β, which is thought to stimulate new blood vessel formation by interacting with endoglin, a TGF-β family co-receptor located on the surface of ECs. A number of studies have reported that there was a positive correlation between the number of endoglin positive blood vessels and cancer growth, progression, and frequency of distant metastases in a wide range of human cancers, whilst there was a negative correlation between endoglin positive blood vessels and disease-free survival or overall survival (Kumar et al., 1999; Brewer et al., 2000; Fonsatti et al., 2003; Shariat et al., 2008; Bernabeu et al., 2009). I sought to test whether endoglin represents a potentially useful therapeutic target to inhibit angiogenesis, tumour growth and metastases in a clinical setting. I therefore investigated whether loss of endoglin would inhibit angiogenesis of the LLC-RFP primary tumour in adult mice and whether this might also affect the frequency of lung metastases.

LLC cells expressing RFP were subdermally implanted in female mice as described in chapter 4. Endoglin was depleted in the experimental group (Eng-iKO^{e}) using i.p. injection of tamoxifen prior to injection of cancer cells. Primary tumour growth was monitored over 18 days and then analysed for vascularity by IHC and ImageJ software (NIH). At the end of the experiment, the number of lung metastases was assessed using fluorescent microscopy. The experimental design including 2 control groups (one with and one without tamoxifen treatment) is illustrated in figure 5.1. In addition, additional early-stage (day6) LLC tumour models were used to investigate the effects of endoglin loss on growth and neovascularization in day6 LLC primary tumour and finally, experimental metastatic models were used to test the effect of endoglin reduction on extravasation.

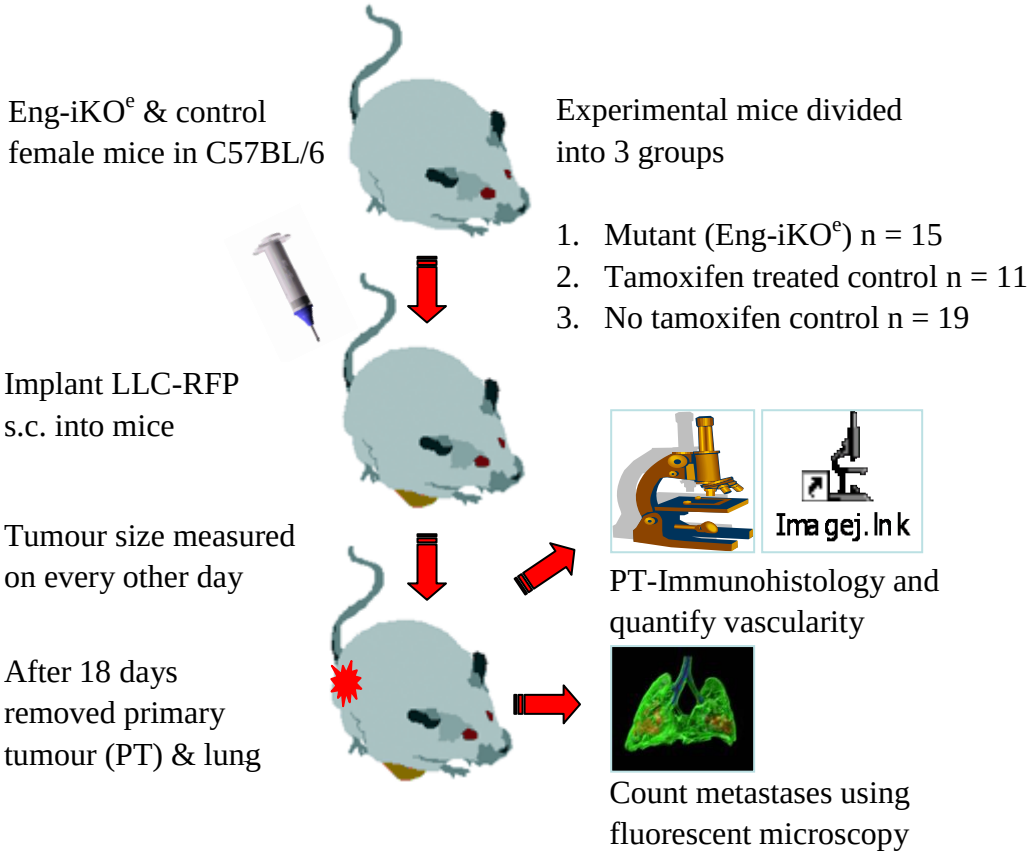

<u>Figure 5.1</u> Sumary of LLC-RFP tumour model and design of the first experimental approaches.

Female mice (aged between 8 and10 weeks, weighed between 19.40 and 28.23 grams and average weight: 24.46 grams) were divided into 3 groups: Eng-iKO^e (n =15), tamoxifen treated control (n =11) and no tamoxifen control (n =19). Mice were implanted subcutaneously into the right flank with 2.5 x 10^6 (50µl) LLC-RFP cancer cells (refinements introduced: identity of number and position of cancer cell injection; uniform "round" shape of primary tumour implanted) and monitored over 18 days. The tumour size was measured using calipers on every other day. Mice were sacrificed and primary tumour masses and lung lobes were removed for analysis. Tissue sections of the primary tumour were stained with anti-CD31 to examine vascularity (using anti-CD31 instead of isolectin to give more precise vascularity measurements) which was then quantified using ImageJ software (calculated from three to five measurements for each sample). Lungs were visualized using the stereomicroscope in both white light phase and fluorescent phase and the number of metastases were counted. Note: s.c. = subcutaneous.

5.2 Results

5.2.1 Effect of endoglin depletion on primary tumour growth

To examine the effect of endoglin depletion on primary tumour growth, the tumour sizes were measured on every other day over 18 days. This generated 10 values in a series of measurements (at day2, day4, day6, day8, day10, day12, day14, day16 and day18) for each individual mouse from both experimental and control groups. These data were analysed following statistical advice from Dr Peter Avery (School of Mathematics & Statistics, Newcastle University). Comparison of the primary tumour growth (slope of the growth curve of best fit) between Eng-iKO^{e} mice and tamoxifen treated control mice was performed using a t-test following normalization (by Log_{10} transformation) of the tumour size data. There was no significant difference in slopes between Eng-iKO^{e} mice and tamoxifen treated control mice (Figure 5.2 A). This indicates there is no effect of endoglin depletion on primary tumour growth. However, we found there was an initial delay in primary tumour progression in Eng-iKO^{e} mice compared to tamoxifen treated control mice which was most obvious at day6 (Figure 5.2 B). Hence, it seems to be reasonable to do a single t-test to compare tumour size at day6, since in principle the depletion of endoglin in ECs might affect primary tumour growth at an early stage of tumour progression. Interestingly, LLC primary tumour sizes at day6 were significantly smaller in Eng-iKO^{e} mice than in tamoxifen treated control mice ($p = 0.018$, Figure 5.2 C&D). Afterwards, It seems that the primary tumour size in Eng-iKO^{e} mice 'caught up with' that of tamoxifen treated control at later stages of primary tumour progression. These data suggest that endoglin depletion may have caused an initial delay in primary tumour growth, perhaps due to a delay in angiogenesis, but that this role can be overcome in the later stages. Therefore, in order to confirm a delay in tumour size and angiogenesis in the early tumour, I performed an additional experiment following the exactly same approach as before to investigate tumour size and vascularity at day 6 of tumour growth, and tissues were harvested at day6. Once again, there was a significant difference in tumour size at day 6 between Eng-iKO^{e} mice and tamoxifen treated control groups ($p =$

0.019, Figure 5.3 A&B). This additional experiment confirms that the loss of endoglin delays subcutaneous LLC-RFP primary tumour growth in Eng-iKO^{e} mice, and this may be due to early defects in angiogenesis.

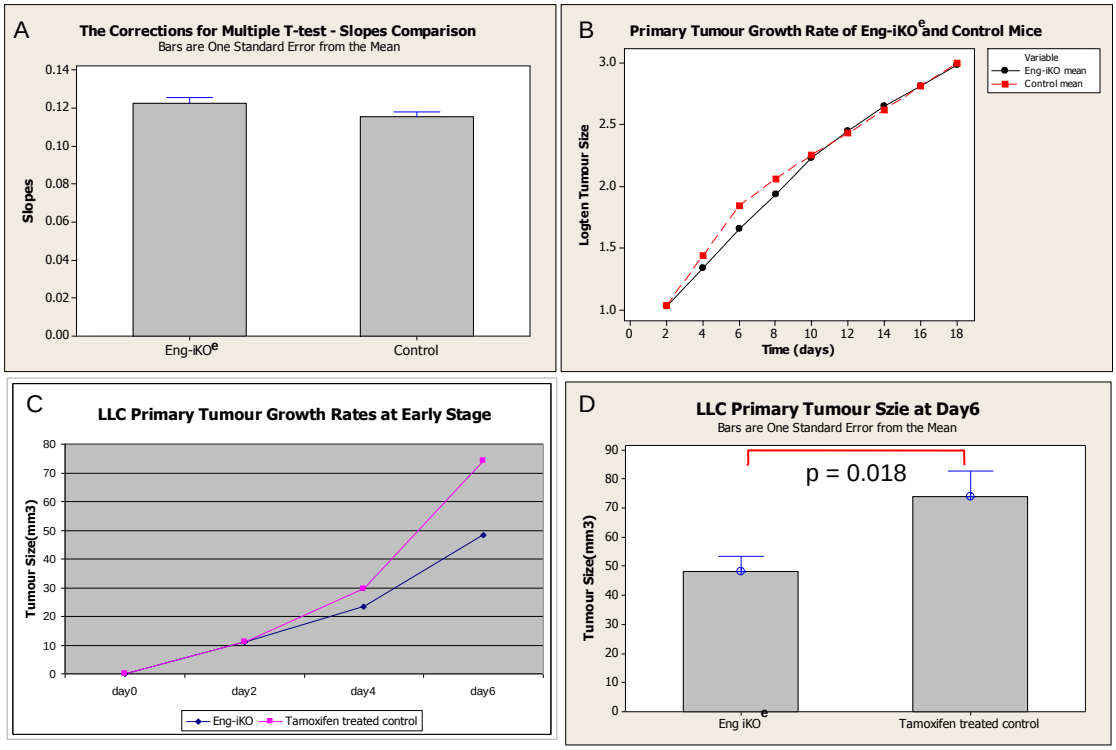

<u>Figure 5.2</u> There is no significant difference in primary tumour size between Eng-iKO^{e} mice and tamoxifen treated control mice, but there appears to be an initial tumour growth delay at day 6 in Eng-iKO^{e} mice.

A. There is no significant difference in primary tumour growth rate base on a slopes comparison between Eng-iKO^{e} mice (n = 15) and tamoxifen treated control mice (n = 11) (Two samples t-test, T-Value = 1.66, P-Value = 0.110).

B. The mean tumour growth curve of Eng-iKO^{e} mice appears to take a different course than that of tamoxifen treated control mice, suggesting an initial delay in tumour growth rate in Eng-iKO^{e} mice and a maximal difference between the two groups at day6.

C, The change in LLC primary tumour size over the first 6 days, suggested that the initial tumour growth rate was slower in Eng-iKO^{e} mice.

D, LLC primary tumour sizes at day6 were significantly smaller in Eng-iKO^{e} mice (n = 15) than in tamoxifen treated control mice (n = 11) (Two samples t-test, T = -2.63, P = 0.018).

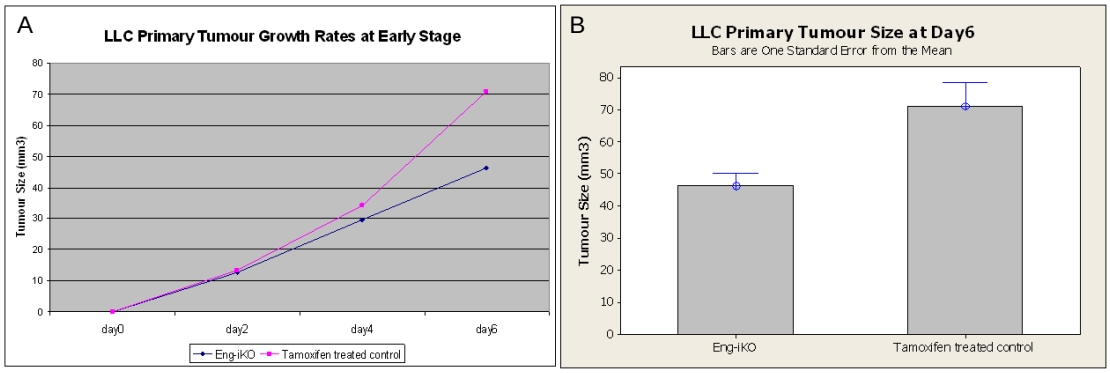

Figure 5.3 An additional experiment confirmed the hypothesis that primary tumour size at day6 was significantly reduced in Eng-iKO^{e} mice compared to tamoxifen treated control mice.

A, LLC primary tumour size over 6 days confirmed that the tumour growth rate was slower at the early stage in Eng-iKO^{e} mice.

B, LLC primary tumour sizes at day6 were significantly smaller in Eng-iKO^{e} mice (n = 9) than in tamoxifen treated control mice (n = 7) (Two samples t-test, T = -2.93, P = 0.019).

5.2.2 Effect of tamoxifen on primary tumour growth

It was important to use an additional control in this study because the tamoxifen used to activate Cre, also has the ability to induce TGF-β in vascular tissues, also tamoxifen influences a number of other cytokines that have been reported to affect angiogenesis (Grainger et al., 1993). I therefore tested whether or not tamoxifen affected primary tumour growth in the LLC mouse tumour model. Primary tumour size was measured from control mice with and without tamoxifen treatment over 18 days. There were no significant differences in the size of primary tumours between the tamoxifen treated control mice and the mice without tamoxifen treatment (Figure 5.4). In addition, there were no significant differences in the size of day6 primary tumours between the tamoxifen treated control mice and the mice without tamoxifen treatment (Figure 5.5 A&B). I therefore concluded that tamoxifen does not significantly affect primary tumour growth at both the early stage and the late stage. Therefore, the treatment of tamoxifen on mice for the induction of the Cre enzyme did not appear to be a confounding factor in this study.

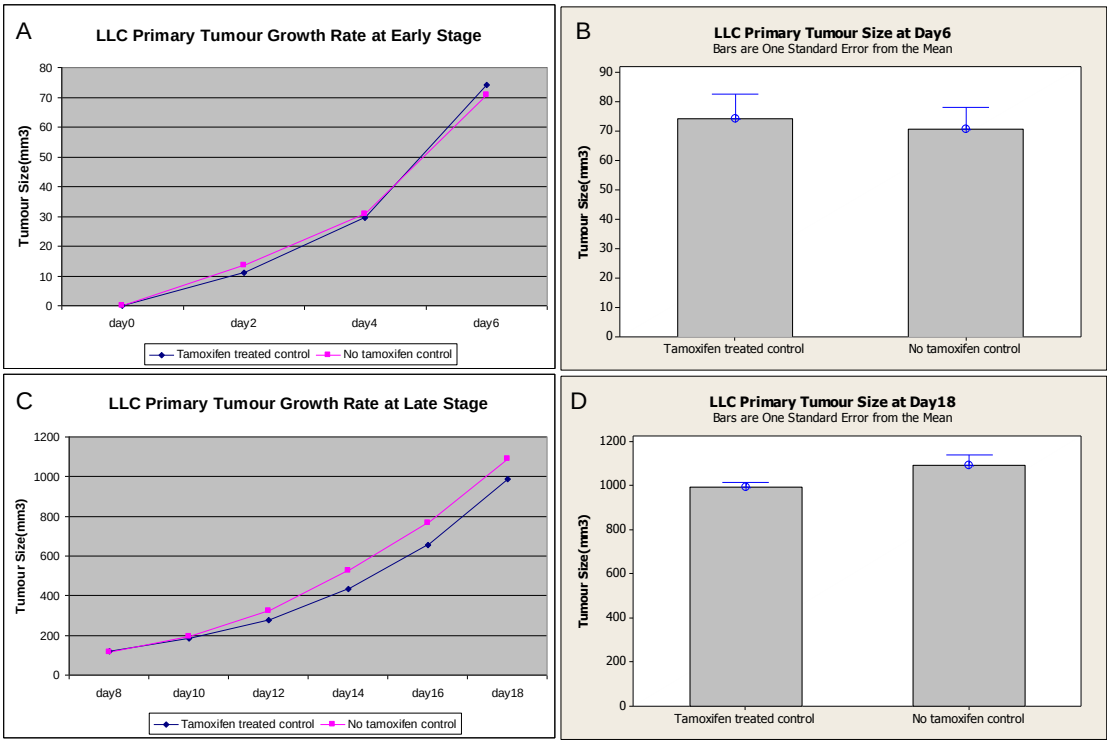

<u>Figure 5.4</u> There is no effect of tamoxifen on primary tumour growth at day 6 or at day 18.

A, Growth rate of primary tumour appears to be similar between tamoxifen treated control and no tamoxifen control from day0 to day6;

B, There was no significant difference in tumour size between tamoxifen treated control (n = 11) and no tamoxifen control (n = 19) at day6 (Two samples t-test, T = 0.30, P = 0.766);

C, Growth rate of primary tumour is slightly different between tamoxifen treated control and no tamoxifen control from day8 to day18;

D, There was no significant difference in tumour size between tamoxifen treated control (n = 11) and no tamoxifen control (n = 19) at day18 (Two samples t-test, T = -1.93, P = 0.066).

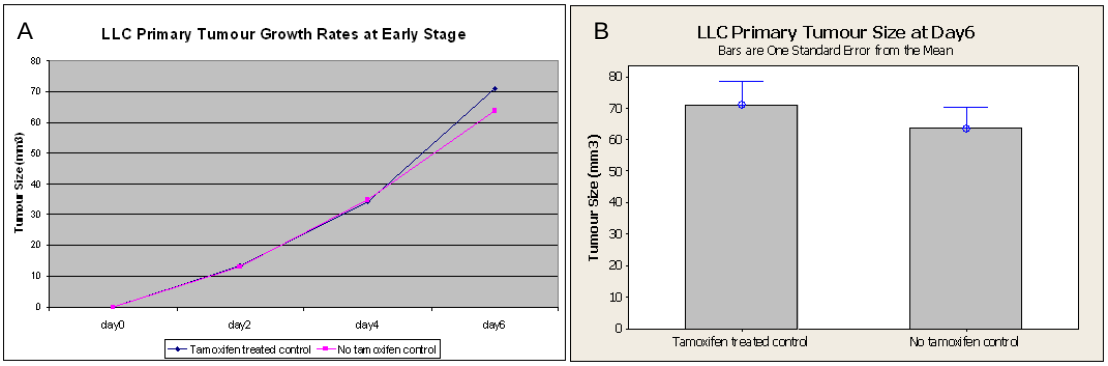

<u>Figure 5.5</u> An additional independent experiment confirmed there is no effect of tamoxifen on primary tumour growth at day6.

A, Growth rate of primary tumour appears to be similar between tamoxifen treated control and no tamoxifen control from day0 to day6;

B, There was no significant difference in tumour size between tamoxifen treated control (n = 7) and no tamoxifen control (n = 7) at day6 (Two samples t-test, T = 0.71, P = 0.490);

5.2.3 Effect of endoglin depletion on primary tumour vascularity

To test whether the loss of endoglin reduces angiogenesis of the primary LLC tumour, adjacent cryosections were taken from the central part of each tumour block at day 18 and at day6 for H&E, CD31 and endoglin staining. To determine the vascularity index of the primary tumours, the percentage CD31 positive stained area on tissue sections was determined using ImageJ software and averaged from 3-5 random fields of view (Figure 5.6), in a similar way to a previously published method (Tammela et al., 2008). CD31 staining was used as this is more specific for ECs than IsolectinB4, used in the previous chapter, which can also stain some inflammatory cells. No significant differences were observed in the vascularity index of primary tumours between Eng-iKO^{e} mice and tamoxifen treated mice at the late stage of tumour growth (day18) (Figure 5.7 A). In the context of the LLC primary tumour model, it seems that there is no significant effect of endoglin loss on primary tumour angogenesis at the later stages of primary tumour progression (day18). In addition, there were no significant differences in the vascularity index of primary tumours between the tamoxifen treated control mice and the mice without tamoxifen treatment (Figure 5.7 B). I therefore concluded that tamoxifen does not significantly affect primary tumour angiogenesis at day 18 in this model.

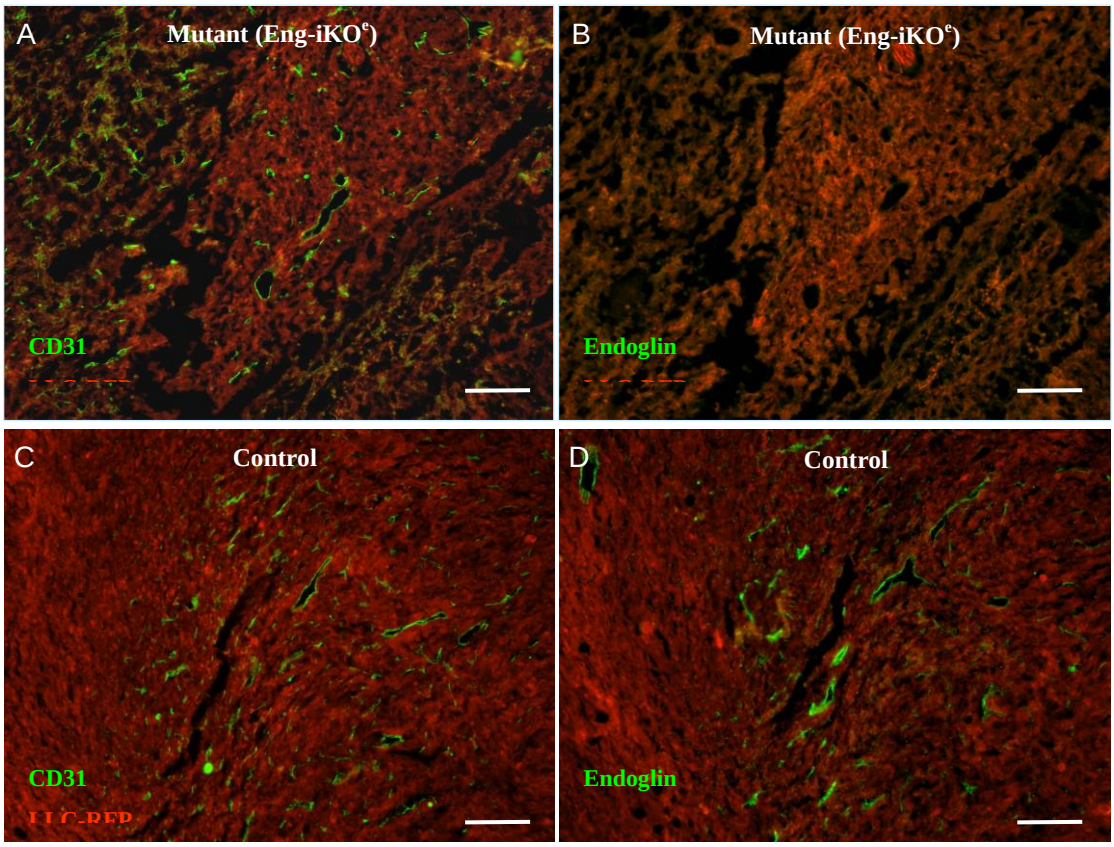

Figure 5.6 Vascularity of LLC-RFP primary tumours at day 18 and the efficacy of endoglin depletion in Eng-iKO^e mice

A, Cryosection of a primary tumour from an Eng-iKO^e mouse stained with CD31 (green) shows extensive microvasculature and the red fluorescence of LLC- RFP primary tumour cells;

B, Endoglin stained serial section of primary tumour in Eng-iKO^e mouse confirms loss of endoglin in the vascular endothelium;

C, CD31 stained primary tumour from a control mouse shows extensive microvasculature;

D, Endoglin stained serial section from a control mouse shows that the vascular endothelium is also endoglin positive

Note that these CD31 stained images also serve as example of images used to determine the vascularity index. Scale bar = 100μm.

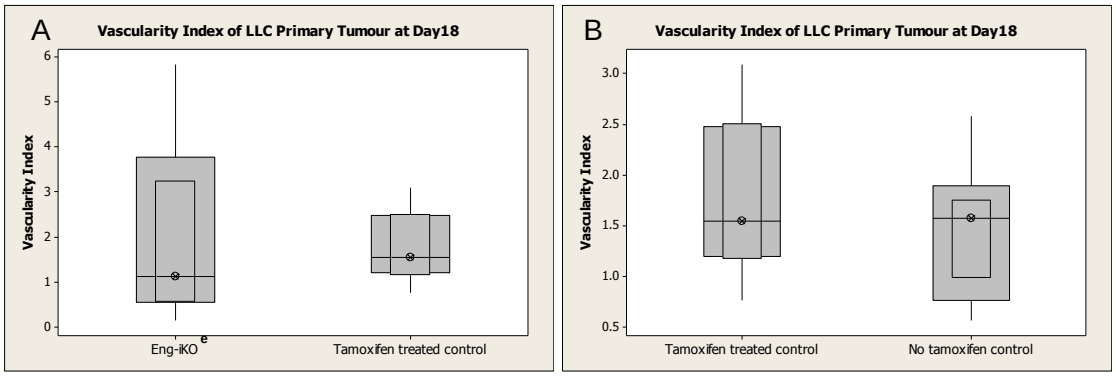

Figure 5.7 There is no effect of endoglin and tamoxifen on tumour vascularity at day18.

A, There was no significant difference in tumour vascularity index between Eng-iKO^{e} mice (Median = 1.127, n = 15) and tamoxifen treated control (Median = 1.548, n = 11) at day18 (Mann-Whitney analysis, W = 185.0, P = 0.3776).

B, There was no significant effect of tamoxifen on tumour vascularity index between tamoxifen treated control (Median = 1.548, n = 11) and no tamoxifen control (Mann-Whitney analysis, Median = 1.575, n = 19) at day18 (Mann-Whitney analysis, W = 187.0, P = 0.4911).

Although I did not find significant effect of endoglin loss on primary tumour angiogenesis at the later stages of primary tumour progression (day18), in order to test whether the loss of endoglin reduces angiogenesis of the primary LLC tumour at an early stage, cryosections from day6 tumours were taken from the three parts of each tumour block including the central part and both sides of the central part; adjacent sections were used for H&E, CD31 and endoglin staining. The tumour vascularity index was determined in a similar way to that used for the day18 tumour study. The LLC-RFP tumour is quite vascular at day 6 and the endoglin gene was effectively deleted in Eng-iKO^{e} mice from both peri-tumour skin tissue and intra-tumour tissue (Figure 5.8). Furthermore, there was a significant decrease in the vascularity index of primary tumours in Eng-iKO^{e} mice compared with tamoxifen treated control tumours at day6 (Figure 5.9 A). In addition, there were no significant differences in the vascularity index of primary tumours between the tamoxifen treated control mice and the mice without tamoxifen treatment (Figure 5.9 B). I therefore concluded that loss of endoglin can significantly reduce LLC-RFP associated neovascularisation in combination with primary tumour growth

delay at day6 and also tamoxifen does not significantly affect primary tumour angiogenesis.

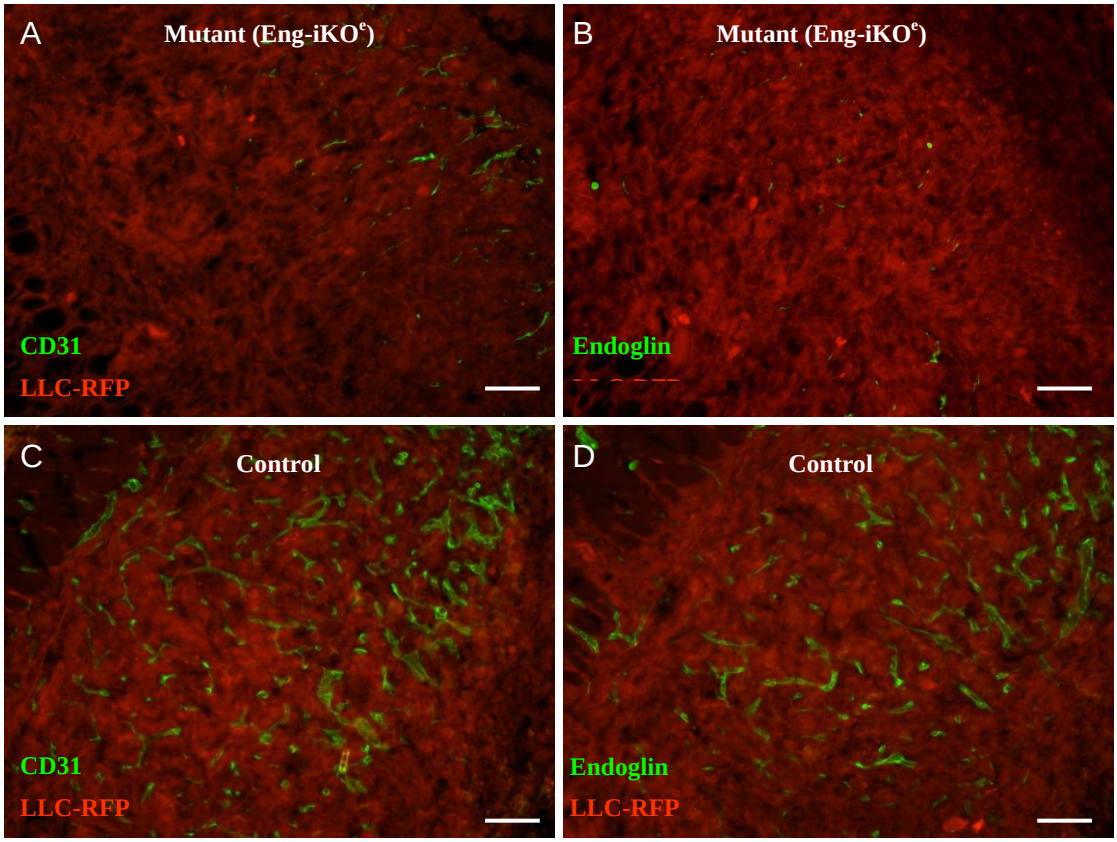

Figure 5.8 Vascularity of LLC-RFP primary tumours at day6 in Eng-iKO^e mouse and control mouse

A, Cryosection stained with CD31(green) shows few microvessels within the red fluorescence of LLC- RFP primary tumour cells at day6 from an Eng-iKO^e mouse.;

B, a serial section of primary tumour stained with endoglin (green) shows reduced endoglin in the tumour-associated vascular endothelium in Eng-iKO^e mouse;

C, CD31 stained primary tumour from a control mouse shows extensive microvasculature;

D, Endoglin stained serial section from a control mouse shows that the vascular endothelium is also endoglin positive

Scale bar = 100µm.

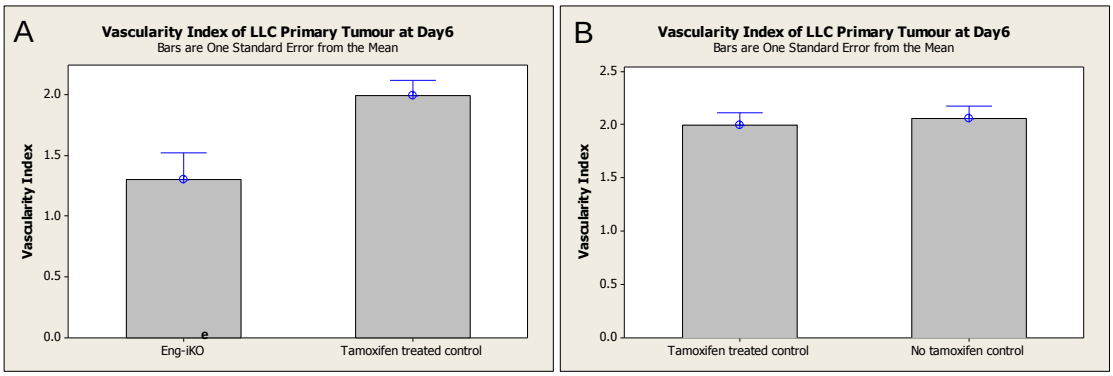

Figure 5.9 There is a significant effect of endoglin and no effect of tamoxifen on tumour vascularity at day6.

A, There was a significant difference in tumour vascularity index between Eng-iKO^{e} mice (Mean = 1.300, n =9) and tamoxifen treated control (Mean = 1.993, n = 7) at day6 (Two sample t-test, T = -2.71, P = 0.019).

B, There was no significant effect of tamoxifen on tumour vascularity index between tamoxifen treated control (Mean = 1.993, n = 7) and no tamoxifen control (Mean = 2.059, n = 7) at day6 (Two sample t-test, T = -0.40, P = 0.699).

Note: Data for above analysis was transformed by square root and then compared by two samples t-test.

5.2.4 Effect of endoglin depletion on metastases at day 18

To test whether the lung metastatic model is consistent between experiments, the incidence of lung metastases was compared between C57BL/6 mice at day 20 (data from Chapter 4) and no tamoxifen treated control mice at day 18 (also in C57BL/6 (N5)) from work described in this chapter. The slightly different time frame applied in these two experiments as the size of primary tumour reached maximum limitation permited by the project licence at day18 in the main study of this chapter. Although there seems to be a higher incidence of lung metastases in C57BL/6 mice compared to no tamoxifen treated control mice, there was no significant difference between them (Figure 5.10). This indicates the lung metastatic model appears to be sufficiently stable to use for investigating differences in metastases incidence.

Next, to investigate the effect of endoglin depletion on metastases, the number of lung metastases was counted directly after the lungs were dissected. There was a dramatic and significant increase in the number of lung metastases in Eng-iKO^{e} mice compared with tamoxifen treated mice at day 18 (Figure 5.11, Figure 5.12 A,

P = 0.0159). Furthermore, there is also a significant difference in the incidence of lung metastases between Eng-iKO^{e} mice (100%) and tamoxifen treated control mice (45.5%) (Table 5.1, X^2 = 10.639, P = 0.002). Therefore, in the context of LLC primary tumour model, this data suggests that targeting endoglin may delay primary tumour progression at an early stage, but this is coupled with a detrimental increase in the frequency of metastases. In addition, there were no significant differences in the number of lung metastases between the tamoxifen treated control mice and the mice without tamoxifen treatment (Figure 5.12 B). Accordingly, we therefore conclude that tamoxifen does not significantly affect the frequency of lung metastases, and the tamoxifen treatment (required for the induction of the Cre enzyme) does not confound our results.

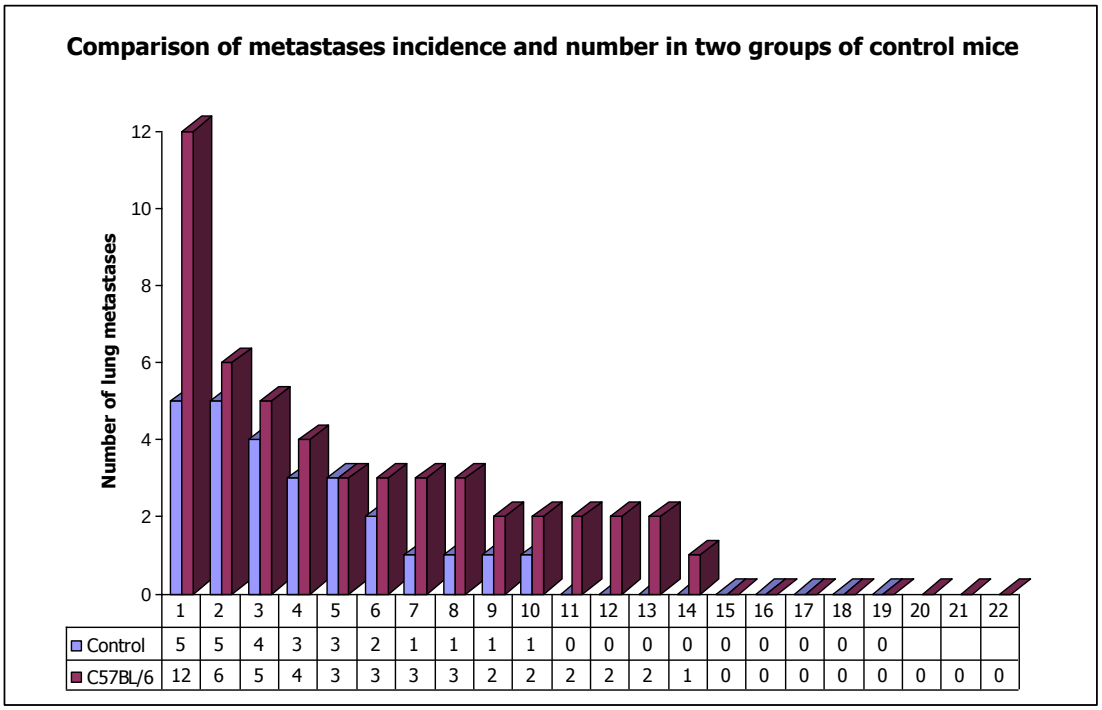

	1	2	3	4	5	6	7	8	9	10	11	12	13	14	15	16	17	18	19	20	21	22
Control	5	5	4	3	3	2	1	1	1	1	0	0	0	0	0	0	0	0	0			
C57BL/6	12	6	5	4	3	3	3	3	2	2	2	2	2	1	0	0	0	0	0	0	0	0

<u>Figure 5.10</u> The incidence and number of lung metastases in C57BL/6 mice (n = 22, pink bars, data from Chapter 4) and in no tamoxifen treated control mice (n = 19, purple bars). Each mouse is represented by a single bar and the height of the bar corresponds to the number of metastases present in the lungs. There is no significant difference between the incidence of metastases in two groups of mice (Mann-Whitney test, W = 500.0, P = 0.3069).
Note: non-parametric Mann-Whitney analysis used to test the above comparisons as data from no tamoxifen control mice was not normally distributed. Attached data table shows the number of mice and the number of lung metastases in each individual mouse.

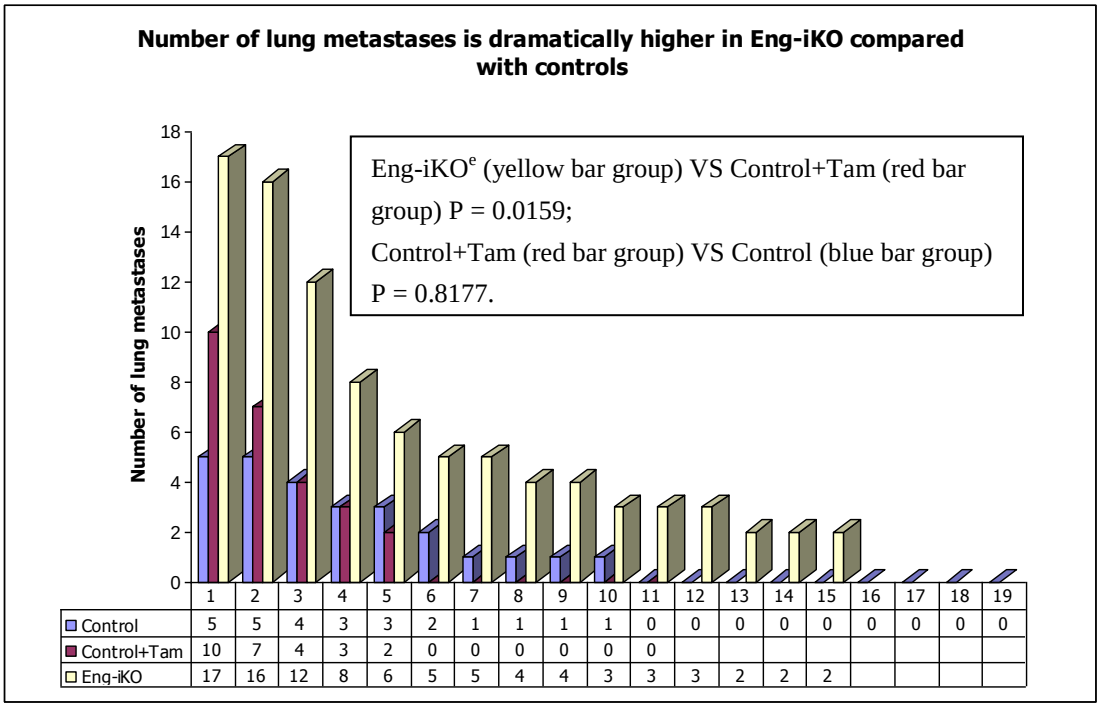

<u>Figure 5.11</u> The incidence and number of lung metastases in Eng-iKO^e mice (n = 15, yellow bars) compared to tamoxifen treated control (n = 11, red bars) and no tamoxifen treated control mice (n = 19, blue bars). Each mouse is represented by a single bar and the height of the bar corresponds to the number of metastases present in the lungs. The table shows the number of lung metastases in each mouse. In light of statistical analysis, the detailed comparison was shown in Figure 5.14.

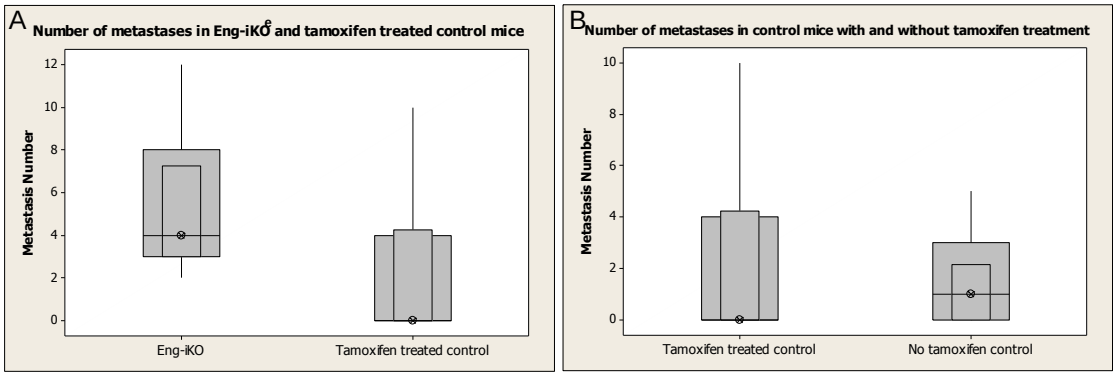

<u>Figure 5.12</u> Box and whisker plots to compare the frequency of lung metastases in Eng-iKO^e mice, tamoxifen treated control mice and control mice without tamoxifen treatment (analysed at day 18).

A, There was a significant difference in lung metastases between Eng-iKO^e mice (Median = 4, n = 15) and tamoxifen treated control (Median = 0, n = 11) at day18 (Mann-Whitney analysis, W = 249.0, P = 0.0159);

B, There was no significant effect of tamoxifen on the number of lung metastases between tamoxifen treated control (Median = 0, n = 11) and no tamoxifen control (Median = 1, n = 19) at day18 (Mann-Whitney analysis, W = 176.0, P =

0.8177).

Group	No. of mice with lung mets	No. of mice without lung mets	Total
Eng-iKO^{e}	15 (11.538)	0 (3.462)	15
Control+Tamoxifen	5 (8.462)	6 (2.538)	11
Total	20	6	26
X^2 = 10.639	**P = 0.0020**		

Table 5.1 X^2 test to compare the incidence of lung metastases between Eng-iKO^{e} mice (100%) and tamoxifen treated control mice (45.45%)

5.2.5 Investigation of potential causes for increased lung metastases in Eng-iKO^{e} mice

There must be some mechanism(s) responsible for increased number of lung metastases in Eng-iKO^{e} mice compared with tamoxifen treated control mice, although this result was not expected. Possible reasons for increased lung metastases in Eng-iKO^{e} mice include (i) increased angiogenesis of the tumour (see section 5.2.3); (ii) increased invasiveness of cancer cells (Blouw et al., 2007; Du et al., 2008; Paez-Ribes et al., 2009); (iii) decreased muscularisation of tumour blood vessels (Carvalho et al., 2004); (iv) reduced integrity of vascular basement membrane (this study); (v) increased lymphangiogenesis of the tumour (Achen and Stacker, 2008); (vi) altered expression of other growth factors (Bergers and Hanahan, 2008; Abdollahi and Folkman, 2010); (vii) altered inflammatory response (Bergers and Hanahan, 2008); (viii) differences in the level of hypoxia and responses to hypoxia (Carmeliet and Jain, 2011a); (ix) differences in interstitial flow pressure and degree of necrosis (Carmeliet and Jain, 2011b); (x) differences in haemorrhage (this study); (xi) altered lung endothelium provided easier growth of metastatic cancer cells (Wels et al., 2008; Psaila and Lyden, 2009; Ebos and Kerbel, 2011); (xii) epithelial to mesenchymal transition (EMT) and or endothelial to mesenchymal transition (EndMT) (unpublished data, Dr. Kristian Pietras). The tumour tissues at day 6 and day 18 were available for analysis, but there was

insufficient time to investigate all of these possibilities. Therefore, the preliminary examination of the primary tumour properties of invasiveness, vascularity, vessel muscularisation, lymphangiogenesis, the level of hypoxia and EndMT were performed. In addition, extravasation of circulating tumour cells was investigated using a different experimental metastatic model.

To investigate whether the primary tumours in Eng-iKO^{e} mice were histologically more invasive than in tamoxifen treated control mice, H&E stained sections (from the central part of primary tumour mass) were quantitively given invasiveness scores based on the criteria described in chapter 4 (Table 4.3). Although the cancer invasiveness score of Eng-iKO^{e} mice (mean ± SE, 4.00 ± 0.38) appeared higher than that of tamoxifen treated control mice (mean ± SE, 3.09 ± 0.56), and by approximately 1 level according to the scoring system described in Table 4.3, there was in fact no significant difference (Figure 5.13 A). To pursue this further the incidence of highest invasiveness score in Eng-iKO^{e} mice (66.67%) was compared with that in tamoxifen treated control mice (45.45%) but was also found to be not statistically significant (Table 5.2). Similarly there was no significant difference between the incidence of lowest invasiveness score in Eng-iKO^{e} mice (0) compared with tamoxifen treated control mice (27.27%) (Table 5.3). In addition, there were no significant differences in the cancer invasiveness between the tamoxifen treated control mice and the mice without tamoxifen treatment (Figure 5.13 B). This suggests that tamoxifen does not significantly affect the invasive ability of LLC cells. Overall, the trend of increased cancer invasiveness in Eng-iKO^{e} mice suggests that an experiment with larger group sizes may reveal a statistically significant difference and that this possible explanation for increased metastases in Eng-iKO^{e} mice should not be ruled out at this stage.

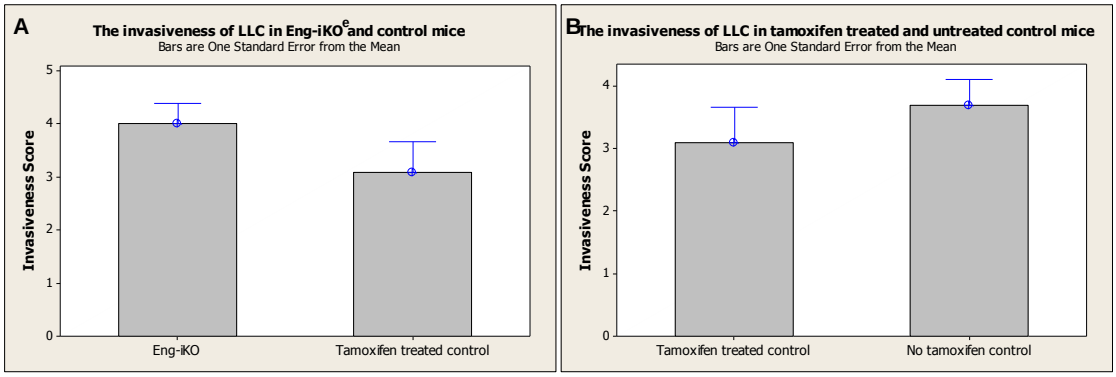

Figure 5.13 There is no dramatic effect of endoglin and tamoxifen on the invasiveness of LLC-RFP cancer cells.

A. There is no significant difference in the invasiveness of LLCs in Eng-iKO^e mice compared with tamoxifen treated control mice (Two samples t-test, T = 1.34, P = 0.197);

B. There is no significant difference in the invasiveness of LLCs in tamoxifen Treated control mice compared with no tamoxifen treated control mice(Two samples t-test, T = -0.85, P = 0.405).

Group	with highest invasiveness	without highest invasiveness	Total
Eng-iKO^e	10 (8.654)	5 (6.346)	15
Control+Tamoxifen	5 (6.346)	6 (4.654)	11
Total	15	11	26
X^2 = 1.170	**P = 0.7603**		

Table 5.2 X^2 test for the incidence of highest invasiveness (scored "5") between Eng-iKO^e mice (66.67%) and tamoxifen treated control mice (45.45%)

Group	with lower invasiveness	without lower invasiveness	Total
Eng-iKO^e	0 (1.731)	15 (13.269)	15
Control+Tamoxifen	3 (1.269)	8 (9.731)	11
Total	3	23	26
X^2 = 4.626	**P = 0.2013**		

Table 5.3 X^2 test for the incidence of lowest invasiveness (scored "1") between Eng-iKO^e mice (0) and tamoxifen treated control mice (27.27%)

To investigate the effect of endoglin depletion on the muscularisation of tumour-associated blood vessels, the integrity of vascular basement membrane and lymphangiogenesis of late stage of primary tumour, α-SMA, Collagen IV and lymphatic vessel endothelial hyaluronan receptor (LYVE)-1 stainings were

performed on day18 primary tumour sections from 3 mice in Eng-iKO^{e} mice and control mice with or without tamoxifen treatment. Representative images from this preliminary analysis shows staining with these three markers are shown in Figure 5.14. In most sections, α-SMA, collagen IV and LYVE-1 staining seemed to be rather patchy and some collagen IV and LYVE-1 staining appears to be non-specific. Therefore, it was difficult to randomly choose fields of view for the analysis. In addition, it would be helpful to perform co-staining for vascular endothelial cells (with anti-CD31) at the same time as α-SMA, collagen IV or LYVE-1. To do this I tried to optimise 4 colour "staining" to include the endogenous m-cherry of LLC-RFP cells, DAPI (nuclei), α-SMA conjugated to Alexa 488 or FITC and anti-CD31 detected by a secondary antibody conjugated to Alexa 647 (Figure 5.15). There remained some technical difficulties to be addressed to optimise this staining. For example, the signal of Alexa 647 was not strong enough to clearly identify the blood vessels and there was bleed-through of the signal from the Texas Red channel (used to visualize m-cherry) into the far red channel used to visualise CD31 staining with Alexa 647. Because of these technical issues together with the large variation of staining both between and within tumour sections, it was not possible within the timeframe of this project to accurately determine whether there were any differences in the muscularisation of tumour-associated blood vessels, the integrity of vascular basement membrane or in the degree of lymphangiogenesis of late stage (day18) primary tumours between Eng-iKO^{e} mice and tamoxifen treated control mice.

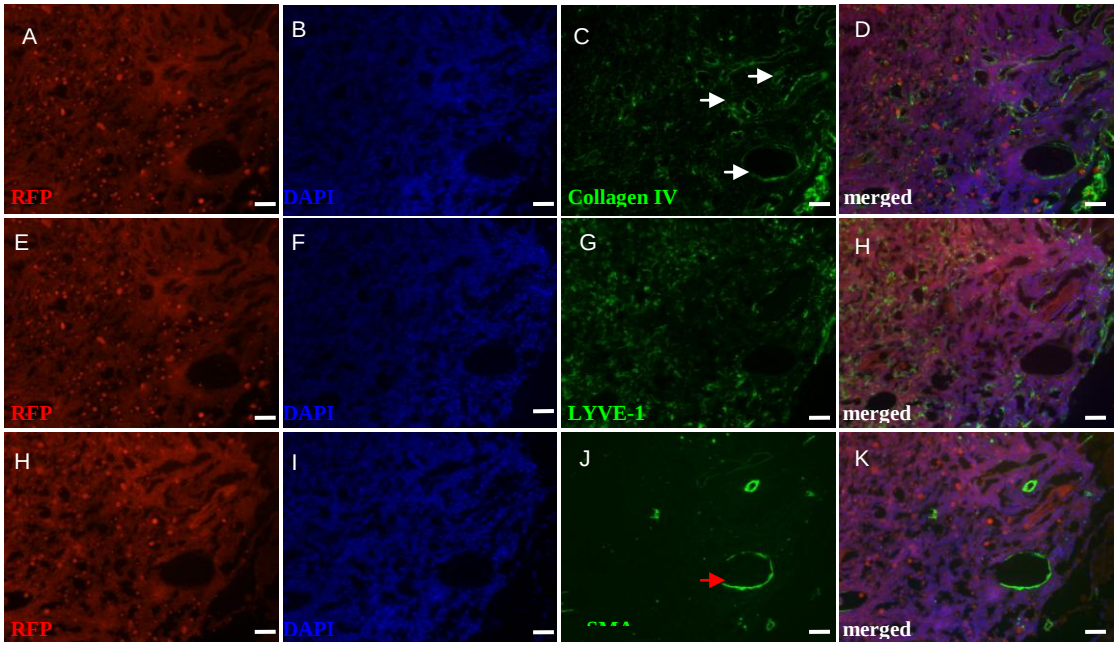

Figure 5.14 Collagen IV, LYVE-1, and α-SMA staining on adjacent primary LLC-RFP tumour sections (day 18).

A, E, H show the endogenous m-cherry of LLC (red) visualized by TexasRed Channel (some red dots seem to be stains on the coverslip);

B, F, I represent nuclei stained with DAPI (blue);

C, Most of Collagen IV staining seems to be localised on the circumference of Blood vessels (white arrows);

G, LYVE-1 staining identifies lymphatic vessels in this field of view, although it is not very specific.

J, shows α-SMA staining which varies in intensity in different blood vessels. staining of only part of the perimeter of one blood vessel is indicated by a red arrow.

D, H, K represent the merged images.

Scale bar = 100µm.

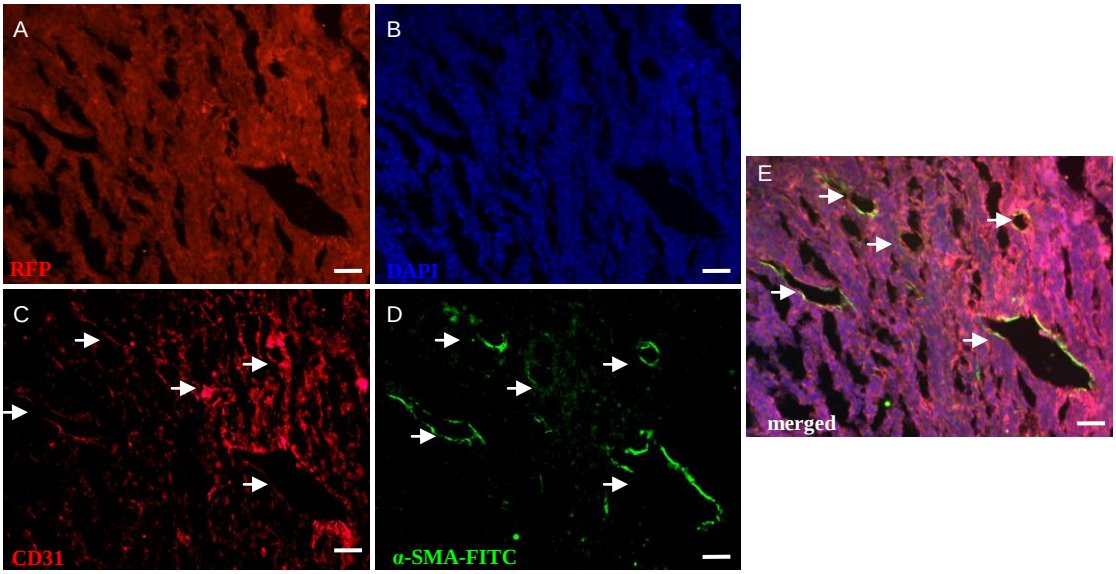

<u>Figure 5.15</u> Colocalisation of CD31-positive endothelial cells and α-SMA-positive pericytes/SMCs in a day 18 primary tumour.

A, shows the endogenous m-cherry RFP of LLC (red) visualized in the TexasRed channel;

B, represents nuclei stained with DAPI (blue);

C, shows CD31-positive blood vessels (far-red) (arrows); there is some bleed through from the m-cherry RFP (see figure A);

D, shows α-SMA-FITC (green) staining of blood vessel walls (arrows); note that The staining of the wall of some vessels is incomplete;

E, merged image shows colocalization of CD31-positive blood vessels and α-SMA-positive pericytes/SMCs (arrows).

Scale bar = 100µm.

To investigate whether the level of hypoxia in the primary tumour of Eng-iKO^{e} mice was significantly higher than that of tamoxifen treated control mice at day 6, the HIF-1α stained sections (from the central part of primary tumour mass) were quantitively given hypoxic scores (1, 2 and 3; Figure 5.16 C) based on the level of HIF-1α expression (Scoring from 1 to 3 was based on the intensity and area of tumor cell and stromal cells staining for HIF-1α. Tumour sections with more than 30-40% of tumor cells staining intensely were scored as 3. Figure 5.16 A&B). Accordingly, each individual tumour tissue was given a hypoxic score that relatively reflected the status of hypoxia (Figure 5.16 C). In comparison, there were significant differences in hypoxic scores between Eng-iKO^{e} mice and tamoxifen treated control mice ($P = 0.026$, Figure 5.16 D). This indicates the depletion of endoglin can cause significant hypoxic status in primary tumours of Eng-iKO^{e} mice

at day 6. More hypoxic cells might be due to reduced neovascularisation (Figure 5.9 A). In addition, there was a possibility that hypoxia occurred at the early stage of primary tumour progression was more likely to regulate hypoxic responses such as stimulating cancer cells to release more growth factors or selection of more aggressive cancer cells. Subsequently, the growth of primary tumour in Eng-iKO^{e} mice caught up with that in control mice and this was associated with increased lung metastases in Eng-iKO^{e} mice. Therefore, additional experiments are required to investigate this dynamic hypoxic process using hypoxic probes perfusion study. In addition to that hypoxic score comparison, to identify whether there was a significant difference in the level of necrosis between Eng-iKO^{e} mice and tamoxifen treated control mice. The degree of necrosis from the central part of primary tumour mass was evaluated based on the histological criteria of necrotic cells (characterized by H&E staining as fat, pink cells without nuclei, personal communication Dr. Brian Angus, Department of Pathology, Newcastle University). There appeared to be slightly more necrotic cells in day6 primary tumour of Eng-iKO^{e} mice compared with that of tamoxifen treated control mice (Figure 5.17), but the difference was small, and difficult to accurately quantify.

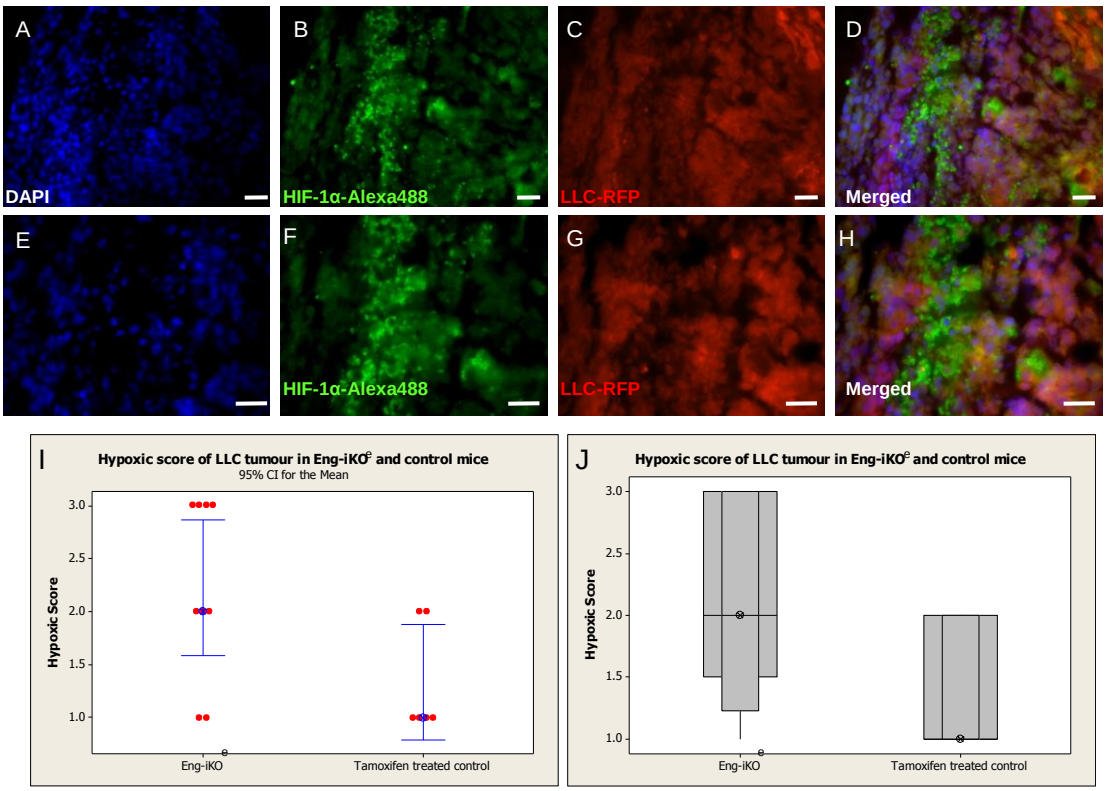

Figure 5.16 Representative images showing the hypoxic cells in an Eng-iKO^{e} tumour and a significant difference in hypoxic score was identified between Eng-iKO^{e} mice and tamoxifen treated control mice.

A - H, Cells nuclei stained with DAPI (A&E, blue), HIF-1α positive hypoxic cells (B&F, green), endogeneous RFP positive LLC cells (C&G, red) and merged images (D&H) shown in cryosections of an Eng-iKO^{e} tumour;

I&J, Red dots indicate the hypoxic score of each individual tumour tissue (I). There is a significant difference in the hypoxic score between Eng-iKO^{e} mice and tamoxifen treated control mice (Mann-Whitney test, W = 88.0, P = 0.026) (J). Scale bar = 200µm.

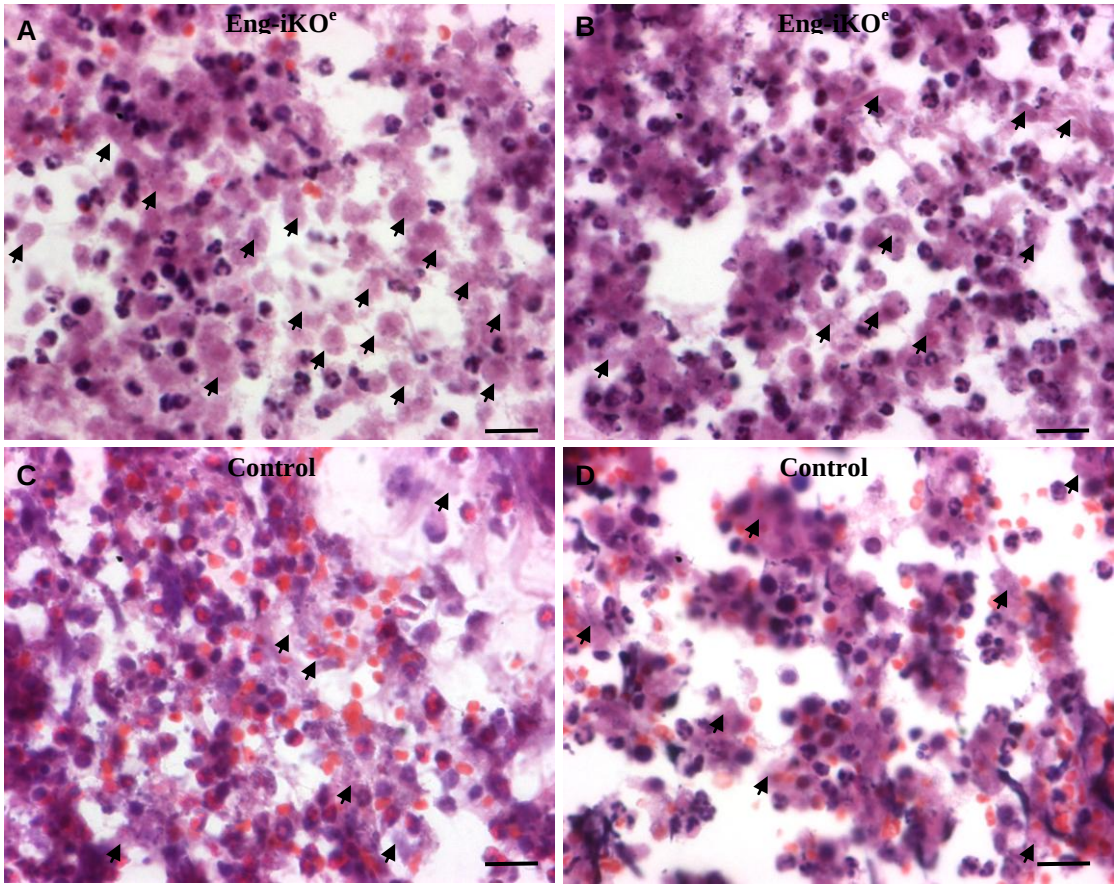

Figure 5.17 Necrotic cells in day6 primary tumours.
A&B, Representative images from day6 primary tumour of Eng-iKO^{e} mice shows presence of necrotic cells recognised by loss of nuclear stain (black arrows);
C&D, Representative images from day6 primary tumour of tamoxifen treated control mice showing necrotic cells (black arrows).
Scale bar = 200µm.

Another possible reason for increased spread of the primary tumour could be changes in the tumour stroma. Cancer-associated fibroblasts (CAFs) are a major component of the tumour stroma so to investigate the level of CAFs, adjacent cryosections were taken from the central part of each tumour block for fibroblast specific protein-1 (FSP-1) and α-SMA staining. Interestingly, FSP-1 and α-SMA seem to be expressed in different parts of the primary tumour. In a control tumour at day6 FSP-1 was more likely to be expressed on myofibroblasts of the intra-tumoural region. However, α-SMA positive myofibroblasts were mostly located in the peri-tumoural area (Figure 5.18). Further experiments are still required to confirm these findings and to compare mutant with control mice.

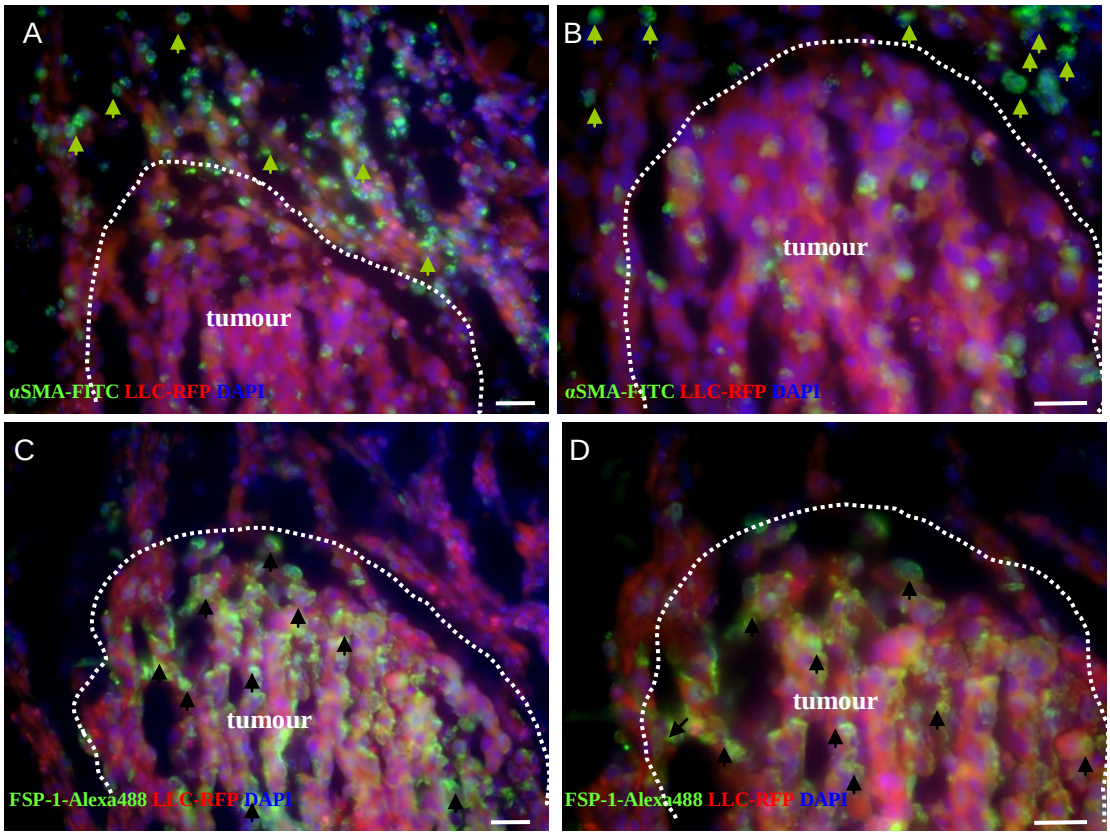

Figure 5.18 Expression patterns of FSP-1 and α-SMA on adjacent cryosections of primary tumour at day 6 in control mice.

A, Most of α-SMA positive mesenchymal cells (green arrows) are located in the peri-tumoural area;

B, shows detailed α-SMA positive mesenchymal cells in higher magnification (x63);

C, A vast majority of FSP-1 positive mesenchymal cells (black arrows) is localised in the intra-tumoural region;

D, shows detailed FSP-1 positive mesenchymal cells in higher magnification (x63).

Note: the dotted line indicate the outer border of the primary tumour. Green arrows indicate α-SMA positive cells in the peri-tumoral area and black arrows indicate FSP-1 positive cells within the intra-tumoral region. Scale bar = 200μm.

To investigate whether the extravasation of LLC-RFP cancer cells was increased in Eng-iKO^{e} mice compared with tamoxifen treated control mice, mice were anesthetised by isofluorane and then injected with 2.5 x 10^{5} LLC-RFP cells in 100ul PBS through the tail vein. Lungs were harvested on day15 and lung lobes were separately examined and lung metastases were identified using fluorescent stemi-microscopy (Figure 5.19 A-D). The number of lung metastases for each mouse was shown in Figure 5.21 E. There were significant differences in the number of lung metastases between Eng-iKO^{e} mice compared with tamoxifen treated control mice (Figure 5.19 F). This suggests that significantly increased extravasations of LLC-RFP cancer cells into the lung might be one of the critical reasons for the previously observed an increased frequency of lung metastases in Eng-iKO^{e} mice.

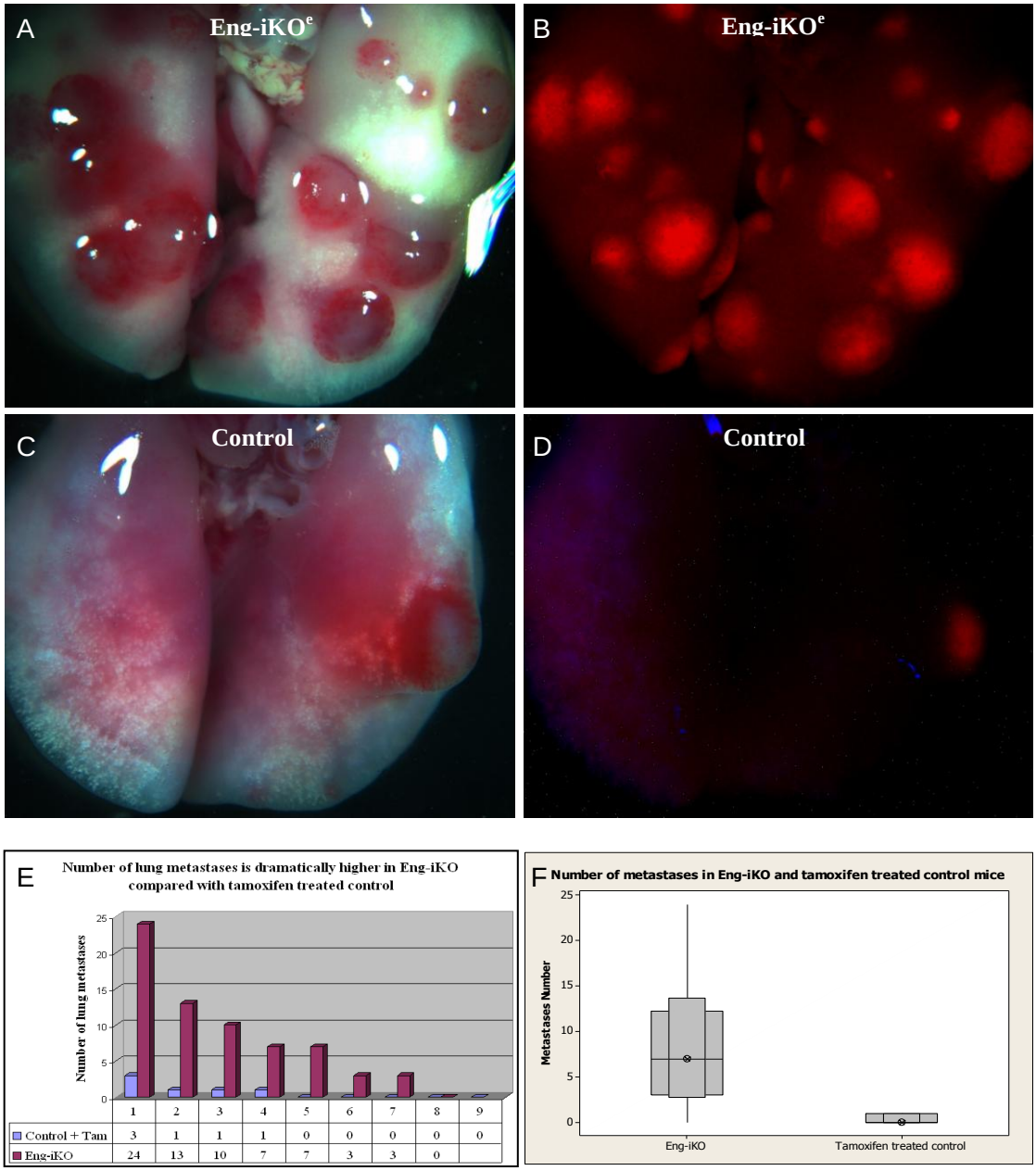

<u>Figure 5.19</u> The number of lung metastases is increased in Eng-iKO^e mice compared to tamoxifen treated control mice following tail vein injection of LLC-RFP cells

A&B, LLC-RFP metastatic lesions visualised using white light (left) and Fluorescent light (right) in lung lobes of an Eng-iKO^e mouse;

C&D, LLC-RFP metastatic lesions visualised using white light (left) and Fluorescent light (right) in lung lobes of a tamoxifen treated control mouse. Metastases are clearly seen in both views;

E, Each mouse is represented by a single bar and the height of the bar corresponds to the number of metastases present in the lungs. The table shows the number of lung metastases in each mouse.

F, There was a significant difference in lung metastases between Eng-iKO^e mice (Median =7, n = 8) and tamoxifen treated control (Median = 0, n = 9), (Mann-

Whitney analysis, W = 100.5, P = 0.0071).

Note: non-parametric Mann-Whitney analysis used to test the above comparisons as data distribution patterns following statistical advice from Dr. Peter Avery (School of Mathematics and Statistics, Newcastle University).

5.3 Discussion

5.3.1 Effect of tamoxifen on tumour progression

An important control for the LLC implanted primary tumour model used in the work described in this chapter was to test whether there were any effects of tamoxifen alone. The results showed no significant effect of tamoxifen on primary tumour size, vascularity or lung metastases. However, tamoxifen has been reported to exert anti-angiogenic effects, since tamoxifen influences a number of cytokines involved in the regulation of angiogenesis, including insulin-like growth factor (IGF) (Huynh and Pollak, 1993; Huynh et al., 1993), TGF- β (Butta et al., 1992), bFGF (Fujimoto et al., 1997) and VEGF (McNamara et al., 2001). One possible reason for not finding an effect of tamoxifen in angiogenesis is that the dose used in this study might be low compared with that used by others where a significant inhibitory effect on tumour growth and/or tissue vascularity was obtained. However, the total dose used to activate Cre-ER^{T2} in the mice described in this chapter (0.4g/kg) is very similar to that used in the rat study described by (McNamara et al., 2001) (0.356g/kg). Furthermore, the data from the matrigel plug angiogenesis experiment (Section 3.2.7, Chapter 3) also showed there was no significant difference in angiogenesis between tamoxifen treated and no tamoxifen control groups, consistent with the findings from the tumour angiogenesis study in this chapter. It is possible that different species or different models have different responses to tamoxifen.

5.3.2 Growth and vascularity of primary tumour in Eng-iKO^{e} mice.

A substantial number of reports have shown that endoglin is overexpressed in vascular ECs of tissues undergoing angiogenesis especially in the tumour-associated angiogenic process (Burrows et al., 1995; Kumar et al., 1999; Miller et al., 1999; Brewer et al., 2000; Fonsatti et al., 2000; Fonsatti et al., 2003; Shariat et al., 2008; Bernabeu et al., 2009; Fonsatti et al., 2010). Furthermore, the potential efficacy of anti-endoglin antibodies for clinical purposes in cancer is supported by a number of available pre-clinical in vitro and in vivo data (Fonsatti et al., 2010; Seon

et al., 2011). Bernabeu and colleagues have investigated the role of endoglin in tumour angiogenesis and growth using endoglin haploinsufficient ($Eng^{+/-}$) and control mice ($Eng^{+/+}$ littermates) that were subcutaneously inoculated with 10^6 LLC cells and tumours harvested after 9 days. The results of these studies indicated that endoglin deficiency decreased tumour vascularization and growth (reduction of tumour weight) in the short time frame used in this study (Duwel et al., 2007). I also observed a significant decrease in the size of primary tumour in Eng-iKO^e mice inoculated with 2.5 x 10^6 LLC cells at the early stage of primary tumour progression (at day 6) compared with control mice. This was confirmed by an additional day6 tumour experiment. However, at day8 and day10 of LLC primary tumour progression, the growth of primary tumour in Eng-iKO^e mice seems to catch up with that in tamoxifen treated control mice. Eventually, at later stages of LLC tumour progression, I observed no significant effect of endoglin loss on primary tumour angiogenesis or tumour size. The data therefore indicates that endoglin appears to promote primary tumour growth only in the initial stages.

Other studies have shown that the tumour response to anti-angiogenic therapy is a highly dynamic one. For example, using a mouse model of pancreatic islet cancer where angiogenesis is inhibited via VEGF receptor inhibition, the initial tumour response is one of 'vascular regression' and tumour growth delay. At a later stage the tumours then adapt and begin regrowing via a process referred to as "evasive resistance". This adaptive response is associated with upregulation of alternative pro-angiogenic signals that include fibroblast growth factor (FGF) ligands (Casanovas et al., 2005). It is therefore possible in our study that endoglin loss inhibits tumour growth at an early stage of primary tumour progression, but that secondary events give rise to revascularization and increased invasiveness. This might be tested by taking advantage of histological analysis on biopsy or dissected samples from discrete stages of tumour growth. In addition, it could be combined with fluorescent reflectance imaging and bioluminescence imaging which can give dynamic data of vascularisation and tumour size over time. Therefore, distinct

phenotypes mediated by endoglin in the different stages of LLC primary tumour progression is possibly due to an emergent resistance to endoglin depletion that might be similar to the resistance that is frequently seen following anti-angiogenic therapy in other preclinical models (Ebos et al., 2009; Paez-Ribes et al., 2009; Ellis and Reardon, 2010; Ebos and Kerbel, 2011).

5.3.3 Increased frequency of lung metastases in Eng-iKO^e mice

In addition to the anticipated effect of anti-angiogenic therapy on primary tumour growth, there is still a promising expectation that this type of therapy will also reduce distant metastases. However, we found a detrimental increase in the frequency of metastases in Eng-iKO^e mice. At first sight, this finding is not only difficult to reconcile with our expectations that endoglin deficiency reduces primary tumour angiogenesis (as metastatic lesions require vessel supply for growth), but is also inconsistent with previous observations that anti-anti-angiogenic therapies reduce metastases (Verheul et al., 2007; Sini et al., 2008). How can we explain these divergent effects of "endoglin-targeted therapy"? There are a number of possibilities, as follows.

First of all, anti-angiogenic treated tumours appear to be more invasive. A number of studies have also associated increased invasiveness with impaired angiogenesis in the context of genetic ablation of the hypoxia reponse and/or the VEGF/VEGFR pathways (Pennacchietti et al., 2003; Blouw et al., 2007; Du et al., 2008). In my study, the invasiveness of day18 primary tumours was compared between Eng-iKO^e mice and tamoxifen treated control mice. It seems that there was a trend of increased cancer invasiveness in Eng-iKO^e mice and this could be one of the explanations for increased metastases in Eng-iKO^e mice. In response to the angiogenesis inhibitors, tumour cells may elevate the activity of a pre-existing cell signalling program that might contribute to intravasation and/or extravasation of invasive cancer cells. This suggests that the invasive growth program induced in

response to therapy may be different from the program occurring in natural tumour progression (Paez-Ribes et al., 2009).

Secondly, tumour hypoxia appears to be a possible mechanism. In theory, the more proficient an anti-angiogenic agent is, the more efficiently it will prune tumour vessels and hence cause hypoxia. In my study, the comparison of HIF-1α staining between Eng-iKO^{e} mice and tamoxifen treated control mice indicates the loss of endoglin leads to significant hypoxic status in primary tumours of Eng-iKO^{e} mice at day 6. In the hypoxic conditions, it is more likely to regulate hypoxic responses such as stimulating cancer cells to release more growth factors or selection of more aggressive hypoxia-tolerant cancer cells, while cancer stem cells in hypoxic niches escape anti-angiogenic treatment (Brahimi-Horn et al., 2007). Subsequently, more malignant aggressive cancer cells appear to be more capable of invading into blood vessels (Yu et al., 2002) and eventually increased lung metastases were found in Eng-iKO^{e} mice.

Thirdly, other up-regulated growth factors might be playing a critical role in promoting angiogenesis and metastases after initial anti-angiogenic therapy. In healthy mice, for instance, the VEGF inhibitors can elevate levels of some other cytokines such as PIGF and IL-6 etc. that promote angiogenesis in a VEGF-independent manner (Ebos et al., 2007). In addition, these elevated cytokines can recruit bone marrow-derived endothelial progenitor cells that contribute to form premetastatic niches (Kaplan et al., 2006). In the tumour of Eng-iKO^{e} mice, some other growth factors might be up-regulated due to the depletion of endoglin and these elevated growth factors may contribute to the detrimental consequence that the growth of primary tumour in Eng-iKO^{e} mice caught up with that in control mice and this was associated with increased lung metastases in Eng-iKO^{e} mice. Therefore, additional experiments are required to investigate this dynamic growth factors up-regulating process in all stages of tumour progression in different cancer types in the future.

In addition, the formation of pre-metastatic niches within the lung may exert extravasation of circulating tumour cells (CTCs). It would be possible that CTCs take advantage of a pre-formed suitably microenmironment within target metastatic sites that might be conducive to extravasation. More likely, the changes of blood vessel integrity occur before the arrival of CTCs at the sites of potential metastases and this could facilitate extravasation (Psaila and Lyden, 2009). In principle, a significant increase in lung metastases in Eng-iKO^{e} may be due to the formation of pre-metastatic niches with leakier vasculature within the lung following vascular specific endoglin depletion. In addition, my further experiments showed the lung vasculature was 'predisposed' to develop metastases in the Eng-iKO^{e} mice using an experimental metastatic model of LLC-RFP cell tail vein injection. However, metastasis seems to be an early event (Psaila and Lyden, 2009; Talmadge and Fidler, 2010; Hanahan and Weinberg, 2011). It will therefore be important to look at the occurrence of micrometastasis in the LLC-RFP model, as well as the macrometastases already examined. Further studies such as analysis of numbers of CTCs in different stages of primary tumour progression are also needed to find out the underlying mechanisms.

Last but not least, more leaky and immature tumour vessels may facilitate intravasation of aggressive cancer cells. These newly developed blood vessels are often characterised by the absence of a smooth muscle wall and the presence of a leaky basement membrane. In theory, these properties allow malignant cells to seep into the circulation and to promote metastatic disease. In fact, some of these agents (especially the more broad-spectrum VEGFR-TKIs, which also inhibit PDGFRβ) or the cytokine response they induce (in the case of osteopontin) may inhibit coverage of tumour vessels by pericytes, which destabilizes vessels, makes them more leaky and immature, and hence facilitates intravasation of tumour cells and metastases (Bergers and Hanahan, 2008). In addition, angiogenesis involves differential growth and sprouting of endothelial tubes and recruitment and differentiation of mesenchymal cells into vascular smooth muscle cells (VSMCs) and pericytes. It

may therefore be important in this context that Carvalho et al. found smooth muscle cell differentiation was impaired in $Eng^{-/-}$ mutant mouse yolk sacs compared with wild-type embryos and this was associated with decreased levels of TGF-β1 protein (Carvalho et al., 2004). In my study, I did not find any significant differences in the muscularisation of neovessels (based on α-SMA immunostaining) between Eng-iKO^e mice and control mice either at day6 or at day18. In fact, tumour cryosections staining with α-SMA can not reflect the comprehensive leakiness of tumour vasculature and also the vascular muscularisation could be a dynamic process. It will therefore be important to perform further studies such as testing the leakiness of tumour-associated blood vessels using a Dextran-FITC perfusion study in Eng-iKO^e mice and control mice.

Taking all these factors into consideration, we can hypothesize that quantitative and qualitative effects of anti-angiogenic therapy may depend on a number of factors. In principle, these will include tumour-intrinsic parameters such as levels of pro-angiogenic factors, vessel number and function, sprouting angiogenesis versus vessel co-option, pericyte coverage, recruitment of bone marrow cells, oxygen tension and lymphangiogenesis. In pre-clinical models, differences in experimental conditions such as type of tumour and metastases model, duration of treatment, class and dose of angiogenesis inhibitor, monotherapy versus combination treatment with cytotoxic or other agents, will all affect the tumour growth and metastatic responses. Pàez-Ribes et al. (2009) speculate that high VEGF levels render tumour vessels immature and facilitate intravasation and metastases while inhibiting VEGF may produce a similar overall effect on metastases, though via qualitatively distinct mechanisms, as explained above. Another unresolved issue is whether metastatic tumours rely as much on angiogenesis as primary tumours, given that metastatic tumour cells often acquire hypoxia-tolerant properties (Brahimi-Horn et al., 2007).

5.3.4 Endoglin might be a major pro-angiogenic agent in tumour angiogenesis and may be a synergistic agent in anti-angiogenic therapy

Judah Folkman proposed that all solid tumour growth is dependent on blood vessel growth and that suppression of tumour angiogenesis would be a valid approach for cancer therapy (Folkman, 1971). In 2004, the first anti-angiogenic cancer drug, bevacizumab (avastin), was approved by the US FDA. There are some small clinical benefits using anti-angiogenic agents for treating only certain types of solid tumours. It seems that anti-angiogenic therapy can potentially overcome several major problems associated with other anti-cancer therapies, for example, the problems of drug resistance, poor drug delivery and tumour heterogeneity. However, current anti-angiogenic drugs for cancer therapy are far from optimal and produce only minor beneficial effects by prolonging the overall survival time of a few months which is effective only in combination with conventional chemotherapy (Kerbel, 2008). This benefit may be because of transient vascular normalisation and consequent improved drug delivery (Jain, 2005b). However, in a certain type of cancer such as pancreatic cancer anti-angiogenic monotherapy or combinations with chemotherapy has not shown significant clinical benefits (Kindler et al., 2005; Kulke et al., 2008). It is unknown why a diversity of tumour types responds differently to anti-angiogenic therapy. Both clinical and experimental results indicate that unconventional drug resistance develops in response to anti-angiogenic therapy (Bergers and Hanahan, 2008). Therefore, the novel and effective anti-angiogenic agents and methods for increasing the efficacy of anti-tumour agents by synergistic combination with monospecific or multitargeted anti-angiogenic agents are required.

Endoglin is one of the most reliable markers of proliferating ECs, and it is overexpressed on tumour neovasculature. The potential of endoglin as vascular target for diagnostic and therapeutic anti-angiogenic strategies in cancer has been investigated at pre-clinical level both *in vitro* and *in vivo*. Recently, Ben K. Seon et.al found that primary tumour growth and metastases were effectively suppressed

by anti-endoglin monoclonal antibodies (mAb) targeting tumour vasculature in a range of pre-clinical cancer models, including orthotopic injection of 4T1 murine mammary carcinoma cells and splenic injection of two types of colon26 murine colorectal carcinoma cells (Uneda et al., 2009; Seon et al., 2011). More recently, a first phase I study in human, with the humanized-murine chimeric anti-endoglin mAb TRC105 in patients with refractory advanced or metastatic solid cancer is ongoing in order to evaluate safety and tolerability of escalating doses of the therapeutic mAb (Fonsatti et al., 2010). Anti-endoglin mAb recognises and binds the target antigen (endoglin) which is upregulated in tumour-associated ECs and subsequently cause failure of binding between TGF-β/BMP9 ligands and endoglin, their endothelial receptor, as well as triggering an immune response to the targeted ECs. In the work described in this chapter, vascular-specific endoglin depletion would be expected to reduce TGF-β/BMP9 binding to the ECs, but would not be expected to trigger the immune system to target ECs. Also, another major difference between these two types of pre-clinical models is the scheduling of the treatments. In the work described in this chapter, endoglin gene depletion occurred prior to primary and secondary tumour establishment. It is possible that endoglin loss pre-conditions the lung micro-environment to make it more favourable for transendothelial migration of tumour cells and/or tumour growth. Therefore, in the context of the subdermal LLC tumour model, our results demonstrate targeting endoglin may delay primary tumour progression at an early stage, but this is coupled with a detrimental increase in the frequency of metastases. Also, these findings possibly indicate evasive resistance to “anti-endoglin therapy”.

A combination of chemotherapy and anti-endoglin therapies might be an effective and beneficial treatment for cancer patients. In an established tumour of MCF-7 in human skin grafted onto SCID mice, Ben K. Seon et.al found improved anti-tumour efficacy by the combination of an anti-endoglin mAb with a chemotherapeutic drug (cyclophosphamide (CPA) or doxorubicin (DPX)) using an anti-angiogenic schedule of drug dosing (Takahashi et al., 2001a; Shiozaki et al., 2006).

Accordingly, another clinically relevant question raised is whether concomitant chemotherapy in some tumour types could alter or even abrogate the increased malignant phenotype caused by certain anti-angiogenic therapies in different models. More recent metronomic chemotherapy could negate or reduce pro-invasive and pro-metastatic responses to anti-angiogenic therapies. On the other hand, abnormal cancer associated neovasculature normalized by anti-angiogenic therapy could contribute to the delivery of chemotherapeutic regiments. To test whether the combination of anti-angiogenic biotherapy and metrotomic chemotherapy is a practical and rational strategy for cancer therapy, Seon et al explored the efficacy of a strategy combining low-dose cisplatin and a recombinant xenogeneic endoglin as a protein vaccine, which was previously demonstrated to have effective anti-angiogenic effects in several mouse models. The results demonstrate the combination therapy resulted not only in significant anti-angiogenic effects but also additional promotion of tumour cell apoptosis and inhibition of tumour cell proliferation. In addition, the combination demonstrated a synergistic relationship, which was shown in all of the synergistic indexes, i.e., tumour volume, angiogenesis, apoptosis and proliferation. These observations may provide the basis for an effective alternative strategy for cancer therapy in the near future (Tan et al., 2004).

Multitargeted antiangiogenic therapies may be another method of increasing the efficacy of anti-angiogenic agents by anti-endoglin antibody. Possibly, the consequence of anti-angiogenic therapy is to upregulate some other cytokines that promote reneovascularization. Therefore, a current priority is to determine whether there are pro-angiogenic agents upregulated due to anti-endoglin therapy.

Taken together, the current pre-clinical data demonstrate endoglin potentially can be developed as a novel antibody-based diagnostic and therapeutic strategy. It seems to be premature timing to apply anti-endoglin therapies to the clinical setting of cancer. Instead the priority must be to investigate mechanisms of response to

anti-endoglin therapy and thereby identify the most appropriate therapeutic applications of endoglin targeting. Moreover, the efficacy of anti-endoglin therapies should be tested at all stages of tumour progression in a variety of clinically relevant animal models. The potential side effects of targeting endoglin are considered in the next chapter.

Chapter 6. Potential Side Effects of Using Endoglin as an Anti-angiogenic Therapeutic Target

6.1 Introduction

Anti-angiogenic therapy is thought to be free of the most severe side effects such as anemia, fatigue, hair loss, appetite changes, swelling, bleeding problems and infection that are usually seen with conventional chemotherapy. But anti-angiogenic drugs are not risk-free and do have their own side effects, which seems to be distinctly caused by anti-angiogenic therapy rather than conventional chemotherapy, when both in combination are used to treat patients with cancer. For example, humanized monoclonal antibody bevacizumab (Avastin) recognises and blocks VEGFA, thereby reducing stimulation of the new blood vessels that are required for tumour growth. There are already clinical trial results supporting its efficacy for the first- and second-line treatment of colorectal cancer in combination with chemotherapy (Hurwitz et al., 2004; Giantonio, 2005; Hochster et al., 2006). The main side effects associated with anti-VEGF treatment in colorectal cancer include hypertension, proteinuria, thrombosis, bleeding, impaired wound healing and gastrointestinal perforation (David Cunningham, 2007). These changes, however, are generally manageable and pose less risk than the tumours being treated. These adverse effects of VEGF inhibitors may be caused by suppressing VEGF signalling in ECs of normal organs, among these, the more likely mechanisms are endothelial cell dysfunction and regression of fenestrated capillaries (Kamba and McDonald, 2007).

Endoglin has also been proposed as an anti-angiogenic target for clinical treatment, and is currently being tested in two phase I clinical trials (http://clinicaltrials.gov/archive/NCT00582985/2008). However, there are also concerns about the potential side effects of such therapy. These might be similar to those of Avastin or other anti-angiogenic agents that are currently used in clinical trials. On the other hand, anti-endoglin therapy could potentially cause vascular defects similar to those present in Hereditary Haemorrhagic Telangiectasia (HHT) patients. HHT type I is caused by an inherited haploinsufficiency of endoglin due to heterozygosity for mutation of endoglin (McAllister et al., 1994). This vascular

disorder is characterized by bleeding from small vascular malformations (telangiectases) in the nose and gastrointestinal tract, and by larger arteriovenous malformations (AVMs) that have most frequently been reported in the lung, brain or liver, but may also occur in the retina (Guttmacher et al., 1995).

To investigate what side effects anti-endoglin therapy may potentially cause, an additional experiment was performed to examine the phenotypes of the Eng-iKO^{e} mice that had been given subdermal matrigel plugs. This model was initially described in Chapter 3 and preliminary data indicated there was some abnormal vascular remodelling in the perimatrigel area. However, the experiment described in Chapter3 was not designed to examine the perimatrigel area in full, nor was control tissue taken for comparison. Therefore, a matrigel plug, supplemented with VEGF (300ng/ml) and bFGF (600ng/ml), as before, was injected subcutaneously into the right flank and examined after 15 days. For the work described in this chapter a full depth sample of dermal tissues (including the skin and subdermal muscle layer surrounding the matrigel plug) was taken at the end of the study to permit investigation of vascular remodelling in the tissue neighbouring the matrigel. Also, in this experiment, a full depth skin tissue sample was taken from the opposite side of the animal to the site of the matrigel plug (in the contra-lateral flank) to analyse unstimulated vessels as an internal control. Tissues were analysed using serial sections as before (Chapter 3).

6.2 Results

6.2.1 The expression of endoglin in different blood vessels in normal skin

In order to formally identify which dermal vessels express endoglin in normal skin, the expression of endoglin in the different blood vessels from control mice without matrigel or tamoxifen stimulation was assessed. From this, I could select which types of blood vessels were most likely to be affected by endoglin depletion. CD31 and endoglin immunohistochemistry was carried out on cryosections of frozen skin tissue that obtained from control mice without matrigel and tamoxifen stimulation. Immunostained adjacent sections using CD31 and endoglin antibodies showed that endoglin similarly was strongly expressed on venules, arterioles and capillaries (Table 6.1). Therefore, I would conclude from this that any of these vessel types might be altered in the absence of endoglin.

Samples	**CD31**			**Endoglin**		
(n = 9)	**Capillaries**	**Venules**	**Arteries**	**Capillaries**	**Venules**	**Arteries**
1	+ + +	+ + (+)	+ + +	+ + +	+ (+)	+ +
2	+ + +	+ + (+)	+ + +	+ + (+)	+ + (+)	+ + (+)
3	+ +	+ (+)	+ +	+	+	+ +
4	+ +	+ (+)	+ +	+ (+)	+ (+)	+ (+)
5	+ + +	+ + +	+ + +	+	+	+ +
6	+ + +	+ + +	+ + +	+ + +	+ + (+)	+ + +
7	+ + +	+ + +	+ + +	+ + +	+ + +	+ + +
8	+ +	+ +	+ +	+ +	+ +	+ +
9	+ + +	+ + +	+ + +	+ + +	+ + (+)	+ + +

Table 6.1 Endoglin and CD31 expression in normal dermal blood vessels
The extent and intensity of vessel staining was scored from 0 (no staining) to +++ (strong staining). The identity of venules and arterioles were determined based the structure of vessels.

6.2.2 Angiogenic stimulation leads to venous enlargement in Eng-iKO^{e} mice

Analysis of paraffin sections of skin samples containing the matrigel plugs showed major remodelling of blood vessels including postcapillary venules close to the matrigel in the Eng-iKO^{e} mice (n=5) that was not seen in the control mice (n=4) and resembled the dilated blood vessels seen in HHT patients (Figure 6.1). This was mirrored by a more modest dilation of the arteries in the Eng-iKO^{e} mice. Blood

vessels distant from the matrigel plug in the contra-lateral flank of the Eng-iKO^{e} mice showed no obvious vascular phenotype (Figure 6.2). Statistical analysis showed there was a significant increase in venous size in distant skin in Eng-iKO^{e} mice compared with control mice (Figure 6.3 A). On the other hand, there was no significant difference in venous size between contra-lateral skin and matrigel-stimulated skin in control mice (Figure 6.3 B). These results indicate endoglin loss alone can cause modest dilated vessels, but angiogenic stimulation alone does not result in dilated vessels. However, there was a significant increase in average venous cross sectional area in veins from the matrigel stimulated region compared with distant skin in the Eng-iKO^{e} mice (Figure 6.4 A). There was also a significantly increased venous size in matrigel skin in Eng-iKO^{e} mice compared with control mice (Figure 6.4 B). Both of these changes suggest there is an abnormal venous enlargement response in the presence of angiogenic stimulation and in the absence of endothelial endoglin. This result may certainly be of clinical relevance. However enlarged venules did not appear to cause any detectable effects on the health or viability of Eng-iKO^{e} mice, and HHT1 patients may harbour enlarged veins without serious morbidity.

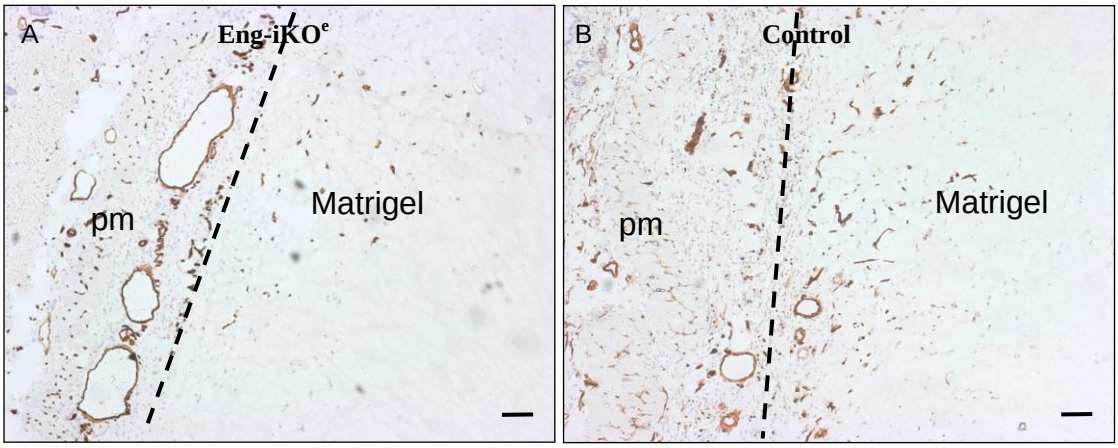

Figure 6.1 Dilated blood vessels in the subdermal tissue adjacent to the matrigel plug in Eng-iKO^{e} mice

A, Three obviously dilated vessels **immunostained with CD31** located on the area adjacent to matrigel in Eng-iKO^{e} mice;

B, Apparently normal vessels in a similar region in control mice.

The dashed line indicates the margin of matrigel plug.

Scale bar = 100μm. Abreviation: pm, panniculus carnosus muscle layer.

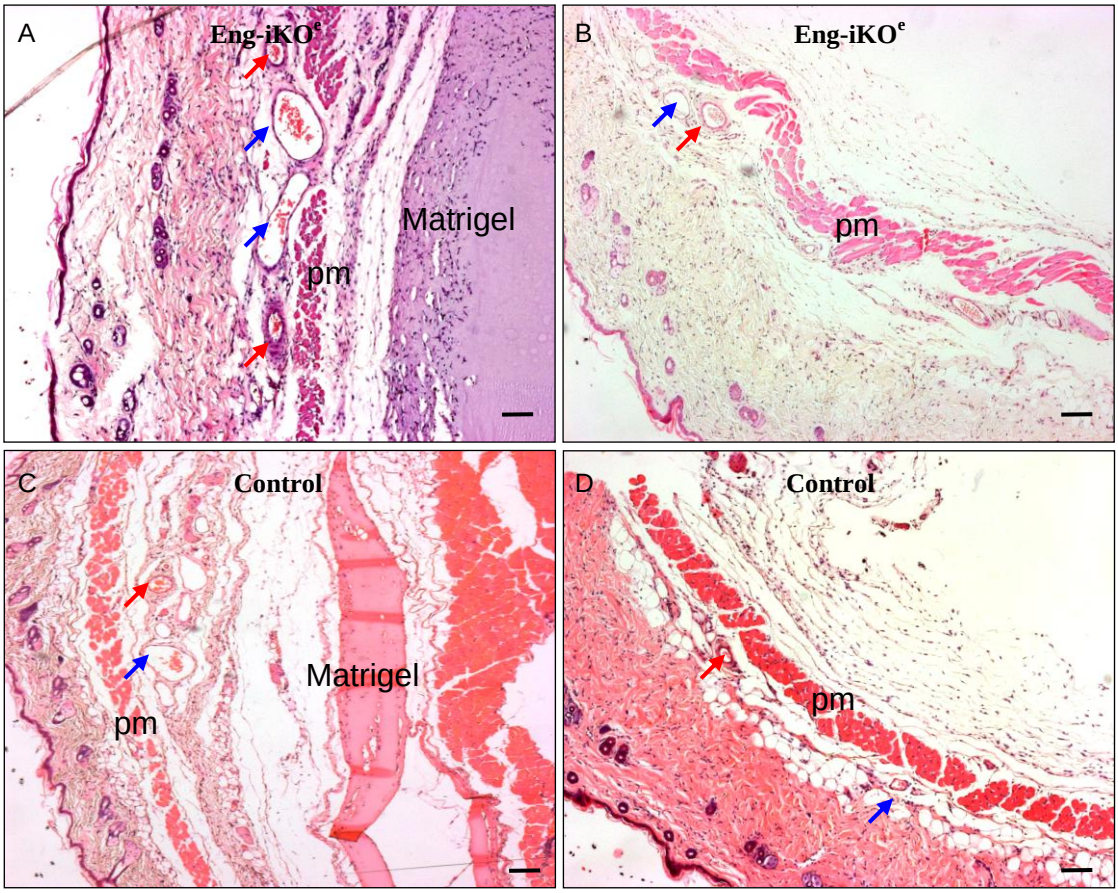

Figure 6.2 Vascular remodelling in response to a matrigel stimulus in Eng-iKO^e mice.

A, H&E staining shows two obviously dilated veins (blue arrows) located on the area adjacent to matrigel plug in the dermis of an Eng-iKO^e mouse;

B, A normal sized venule (blue arrow) and artery (red arrow) sitting aside the panniculus carnosus muscle layer in Eng-iKO^e mouse in the unstimulated contralateral skin;

C, Modest dilation of a vein (blue arrow) located on the area adjacent to matrigel plug in a control mouse;

D, Normal microvasculature in the contralateral skin in control mouse (blue arrows indicate veins, red arrows indicate arteries).

Scale bar 100μm. Abbreviation: pm, panniculus carnosus muscle layer.

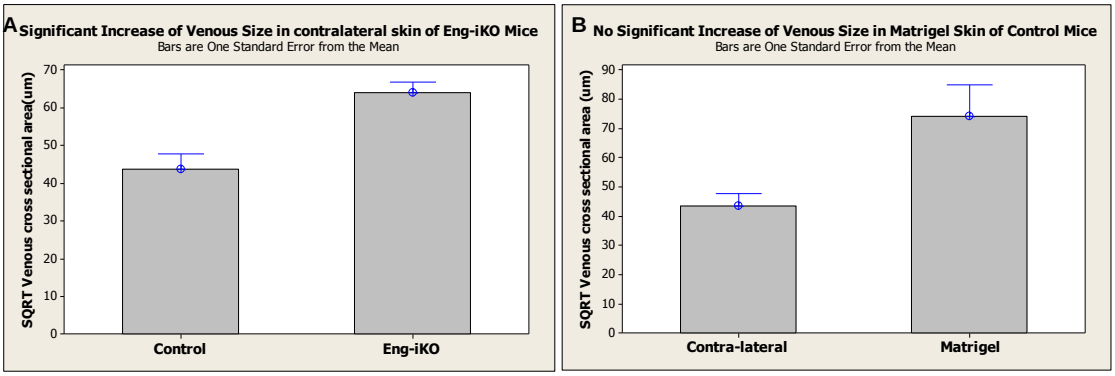

Figure 6.3 Endoglin loss alone causes dilated vessels.

A, There is a significant increase in venous size in contralateral skin between Eng-iKO^{e} mice (n = 5) and control mice (n = 4) (t-test, T = -4.06, P = 0.010).

B, There is no significant difference of venous size between contra-lateral skin and matrigel skin in control mice (n = 4) (Paired t-test, T = -2.76, P = 0.070).

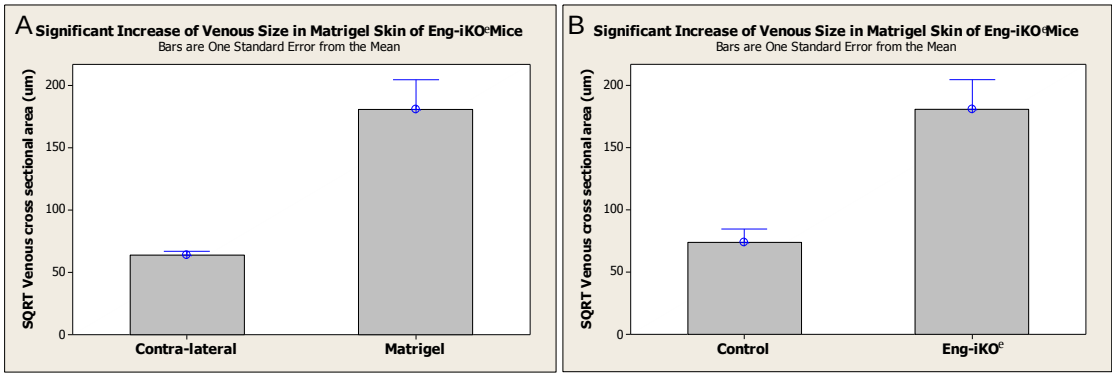

Figure 6.4 The combination of endoglin loss and angiogenic stimulation results in enlarged veins.

A, There is a significant increase in venous size in matrigel-stimulated skin compared with contra-lateral skin in Eng-iKO^{e} mice (n = 5). (Paired t-test, T = -4.83, P = 0.008).

B, There is a significant increase in venous size in matrigel-stimulated skin in Eng-iKO^{e} mice (n = 5) compared with matrigel-stimulated skin of control mice (n = 4). (t-test, T = -4.00, P = 0.010).

6.2.3 Veins are the major responsive vessels

To investigate this vessel enlargement in more detail and to better define the physical extent of the response, we undertook a systematic analysis of serial sections of dermal blood vessels in tamoxifen treated control and Eng-iKO^{e} mice, from near the matrigel plugs in skin and in the skin that was distant from the matrigel, taken from the contra-lateral flank. The analysis was focussed on the

postcapillary venules and neighbouring arterioles located close to the panniculus carnosus muscle layer in each case.

The average venous cross sectional area of maximally enlarged vessels showed the postcapillary venules enlarged dramatically as shown above (Figure 6.2, 6.3 & 6.4), whereas the arteries only slightly increased (Figure 6.5).

In order to examine this finding in more detail, multiple serial sections that contained at least one pair of veins and arteries close to the panniculus carnosus were examined and photographed for 3-D reconstruction. This further illustrates the obvious venous enlargement in the Eng-iKO^{e} mouse compared with the control (Figure 6.6). There were six 3D reconstructions (three from Eng-iKO^{e} mice and three from control mice) that were performed similarly in this study and were consistent with the results from the analysis of venous and arterial cross sectional area shown above. This provided additional support to the conclusion that veins are the major responsive vessels compared to arteries.

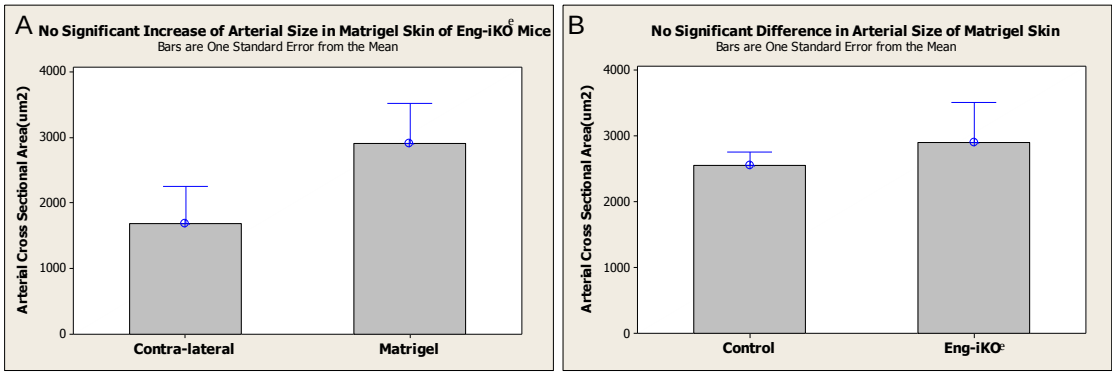

<u>Figure 6.5</u> No significant increase of arterial size in matrigel skin in Eng-iKO^{e} mice.

A, There is no significant difference of arterial size between matrigel skin and contra-lateral skin in Eng-iKO^{e} mice (n = 5) (Paired t-test, T = -1.29, P = 0.267).

B, There is no significant difference of arterial size in matrigel skin between Eng-iKO^{e} mice (n = 5) and control mice (n = 3) (t-test, T = -0.54, P = 0.615).

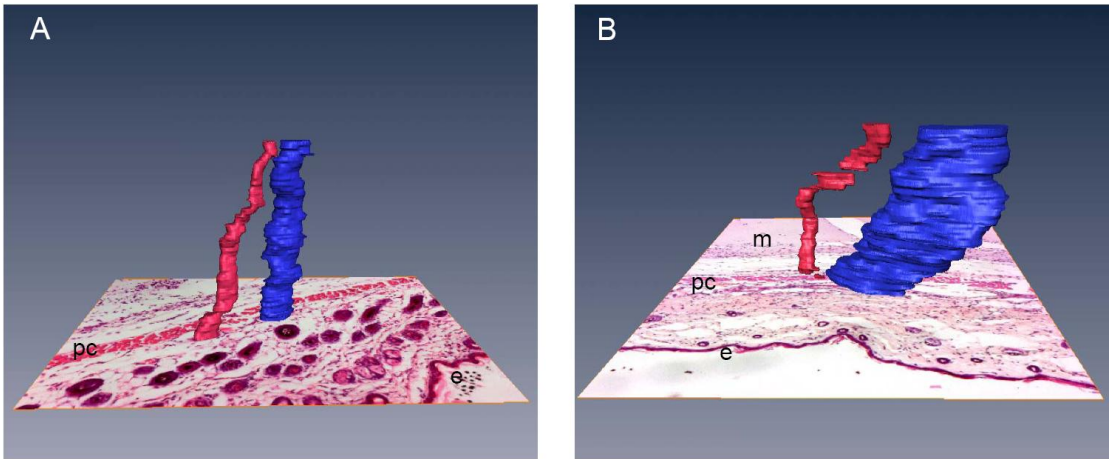

Figure 6.6 3D reconstructions of veins (blue) and arteries (red) from serial sections of adult mouse skin.

Images show how the reconstructions are based on individual sections and the lowest section has been kept for illustration purposes. The position of the epidermis (e) is marked for orientation.

A, A parallel vein and artery close to the Panniculus Carnosus (pc) in normal skin from a control mouse.

B, An enlarged vein running parallel to an artery from an equivalent region of skin but close to matrigel (m) in an Eng-iKO^{e} mouse. Slight imperfections in the serial sectioning lead to the small 'gap'seen here in the artery.

Approximately 60 serial 5µm sections were reconstructed in each case using Amira 4.0 software.

6.2.4 Vascular remodeling occurs close to the source of the angiogenic stimulus

The significant feature of vascular remodeling in the matrigel plug implanted Eng-iKO^{e} mice is primarily the change in venous luminal dimensions. As the increase in venous size was far greater than could be explained simply from vasodilation, I examined the numbers of cells lining the vessels (assumed ECs, Figure 6.7) and found a significant increase of venous EC number in matrigel skin of Eng-iKO^{e} mice compared to control mice (Figure 6.8). These results indicate this vascular remodelling was not due to venous dilation alone, but that EC proliferation also made a contribution to the venous enlargement.

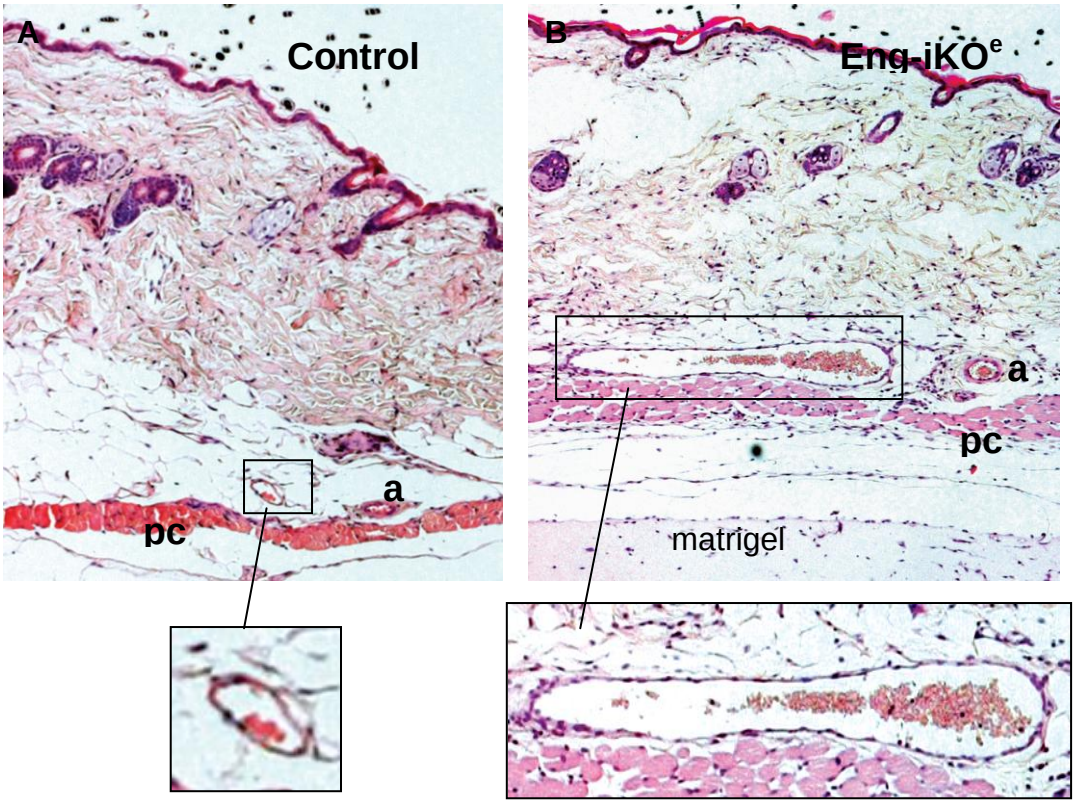

Figure 6.7 The number of cells lining the vessels counted based on serial skin sections stained with H&E from control mice and Eng-iKO^{e} mice

A, Skin section stained with H&E from a control mouse show normal appearance of post capillary venule (boxed area, and in digital zoom) adjacent to a small artery (a) running next to the Panniculus Carnosus (pc).

B, A similar section from an Eng-iKO^{e} mouse shows major venous enlargement (boxed area, and in digital zoom) adjacent to matrigel plug.

Note: Nuclei of cells lining the vessles (identified as nuclei protruding into the vessel lumen) were counted on 3 adjacent sections for each vein. Dilated blood vessels were discriminated from longitudinal sections through blood vessels fusion by performing serial sectioning and 3-D reconstructions with Amira software.

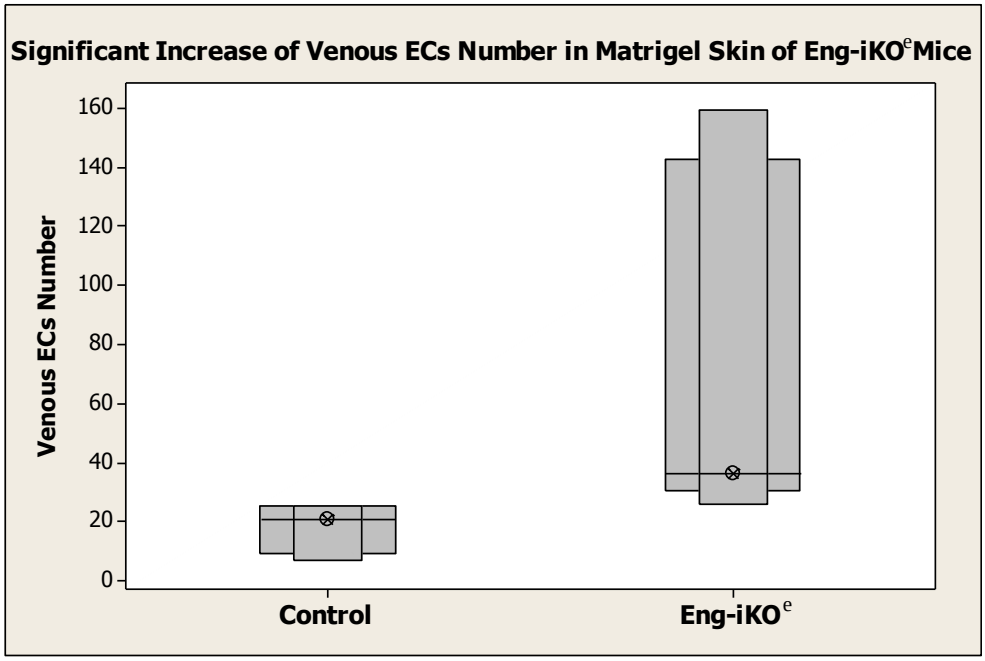

Figure 6.8 Significant increase in the number of venous endothelial cells in matrigel skin of Eng-iKO^{e} mice

There is a significant increase in venous endothelial cell number comprising the enlarged vessels in matrigel skin of Eng-iKO^{e} mice (Median = 36, n = 5) compared with that of control mice (Median = 20.33, n = 4) (Mann-Whitney test, W = 10.0, P = 0.020).

Note: there is not normal distribution in the number of venous endothelial cells in matrigel skin of Eng-iKO^{e} mice, therefore the non-parametric Mann-Whitney test was used in this analysis. Circle dots indicate the median, external bar and internal bar represents Inter-Quartile Range (IQR) and 95% confidence interval for median, respectively.

6.3 Discussion

6.3.1 The potential development of HHT in patients treated with anti-endoglin therapy

HHT is characterized by a highly variable expressivity and age-dependent penetrance. Diagnosis is based on a combination of some or all of the following symptoms: spontaneous epistaxis, cutaneous telangiectases and arteriovenous malformations in some internal organs including the lung, brain or liver (Lebrin and Mummery, 2008). Mutations in the endoglin gene are associated with HHT type I. In Chapters 3 and 5, the data showed evidence for reduced new blood vessel formation due to the absence of endoglin, potentially supporting the idea that anti-endoglin therapy will be effective against new blood vessel formation in tumours. However, a major concern is that patients may develop HHT1 during long-term anti-endoglin therapy.

6.3.2 Endothelial specific endoglin depletion does not appear to cause major health problems

To investigate whether anti-endoglin therapy can cause HHT1, the experimental data from the matrigel plug implanted mice indicates that mutation of endoglin alone causes minor changes in venous size that may be due to venous dilations rather than major vascular remodeling. However, an angiogenic stimulus in combination with loss of endoglin can cause significant dilation of veins and increased proliferation of venous ECs. Therefore, this finding indicated that any angiogenic stimulus within a growing tumour might lead to abnormal venous enlargement during anti-endoglin therapy. However, in my tumour study, I did not find abnormally enlarged veins in peritumoural regions of day6 or day18 tumours in Eng-iKO^{e} mice. There is a possibility that the different experimental procedures between the matrigel plugs implantation study and the subdermal LLC-RFP tumour study may explain this difference in venous response. The matrigel mixed with growth factors was injected on the same day as the tamoxifen i.p. injections began. In contrast, in prior to subdermal LLC-RFP injection, 5 consecutive i.p. tamoxifen

injection were applied and endoglin gene were deleted. In addition, the growth of tumour was more aggressive and these aggressive cancer cells were more likely to 'destroy' the peritumoural tissues, unlike the compact matrigel plugs. Moreover, the matrigel plugs containing high levels of FGF and VEGF growth factors can immediately affect surrounding vasculature after matrigel plug implantation, whereas injected cancer cells might experience a 'dormancy' period before releasing growth factors.

The expression of endoglin is not tumour specific, it is expressed in tumour-associated blood vessels but is also variably expressed in the vasculature of normal tissues (Takahashi et al., 2001a). This finding is in line with our results from immunostaining. We found endoglin was highly expressed in the vasculature of solid tumours such as lewis lung carcinoma and neuroblastoma, but was also expressed in varying degrees in the vasculature of skin (Table 6.1). It is also expressed in adult lung vasculature (Mahmoud et al., 2009), and adult heart valves and capillaries (Arthur et al., 2000). Therefore, it is possible that anti-endoglin therapy could affect the function of major organs and tissues. From my experimental metastatic model study (introduced in Chapter 5), I found that metastases in lung were significantly increased in Eng-iKO^{e} mice compared with control mice. This indicates the vasculature in lung might be affected due to the loss of endoglin. Therefore, it would be very advantageous if different specificities of anti-endoglin mAbs allowed specificity for tumour vasculature compared with normal tissue vasculature. For example, SN6j and SN6k show higher selective reactivity with human tumour vasculature compared with normal human tissue vasculature (Matsuno et al., 1999). In principle, if an anti-endoglin mAb reacts only with tumour-associated vascular endothelium, this would minimize any side effects caused by cross interaction with vascular endothelium in normal tissues (Matsuno et al., 1999; Fonsatti et al., 2000).

However, endoglin is also an endothelial cell-associated proliferating antigen and its expression is upregulated in tumour-associated vascular endothelium (Seon et al., 1997; Takahashi et al., 2001a). Therefore, the endoglin upregulation in ECs of tumour vasculature are likely to be more susceptible to targeting by anti-endoglin mAbs than any normal tissues showing low endoglin expression.

An open label phase-I dose finding study of TR105 (a human/murine chimeric IgG1 anti-endoglin antibody) in patients with advanced solid tumour is now in progress (http://www.cancer.gov/search/ViewClinicalTrials.aspx). This phase-I study is aiming to evaluate safety, tolerability and dose limiting toxicities during an evaluation period (a month to years). Although the evaluation is only based on a small number of patients (up to date n = 50) with advanced solid tumours, it is the first clinical trial of anti-endoglin therapy and the preliminary data indicates the majority patients can tolerate doses of TRC105 that generate anti-angiogenic and anti-cancer activity (Goldman et al., 2011).

6.3.3 Limitations of the matrigel skin model to investigate abnormal vascular remodelling in Eng-iKO^{e} mice

The matrigel implanted skin model described in this chapter had a number of limitations. The most important problem was that of a rather variable response, despite the fact that the experimental design aimed to minimise variations, by using age matched and similar weight mice. However, there were some unavoidable sources of variation that might have altered the effect of endoglin or angiogenic stimulation on vascular remodelling. First of all, the responsive arteries and veins of interest, close to the panniculus carnosus muscle layer in mouse skin, are not visible at the time of injection of the matrigel. It was therefore not possible to inject the matrigel plug in exactly the same place close to the responsive vessels. Therefore, minor variation in the location of the matrigel plug is an important factor potentially affecting vascular remodelling within the study group. Secondly, the mouse models

used in this study were of a mixed genetic background due to the intercrossing of several transgenic lines to generate the required genotype (in contrast to the work described in chapter 5 that used a backcrossed line). In addition, there were some difficulties of examining vessels in 3-D, for example, it was difficult to obtain consistent serial sections including an artery and vein that ran in parallel through the skin tissue and also it was difficult to align the images from any damaged or folded sections for 3-D reconstruction. Although the Amira software can automatically fill the gap generated by missing sections, this did affect the accuracy of the study.

To avoid the shortcomings of matrigel skin and minimize variations generated by models, an alternative retinal angiogenesis model was recommended by Dr. Marcus Fruttiger. This is a good model system for study of the development of blood vessels, because arteries and veins develop during the first week of neonatal life in a regular alternating pattern with an intervening capillary network. This vasculature forms a highly organised vascular plexus in two dimensions, which simplifies the study of a vascular plexus in its entirety (Fruttiger, 2002; Fruttiger, 2007). Colleagues in my host laboratory have shown similar responses of vessel enlargement in the absence of endoglin in this more readily visualised physiological model (Mahmoud et al., 2010). The enlarged vessel phenotype appears to be caused by a deregulated EC proliferation response, the response that was initially indicated in the dermal model described in this chapter.

In order to investigate the abnormal cell proliferation responses and any TGF-β family signalling defects in endoglin deficient ECs in more detail, the final part of this study was to isolate primary cell lines from the inducible endoglin knockout mice and is described in the next chapter.

Chapter 7. Effect of Endoglin Depletion on Endothelial Cell Phenotypes *In Vitro*

7.1 Introduction

During angiogenesis, ECs organize to form three-dimensional (3D) capillary networks, which encompasses a range of cellular processes including migration, proliferation and differentiation of ECs (Whelan and Senger, 2003). Endoglin, an auxillary receptor for TGF-β, is predominantly expressed on proliferating ECs and is required for efficient angiogenesis *in vivo* (as described in Chapter 3) (Lopez-Novoa and Bernabeu, 2010; Mahmoud et al., 2010). To investigate the effects of endoglin depletion on individual aspects of ECs migration, proliferation and differentiation, a more readily manipulated system was required that could mimic some aspects of EC phenotype *in vitro*. I therefore aimed to derive inducible endoglin deficient endothelial cell lines for functional *in vitro* analyses that would complement the *in vivo* mouse model.

ECs were purified from mouse lungs using antibody-dynabead conjugates (Figure 4.1, & Chapter2). Primary mouse lung endothelial cells (MLECs) were isolated and survived well in culture for at least 4-5 passages. Cells were prepared from *Eng*$^{fl/fl}$ *Cdh5*(PAC)Cre-ER^{T2} mice and the endoglin gene was deleted by treatment with 4-hydroxytamoxifen (4-OHT). (Activation of Cre-ER^{T2} by tamoxifen itself is not effective in vitro as it requires the active metabolite, 4-OHT; conversion of tamoxifen to 4-OHT normally occurs in the liver *in vivo*). I confirmed that endoglin protein was lost in *Eng*$^{fl/fl}$ *Cdh5*(PAC)Cre-ER^{T2} MLECs within 48 hours of 1μM 4-OHT treatment. However, isolation of primary MLECs is very challenging, due to a slow growth rate and early senescence, so these cells are unsuitable for more than 6 passages. I therefore decided to generate conditionally immortalised Eng-iKO lines using the immortomouse (transgenic line H-2K^{b}-tsA58) (Jat et al., 1991). The immortomouse transgene allowed the derivation of longer lasting endothelial cell lines from primary cells. I also used a different transgene to drive Cre expression. RosaCre-ER^{T2} expresses a tamoxifen activated Cre protein in most cells, including ECs, driven by the ubiquitous Rosa26 promoter. All mice used in this part of the study were in C57BL/6 background (approximately N5).

A temperature sensitive Simian Virus 40 Large T Antigen (SV40 TAg) expressed by the immorto allele, allows cell proliferation at 33°C to bypass G1 checkpoint control, increasing the growth rate (Lidington et al., 2002). Returning to 37°C allows orthodox growth at the physiological temperature. Subsequently, to investigate the effect of endoglin-loss on the ability of ECs to undergo the cellular activities required for angiogenesis, 4-OHT was used to deplete endoglin at a time of choice. The resultant conditionally immortalised Eng-iKO ECs were tested in the following assays: MTT assay to measure cell viability, cell counts to monitor proliferation, and a "wound healing" (scratch assay) to measure migration.

7.2 Results

7.2.1 Effect of 4-Hydroxytamoxifen on viability of ECs

Transient exposure to 4-OHT was required to bring about endoglin deletion. However, to identify any confounding effects of 4-OHT on viability and proliferation of ECs, an MTT assay on a mouse skin dermal vascular endothelial cell line (sEND-1) was performed. The MTT assay gives an indication of the metabolic activity of cells which reflects their viability and proliferation rate. Cells reduce the tetrazolium component of MTT into a water insoluble formazan product, resulting in purple crystals being deposited. The reaction occurs only in the mitochondria of healthy cells (van de Loosdrecht et al., 1993). Therefore, cells undergoing apoptosis or in senescence convert less MTT compared to healthy or actively dividing cells.

The MTT assay revealed that there was no apparent effect of 4-OHT treatment on cell viability at doses ranging from 0.1µM to 2.0 µM and that there was no difference between treated and untreated sEND-1 cells (Figure 7.1). This was confirmed statistically, using an unpaired student's t-test (Figure 7.1). These data indicate that these doses of 4-OHT may be safely used for activating Cre recombinase in MLECS derived from *Eng*$^{fl/fl}$ *Cdh5*(PAC)Cre-ER^{T2} and *Eng*$^{fl/fl}$ RosaCre-ER^{T2} mice.

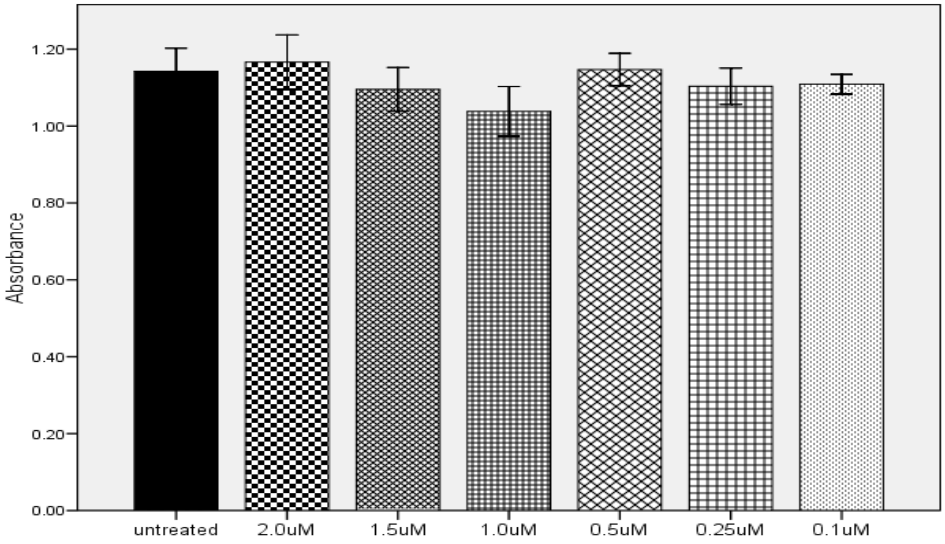

Figure 7.1 The effect of 4-OHT on sEND-1 viability using MTT assay.

Cells were seeded at 5,000 per 96-well plate and incubated for 48 hours with or without 4-OHT (ranging from 0.1µM to 2.0 µM). There are no significant changes in cell viability/proliferation of untreated versus 4-OHT treated sEND-1 ($P > 0.05$, two sample *t*-test, error bars: ±1 standard error (SE); the figure was generated using SPSS Statistics 17 analysis package)

7.2.2 Optimising methods for cell staining

In order to examine the purity of mouse lung ECs and evaluate endoglin depletion in Eng-iKO^{e} MLECs, the methods of immunocytochemistry were optimised (Figure 7.2; Table 2.6).

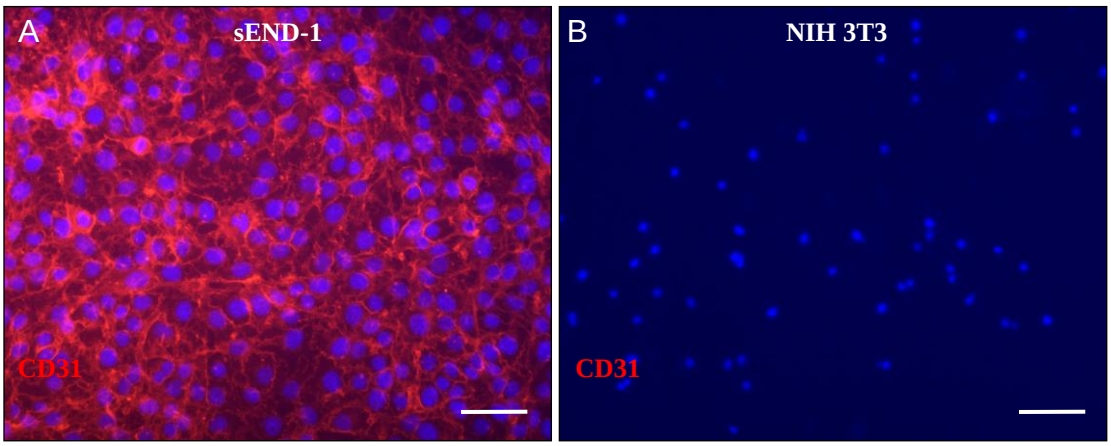

Figure 7.2 Immunocytochemistry staining of sEND-1 and NIH 3T3 (fibroblast cell line) with anti-CD31

A, sEND-1 cell line stained with anti-CD31 and an anti-rat secondary antibody conjugated to Alexa-594 (red);

B, NIH 3T3 cell line stained with anti-CD31 and an anti-rat secondary antibody conjugated to Alexa-594 (red) shown as a negative cell control.
Scale bar = 100µm.

7.2.3 Yield and purity of Mouse Lung Endothelial Cells

To examine the purity of primary MLECs, immunocytochemisty using anti-CD31 was used and the CD31-positive ECs and CD31-negative non-ECs were counted (based on random fields of view in several wells of a multichamber slide to give a total of 6 images per cell line). The percentage of CD31 positive MLECs for each cell type were calculated and summarized in Table 7.1. The purity of MLECs was good enough for subsequent experiments, however the yield was not sufficient for the subsequent functional assays due to the slow growth rate and limited passage number.

Cell type	FOV	Antibody	No. of ECs	No. of NCs	Total	ECs %	Average
Control	1	CD31	49	3	52	94.2%	92.9%
	2	CD31	40	5	45	88.9%	
	3	CD31	51	5	56	91.1%	
	4	CD31	50	5	55	90.9%	
	5	CD31	65	4	69	94.2%	
	6	CD31	50	1	51	98.0%	
Mutant	1	CD31	58	5	63	92.1%	94.0%
	2	CD31	35	3	38	92.1%	
	3	CD31	30	3	33	90.9%	
	4	CD31	62	2	64	96.9%	
	5	CD31	43	1	44	97.7%	
	6	CD31	34	2	36	94.4%	

Table 7.1 Summary of MLECs purity based on CD31 staining.
Note: genotype of control and mutant cells was *Eng*$^{fl/fl}$ and *Eng*$^{fl/fl}$ *Cdh5*(PAC)Cre-ER^{T2} respectively. Abbreviation: FOV = field of view, ECs = CD31 positive cells, NCs = CD31 negative cells.

7.2.4 The lowest effective dose and timing of 4-OHT treatment for endoglin deletion on MLECs

To determine the lowest effective dose and optimal time of 4-OHT treatment to efficiently bring about endoglin gene deletion in *Eng*$^{fl/fl}$*Cdh5*(PAC)Cre-ER^{T2} MLECs, a series of titration experiments with different time points were performed (Table 7.2). These results indicate that increasing dose and timing of 4-OHT treatment do lead to an increasing percentage of cells with endoglin gene deletion. However, 0.1µM was too low to generate efficient endoglin deletion even after 9 days. Therefore, based on this preliminary data and the published data (Loonstra et al., 2001), I used 1µM 4-OHT to treat primary MLECs (*Eng*$^{fl/fl}$ and *Eng*$^{fl/fl}$ *Cdh5*(PAC)Cre-ER^{T2}) over 48 hours. This was sufficient to activate lacZ expression from the Rosa26R reporter transgene (Figure 3.2), which was shown by X-gal staining (Figure 7.3). This experiment was used not only to test the induction efficiency of Cre recombinase, but also to indirectly check the purity of MLECs. The majority of cells are blue cells, which are Cre induced ECs. Figure 7.4 shows almost 100% of Eng gene depletion in MLECs. Therefore, these results show that the dose of 1µM 4-OHT for 48 hours leads to efficient Cre activation, and Endoglin gene deletion (according to the principle shown in Figure 1.6). This protocol for 1µM 4-OHT treatment for 48 hours was used for all subsequent experiments.

Immunostain	**Dose of 4-OHT**	**Time course of treatment**	**Approx. efficiency of endoglin gene deletion**
Anti-endoglin + Alexas-594 IgG	0.05 µM	5 days	30%
		9 days	50%
	0.1 µM	5 days	40%
		9 days	60%
Anti-endoglin + Alexas-594 IgG	1.0 µM	2 days	~100%

Table 7.2 Titration of 4-OHT to optimise endoglin gene deletion in *Eng*$^{fl/fl}$ *Cdh5*(PAC)Cre-ER^{T2} MLECs.

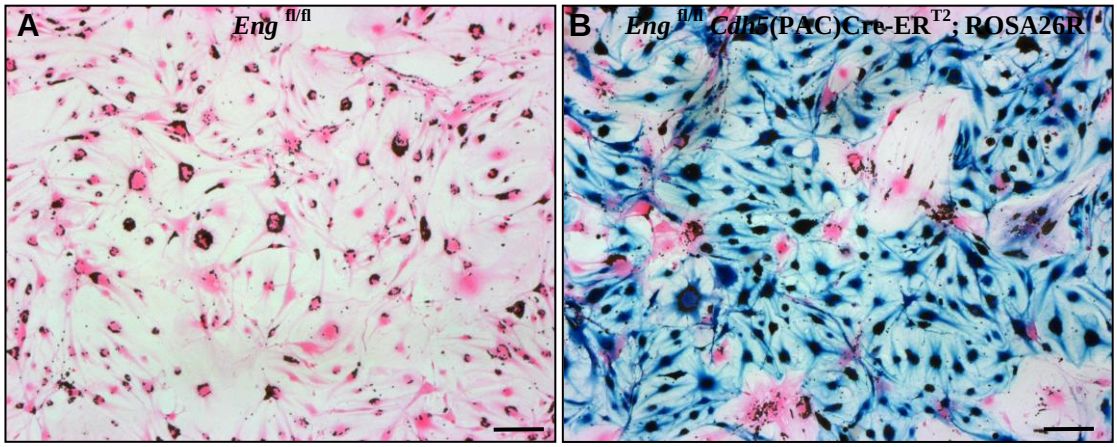

Figure 7.3 X-gal staining on primary mouse lung endothelial cells carrying the Rosa26R Cre reporter

A, X-gal staining on *Eng* $^{fl/fl}$ MLECs with 1µM 4-OHT treatment for 48hrs, there are no blue cells detected without Cre activation.

B, X-gal staining on *Eng* $^{fl/fl}$ *Cdh5*(PAC)Cre-ER^{T2} ROSA26R MLECs with 1µM 4-OHT treatment for 48 hours, there are blue cells present following Cre activation. Scale bar = 100µm.

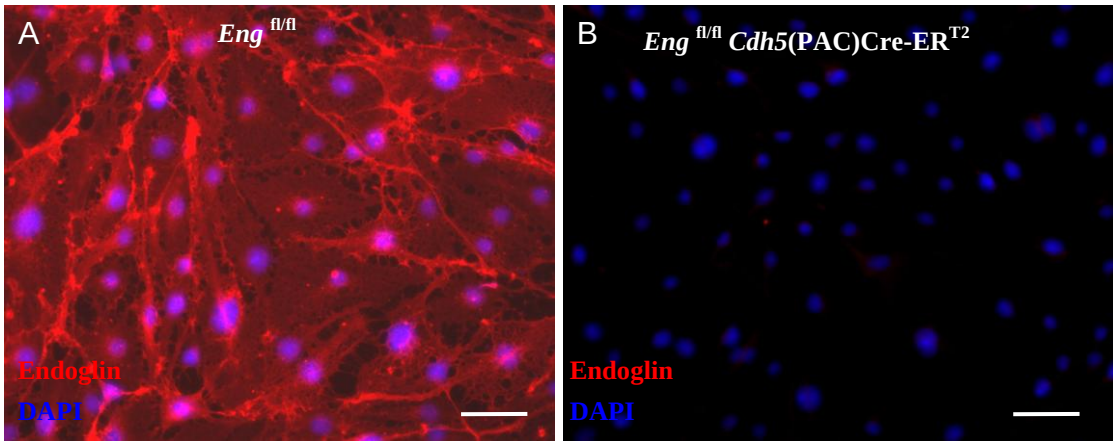

Figure 7.4 The efficiency of Eng deletion in primary MLECs is detected using immunocytochemistry.

A, The expression of endoglin on primary *Eng* $^{fl/fl}$ MLECs treated with 1µM 4-OHT is detected by anti-endoglin and an anti-rat secondary antibody conjugated to Alexa-594 (positive cells in red, nuclei stained with DAPI in blue).

B, The absence of endoglin on primary *Eng* $^{fl/fl}$ *Cdh5*(PAC)Cre-ER^{T2} MLECs Treated with 1µM 4-OHT is detected by anti-endoglin and an anti-rat secondary antibody conjugated to Alexa-594 (nearly 100% cells show endoglin depletion, nuclei stained with DAPI in blue). Scale bar = 100µm.

7.2.5 Derivation of novel conditionally immortalised cell lines using Immortomouse

In order to overcome the shortcomings of primary ECs such as early senesence and slow growth rate, we took advantage of the immortomouse transgene to generate conditionally immortalized MLEC cell lines. The cell isolation protocol was exactly same as that used for the isolation and purifying of primary MLECs (Chapter 2, Figure 2.1). As explained above, the Immorto allele, allows cell proliferation at 33°C to bypass G1 checkpoint control, increasing the growth rate. In addition, interferon-gamma (IFN-γ, 20U/ml) was used to stimulate Immorto gene expression and was removed before returning to 37°C to allow orthodox growth at the physiological temperature, where cells regained checkpoint control and assumed a growth phenotype similar to primary ECs.

To identify the purity of these conditionally immortalized MLECs, immunocytochemistry staining was performed and also morphology of MLECs was shown in Figure 7.5. As similar results were obtained using both anti-endoglin and anti-CD31 antibodies, anti-CD31 antibody staining was subsequently used for determining the degree of EC purity (Figure 7.6). Purity of higher than 95% ECs was considered sufficient for the subsequent functional assays.

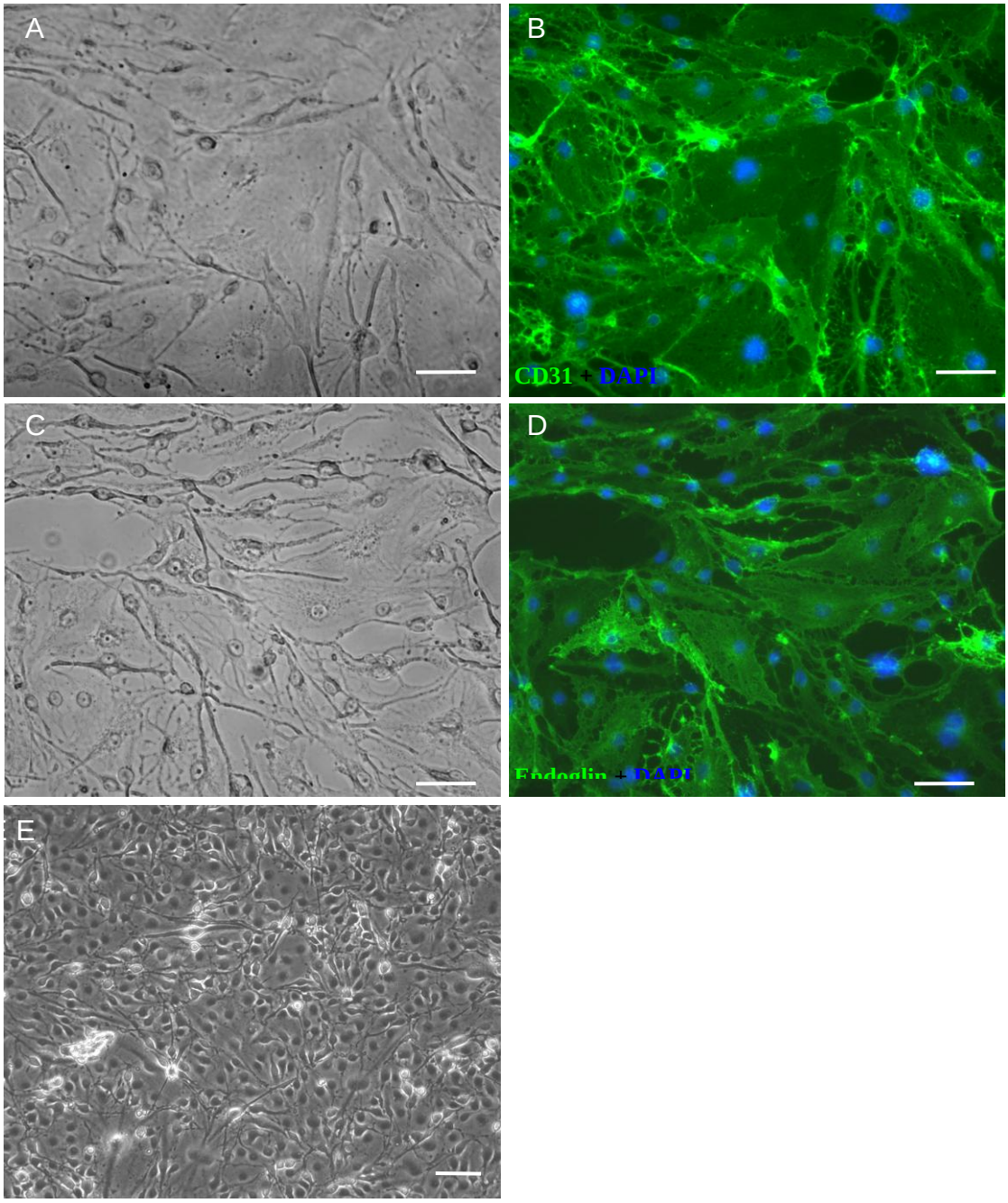

<u>Figure 7.5</u> Immunocytochemistry staining and morphology of the purified endothelial cell population.

A & C show EC morphology and phenotype through phase contrast images; the nuclei are elliptical or round and located in the centre of cell body some cells are spindle shaped in the relatively sparse cultures.

B & D confirm EC phenotype and purity through immunofluorescence staining of EC markers CD31(B) and endoglin(D), both present on the EC surface and stained green (Alexa-488). The nuclei of all cells can be seen with DAPI in blue.

E, MLECs show typical cobblestone morphology of ECs at higher density.
Scale bar = 100 µm.

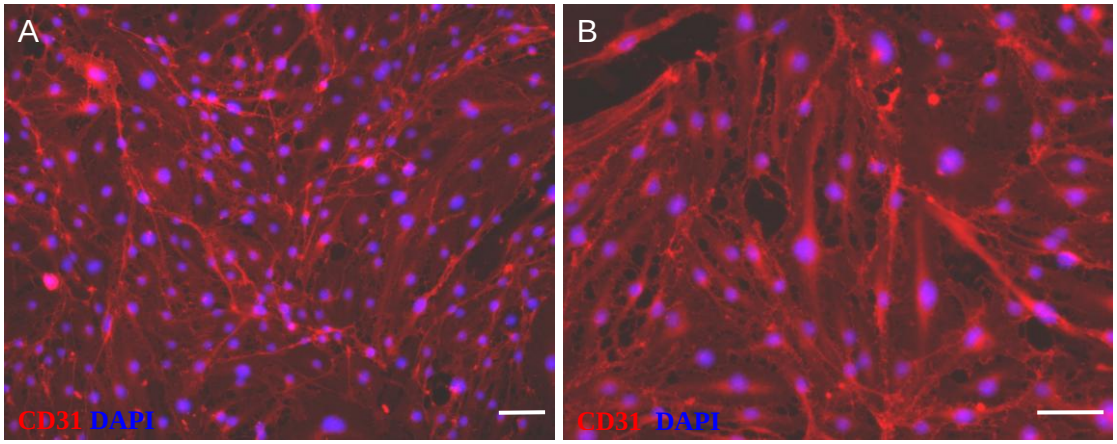

Figure 7.6 Purity of immortalized MLECs using immunocytochemistry staining with anti-CD31.

A&B confirm the purity of immortalized MLECs through fluorescence staining with anti-CD31. To analyse cell purity, three fields of view at magnification of x10 were analysed using Image J software and 4 replicates were performed. The nuclei of all cells can be seen with DAPI in blue.

Scale bar = 100µm.

7.2.6 Accelerated growth rate of immortalized Mouse LungEndothelial Cells

Having generated pure MLEC populations, it was important to test whether the Immorto allele helps the cells incubated at the lower temperature in the presence of IFN-γ to proliferate more quickly. A simple cell count over 7 days showed that from a similar seeding density, the number of cells at 37°C increased by approximately 20%, whereas at 33^{o}C the number of cells increased by around 80% (Figure 7.7). In this way, the continuous expression of immorto gene at the lower temperature permitted the yield of the conditionally immortalised MLECs to be increased for subsequent in vitro analyses.

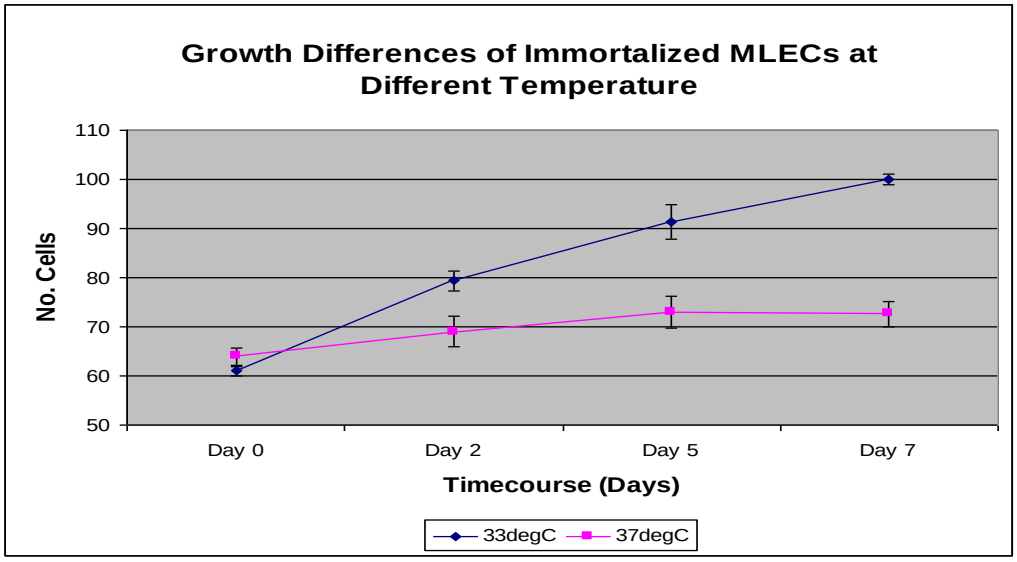

Figure 7.7 Cell count of immortalised MLECs shows different growth rate at different temperatures.
Cell counts show the proliferation rates of immortalised MLECs at different temperatures. Over 7 days cell counts were taken from phase contrast pictures of the same area of 3 different wells from both 37°C, and 33°C + IFN-γ incubation. This figure was generated by Dave Burn during his BSc project (which I supervised).

7.2.7 Optimising methods for cell PCR

In order to examine the DNA level of Eng gene depletion, PCR conditions were optimized first using the primary MLEC and wild type sEND-1 cell line (Figure 7.8). The minimal cell number required to detect PCR products corresponding to the Eng gene was found to be approximately 50 cells. In addition, following this protocol, exons 5 and 6 of the Eng gene were deleted in 4-OHT treated *Eng*$^{fl/fl}$ Rosa-CreER^{T2} MLECs (Figure 7.9).

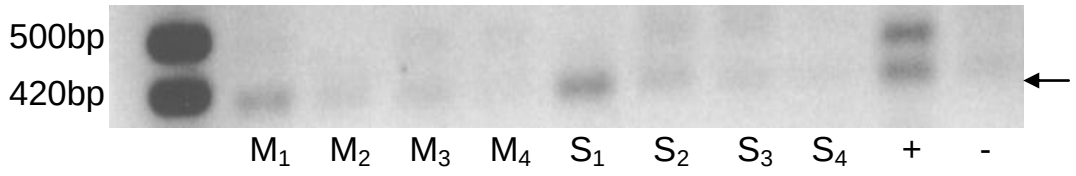

Figure 7.8 Determining the minimal cell number required for genotyping cells by PCR
This PCR on genomic DNA isolated from ECs used primers F6 and R7 (Table 2.1) and shows a clear product for endoglin corresponding to the wild type allele (arrow) in both MLEC (M) and sEND-1(S) cells. The cell number used to prepare template

DNA was critical. Genotyping was possible from 50 MLEC cells and 50 sEND-1 cells. M1 and S1 samples contain DNA from 50 cells, M2 and S2 samples contain DNA from 5 cells, M3 and S3 samples contain DNA from 0.5 cell, M4 and S4 samples contain DNA from 0.05 cell. PCR products are 430bp for WT and 500bp for Eng^{fl} allele. Positive control (+) is a PCR from a standard preparation of DNA from a mouse ear clip (genotype is $Eng^{fl/+}$) and negative PCR control (-) used water as a template in place of DNA.

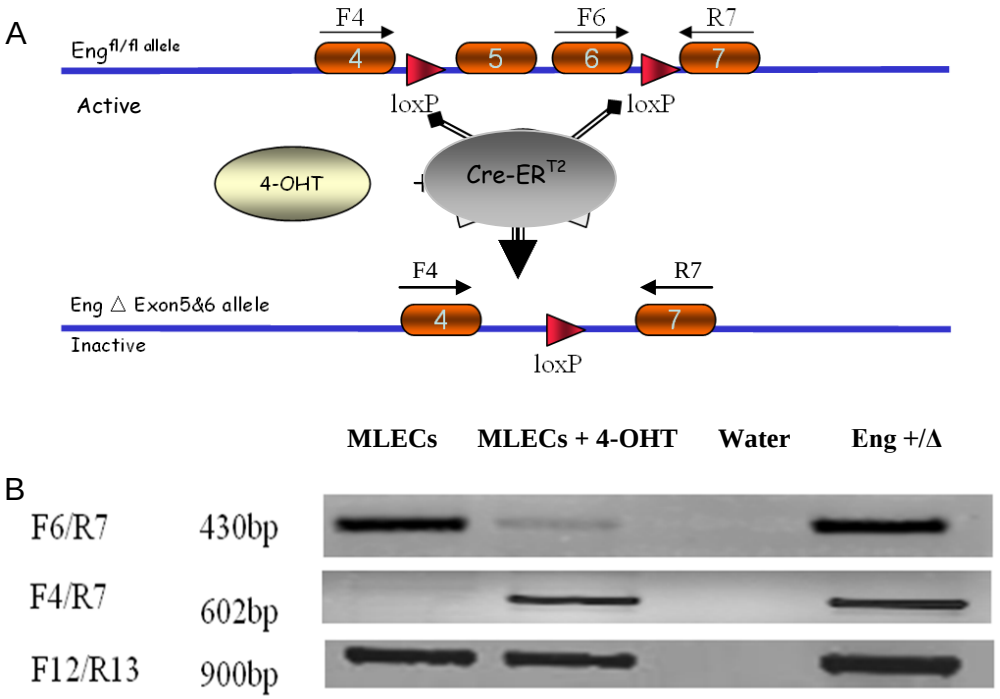

Figure 7.9 Endoglin gene depletion at the DNA level identified by cell PCR

A, a cartoon shows the position of the primers over the floxed endoglin allele and the principle of endoglin gene depletion.

B, Three PCR reactions using primers F6 & R7, F4 & R7, and F12& R13 shows PCR products for three different regions of the endoglin gene (the primers and PCR product sizes are also shown in Table 2.1). Lanes 1 & 2 show PCR products from MLEC DNA isolated from untreated $Eng^{fl/fl}$ Rosa-$CreER^{T2}$ cells (lane 1) and DNA isolated from similar cells following 4-OHT treatment (lane 2). Lane 3 is a negative control (no DNA template) whereas lane 4 contains positive control (from an earclip of Eng +/Δ mouse) DNA for a deleted endoglin allele. Note that the size of DNA sequence flanked by LoxP sites is approx. 2kbs. Therefore, primer pair F4/R7 does not generate a product with the conditions used. PCR using primers F6 and R7 detects the floxed allele, which is present in the untreated cells (lane 1) but at reduced levels in the 4-OHT treated MLECs (Eng-iKO MLECs). In contrast, PCR using primers F4 and R7 detects the Eng delete allele, which is present in MLECs only after 4-OHT treatment (lane 2). There are clear PCR products in Eng-iKO and control MLECs using

primers F12 and R13 that detect DNA in both endoglin floxed and delete alleles. Template DNA used in this PCR was prepared from 50 cells, as optimized in figure 7.8. This MLECs PCR figure is courtesy of Rachael Redgrave.

7.2.8 Efficiency of endoglin depletion on immortalized MLECs

Immorto-MLEC cells were tested for the loss of endoglin protein following 4-OHT treatment by immunocytochemistry. Endoglin protein was not detected in the *Eng*$^{fl/fl}$ RosaCre-ER^{T2} cell lines following 4-OHT treatment (Figure 7.10). This shows that 4-OHT effectively generated Eng null cell lines, which can be used in subsequent experiments.

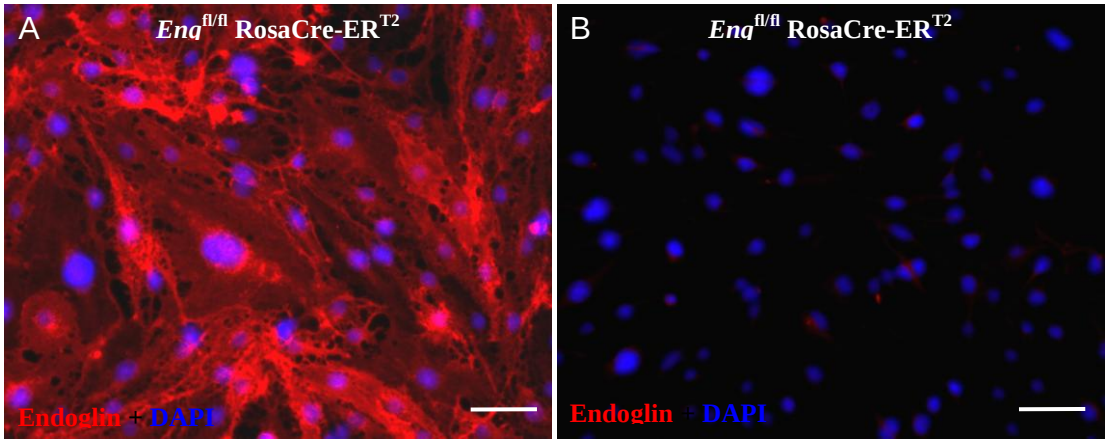

Figure 7.10 Endoglin protein was efficiently depleted in *Eng*$^{fl/fl}$ RosaCre-ER^{T2} immortalized MLECs with 1 µM 4-OHT treatment for 48 hours.

A, Nearly 100% cells expressed endoglin (anti-endoglin and an anti-rat secondary antibody conjugated to Alexa-594 in red) in *Eng*$^{fl/fl}$ RosaCre-ER^{T2} MLECs without 4-OHT treatment;

B, There was almost 100% deletion of endoglin (nuclei with DAPI staining in blue) in *Eng* $^{fl/fl}$ RosaCre-ER^{T2} MLECs following 1µM 4-OHT treatment for 48 hours. Scale bar = 100µm.

7.2.9 Effect of endoglin depletion on viability of Eng-iKO MLECs (MTT Assay)

To investigate the effect of endoglin depletion on viability of MLECs, an MTT assay was performed (as described in Figure 2.2). There was no significantly reduced viability and or proliferation found in mutant MLECs compared with control MLECs (Figure 7.11, P = 0.341). As the MTT assay measures a combination of cell viability and cell proliferation properties, a cell counting method to investigate cell proliferation was performed as a separate analysis (Section 7.2.10).

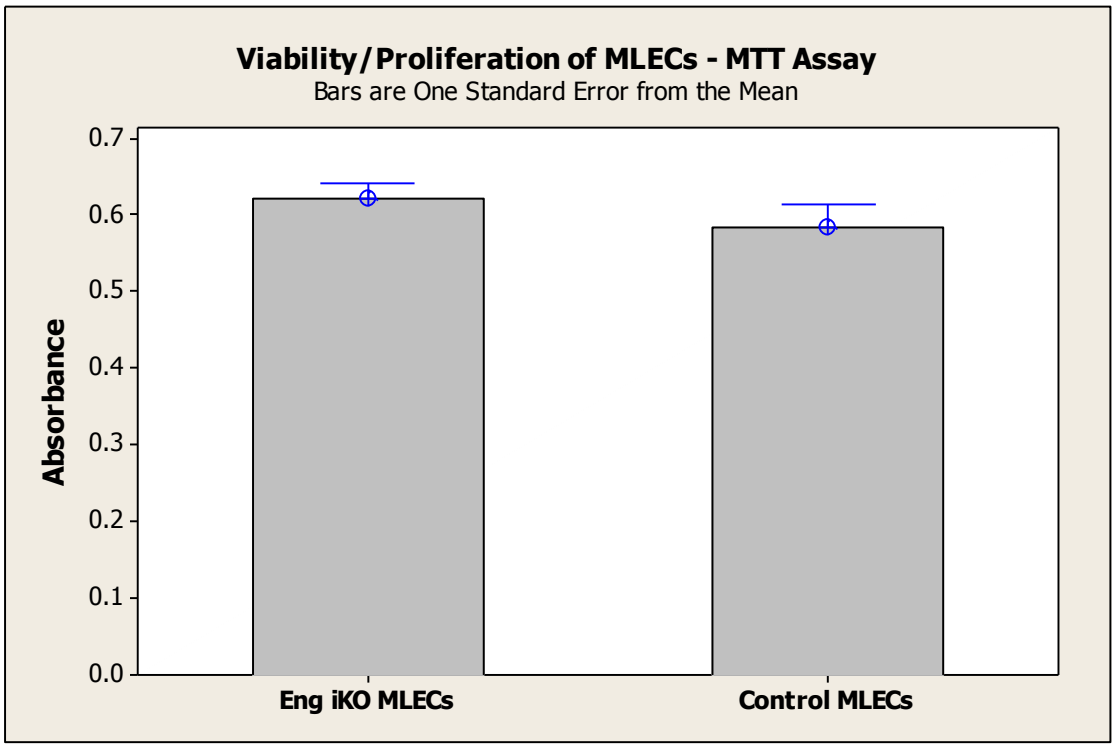

Figure 7.11 A representative MTT assay demonstrates no influence of endoglin on the viability of MLECs

There is no significant difference in viability/proliferation between Eng-iKO MLECs and control MLECs (Two samples t-test, T-Value = 0.98, P-Value = 0.341, n = 10).

Qualitatively similar results were found in three independent MTT assays.

7.2.10 Effect of endoglin depletion on proliferation of Eng-iKO MLECs using cell number counting

To test the effect of endoglin depletion on proliferation of Eng-iKO MLECs, an approach of simple cell number counting was used (as described in Figure 2.4). Overall, there were similar growth rates in both Eng-iKO MLECs and control MLECs (Figure 7.12 A). I observed increasing cell growth rate in the first 24 hr, decreasing growth rate in the next 24 hr, and then replication of these cycles during alternate days (Figure 7.12 B). It appears that cells stop growing after 64 hours and some cells also migrate out of the field of view. In addition, there is a slightly decreased proliferation rate in Eng-iKO MLECs compared with control MLECs during the 80 hr period, but this was not statistically significant (Figure 7.13). This result indicates that endoglin is not important for EC proliferation in MLECs cultured in microvascular endothelial cell growth medium MV2 (Promocell)

including a variety of growth factors.

<u>Figure 7.12</u> The growth rate of Eng-iKO MLECs and Control MLECs in the period of 80 hours.

A, There are similar growth rate and trends between Eng-iKO MLECs and Control

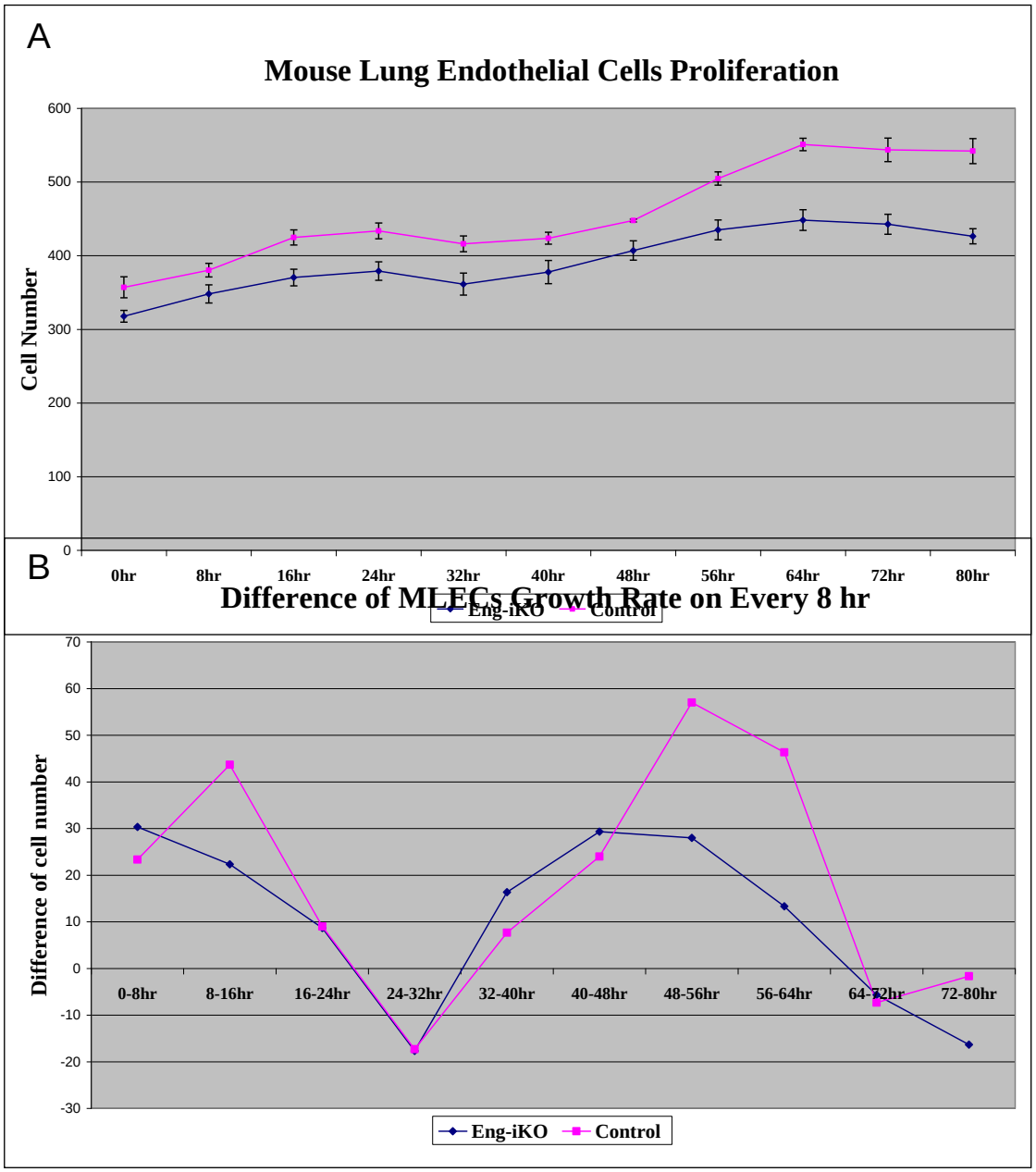

MLECs, the graph shows increasing cell growth rate in the first 24 hours, a reduced growth rate in the next 24 hours, and then it increases again.

B, shows the difference of MLECs growth every 8 hours within 80 hours. In the periods of 24-32 hours, 64-72 hours and 72-80 hours, there are negative growth rates. Cell confluence was not reached within this 80-hour observation period.

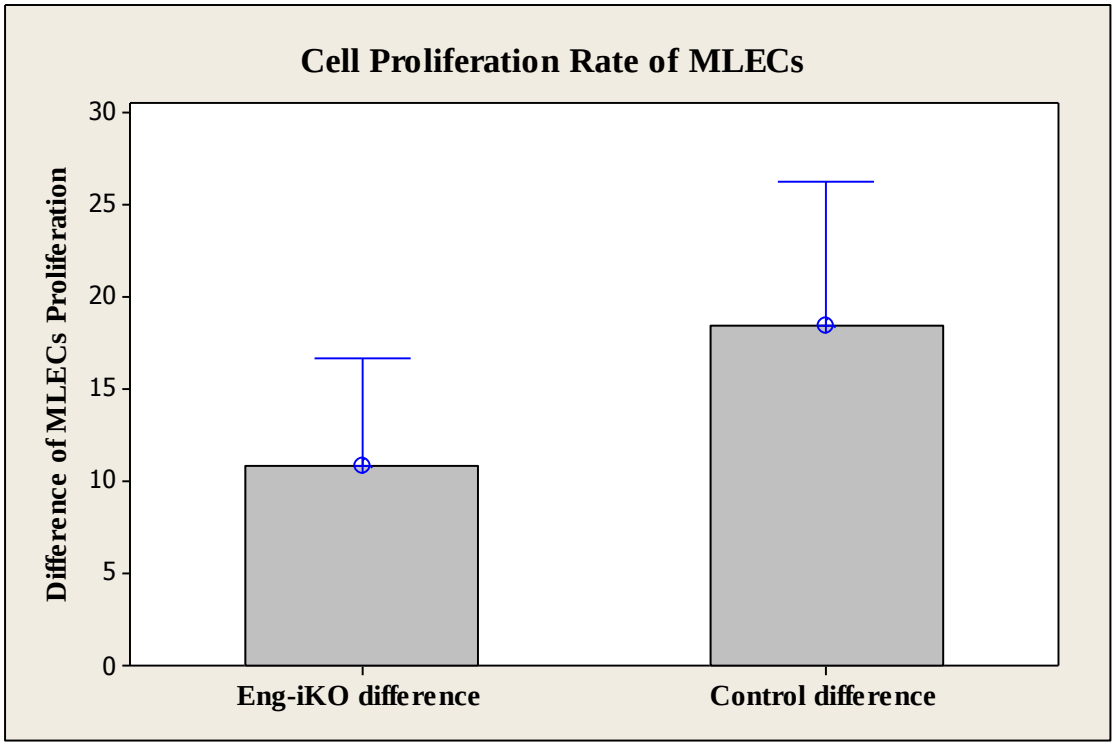

Figure 7.13 No significant difference in cell proliferation rate between control MLECs compared and Eng-iKO MLECs

There is no significant difference between control MLECs (18.5 ± 7.8) compared with Eng-iKO MLECs (10.9 ± 5.8) (T-Value = -0.78, P-Value = 0.446, n = 10). Bars are one standard error from mean.

7.2.11 Effect of endoglin depletion on migration of Eng-iKO MLECs (Scratch Healing Assay)

The migration of MLECs in response to endoglin depletion during a period of 28 hours was investigated in an in vitro monolayer wound-healing model (as described in Figure 2.3). The initial wound in the MLECs monolayer culture was scratched using a trimmed cell scraper (approx. 1.5-2 mm width). The effect of endoglin on the EC migration of the wound-healing process obtained in one representative experiment is shown in Figure 7.14. The quantification of the wound-healing process was judged by the following formula: Healed area= (area of original wound – area of wound during healing)/area of original wound. There appeared to be a slightly faster migration rate in control MLECs compared with Eng-iKO MLECs during the period of 28-hour wound healing (Figure 7.15). However statistical analysis showed there was no significant difference in the average percentage of healed wound area between control MLECs and Eng-iKO MLECs (Figure 7.16, P =

0.320). Qualitatively similar results were found in 3 replicates of wound-healing assays. This result indicates endoglin is not important for endothelial cell migration in MLECs cultured in microvascular endothelial cell growth medium MV2 (Promocell) including a variety of growth factors.

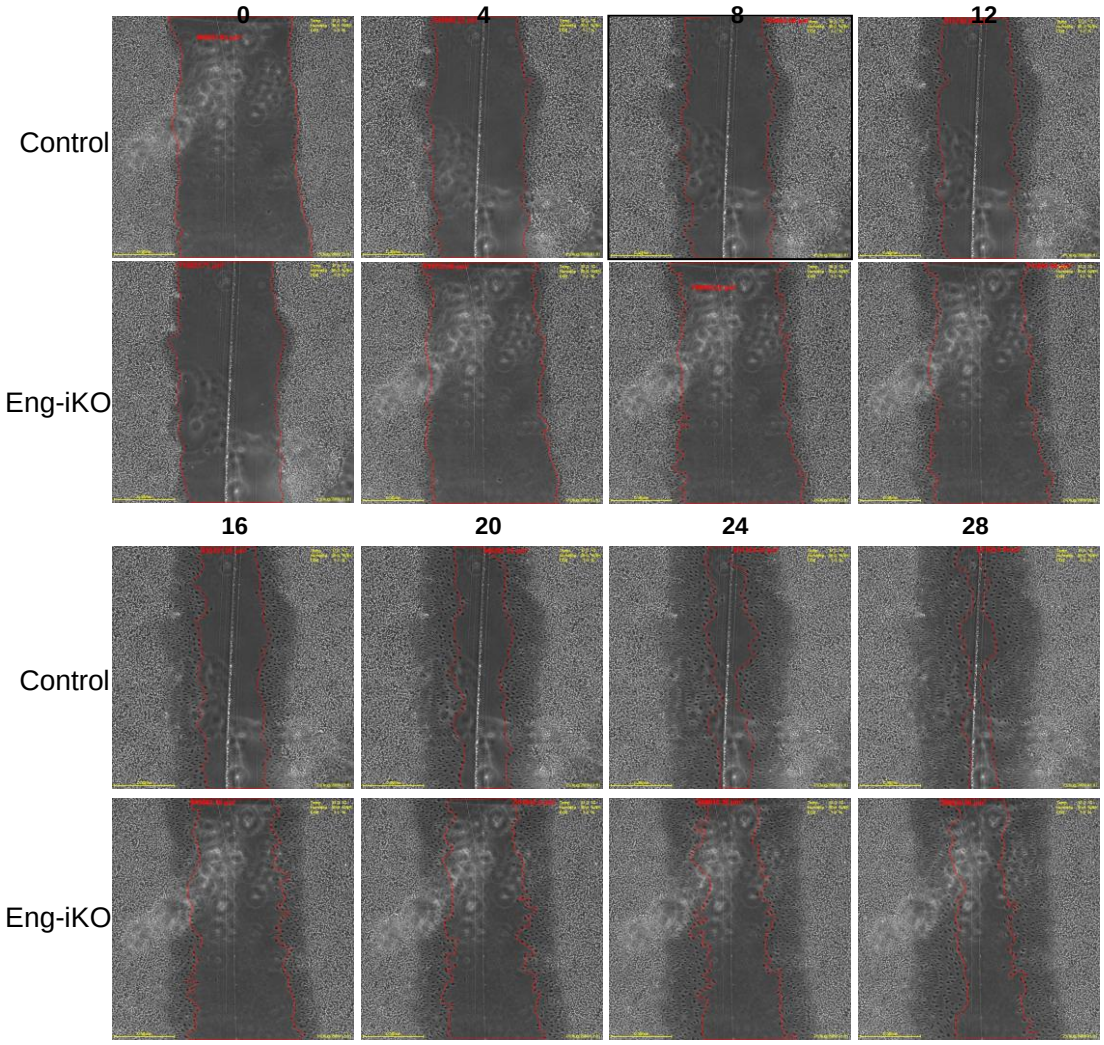

<u>Figure 7.14</u> Influence of Eng loss on MLECs migration using a scratch assay
The original images were taken every 2 hours and representative images selected at 4- hour time intervals are shown in the figure. The migrating process of Eng-iKO MLECs and control MLECs over 28 hours is indicated by the area outlined with red lines which marks the migrating cell front. The wound region was measured using Axiovision software, and the rate of closure of the wound was calculated from the difference between measurements from two time points. These images indicate that there is no significant difference in healing rate between control MLECs and Eng-iKO MLECs. See also Figure 7.16.

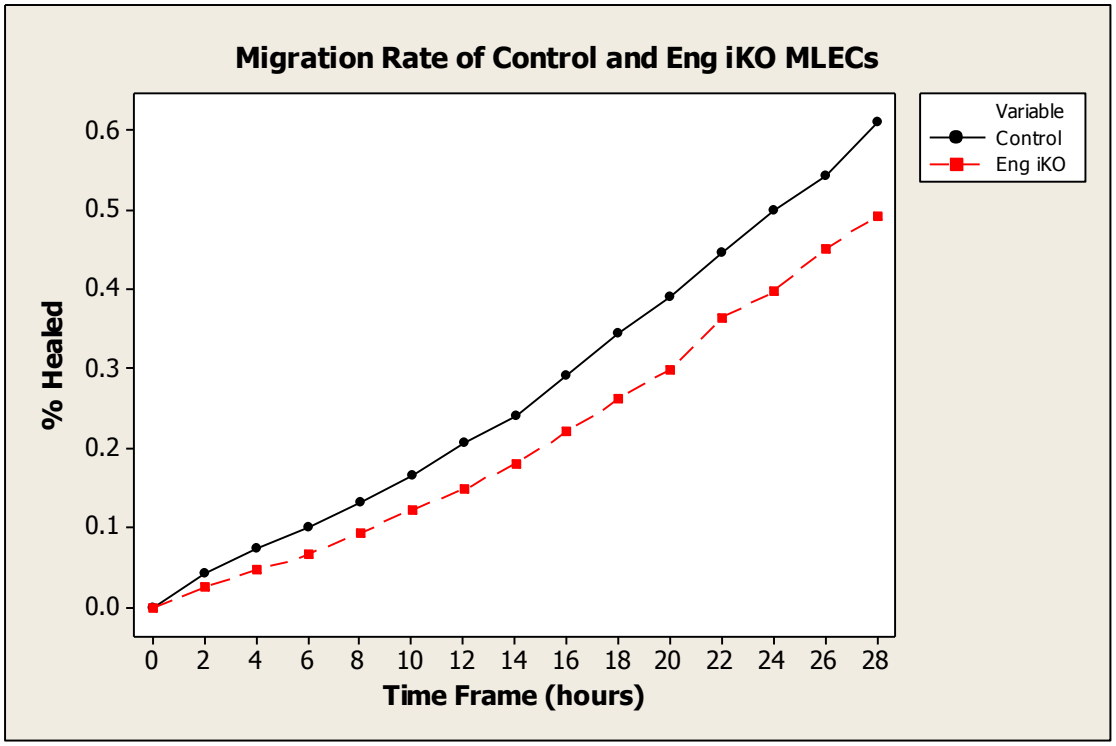

Figure 7.15 Cell migration rate of control MLECs and Eng- iKO MLECs during the period of 28 hours wound healing

It appears that there is a higher migration rate in control MLECs compared with that in Eng-iKO MLECs. Each dot represents average migration rate from three measurements and calculations of three fields of view within wound area.

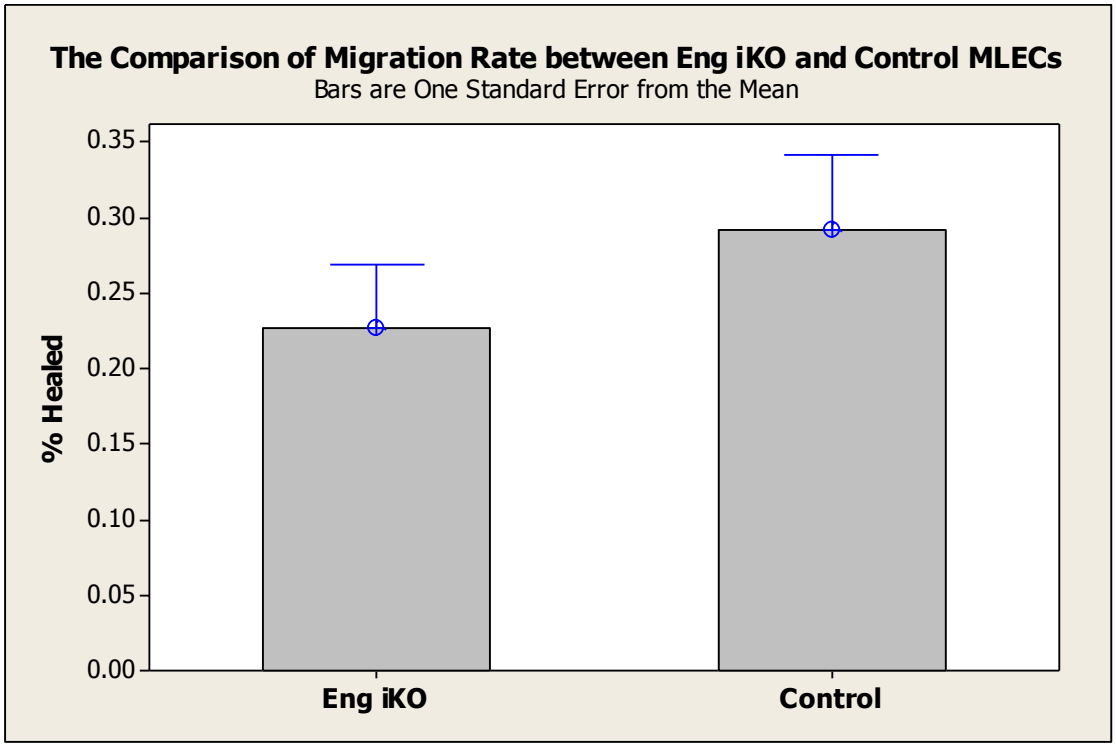

Figure7.16 Cell migration rate in Eng-iKO MLECs is not significantly different from control MLECs

There is no significant difference in percentage of healed wound area between Eng-iKO MLECs and control MLECs during the healing period of wound (Two samples t-test, T-Value = 1.01, P-Value = 0.320, n = 14).

7.2.12 Effect of endoglin depletion on viability of MLECs following titration of growth factors

To investigate whether a variety of growth factors in microvascular endothelial cell growth medium MV2 (Table 2.5) could mask any effect of endoglin depletion on viability of control and Eng-iKO MLECs, additional MTT assays were performed. Eng-iKO and control MLECs were cultured with growth medium, with serially diluted growth factors for 24 and 48 hours. In this experiment, there were significant differences in viability between Eng-iKO MLECs and control MLECs even in full medium (Figure 7.17 A and Figure 7.18 A). This difference increased at 1/4 and 1/8 dilutions. However, the viability of both Eng-iKO MLECs and control MLECs decreased as the growth factors were titrated and this was particularly evident at 1/16 and 1/32 dilutions (Figure 7.17 B and Figure 7.18 B). A significant drop in viability of control cells was firstly seen at 1/4 dilution compared with full medium. These results suggest the depletion of endoglin does influence the viability of MLECs, and that this may be partially rescued by growth factors present in the medium.

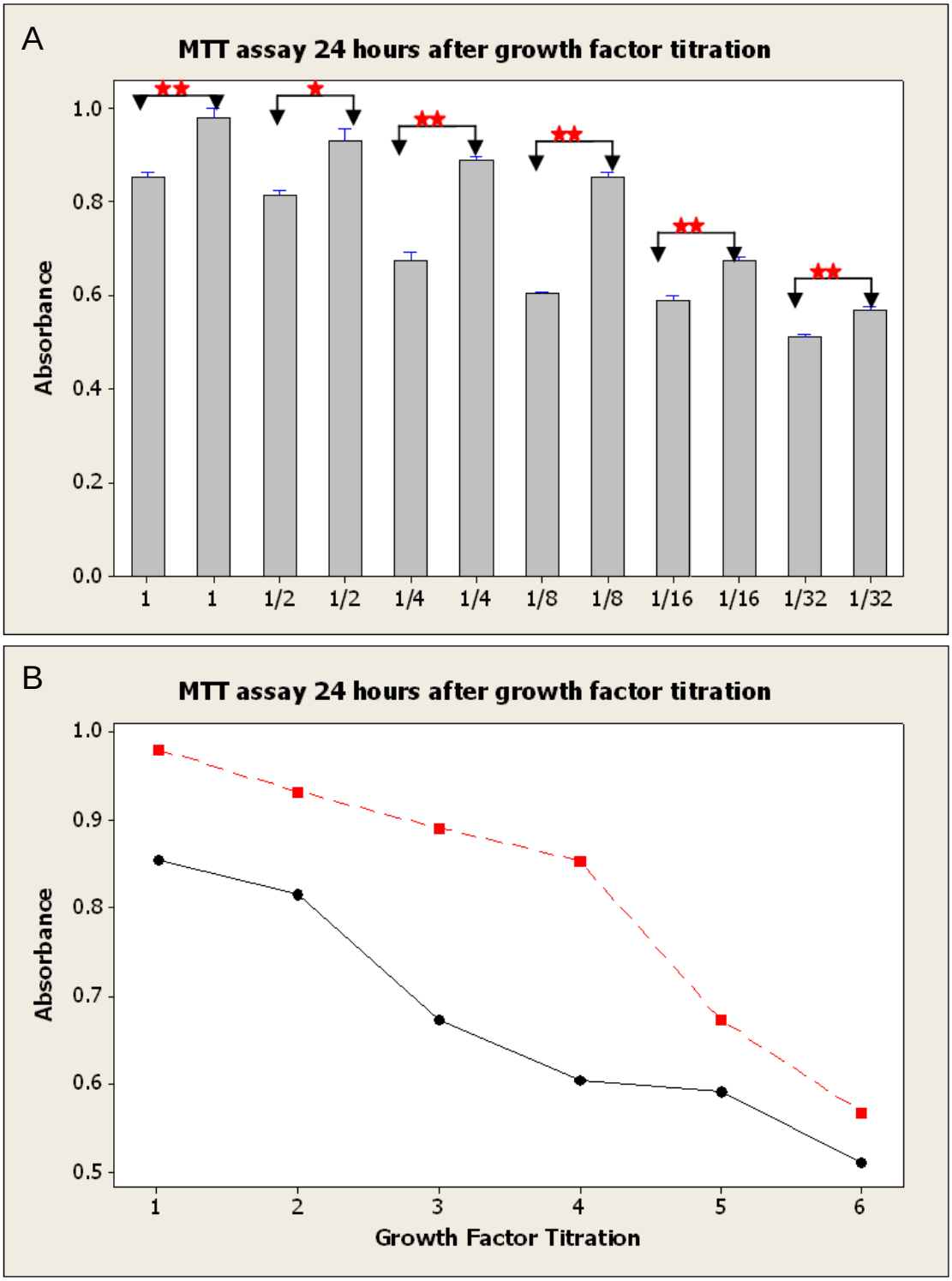

Figure 7.17 A loss of endoglin reduces viability of MLECs grown in normal and growth factor-reduced medium for 24 hours.

A, MTT assay readings for Eng-iKO MLECs and control MLECs grown in normal and growth factor-reduced medium for 24 hours. Growth factor supplement was titrated in 2-fold dilution steps from 1/2 to 1/32 of that used to prepare normal microvascular growth medium MV2 (Table 2.5). There are significant differences in viability between the viability of Eng-iKO and Control cells at all dilutions (Two samples t-test, n = 8, ★ indicates P < 0.001, ★★ presents P <

0.000).

B, Same MTT assay data as in A represented in graph format. Red squares and black dots represent Eng-iKO MLECs and control MLECs respectively.

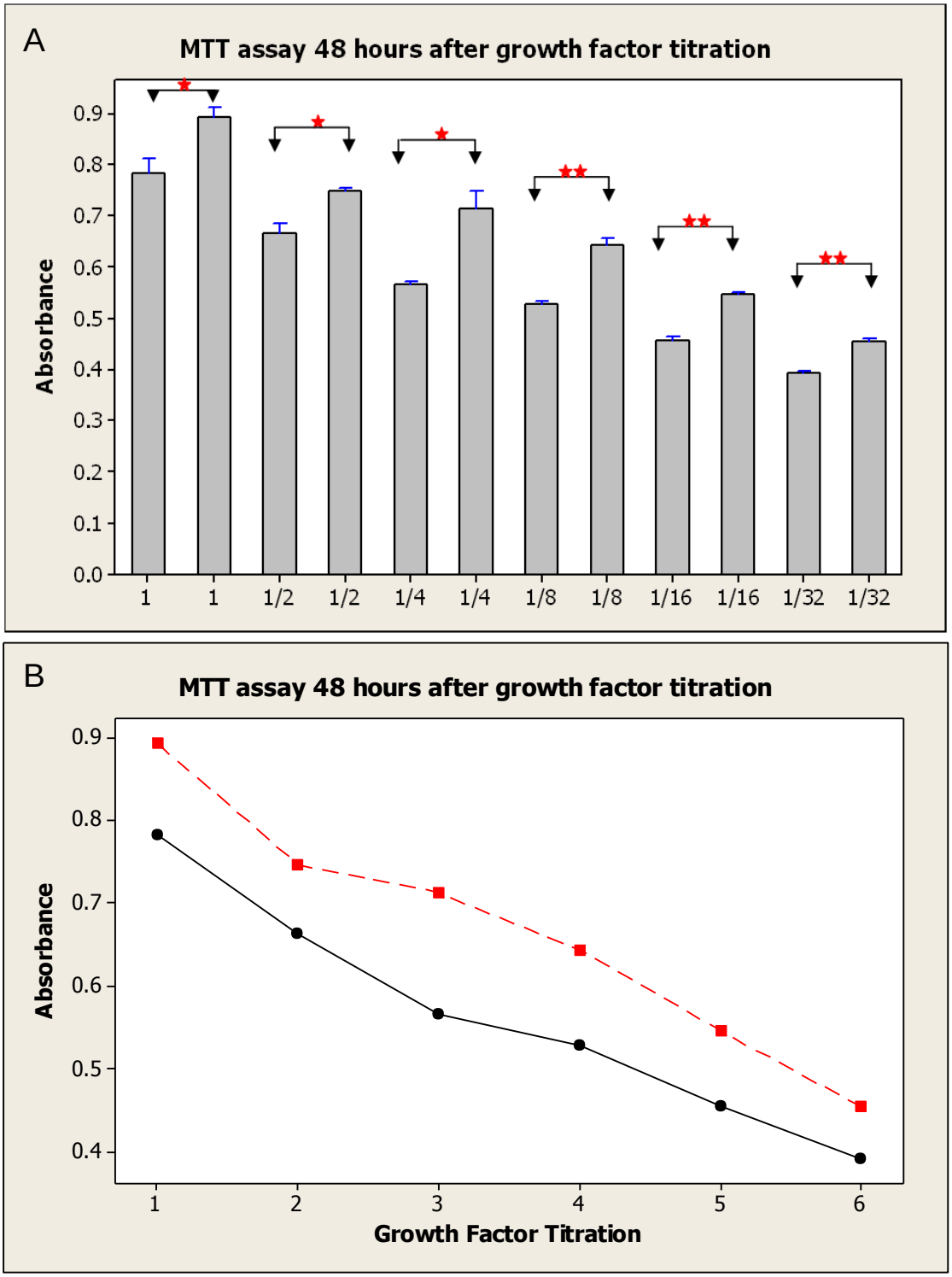

Figure 7.18 A loss of endoglin reduces viability of MLECs grown in normal and growth factor-reduced medium for 48 hours.

A, MTT assay readings for Eng-iKO MLECs and control MLECs grown in normal and growth factor-reduced medium for 48 hours. Growth factor supplement was

titrated as in Figure 7.17 (Two samples t-test, n = 8; ★ indicates P < 0.001; ★★ presents P < 0.000).

B, The same data as in A represented in graph format. Red squares and black dots represent Eng-iKO MLECs and control MLECs respectively.

7.2.13 Effect of endoglin depletion on cytoskeleton of MLECs

The cytoskeleton generates contractile and stretching forces existing at equilibrium in normal endothelium. However, cytoskeletal rearrangements and actinomyosin contractility (formation of paracellular gaps between ECs) are coupled to vascular endothelium dysfunction (Garbi et al., 1990; Miettinen et al., 1994; Lum and Malik, 1996; Dudek and Garcia, 2001; Birukova et al., 2004). In addition TGF- β signalling is known to regulate re-arrangements of the cytoskeleton. Therefore, to investigate the effect of endoglin depletion on the actin cytoskeleton of MLECs, fluorescent-phalloidin staining was performed. There seems to be no difference between overall cell shape between Eng-iKO MLECs and control MLECs. In addition, actin filaments stained with a phalloidin-FITC conjugate indicates there are similar cytoskeletal structures in Eng-iKO MLECs and control MLECs. However, I found the formation of dense peripheral bands in between Eng-iKO MLECs (Figure 7.19). These findings suggest that loss of endoglin does not affect the distribution of actin cytoskeleton network on MLECs, but contributes to the formation of dense paracellular bundles. It would be interesting to replicate this experiment and investigate this phenotype in more detail. The recent purchase of a super resolution microscope by Newcastle University may also help to gain further information.

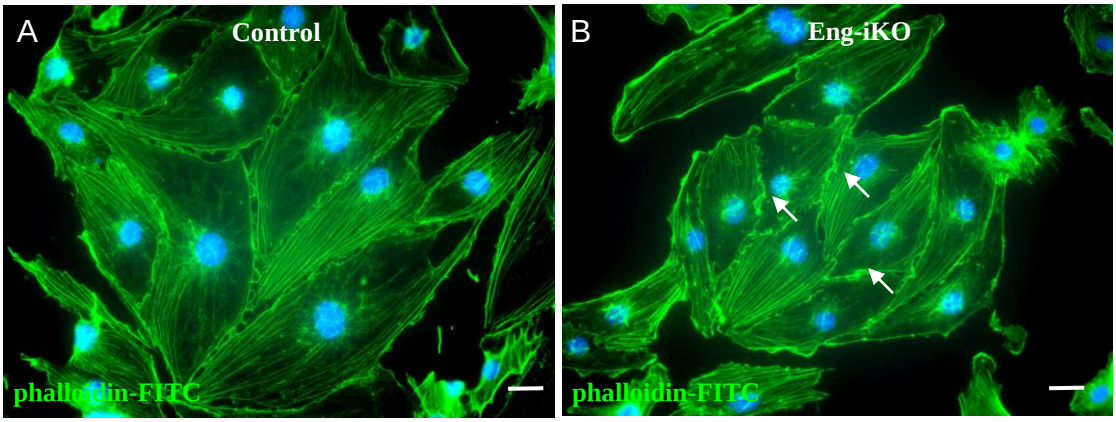

Figure 7.19 Comparison of actin cytoskeleton of Eng-iKO and control MLECs.

MLECs are stained with phalloidin-FITC (green) conjugate and nuclei stained with DAPI (blue). The distribution of actin filaments seems to be similar between control MLECs (A) and Eng-iKO MLECs (B), but the dense paracellular bands (arrows) are formed in between Eng-iKO MLECs. Scale bar = 200μm.

7.3 Discussion

7.3.1 Challenges of purifying and passaging primary endothelial cells

Endothelial cells play a major role in tissue homeostasis, as well as diverse pathologies, such as cancer, arthritis and atherosclerosis (Folkman, 1995; Griffioen and Molema, 2000), therefore, to understand the biology of ECs, characterization of this cell population is highly desirable. Cultured ECs are indispensable tools for functional assays and some signalling pathway studies, even though these may not completely mimic the phenotype of tissue ECs because the proper microenvironment is lacking. In 1973, ECs derived from human umbilical veins were first successfully cultured *in vitro*, since then, a substantial number of vascular cells have been cultured. However, it is fairly challenging to obtain sufficient purified primary ECs for subsequent functional studies.

First of all, the protocol used to isolate mouse lung ECs in this study required multiple steps and considerable optimisation. Therefore, the critical criteria have been emphasized in the final protocol (described in Chapter2). For example, trimming off obvious bronchi and connective tissue is critical to avoid non-EC contamination; mouse lung lobes are rapidly minced as small as possible and subsequently digested enzymatically once with collagenase at 37 ^{o}C for exactly 1 hour; MLECs in the single-cell suspension are labelled with CD31 antibody combined with magnetic beads using approximate 5 beads per target ECs; in order to obtain "pure" ECs, a second (or even a third) cell sorting is required using anti-CD102 conjugated beads. This proved to be a really challenging technique.

Secondly, ECs make up a minor population of cells in a tissue, ECs comprise only 1-2 % of the total amount of cells in the tissue, and they are embedded in matrix components and tightly surrounded by various other cell types (Griffioen and Molema, 2000). The yield of ECs will also depend on the vascular density of the tissue, the expression of CD31, as well as the tissue composition which will affect

the efficiency of digestion (van Beijnum et al., 2008). For this reason the highly vascular mouse lung was used as the source of ECs in this study. On the other hand, the size of mouse tissue is rather small so the yield of ECs was not sufficient for downstream applications directly. Our solution was to culture those "pure" primary MLECs to build up the number of cells. However, these cells can only be passaged for 5-6 generations, since the majority of primary cells rapidly become senescent during cell culture. One report suggested single-cell suspensions might be expanded in vitro for 3-5 days and subsequently sorted for ECs (Dirkx et al., 2003). However, this culture step may induce unwanted phenotypic changes in the ECs, as contaminating cell types may grow more rapidly and take over the ECs population. On the other hand, the growth rate of primary MLECs is rather slow, it will take a long time to expand the cell number. Hence, these two limitations make passaging primary MLECs particularly challenging. Despite this problem, I successfully used a vascular specific inducible Cre enzyme, activated by 4-OHT, to obtain endoglin null ECs demonstrating that the inducible endoglin knockout system was workable *in vitro*. However, maintenance of a pure population of primary ECs was fairly difficult and restricted the use of these cells in angiogenesis assay systems. The progressive loss of cell viability and expression of endothelial markers in the course of *in vitro* propagation may have been due to increased numbers of senescent cells, de-differentiated cells, as well as the presence of contaminated non-ECs (Unger et al., 2002). Therefore, an alternative approach was required to generate larger numbers of ECs that could be maintained in culture for longer periods than 5-6 passages.

7.3.2 Conditionally immortalized endothelial cell lines

To overcome these limitations, I took advantage of the 'immortomouse' to isolate and purify conditionally immortalized MLECs. The cell numbers were expanded at 33°C to bypass G1 checkpoint control, to generate sufficient cells for subsequent experiments, which were performed at 37°C where cells regained checkpoint control and assumed a phenotype similar to primary ECs. Subsequently, using a

ubiquitous Rosa-Cre-ER^{T2} enzyme activated by 4-OHT, I also obtained sufficient numbers of Eng null ECs for analysis.

7.3.3 Effect of endoglin depletion on endothelial cell phenotypes

It is not clear whether endoglin mediates an enhanced migration and proliferative rate of ECs or how endoglin functions through the TGF-β/BMP signalling pathways in ECs. A better understanding of these functions will contribute to understanding the mechanisms of its role in angiogenesis. It was reported that endoglin is essential for angiogenesis in the mouse embryonic development and its expression is up-regulated on proliferating ECs during angiogenesis (Arthur et al., 2000; Lebrin et al., 2004). Using the conditionally immortalised Eng-iKO MLECs, I investigated the role of endoglin in regulating cell viability, cell proliferation and migration. In previously published work, *Eng*$^{+/-}$ ECs displayed significantly reduced proliferation and migration and impaired tube formation *in vitro* and endoglin positively mediated proliferation of ECs (Jerkic et al., 2006). In contrast, the initial work described in this chapter revealed that MLECs showed slightly reduced cell viability, proliferation and migration in the absence of endoglin, but this difference was not statistically significant. There might be two possible explanations, first of all, the media used to culture these cells was rich in growth factor supplements (including VEGF (0.5ng/ml), bFGF (10ng/ml), IGF (20ng/ml), EGF (5ng/ml) and it is possible that one or more of these growth factors can rescue any effects of endoglin depletion in these assays. In addition, Eng-iKO MLECs were cultures at 37^{o}C for 72 hours before the MTT assay. This relatively long period of time may make MLECs in orthodox growth conditions more susceptible to become senescent. Therefore, I determined to reduce the culture time under growth restrictive conditions during preparation of MLECs prior to the MTT assay. I also titrated the growth factor supplement used to prepare MV2 growth medium. Under these conditions, there were significant differences in viability/proliferation between Eng-iKO MLECs and control MLECs for 24 and 48 hours. This result suggests endoglin is important for maintaining viability of MLECs. Unfortunately,

there was insufficient time to use these cells to study the role of endoglin in TGF-β receptor superfamily signalling pathway as well. It is known that endoglin associates with TGF-β receptors and TGF-β is a multifunctional cytokine that controls proliferation, migration, adhesion, and apoptosis of a diversity of cell types (Lebrin et al., 2005; ten Dijke and Arthur, 2007; Holderfield and Hughes, 2008; Massague, 2008; Bernabeu et al., 2009; Pardali et al., 2010).

In principle, VEGF is a crucial pro-angiogenic factor that promotes migration and proliferation of ECs and is essential for initiation of angiogenic sprouting. In addition, TGF-β has also been implicated in the regulation of EC migration and proliferation, as well as matrix synthesis (Holderfield and Hughes, 2008). It is still elusive how crosstalk between these two pathways can control proper patterning of the vasculature and how these pathways might interact to generate new ECs during pathological angiogenesis. It was thought that VEGF signal predominantly drives migration but does not stimulate proliferation, TGF-β signalling synergizes with VEGF to drive migration, while also blocking proliferation. Therefore, the switch between migration and proliferation in response to VEGF may involve synergistic and/or antagonistic interactions with TGF-β/BMP signalling (Holderfield and Hughes, 2008).

In fact, there are surprisingly different conclusions regarding the specific role of endoglin in ECs based on published reports. For example, Michelle Letarte et al. demonstrated that Endoglin null ECs proliferate faster and are more responsive to TGF-β1 using mouse embryonic endothelial cells (MEECs) (Pece-Barbara et al., 2005). Jerkic et al, in contrast, reported that $Eng^{+/-}$ ECs from mouse aortic ECs showed significantly reduced proliferation and migration (Jerkic et al., 2006). This phenotype is consistent with what is seen when human umbilical vein endothelial cells (HUVEC) are treated with antisense endoglin (Goumans et al., 2002; Ota et al., 2002). The discrepancies among these similar studies are now awaiting resolution but probably relate to the origins of the cells used, such as human/murine

primary micro/macro endothelial cell and cell lines. There are some significant differences in phenotype between primary cells and cell lines. For example, the distinctive endothelial phenotypes such as constitutive expression of EC markers and angiogenic responses were typically observed in primary ECs. However, most endothelial cell lines only exhibit a few of these endothelial characteristics (van Beijnum et al., 2008). Furthermore, gene expression profiles might be changed over time possibly because of different types of medium and growth factor supplements used in culture. In addition, the different cells may respond distinctively to TGF-β signalling due to crosstalk between different TGF-β receptors and/or the other signalling pathways involved in phenotypic regulation of ECs.

In conclusion, I have successfully derived several new EC lines that will be extremely useful in future studies to investigate the role of endoglin in experiments using defined culture media to try to resolve the disparate results obtained in different laboratories that have lead to current uncertainty of the role of endoglin in angiogenesis.

Chapter 8. General Discussion and Future Directions

8.1 Evasive resistance to anti-angiogenic therapy

The overall aim of my project was to investigate the role of endoglin in angiogenesis and its potential as an anti-angiogenic therapeutic target. Angiogenesis was tested *in vivo* using the matrigel subdermal plug assay and was significantly reduced in endoglin-deficient adult mice compared with controls. Subsequently, angiogenesis and lung metastases were investigated using a subdermal LLC model. My findings indicate that targeting endoglin may delay tumour progression at an early stage (day6), but that loss of endoglin was associated with a significant increase in the frequency of lung metastases by day 18. This is a similar finding to two recent investigations of anti-VEGF treatments in pre-clinical mouse tumour models published in Cancer Cell. Hanahan et al. (2009) reported that anti-angiogenic therapy elicits malignant propression of tumours to increased local invasion and distant metastases (Paez-Ribes et al., 2009). Likewise, Kerbel and colleagues reported accelerated metastases after anti-angiogenic therapy (Ebos et al., 2009). Possible causes for increased metastases following this anti-angiogenic treatment might be because the resultant hypoxia promotes tumour cell invasion into the surrounding tissue. Also, tumours may develop a number of mechanisms to evade anti-angiogenic therapy. First, evolutionary selection following anti-angiogenic therapy to neutralize the effect of a single angiogenic factor (e.g., VEGF) selects for tumour cells that express alternative pro-angiogenic factors (e.g., bFGF or PDGF). Second, a compensatory switch (a physiologically coordinated compensatory program) is activated in response to perturbations of homoeostatic systems after single pathway inhibition. Third, a genetic switch (comprising a dynamic change in expression of angiogenic factors via genetic or epigenetic alterations of, for example, oncogenes in tumour cells) would provide alternate angiogenic stimulation. Finally, a stromal switch would involve paracrine stimulation of angiogenesis via tumour recruitment and activation of diverse cell types, such as bone marrow-derived cells, immune cells and tumour associated fibroblasts. Any or all of these mechanisms might help the tumour to evade anti-angiogenic therapy with a single target. Therefore, it is important to know which

evading mechanisms the tumour cells and microenvironment can develop over the time of therapy. In this regard, knowing the changes that occur following loss of endoglin or during anti-endoglin therapy would be very useful to determine which combination therapy can be used to supplement anti-endoglin therapy.

8.2 Potential side effects of anti-endoglin therapy

It is thought that anti-angiogenic therapy is generally safe and well tolerated, although it can be accompanied by a variety of adverse effects. In fact, Eng-iKO^{e} mice did not lose weight and appeared healthy until the end point of the study (approximately 3 weeks after endoglin depletion). Also, there were no haemorrhagic symptoms found during this time, but these mutant mice did exhibit abnormal venous enlargement close to sites of local angiogenic stimulation. However, enlarged venules did not appear to cause any adverse effects in Eng-iKO^{e} mice. It is important to note that no similar abnormal venous enlargement was found in the peripheral tumour tissue of Eng-iKO^{e} mice.

8.3 Endoglin may be important for maintaining EC viability

In parallel to the *in vivo* studies, ECs were isolated from the floxed endoglin mice for *in vitro* studies. Surprisingly, and in contrast to previously published works (Goumans et al., 2002; Ota et al., 2002; Jerkic et al., 2006), MLECs initially showed 'normal' cell proliferation and migration in the absence of endoglin. In addition, these *in vitro* findings seemed to be inconsistent with the results achieved using the *in vivo* matrigel plug angiogenesis assay, where endoglin depletion caused an angiogenesis defect. A possible explanation for this difference is that the media used to culture these cells was rich in growth factor supplements (including VEGF, bFGF, IGF & EGF) and that one or more of these growth factors rescued the effects of endoglin depletion in these assays. Two further MTT assays were performed using Eng-iKO and control MLECs cultured with MV2 growth medium in which the growth factor supplements had been serially titrated. In these experiments there was a significant reduction in viability in Eng-iKO MLECs compared with control

MLECs. Although this was only preliminary data, this result suggests endoglin might be important for maintaining viability of MLECs. Future experiments to investigate the role of endoglin should use defined culture medium and take advantage of successfully derived endothelial cell lines from this project to resolve the disparate results obtained in different laboratories that have lead to current uncertainty of the role of endoglin in angiogenesis. An important consideration in relating this to the EC responses *in vivo* will be to compare levels of these growth factors in endogenous tissues (with and without endoglin) to those used in tissue culture.

8.4 The selection of mouse tumour model

The LLC-RFP subcutaneous cancer model generated a very useful tumour model with which to investigate the effect of endoglin depletion on tumour angiogenesis, growth and metastases. The LLC primary tumour (originally derived from mouse lung carcinoma) is characterised by rapid growth, high vascularity and frequent metastases to the lungs. However, this model also has some limitations when compared to the complexity of cancer development in patients. First of all, the subdermal LLC tumour model is a very simple one, comprising one rapidly proliferating cell type, that is not able to mimic the more complex tumour microenvironment found in patients. This complexity leads to more varied interactions between transplanted cancer cells and surrounding constituents, such as normal cells, stromal cells and immune cells (Hanahan and Weinberg, 2000; Hanahan and Weinberg, 2011). In addition, the LLC cancer is not a human cancer. However, an alternative pre-clinical mouse model which is often used in these types of studies is the human xenograft model. This involves injecting human cancer cells into immunocompromised mice. It aims to permit therapeutic assessment using cancer tissue from human, rather than from another species. Unfortunately, the results obtained from a number of xenograft studies (Boehm et al., 1997; Sarraf et al., 1998) have not translated well into the clinic (Kulke et al., 2002; Twombly, 2002). It has been estimated that cancer drugs that enter clinical testing have a 95%

rate of failing to make it to market. The xenograft data from 39 cancer drugs that had already successfully completed Phase II trails in humans shows that only one of the xenograft models showed a similar response to the cancer drug as the patients who received it (Johnson et al., 2001). It seems, on the one hand, that there are histological differences in tumour structure and vasculature between tumours from xenograft or congenic graft models and tumours found in human maliganancies. In addition, the immunocompromised mouse involves knocking out the immune system to allow human cancer xenograft transplantion, at the same time it also fundamentally alters the interaction between cancers and the immune system during cancer progression, which can change the course and outcome of the disease (http://www.the-scientist.com/article/display/56084/). Moreover, the scheduling of anti-angiogenic therapy is different in pre-clinical and clinical settings. Treatments can be started at a much earlier stage of primary tumour progression in laboratory models compared with the clinic where cancers often present at a much later stage and/or metastatic condition may manifest before treatment begins. These differences may affect the response of the tumour to an anti-angiogenic therapy and might explain some clinical failures of anti-angiogenic approaches. Therefore, genetically engineered mouse (GEM) models which not only keep the mouse's immune system intact, but also genetically predispose the mouse to develop cancer by inducing the same genetic mutations in the mouse that cause cancer in humans, may have better predictive capability as models for human cancer. To date, GEM models have been developed for many common tumour types including lung, prostate, breast, colon and pancreatic cancers (Frese and Tuveson, 2007). There are a growing number of anti-angiogenic pre-clinical trials that take advantage of GEM models (Casneuf et al., 2009; Ebos et al., 2009; Noguchi et al., 2009; Paez-Ribes et al., 2009). However, it is still unclear whether this type of pre-clinical model is going to be optimal for facilitating tumour angiogenesis studies and anti-angiogenic drug development.

In addition, the metastatic process is often difficult to accurately model in xenografts or congeneric graft pre-clinical models owing to the rapid growth of primary ectopic tumours, although orthotopic implantation followed by resection (Vantyghem et al., 2005; Francia et al., 2011) and direct intravascular tumour cell injection can generate useful models of distant spread (Cruz-Munoz and Kerbel, 2011). Even if it seems to be probably impossible to accurately mimic tumour metastatic cascades of human cancers, GEM tumour models are perhaps the closest approximation as they are more likely to develop tumours that can metastasize in 'natural' ways and may offer a more optimal model to evaluate therapeutics directed against this process. Taken together, all of this work is for one purpose – to find a better cancer mouse model that can successfully predict how a human cancer will progress and respond to an experimental cancer drug before the drug is ever tried in humans. The different types of pre-clinical tumour mouse models have individual strengths and weaknesses. Therefore, it is critical to determine which xenografts, congeneric graft or GEM models will be optimal for evaluating novel anti-tumour or anti-angiogenesis agents prior to clinical testing (Francia and Kerbel, 2010; Francia et al., 2011).

8.5 *In vivo* imaging tumour angiogenesis and the response to anti-angiogenic therapies

To monitor anti-angiogenic responses, immunofluorescent and histological analyses of tissue sections can supply detailed information about the tumour vasculature. However, the information provided from tissue sections is not dynamic and just represents the situation at a single time point. In the past three decades, there have been huge advances in imaging technologies and their applications, particularly in the field of tumour angiogenesis and vascular targeting. A number of imaging systems that provide anatomical and physiological information are now used in a variety of pre-clinical and clinical applications and include magnetic resonance imaging (MRI), computed tomography (CT), positron emission tomography (PET), single-photon-emission (SPECT), ultrasound, fluorescence reflectance imaging,

fluorescence-mediated tomography (FMT) and bioluminescence imaging (Weissleder and Pittet, 2008). Some of these technologies are widely used in the elucidation of morphological, functional and molecular characteristics of tumour vasculature and can be used to follow tumour growth and metastases in response to anti-angiogenic therapies. Ideally the read-outs from imaging systems should be quantitative, high resolution, longitudinal (allow imaging over time), comprehensive and standardized (Weissleder and Pittet, 2008). But several challenges remain, because each technology has its own strengths and limitations. In my project, pilot studies to image tumour angiogenesis and metastases were performed by applying PET-CT and MRI to the LLC mouse model. This work showed that MRI scanning detected lung micrometastases down to 1mm in diameter (or even less). In contrast, PET-CT was unable to detect even large metastatic lesions in preliminary studies. MRI would therefore be a useful modality for a longitudinal study of tumour metastases after they had reached approximately 1mm in size. It also has the advantage of being able to detect metastatic lesions without additional cell labelling. However, MRI has the disadvantage of being relatively time consuming and expensive. Fluorescence reflectance imaging and bioluminescence imaging are much less time consuming, can be used on multiple occasions to viualise tumour metastases over time but require labelled tumour cells to allow visualization. For example, cancer cells can be labelled with far-red (eg. TomatoRed) or bioluminescence and visualized in orthotopic locations and metastatic sites by the IVIS imaging system (Caliper). However, all the imaging systems mentioned above are also limited by their lack of detailed histological information. Therefore, the combination of histological analysis and *in vivo* imaging systems provide the most powerful approach for investigating tumour angiogenesis and assessing anti-angiogenic targets.

Endoglin provides a potential anti-angiogenic target because it is predominantly expressed in the active and angiogenic tumour associated endothelium. Its location on the luminal surface of blood vessels makes it an ideal target for tumour

vasculature detection by an antibody. Labelled anti-endoglin antibodies can potentially be used to distinguish malignant neoplasm from benign tissue. This information may also be used to select patients who would be suitable for endoglin-targeted anti-angiogenic therapy and further imaging could be used to evaluate the response to this anti-angiogenic therapy. Published work showed that ^{99}Tcm-labeled anti-endoglin mAb E9 (Costello et al., 2004), ^{125}I-labeled anti-endoglin mAb MAEND3 (Fonsatti et al., 2000) and ^{111}In-labeled rat anti-mouse endoglin mAb MJ7/18 (Bredow et al., 2000) have been used to detect and monitor primary tumour growth and metastases either in human or in mouse. In the future, there might be additional options for labelled anti-endoglin antibodies to be used in other *in vivo* imaging systems such as MRI or PET scanning. In terms of anti-endoglin mAb labels for MRI, antibodies could be labelled with ferrous iron to be visualized. The gadolinium-modified nanoparticles are currently applied to pre-clinical and clinical MRI scans. Recently, iron-oxide nanoparticles (IONPs) represent a significant class of inorganic nanomaterial that is characterized with unique physical properties including high surface area to volume ratios and superparamagnetism (Jun et al., 2008; Laurent et al., 2008). It might be possible to label anti-endoglin mAb with IONPs in order to improve its stability in biological fluids and its ability to concentrate at the angiogenic target area. In contrast to MRI, PET uses radiotracers to image, map and measure target site activities such as angiogenesis, metabolism, apoptosis and proliferation. For visualization with PET, anti-endoglin antibody could be labelled using chemistries which are frequently used in the preparation of radiotracers including covalent (^{18}F, ^{123}I, ^{131}I, ^{75}Br, ^{68}Ga and ^{11}C) and ionic binding (a chelator is required to trap metal isotopes in complex chemistry) (Yang et al., 2006). A new method using N-succinimidyl 4-[18F] fluorobenzoate ([18F]SFB) to label peptides of proteins was performed by Dr. Michael Carroll, and this may be suitable for labeling anti-endoglin antibodies. In addition, in terms of half time, ^{124}I might be a good alternative to ^{18}F as this has a much longer half-life (4 days) than that of ^{18}F (110 mins) (personal communication, Dr. Ross Maxwell). Therefore, tumour imaging might be hugely improved by

taking advantage of endoglin labelled targets, and this approach may also be valuable to monitor the response to anti-cancer therapies. Through the development of a robust tumour angiogenesis imaging platform, molecular imaging can dramatically facilitate and speed up many steps of anti-angiogenic drug development in both the pre-clinical stages and clinical settings (Cai et al., 2006).

8.6 Endoglin as an anti-angiogenic therapeutic target

In order to examine the role of a novel agent in tumour angiogenesis and potential as an anti-angiogenic therapeutic target, a variety of methods have been applied in experimental animals. Those can be broadly divided into three categories: genetic depletion of target gene, RNA interference (RNAi) therapeutics and injectable or orally administered antibodies/drugs. In my project, the Eng-iKO^{e} mouse model was used to genetically deplete the endoglin gene in ECs to address the question of whether endoglin might be a good anti-angiogenic therapeutic target. Endoglin siRNA techniques have not yet been applied to tumour studies *in vivo*, but this approach has been used to silence other angiogenic target genes. For example, atelocollagen-complexed siRNA effectively silenced VEGF to inhibit tumour angiogenesis and growth in mouse xenograft model (Takei et al., 2004). Finally, a number of anti-endoglin antibodies, such as the immunotoxin conjugated (Seon et al., 1997; Matsuno et al., 1999), radiolabelled (Tabata et al., 1999), or naked anti-endoglin mAb (Takahashi et al., 2001a; Tsujie et al., 2006; Tsujie et al., 2008; Uneda et al., 2009) termed SN6f, SN6j, and SN6k, were tested in pre-clinical studies that revealed a long-lasting regression/suppression of tumour growth and metastases in SCID mice, that was likely mediated by the inhibition of tumour-associated angiogenesis (Seon et al., 2011). In addition, a phase I study which is aiming to evaluate safety and tolerability of escalating doses of the therapeutic anti-CD105 mAb, its pharmacokinetics and immunogenicity, as well as signs of clinical activity is now in progress in a multi-centre phase I clinical trial. Patients with advanced and/or metastatic cancer were given naked human/murine chimeric anti-endoglin mAb (TRC105) as a tumour vascular targeting agent

(http://clinicaltrials.gov/archive/NCT00582985). Preliminary data from 50 patients with advanced refractory cancer in this clinical trial suggest clinical activity and good tolerability of the TRC105 antibody at a wide range of doses used (0.01-1 mg/kg every two weeks, 0.3-15 mg/kg every two weeks or 10-15 mg/kg/ every week). The preliminary data indicates the majority patients can tolerate doses of TRC105 that generate anti-angiogenic and anti-cancer activity (Goldman et al., 2011). Subsequently further clinical trials will focus on the evaluation of single TRC105 agent and combination therapy in a variety of indications (Rosen et al., 2008; Rosen et al., 2009; Goldman et al., 2011).

8.7 Current combination therapies and future directions

In fact, current data from pre-clinical and clinical trials of anti-angiogenic therapies indicates these therapies benefit a variety of patients with malignant neoplasm in different stages. However, the data also raise a number of important questions of how to effectively combat cancer with anti-angiogenic medicine in the future. It seems that chemotherapy and anti-angiogenic combination therapies might be a beneficial treatment for cancer patients. This type of combination therapy exerted synergistic benefits simply because cytotoxic agents directly kill cancer cells and anti-angiogenic drugs indirectly kill cancers by blocking the blood supply and starving cancer cells. Also, it was proposed that anti-angiogenic therapy can promote drug delivery by transiently normalizing tumour vasculature (Jain, 2005b). Interestingly, a synergistic effect was also reported between naked anti-endoglin antibodies and conventional chemotherapeutic schedules in a human skin/SCID mouse chimera model (Takahashi et al., 2001a). Furthermore, the combination of anti-angiogenic biotherapy and metronomic chemotherapy seems to be a more hopeful strategy for cancer therapy. The metronomic chemotherapy not only can inhibit cancer cell proliferation and speed up cancer cell apoptosis, but it can also have an anti-angiogenic effect (Tan et al., 2004; Emmenegger et al., 2010).

Multi-targeted anti-angiogenic therapies may be another method of increasing the efficacy of anti-angiogenic agents by an anti-endoglin antibody. Numerous angiogenic factors, including VEGF, PDGF, EGF, TGF-α TGF-β, acidic and basic FGF have been shown to contribute to tumour angiogenesis (Ferrara and Kerbel, 2005; Kerbel, 2008; Chung et al., 2010). Therefore, blocking a single angiogenic molecule was expected to have little or no impact on tumour growth. Nevertheless, among a large array of novel therapeutic agents with anti-angiogenic activity tested in the clinical setting in the past decade, anti-VEGF/VEGFR signalling agents such as Bevacizumab(Avastin), Sunitinib (Sutent), Sorafenib (Nexavar) and Pazopanib (Votvient) were approved by FDA. Among the most promising member of this growing 'family' of novel therapeutic targets, it must be carefully considered and investigated which type of multi-targeted anti-angiogenic combination therapy is ideally suitable for cancer patients. However, it is truly difficult to determine which type of combination and model is ideal for a certain investigation before the expression of target gene is manipulated on biopsy or clinical samples from cancer patients. Therefore, researchers should be encouraged to identify the potential synergy of the combination therapy using a variety of anti-angiogenic agents based on bench to bedside and back to bench studies. On the other hand, effective multi-targeted anti-angiogenic therapies are now required since the consequence of single target anti-angiogenic therapy may be to upregulate some other cytokines that promote reneovascularization. Therefore, a priority in the anti-endoglin therapy field is to identify any pro-angiogenic agents that are upregulated due to anti-endoglin therapy, in order to impede this insidious consequence of single anti-angiogenic therapy. It is certainly important to investigate the potential of mechanism-based combination therapies in the future.

Anti-angiogenic agents predominantly interfere with new blood vessel formation, whereas vascular disrupting agents (VDAs) are designed to target established tumour vasculature causing rapid and sustained inhibition of tumour blood flow and extensive tumour necrosis (Baguley, 2003; Siemann et al., 2005). Tumour-VDAs

have the potential to affect the areas of the tumour that are resistant to conventional cytotoxic therapies used for cancer treatment. Indeed, when combined with conventional chemotherapy, tumour-VDAs demonstrated synergy in pre-clinical models and activity in Phase II/III clinical trials (Hinnen and Eskens, 2007; Heath and Bicknell, 2009).

Taken together, the current pre-clinical data significantly demonstrate endoglin has the potential to be developed as a novel antibody-based diagnostic and therapeutic target. However, it seems to be a little premature to apply anti-endoglin drugs in the clinical setting of cancer and it is essential to investigate the mechanisms of response to anti-endoglin therapy and identify the most appropriate therapeutic applications of endoglin targeting. This will involve using an appropriate pre-clinical model and should take advantage of the latest imaging systems. Therapeutic strategies relying on targeting a single biological agent may have initial benefit but their ultimate impact on treatment efficacy is likely to be limited. Angiogenic inhibitors (AIs) and/or VDAs can augment conventional anti-cancer therapies, but better cytotoxics are required and the application of combined biological targeting strategies needs to be considered. For example, multi-target anti-angiogenic therapies in conjuction with anti-metastatic therapies might represent the best combination to address the increased metastases problem caused by anti-angiogenic therapy.

In conclusion, in the context of a subdermal LLC-RFP primary tumour and 'spontaneous' lung metastatic secondary tumour model, targeting endoglin alone is likely to delay early stages of primary tumour progression in association with reduced angiogenesis. However, targeting endoglin alone is unlikely to have a major anti-cancer effect at later stages of primary tumour progression and also this is associated with a detrimental increase in lung metastases. Apart from the benefit of targeting endoglin at early stages of tumour progression, the finding of significant increase lung metastases in Eng-iKO^{e} mice must be highlighted in the

context of anti-endoglin therapies currently being tested in phase I and phase I and II clinical trials. This increase may be due to the changes in lung vasculature and the formation of pre-metastatic niches within the lung following vascular specific endoglin depletion. Despite this major problem, endoglin may still represent an effective agent as a component target in anti-angiogenic multi-target combination therapy. Additional preclinical studies of anti-endoglin therapy (alone and in combination with other targets such as VEGF) in a wide range of clinically relevant mouse models are required to establish the broader validity of these conclusions and to direct the way for future clinical applications

References

Abdollahi A, Folkman J. 2010. Evading tumor evasion: current concepts and perspectives of anti-angiogenic cancer therapy. Drug Resist Updat 13:16-28.

Achen MG, Stacker SA. 2008. Molecular control of lymphatic metastasis. Ann N Y Acad Sci 1131:225-234.

Ahmadvand D, Rasaee MJ, Rahbarizadeh F, Mohammadi M. 2008. Production and characterization of a high-affinity nanobody against human endoglin. Hybridoma (Larchmt) 27:353-360.

Aird WC. 2009. Molecular heterogeneity of tumor endothelium. Cell Tissue Res 335:271-281.

Akagi K, Ikeda Y, Sumiyoshi Y, Kimura Y, Kinoshita J, Miyazaki M, Abe T. 2002. Estimation of angiogenesis with anti-CD105 immunostaining in the process of colorectal cancer development. Surgery 131:S109-113.

Alessandri G, Chirivi RG, Fiorentini S, Dossi R, Bonardelli S, Giulini SM, Zanetta G, Landoni F, Graziotti PP, Turano A, Caruso A, Zardi L, Giavazzi R, Bani MR. 1999. Phenotypic and functional characteristics of tumour-derived microvascular endothelial cells. Clin Exp Metastasis 17:655-662.

Allinson KR, Carvalho RL, van den Brink S, Mummery CL, Arthur HM. 2007. Generation of a floxed allele of the mouse Endoglin gene. Genesis 45:391-395.

Alva JA, Zovein AC, Monvoisin A, Murphy T, Salazar A, Harvey NL, Carmeliet P, Iruela-Arispe ML. 2006. VE-Cadherin-Cre-recombinase transgenic mouse: a tool for lineage analysis and gene deletion in endothelial cells. Dev Dyn 235:759-767.

Arthur HM, Ure J, Smith AJ, Renforth G, Wilson DI, Torsney E, Charlton R, Parums DV, Jowett T, Marchuk DA, Burn J, Diamond AG. 2000. Endoglin, an ancillary TGFbeta receptor, is required for extraembryonic angiogenesis and plays a key role in heart development. Dev Biol 217:42-53.

Baguley BC. 2003. Antivascular therapy of cancer: DMXAA. Lancet Oncol 4:141-148.

Barbara NP, Wrana JL, Letarte M. 1999. Endoglin is an accessory protein that interacts with the signaling receptor complex of multiple members of the transforming growth factor-beta superfamily. J Biol Chem 274:584-594.

Bates DO, Cui TG, Doughty JM, Winkler M, Sugiono M, Shields JD, Peat D, Gillatt D, Harper SJ. 2002. VEGF165b, an inhibitory splice variant of vascular endothelial growth factor, is down-regulated in renal cell carcinoma. Cancer Res 62:4123-4131.

Bellon T, Corbi A, Lastres P, Cales C, Cebrian M, Vera S, Cheifetz S, Massague J, Letarte M, Bernabeu C. 1993. Identification and expression of two forms of the human transforming growth factor-beta-binding protein endoglin with distinct cytoplasmic regions. Eur J Immunol 23:2340-2345.

Benetti A, Berenzi A, Gambarotti M, Garrafa E, Gelati M, Dessy E, Portolani N, Piardi T, Giulini SM, Caruso A, Invernici G, Parati EA, Nicosia R, Alessandri

G. 2008. Transforming growth factor-beta1 and CD105 promote the migration of hepatocellular carcinoma-derived endothelium. Cancer Res 68:8626-8634.
Bergers G, Benjamin LE. 2003. Tumorigenesis and the angiogenic switch. Nat Rev Cancer 3:401-410.
Bergers G, Hanahan D. 2008. Modes of resistance to anti-angiogenic therapy. Nat Rev Cancer 8:592-603.
Bergers G, Javaherian K, Lo KM, Folkman J, Hanahan D. 1999. Effects of angiogenesis inhibitors on multistage carcinogenesis in mice. Science 284:808-812.
Bergers G, Song S, Meyer-Morse N, Bergsland E, Hanahan D. 2003. Benefits of targeting both pericytes and endothelial cells in the tumor vasculature with kinase inhibitors. J Clin Invest 111:1287-1295.
Bernabeu C, Lopez-Novoa JM, Quintanilla M. 2009. The emerging role of TGF-beta superfamily coreceptors in cancer. Biochim Biophys Acta 1792:954-973.
Bertolino P, Deckers M, Lebrin F, ten Dijke P. 2005. Transforming growth factor-beta signal transduction in angiogenesis and vascular disorders. Chest 128:585S-590S.
Bertram JS, Janik P. 1980. Establishment of a cloned line of Lewis Lung Carcinoma cells adapted to cell culture. Cancer Lett 11:63-73.
Birukova AA, Birukov KG, Smurova K, Adyshev D, Kaibuchi K, Alieva I, Garcia JG, Verin AD. 2004. Novel role of microtubules in thrombin-induced endothelial barrier dysfunction. FASEB J 18:1879-1890.
Blackwell KL, Haroon ZA, Shan S, Saito W, Broadwater G, Greenberg CS, Dewhirst MW. 2000. Tamoxifen inhibits angiogenesis in estrogen receptor-negative animal models. Clin Cancer Res 6:4359-4364.
Blouw B, Haase VH, Song H, Bergers G, Johnson RS. 2007. Loss of vascular endothelial growth factor expression reduces vascularization, but not growth, of tumors lacking the Von Hippel-Lindau tumor suppressor gene. Oncogene 26:4531-4540.
Bocci G, Falcone A, Fioravanti A, Orlandi P, Di Paolo A, Fanelli G, Viacava P, Naccarato AG, Kerbel RS, Danesi R, Del Tacca M, Allegrini G. 2008. Antiangiogenic and anticolorectal cancer effects of metronomic irinotecan chemotherapy alone and in combination with semaxinib. Br J Cancer 98:1619-1629.
Bodey B, Bodey B, Jr., Siegel SE, Kaiser HE. 1998a. Immunocytochemical detection of endoglin is indicative of angiogenesis in malignant melanoma. Anticancer Res 18:2701-2710.
Bodey B, Bodey B, Jr., Siegel SE, Kaiser HE. 1998b. Over-expression of endoglin (CD105): a marker of breast carcinoma-induced neo-vascularization. Anticancer Res 18:3621-3628.
Bodey B, Bodey B, Jr., Siegel SE, Kaiser HE. 1998c. Upregulation of endoglin (CD105) expression during childhood brain tumor-related angiogenesis. Anti-angiogenic therapy. Anticancer Res 18:1485-1500.

Boehm T, Folkman J, Browder T, O'Reilly MS. 1997. Antiangiogenic therapy of experimental cancer does not induce acquired drug resistance. Nature 390:404-407.

Bomken S, Fiser K, Heidenreich O, Vormoor J. 2010. Understanding the cancer stem cell. Br J Cancer 103:439-445.

Bourdeau A, Dumont DJ, Letarte M. 1999. A murine model of hereditary hemorrhagic telangiectasia. J Clin Invest 104:1343-1351.

Bourdeau A, Faughnan ME, McDonald ML, Paterson AD, Wanless IR, Letarte M. 2001. Potential role of modifier genes influencing transforming growth factor-beta1 levels in the development of vascular defects in endoglin heterozygous mice with hereditary hemorrhagic telangiectasia. Am J Pathol 158:2011-2020.

Brahimi-Horn MC, Chiche J, Pouyssegur J. 2007. Hypoxia and cancer. J Mol Med 85:1301-1307.

Bredow S, Lewin M, Hofmann B, Marecos E, Weissleder R. 2000. Imaging of tumour neovasculature by targeting the TGF-beta binding receptor endoglin. Eur J Cancer 36:675-681.

Brekken RA, Thorpe PE. 2001. VEGF-VEGF receptor complexes as markers of tumor vascular endothelium. J Control Release 74:173-181.

Breviario F, Caveda L, Corada M, Martin-Padura I, Navarro P, Golay J, Introna M, Gulino D, Lampugnani MG, Dejana E. 1995. Functional properties of human vascular endothelial cadherin (7B4/cadherin-5), an endothelium-specific cadherin. Arterioscler Thromb Vasc Biol 15:1229-1239.

Brewer CA, Setterdahl JJ, Li MJ, Johnston JM, Mann JL, McAsey ME. 2000. Endoglin expression as a measure of microvessel density in cervical cancer. Obstet Gynecol 96:224-228.

Browder T, Butterfield CE, Kraling BM, Shi B, Marshall B, O'Reilly MS, Folkman J. 2000. Antiangiogenic scheduling of chemotherapy improves efficacy against experimental drug-resistant cancer. Cancer Res 60:1878-1886.

Brown DM, Ruoslahti E. 2004. Metadherin, a cell surface protein in breast tumors that mediates lung metastasis. Cancer Cell 5:365-374.

Burrows FJ, Derbyshire EJ, Tazzari PL, Amlot P, Gazdar AF, King SW, Letarte M, Vitetta ES, Thorpe PE. 1995. Up-regulation of endoglin on vascular endothelial cells in human solid tumors: implications for diagnosis and therapy. Clin Cancer Res 1:1623-1634.

Bussolati B, Deregibus MC, Camussi G. 2010. Characterization of molecular and functional alterations of tumor endothelial cells to design anti-angiogenic strategies. Curr Vasc Pharmacol 8:220-232.

Butta A, MacLennan K, Flanders KC, Sacks NP, Smith I, McKinna A, Dowsett M, Wakefield LM, Sporn MB, Baum M, et al. 1992. Induction of transforming growth factor beta 1 in human breast cancer in vivo following tamoxifen treatment. Cancer Res 52:4261-4264.

Cai W, Rao J, Gambhir SS, Chen X. 2006. How molecular imaging is speeding up antiangiogenic drug development. Mol Cancer Ther 5:2624-2633.

Carmeliet P. 2005. Angiogenesis in life, disease and medicine. Nature 438:932-936.

Carmeliet P, Jain RK. 2011a. Molecular mechanisms and clinical applications of angiogenesis. Nature 473:298-307.
Carmeliet P, Jain RK. 2011b. Principles and mechanisms of vessel normalization for cancer and other angiogenic diseases. Nat Rev Drug Discov 10:417-427.
Carvalho RL, Jonker L, Goumans MJ, Larsson J, Bouwman P, Karlsson S, Dijke PT, Arthur HM, Mummery CL. 2004. Defective paracrine signalling by TGFbeta in yolk sac vasculature of endoglin mutant mice: a paradigm for hereditary haemorrhagic telangiectasia. Development 131:6237-6247.
Casanovas O, Hicklin DJ, Bergers G, Hanahan D. 2005. Drug resistance by evasion of antiangiogenic targeting of VEGF signaling in late-stage pancreatic islet tumors. Cancer Cell 8:299-309.
Casneuf VF, Demetter P, Boterberg T, Delrue L, Peeters M, Van Damme N. 2009. Antiangiogenic versus cytotoxic therapeutic approaches in a mouse model of pancreatic cancer: an experimental study with a multitarget tyrosine kinase inhibitor (sunitinib), gemcitabine and radiotherapy. Oncol Rep 22:105-113.
Chang YS, di Tomaso E, McDonald DM, Jones R, Jain RK, Munn LL. 2000. Mosaic blood vessels in tumors: frequency of cancer cells in contact with flowing blood. Proc Natl Acad Sci U S A 97:14608-14613.
Charalambous C, Chen TC, Hofman FM. 2006. Characteristics of tumor-associated endothelial cells derived from glioblastoma multiforme. Neurosurg Focus 20:E22.
Charalambous C, Hofman FM, Chen TC. 2005. Functional and phenotypic differences between glioblastoma multiforme-derived and normal human brain endothelial cells. J Neurosurg 102:699-705.
Cheifetz S, Bellon T, Cales C, Vera S, Bernabeu C, Massague J, Letarte M. 1992. Endoglin is a component of the transforming growth factor-beta receptor system in human endothelial cells. J Biol Chem 267:19027-19030.
Chen CZ, Li M, de Graaf D, Monti S, Gottgens B, Sanchez MJ, Lander ES, Golub TR, Green AR, Lodish HF. 2002. Identification of endoglin as a functional marker that defines long-term repopulating hematopoietic stem cells. Proc Natl Acad Sci U S A 99:15468-15473.
Choi WW, Lewis MM, Lawson D, Yin-Goen Q, Birdsong GG, Cotsonis GA, Cohen C, Young AN. 2005. Angiogenic and lymphangiogenic microvessel density in breast carcinoma: correlation with clinicopathologic parameters and VEGF-family gene expression. Mod Pathol 18:143-152.
Chung AS, Lee J, Ferrara N. 2010. Targeting the tumour vasculature: insights from physiological angiogenesis. Nat Rev Cancer 10:505-514.
Clasper S, Royston D, Baban D, Cao Y, Ewers S, Butz S, Vestweber D, Jackson DG. 2008. A novel gene expression profile in lymphatics associated with tumor growth and nodal metastasis. Cancer Res 68:7293-7303.
Conley BA, Smith JD, Guerrero-Esteo M, Bernabeu C, Vary CP. 2000. Endoglin, a TGF-beta receptor-associated protein, is expressed by smooth muscle cells in human atherosclerotic plaques. Atherosclerosis 153:323-335.

Costello B, Li C, Duff S, Butterworth D, Khan A, Perkins M, Owens S, Al-Mowallad AF, O'Dwyer S, Kumar S. 2004. Perfusion of 99Tcm-labeled CD105 Mab into kidneys from patients with renal carcinoma suggests that CD105 is a promising vascular target. Int J Cancer 109:436-441.

Cruz-Munoz W, Kerbel RS. 2011. Preclinical approaches to study the biology and treatment of brain metastases. Semin Cancer Biol 21:123-130.

Cunha SI, Pardali E, Thorikay M, Anderberg C, Hawinkels L, Goumans MJ, Seehra J, Heldin CH, ten Dijke P, Pietras K. 2010. Genetic and pharmacological targeting of activin receptor-like kinase 1 impairs tumor growth and angiogenesis. J Exp Med 207:85-100.

Daenen LG, Shaked Y, Man S, Xu P, Voest EE, Hoffman RM, Chaplin DJ, Kerbel RS. 2009. Low-dose metronomic cyclophosphamide combined with vascular disrupting therapy induces potent antitumor activity in preclinical human tumor xenograft models. Mol Cancer Ther 8:2872-2881.

Dalerba P, Cho RW, Clarke MF. 2007. Cancer stem cells: models and concepts. Annu Rev Med 58:267-284.

Dallas NA, Samuel S, Xia L, Fan F, Gray MJ, Lim SJ, Ellis LM. 2008. Endoglin (CD105): a marker of tumor vasculature and potential target for therapy. Clin Cancer Res 14:1931-1937.

David Cunningham YJC. 2007. Antiangiogenic Therapy in Colorectal Cancer: Managing Side Effects. Medscape Hematology-Oncology webpage:http://cme.medscape.com/viewarticle/552181.

David L, Mallet C, Mazerbourg S, Feige JJ, Bailly S. 2007. Identification of BMP9 and BMP10 as functional activators of the orphan activin receptor-like kinase 1 (ALK1) in endothelial cells. Blood 109:1953-1961.

Davies MM, Mathur P, Carnochan P, Saini S, Allen-Mersh TG. 2002. Effect of manipulation of primary tumour vascularity on metastasis in an adenocarcinoma model. Br J Cancer 86:123-129.

di Tomaso E, Capen D, Haskell A, Hart J, Logie JJ, Jain RK, McDonald DM, Jones R, Munn LL. 2005. Mosaic tumor vessels: cellular basis and ultrastructure of focal regions lacking endothelial cell markers. Cancer Res 65:5740-5749.

Dirkx AE, Oude Egbrink MG, Kuijpers MJ, van der Niet ST, Heijnen VV, Bouma-ter Steege JC, Wagstaff J, Griffioen AW. 2003. Tumor angiogenesis modulates leukocyte-vessel wall interactions in vivo by reducing endothelial adhesion molecule expression. Cancer Res 63:2322-2329.

Djonov V, Schmid M, Tschanz SA, Burri PH. 2000. Intussusceptive angiogenesis: its role in embryonic vascular network formation. Circ Res 86:286-292.

Du R, Lu KV, Petritsch C, Liu P, Ganss R, Passegue E, Song H, Vandenberg S, Johnson RS, Werb Z, Bergers G. 2008. HIF1alpha induces the recruitment of bone marrow-derived vascular modulatory cells to regulate tumor angiogenesis and invasion. Cancer Cell 13:206-220.

Dudek SM, Garcia JG. 2001. Cytoskeletal regulation of pulmonary vascular permeability. J Appl Physiol 91:1487-1500.

Duwel A, Eleno N, Jerkic M, Arevalo M, Bolanos JP, Bernabeu C, Lopez-Novoa JM. 2007. Reduced tumor growth and angiogenesis in endoglin-haploinsufficient mice. Tumour Biol 28:1-8.

Ebos JM, Kerbel RS. 2011. Antiangiogenic therapy: impact on invasion, disease progression, and metastasis. Nat Rev Clin Oncol 8:210-221.

Ebos JM, Lee CR, Christensen JG, Mutsaers AJ, Kerbel RS. 2007. Multiple circulating proangiogenic factors induced by sunitinib malate are tumor-independent and correlate with antitumor efficacy. Proc Natl Acad Sci U S A 104:17069-17074.

Ebos JM, Lee CR, Cruz-Munoz W, Bjarnason GA, Christensen JG, Kerbel RS. 2009. Accelerated metastasis after short-term treatment with a potent inhibitor of tumor angiogenesis. Cancer Cell 15:232-239.

Ellis LM, Hicklin DJ. 2008. VEGF-targeted therapy: mechanisms of anti-tumour activity. Nat Rev Cancer 8:579-591.

Ellis LM, Reardon DA. 2010. Is there really a yin and yang to VEGF-targeted therapies? Lancet Oncol 11:809-811.

Emmenegger U, Francia G, Shaked Y, Kerbel RS. 2010. Metronomic chemotherapy: principles and lessons learned from applications in the treatment of metastatic prostate cancer. Recent Results Cancer Res 180:165-183.

Escudier B, Eisen T, Stadler WM, Szczylik C, Oudard S, Siebels M, Negrier S, Chevreau C, Solska E, Desai AA, Rolland F, Demkow T, Hutson TE, Gore M, Freeman S, Schwartz B, Shan M, Simantov R, Bukowski RM. 2007. Sorafenib in advanced clear-cell renal-cell carcinoma. N Engl J Med 356:125-134.

F.J. Burrows EJD, P.L. Tazzari, P. Amlot, A.F. Gazdar and S.W. King et al., . 1995. Up-regulation of endoglin on vascular endothelial cells in human solid tumors: implications for diagnosis and therapy. Clin Cancer Res 1:1623-1634.

Fathers KE, Stone CM, Minhas K, Marriott JJ, Greenwood JD, Dumont DJ, Coomber BL. 2005. Heterogeneity of Tie2 expression in tumor microcirculation: influence of cancer type, implantation site, and response to therapy. Am J Pathol 167:1753-1762.

Feng XH, Derynck R. 2005. Specificity and versatility in tgf-beta signaling through Smads. Annu Rev Cell Dev Biol 21:659-693.

Ferrara N, Kerbel RS. 2005. Angiogenesis as a therapeutic target. Nature 438:967-974.

Fidler IJ. 2003. The pathogenesis of cancer metastasis: the 'seed and soil' hypothesis revisited. Nat Rev Cancer 3:453-458.

Folkman J. 1971. Tumor angiogenesis: therapeutic implications. N Engl J Med 285:1182-1186.

Folkman J. 1995. Angiogenesis in cancer, vascular, rheumatoid and other disease. Nat Med 1:27-31.

Fonsatti E, Altomonte M, Nicotra MR, Natali PG, Maio M. 2003. Endoglin (CD105): a powerful therapeutic target on tumor-associated angiogenetic blood vessels. Oncogene 22:6557-6563.

Fonsatti E, Del Vecchio L, Altomonte M, Sigalotti L, Nicotra MR, Coral S, Natali PG, Maio M. 2001. Endoglin: An accessory component of the TGF-beta-binding receptor-complex with diagnostic, prognostic, and bioimmunotherapeutic potential in human malignancies. J Cell Physiol 188:1-7.

Fonsatti E, Jekunen AP, Kairemo KJ, Coral S, Snellman M, Nicotra MR, Natali PG, Altomonte M, Maio M. 2000. Endoglin is a suitable target for efficient imaging of solid tumors: in vivo evidence in a canine mammary carcinoma model. Clin Cancer Res 6:2037-2043.

Fonsatti E, Nicolay HJ, Altomonte M, Covre A, Maio M. 2010. Targeting cancer vasculature via endoglin/CD105: a novel antibody-based diagnostic and therapeutic strategy in solid tumours. Cardiovasc Res 86:12-19.

Forsythe JA, Jiang BH, Iyer NV, Agani F, Leung SW, Koos RD, Semenza GL. 1996. Activation of vascular endothelial growth factor gene transcription by hypoxia-inducible factor 1. Mol Cell Biol 16:4604-4613.

Francia G, Cruz-Munoz W, Man S, Xu P, Kerbel RS. 2011. Mouse models of advanced spontaneous metastasis for experimental therapeutics. Nat Rev Cancer 11:135-141.

Francia G, Kerbel RS. 2010. Raising the bar for cancer therapy models. Nat Biotechnol 28:561-562.

Fruttiger M. 2002. Development of the mouse retinal vasculature: angiogenesis versus vasculogenesis. Invest Ophthalmol Vis Sci 43:522-527.

Fruttiger M. 2007. Development of the retinal vasculature. Angiogenesis 10:77-88.

Fujimoto J, Hori M, Ichigo S. 1997. Antioestrogenic compounds inhibit estrogen-induced expressions of basic fibroblast growth factor and its mRNA in well-differentiated endometrial cancer cells. Gen Pharmacol 28:215-219.

Gagliardi A, Hennig B, Collins D. 1996. Antioestrogens inhibit endothelial cell growth stimulated by angiogenic growth factors. Anticancer Res 16:1101-1106.

Gao DC, Nolan DJ, Mellick AS, Bambino K, McDonnell K, Mittal V. 2008. Endothelial progenitor cells control the angiogenic switch in mouse lung metastasis. Science 319:195-198.

Garbi C, Colletta G, Cirafici AM, Marchisio PC, Nitsch L. 1990. Transforming growth factor-beta induces cytoskeleton and extracellular matrix modifications in FRTL-5 thyroid epithelial cells. Eur J Cell Biol 53:281-289.

Garcia-Pozo L, Miquilena-Colina ME, Lozano-Rodriguez T, Garcia-Monzon C. 2008. [Endoglin: structure, biological functions, and role in fibrogenesis]. Rev Esp Enferm Dig 100:355-360.

Gerhardt H, Golding M, Fruttiger M, Ruhrberg C, Lundkvist A, Abramsson A, Jeltsch M, Mitchell C, Alitalo K, Shima D, Betsholtz C. 2003. VEGF guides angiogenic sprouting utilizing endothelial tip cell filopodia. J Cell Biol 161:1163-1177.

Giantonio BJ. 2005. Gastrointestinal perforation and cancer therapy: managing risk to achieve benefit. Onkologie 28:177-178.

Goldman JW, Gordon MS, Hurwitz H, Pili R, Mendelson DS, Adams BJ, Alvarez D, Seon BK, Theuer CP, Leigh BR, Rosen LS. 2011. A phase I study of TRC105 (anti-CD105 antibody) in patients with advanced solid tumors. J Clin Oncol 29.

Gordon KJ, Blobe GC. 2008. Role of transforming growth factor-beta superfamily signaling pathways in human disease. Biochim Biophys Acta 1782:197-228.

Gougos A, Letarte M. 1990. Primary structure of endoglin, an RGD-containing glycoprotein of human endothelial cells. J Biol Chem 265:8361-8364.

Goumans MJ, Valdimarsdottir G, Itoh S, Lebrin F, Larsson J, Mummery C, Karlsson S, ten Dijke P. 2003. Activin receptor-like kinase (ALK)1 is an antagonistic mediator of lateral TGFbeta/ALK5 signaling. Mol Cell 12:817-828.

Goumans MJ, Valdimarsdottir G, Itoh S, Rosendahl A, Sideras P, ten Dijke P. 2002. Balancing the activation state of the endothelium via two distinct TGF-beta type I receptors. EMBO J 21:1743-1753.

Grainger D, Metcalfe J. 1996. Tamoxifen: teaching an old drug new tricks? . Nature Med 2:381-385.

Grainger DJ, Weissberg PL, Metcalfe JC. 1993. Tamoxifen decreases the rate of proliferation of rat vascular smooth-muscle cells in culture by inducing production of transforming growth factor beta. Biochem J 294 (Pt 1):109-112.

Grainger DJ, Witchell CM, Metcalfe JC. 1995. Tamoxifen elevates transforming growth factor-beta and suppresses diet-induced formation of lipid lesions in mouse aorta. Nat Med 1:1067-1073.

Gressett SM, Shah SR. 2009. Intricacies of bevacizumab-induced toxicities and their management. Ann Pharmacother 43:490-501.

Griffioen AW, Molema G. 2000. Angiogenesis: potentials for pharmacologic intervention in the treatment of cancer, cardiovascular diseases, and chronic inflammation. Pharmacol Rev 52:237-268.

Gudjonsson JE, Johnston A, Dyson M, Valdimarsson H, Elder JT. 2007. Mouse models of psoriasis. J Invest Dermatol 127:1292-1308.

Guerrero-Esteo M, Sanchez-Elsner T, Letamendia A, Bernabeu C. 2002. Extracellular and cytoplasmic domains of endoglin interact with the transforming growth factor-beta receptors I and II. J Biol Chem 277:29197-29209.

Guttmacher AE, Marchuk DA, White RI, Jr. 1995. Hereditary hemorrhagic telangiectasia. N Engl J Med 333:918-924.

Hanahan D, Weinberg RA. 2000. The hallmarks of cancer. Cell 100:57-70.

Hanahan D, Weinberg RA. 2011. Hallmarks of cancer: the next generation. Cell 144:646-674.

Hashimoto K, Man S, Xu P, Cruz-Munoz W, Tang T, Kumar R, Kerbel RS. 2010. Potent preclinical impact of metronomic low-dose oral topotecan combined with the antiangiogenic drug pazopanib for the treatment of ovarian cancer. Mol Cancer Ther 9:996-1006.

Hawinkels LJ, Kuiper P, Wiercinska E, Verspaget HW, Liu Z, Pardali E, Sier CF, ten Dijke P. 2010. Matrix metalloproteinase-14 (MT1-MMP)-mediated endoglin shedding inhibits tumor angiogenesis. Cancer Res 70:4141-4150.

Heath VL, Bicknell R. 2009. Anticancer strategies involving the vasculature. Nat Rev Clin Oncol 6:395-404.

Hellebrekers DM, Melotte V, Vire E, Langenkamp E, Molema G, Fuks F, Herman JG, Van Criekinge W, Griffioen AW, van Engeland M. 2007. Identification of epigenetically silenced genes in tumor endothelial cells. Cancer Res 67:4138-4148.

Henriksen R, Gobl A, Wilander E, Oberg K, Miyazono K, Funa K. 1995. Expression and prognostic significance of TGF-beta isotypes, latent TGF-beta 1 binding protein, TGF-beta type I and type II receptors, and endoglin in normal ovary and ovarian neoplasms. Lab Invest 73:213-220.

Hinnen P, Eskens FA. 2007. Vascular disrupting agents in clinical development. Br J Cancer 96:1159-1165.

Hochster HS, Hart LL, Ramanathan RK, Hainsworth JD, Hedrick EE, Childs BH. 2006. Safety and efficacy of oxaliplatin/fluoropyrimidine regimens with or without bevacizumab as first-line treatment of metastatic colorectal cancer (mCRC): final analysis of the TREE-Study. Proc Am Soc Clin Oncol 26:148s.

Holderfield MT, Hughes CC. 2008. Crosstalk between vascular endothelial growth factor, notch, and transforming growth factor-beta in vascular morphogenesis. Circ Res 102:637-652.

Horak ER, Leek R, Klenk N, LeJeune S, Smith K, Stuart N, Greenall M, Stepniewska K, Harris AL. 1992. Angiogenesis, assessed by platelet/endothelial cell adhesion molecule antibodies, as indicator of node metastases and survival in breast cancer. Lancet 340:1120-1124.

Hurwitz H, Fehrenbacher L, Novotny W, Cartwright T, Hainsworth J, Heim W, Berlin J, Baron A, Griffing S, Holmgren E, Ferrara N, Fyfe G, Rogers B, Ross R, Kabbinavar F. 2004. Bevacizumab plus irinotecan, fluorouracil, and leucovorin for metastatic colorectal cancer. N Engl J Med 350:2335-2342.

Huynh HT, Pollak M. 1993. Insulin-like growth factor I gene expression in the uterus is stimulated by tamoxifen and inhibited by the pure antiestrogen ICI 182780. Cancer Res 53:5585-5588.

Huynh HT, Tetenes E, Wallace L, Pollak M. 1993. In vivo inhibition of insulin-like growth factor I gene expression by tamoxifen. Cancer Res 53:1727-1730.

Isaac Yi Kim, Moses M Kim, Seong-Jin Kim. 2005. Transforming growth factor-beta: biology and clinical relevance. Journal of Biochemistry and Molecular Biology 38:1-8.

Ivy SP, Wick JY, Kaufman BM. 2009. An overview of small-molecule inhibitors of VEGFR signaling. Nat Rev Clin Oncol 6:569-579.

Jain RK. 2005a. Antiangiogenic therapy for cancer: current and emerging concepts. Oncology (Williston Park) 19:7-16.

Jain RK. 2005b. Normalization of tumor vasculature: an emerging concept in antiangiogenic therapy. Science 307:58-62.

Jat PS, Noble MD, Ataliotis P, Tanaka Y, Yannoutsos N, Larsen L, Kioussis D. 1991. Direct derivation of conditionally immortal cell lines from an H-2Kb-tsA58 transgenic mouse. Proc Natl Acad Sci U S A 88:5096-5100.

Jerkic M, Rodriguez-Barbero A, Prieto M, Toporsian M, Pericacho M, Rivas-Elena JV, Obreo J, Wang A, Perez-Barriocanal F, Arevalo M, Bernabeu C, Letarte M, Lopez-Novoa JM. 2006. Reduced angiogenic responses in adult Endoglin heterozygous mice. Cardiovasc Res 69:845-854.

Jiang P, Yamauchi K, Yang M, Tsuji K, Xu M, Maitra A, Bouvet M, Hoffman RM. 2006. Tumor cells genetically labeled with GFP in the nucleus and RFP in the cytoplasm for imaging cellular dynamics. Cell Cycle 5:1198-1201.

Johnson JI, Decker S, Zaharevitz D, Rubinstein LV, Venditti JM, Schepartz S, Kalyandrug S, Christian M, Arbuck S, Hollingshead M, Sausville EA. 2001. Relationships between drug activity in NCI preclinical in vitro and in vivo models and early clinical trials. Br J Cancer 84:1424-1431.

Josep M. Llovet SR, Vincenzo Mazzaferro, Philip Hilgard, Edward Gane, Jean-Frédéric Blanc, Andre Cosme de Oliveira. 2008. Sorafenib in Advanced Hepatocellular Carcinoma. N Engl J Med 359:378-390.

Jovine L, Darie CC, Litscher ES, Wassarman PM. 2005. Zona pellucida domain proteins. Annu Rev Biochem 74:83-114.

Jovine L, Qi H, Williams Z, Litscher E, Wassarman PM. 2002. The ZP domain is a conserved module for polymerization of extracellular proteins. Nat Cell Biol 4:457-461.

Jun YW, Lee JH, Cheon J. 2008. Chemical design of nanoparticle probes for high-performance magnetic resonance imaging. Angew Chem Int Ed Engl 47:5122-5135.

Kamba T, McDonald DM. 2007. Mechanisms of adverse effects of anti-VEGF therapy for cancer. Br J Cancer 96:1788-1795.

Kaplan RN, Psaila B, Lyden D. 2006. Bone marrow cells in the 'pre-metastatic niche': within bone and beyond. Cancer Metastasis Rev 25:521-529.

Kaplan RN, Riba RD, Zacharoulis S, Bramley AH, Vincent L, Costa C, MacDonald DD, Jin DK, Shido K, Kerns SA, Zhu Z, Hicklin D, Wu Y, Port JL, Altorki N, Port ER, Ruggero D, Shmelkov SV, Jensen KK, Rafii S, Lyden D. 2005. VEGFR1-positive haematopoietic bone marrow progenitors initiate the pre-metastatic niche. Nature 438:820-827.

Kassouf W, Ismail HR, Aprikian AG, Chevalier S. 2004. Whole-mount prostate sections reveal differential endoglin expression in stromal, epithelial, and endothelial cells with the development of prostate cancer. Prostate Cancer Prostatic Dis 7:105-110.

Kerbel RS. 2008. Tumor angiogenesis. N Engl J Med 358:2039-2049.

Kerbel RS, Kamen BA. 2004. The anti-angiogenic basis of metronomic chemotherapy. Nat Rev Cancer 4:423-436.

Kindler HL, Friberg G, Singh DA, Locker G, Nattam S, Kozloff M, Taber DA, Karrison T, Dachman A, Stadler WM, Vokes EE. 2005. Phase II trial of bevacizumab plus gemcitabine in patients with advanced pancreatic cancer. J Clin Oncol 23:8033-8040.

Korn T, Muller R, Kontermann RE. 2004. Bispecific single-chain diabody-mediated killing of endoglin-positive endothelial cells by cytotoxic T lymphocytes. J Immunother 27:99-106.

Kulke MH, Demetri GD, Sharpless NE, Ryan DP, Shivdasani R, Clark JS, Spiegelman BM, Kim H, Mayer RJ, Fuchs CS. 2002. A phase II study of troglitazone, an activator of the PPARgamma receptor, in patients with chemotherapy-resistant metastatic colorectal cancer. Cancer J 8:395-399.

Kulke MH, Lenz HJ, Meropol NJ, Posey J, Ryan DP, Picus J, Bergsland E, Stuart K, Tye L, Huang X, Li JZ, Baum CM, Fuchs CS. 2008. Activity of sunitinib in patients with advanced neuroendocrine tumors. J Clin Oncol 26:3403-3410.

Kumar S, Ghellal A, Li C, Byrne G, Haboubi N, Wang JM, Bundred N. 1999. Breast carcinoma: vascular density determined using CD105 antibody correlates with tumor prognosis. Cancer Res 59:856-861.

Kyzas PA, Agnantis NJ, Stefanou D. 2006. Endoglin (CD105) as a prognostic factor in head and neck squamous cell carcinoma. Virchows Arch 448:768-775.

Lamouille S, Mallet C, Feige JJ, Bailly S. 2002. Activin receptor-like kinase 1 is implicated in the maturation phase of angiogenesis. Blood 100:4495-4501.

Langenkamp E, Molema G. 2009. Microvascular endothelial cell heterogeneity: general concepts and pharmacological consequences for anti-angiogenic therapy of cancer. Cell Tissue Res 335:205-222.

Langley RR, Fidler IJ. 2007. Tumor cell-organ microenvironment interactions in the pathogenesis of cancer metastasis. Endocr Rev 28:297-321.

Lastres P, Bellon T, Cabanas C, Sanchez-Madrid F, Acevedo A, Gougos A, Letarte M, Bernabeu C. 1992. Regulated expression on human macrophages of endoglin, an Arg-Gly-Asp-containing surface antigen. Eur J Immunol 22:393-397.

Lastres P, Letamendia A, Zhang H, Rius C, Almendro N, Raab U, Lopez LA, Langa C, Fabra A, Letarte M, Bernabeu C. 1996. Endoglin modulates cellular responses to TGF-beta 1. J Cell Biol 133:1109-1121.

Lastres P, Martin-Perez J, Langa C, Bernabeu C. 1994. Phosphorylation of the human-transforming-growth-factor-beta-binding protein endoglin. Biochem J 301 (Pt 3):765-768.

Laurent S, Forge D, Port M, Roch A, Robic C, Vander Elst L, Muller RN. 2008. Magnetic iron oxide nanoparticles: synthesis, stabilization, vectorization, physicochemical characterizations, and biological applications. Chem Rev 108:2064-2110.

Lebrin F, Deckers M, Bertolino P, Ten Dijke P. 2005. TGF-beta receptor function in the endothelium. Cardiovasc Res 65:599-608.

Lebrin F, Goumans MJ, Jonker L, Carvalho RL, Valdimarsdottir G, Thorikay M, Mummery C, Arthur HM, ten Dijke P. 2004. Endoglin promotes endothelial cell proliferation and TGF-beta/ALK1 signal transduction. EMBO J 23:4018-4028.

Lebrin F, Mummery CL. 2008. Endoglin-mediated vascular remodeling: mechanisms underlying hereditary hemorrhagic telangiectasia. Trends Cardiovasc Med 18:25-32.

Letamendia A, Lastres P, Botella LM, Raab U, Langa C, Velasco B, Attisano L, Bernabeu C. 1998. Role of endoglin in cellular responses to transforming growth factor-beta. A comparative study with betaglycan. J Biol Chem 273:33011-33019.

Li C, Guo B, Bernabeu C, Kumar S. 2001. Angiogenesis in breast cancer: the role of transforming growth factor beta and CD105. Microsc Res Tech 52:437-449.

Li C, Hampson IN, Hampson L, Kumar P, Bernabeu C, Kumar S. 2000. CD105 antagonizes the inhibitory signaling of transforming growth factor beta1 on human vascular endothelial cells. FASEB J 14:55-64.

Li C, Issa R, Kumar P, Hampson IN, Lopez-Novoa JM, Bernabeu C, Kumar S. 2003. CD105 prevents apoptosis in hypoxic endothelial cells. J Cell Sci 116:2677-2685.

Li DY, Sorensen LK, Brooke BS, Urness LD, Davis EC, Taylor DG, Boak BB, Wendel DP. 1999. Defective angiogenesis in mice lacking endoglin. Science 284:1534-1537.

Lidington EA, Rao RM, Marelli-Berg FM, Jat PS, Haskard DO, Mason JC. 2002. Conditional immortalization of growth factor-responsive cardiac endothelial cells from H-2K(b)-tsA58 mice. Am J Physiol Cell Physiol 282:C67-74.

Lindmark G, Gerdin B, Sundberg C, Pahlman L, Bergstrom R, Glimelius B. 1996. Prognostic significance of the microvascular count in colorectal cancer. J Clin Oncol 14:461-466.

Llorca O, Trujillo A, Blanco FJ, Bernabeu C. 2007. Structural model of human endoglin, a transmembrane receptor responsible for hereditary hemorrhagic telangiectasia. J Mol Biol 365:694-705.

Llovet JM, Ricci S, Mazzaferro V, Hilgard P, Gane E, Blanc JF, de Oliveira AC, Santoro A, Raoul JL, Forner A, Schwartz M, Porta C, Zeuzem S, Bolondi L, Greten TF, Galle PR, Seitz JF, Borbath I, Haussinger D, Giannaris T, Shan M, Moscovici M, Voliotis D, Bruix J. 2008. Sorafenib in advanced hepatocellular carcinoma. N Engl J Med 359:378-390.

Loonstra A, Vooijs M, Beverloo HB, Allak BA, van Drunen E, Kanaar R, Berns A, Jonkers J. 2001. Growth inhibition and DNA damage induced by Cre recombinase in mammalian cells. Proc Natl Acad Sci U S A 98:9209-9214.

Lopez-Casillas F, Wrana JL, Massague J. 1993. Betaglycan presents ligand to the TGF beta signaling receptor. Cell 73:1435-1444.

Lopez-Novoa JM, Bernabeu C. 2010. The physiological role of endoglin in the cardiovascular system. Am J Physiol Heart Circ Physiol 299:H959-974.

Lum H, Malik AB. 1996. Mechanisms of increased endothelial permeability. Can J Physiol Pharmacol 74:787-800.

Mahmoud M, Allinson KR, Zhai Z, Oakenfull R, Ghandi P, Adams RH, Fruttiger M, Arthur HM. 2010. Pathogenesis of arteriovenous malformations in the absence of endoglin. Circ Res 106:1425-1433.

Mahmoud M, Borthwick GM, Hislop AA, Arthur HM. 2009. Endoglin and activin receptor-like-kinase 1 are co-expressed in the distal vessels of the lung: implications for two familial vascular dysplasias, HHT and PAH. Lab Invest 89:15-25.

Majmundar AJ, Wong WJ, Simon MC. 2010. Hypoxia-inducible factors and the response to hypoxic stress. Mol Cell 40:294-309.

Manalo DJ, Rowan A, Lavoie T, Natarajan L, Kelly BD, Ye SQ, Garcia JG, Semenza GL. 2005. Transcriptional regulation of vascular endothelial cell responses to hypoxia by HIF-1. Blood 105:659-669.

Mancini ML, Verdi JM, Conley BA, Nicola T, Spicer DB, Oxburgh LH, Vary CP. 2007. Endoglin is required for myogenic differentiation potential of neural crest stem cells. Dev Biol 308:520-533.

Mancuso MR, Davis R, Norberg SM, O'Brien S, Sennino B, Nakahara T, Yao VJ, Inai T, Brooks P, Freimark B, Shalinsky DR, Hu-Lowe DD, McDonald DM. 2006. Rapid vascular regrowth in tumors after reversal of VEGF inhibition. J Clin Invest 116:2610-2621.

Mao X, Fujiwara Y, Orkin SH. 1999. Improved reporter strain for monitoring Cre recombinase-mediated DNA excisions in mice. Proc Natl Acad Sci U S A 96:5037-5042.

Martone T, Rosso P, Albera R, Migliaretti G, Fraire F, Pignataro L, Pruneri G, Bellone G, Cortesina G. 2005. Prognostic relevance of CD105+ microvessel density in HNSCC patient outcome. Oral Oncol 41:147-155.

Massague J. 2008. TGFbeta in Cancer. Cell 134:215-230.

Matsuno F, Haruta Y, Kondo M, Tsai H, Barcos M, Seon BK. 1999. Induction of lasting complete regression of preformed distinct solid tumors by targeting the tumor vasculature using two new anti-endoglin monoclonal antibodies. Clin Cancer Res 5:371-382.

McAllister KA, Grogg KM, Johnson DW, Gallione CJ, Baldwin MA, Jackson CE, Helmbold EA, Markel DS, McKinnon WC, Murrell J, et al. 1994. Endoglin, a TGF-beta binding protein of endothelial cells, is the gene for hereditary haemorrhagic telangiectasia type 1. Nat Genet 8:345-351.

McNamara DA, Harmey J, Wang JH, Kay E, Walsh TN, Bouchier-Hayes DJ. 2001. Tamoxifen inhibits endothelial cell proliferation and attenuates VEGF-mediated angiogenesis and migration in vivo. Eur J Surg Oncol 27:714-718.

Miettinen PJ, Ebner R, Lopez AR, Derynck R. 1994. TGF-beta induced transdifferentiation of mammary epithelial cells to mesenchymal cells: involvement of type I receptors. J Cell Biol 127:2021-2036.

Miller DW, Graulich W, Karges B, Stahl S, Ernst M, Ramaswamy A, Sedlacek HH, Muller R, Adamkiewicz J. 1999. Elevated expression of endoglin, a component of the TGF-beta-receptor complex, correlates with proliferation of tumor endothelial cells. Int J Cancer 81:568-572.

Monvoisin A, Alva JA, Hofmann JJ, Zovein AC, Lane TF, Iruela-Arispe ML. 2006. VE-cadherin-CreERT2 transgenic mouse: a model for inducible recombination in the endothelium. Dev Dyn 235:3413-3422.

Motzer RJ, Hutson TE, Tomczak P, Michaelson MD, Bukowski RM, Rixe O, Oudard S, Negrier S, Szczylik C, Kim ST, Chen I, Bycott PW, Baum CM, Figlin RA. 2007. Sunitinib versus interferon alfa in metastatic renal-cell carcinoma. N Engl J Med 356:115-124.

Murukesh N, Dive C, Jayson GC. 2010. Biomarkers of angiogenesis and their role in the development of VEGF inhibitors. Br J Cancer 102:8-18.

Noguchi R, Yoshiji H, Ikenaka Y, Namisaki T, Kitade M, Kaji K, Yoshii J, Yanase K, Yamazaki M, Tsujimoto T, Kawaratani H, Fukui H. 2009. Synergistic inhibitory effect of gemcitabine and angiotensin type-1 receptor blocker, losartan, on murine pancreatic tumor growth via anti-angiogenic activities. Oncol Rep 22:355-360.

Nowak DG, Amin EM, Rennel ES, Hoareau-Aveilla C, Gammons M, Damodoran G, Hagiwara M, Harper SJ, Woolard J, Ladomery MR, Bates DO. 2010. Regulation of vascular endothelial growth factor (VEGF) splicing from pro-angiogenic to anti-angiogenic isoforms: a novel therapeutic strategy for angiogenesis. J Biol Chem 285:5532-5540.

O'Connell PJ, McKenzie A, Fisicaro N, Rockman SP, Pearse MJ, d'Apice AJ. 1992. Endoglin: a 180-kD endothelial cell and macrophage restricted differentiation molecule. Clin Exp Immunol 90:154-159.

Oh SP, Seki T, Goss KA, Imamura T, Yi Y, Donahoe PK, Li L, Miyazono K, ten Dijke P, Kim S, Li E. 2000. Activin receptor-like kinase 1 modulates transforming growth factor-beta 1 signaling in the regulation of angiogenesis. Proc Natl Acad Sci U S A 97:2626-2631.

Ota T, Fujii M, Sugizaki T, Ishii M, Miyazawa K, Aburatani H, Miyazono K. 2002. Targets of transcriptional regulation by two distinct type I receptors for transforming growth factor-beta in human umbilical vein endothelial cells. J Cell Physiol 193:299-318.

Paez-Ribes M, Allen E, Hudock J, Takeda T, Okuyama H, Vinals F, Inoue M, Bergers G, Hanahan D, Casanovas O. 2009. Antiangiogenic therapy elicits malignant progression of tumors to increased local invasion and distant metastasis. Cancer Cell 15:220-231.

Page DL, Jensen RA. 1995. Angiogenesis in human breast carcinoma: what is the question? Hum Pathol 26:1173-1174.

Pardali E, Goumans MJ, ten Dijke P. 2010. Signaling by members of the TGF-beta family in vascular morphogenesis and disease. Trends Cell Biol 20:556-567.

Pardali E, ten Dijke P. 2009. Transforming growth factor-beta signaling and tumor angiogenesis. Front Biosci 14:4848-4861.

Pardali E, van der Schaft DW, Wiercinska E, Gorter A, Hogendoorn PC, Griffioen AW, ten Dijke P. Critical role of endoglin in tumor cell plasticity of Ewing sarcoma and melanoma. Oncogene 30:334-345.

Pece-Barbara N, Vera S, Kathirkamathamby K, Liebner S, Di Guglielmo GM, Dejana E, Wrana JL, Letarte M. 2005. Endoglin null endothelial cells proliferate faster and are more responsive to transforming growth factor beta1 with higher

affinity receptors and an activated Alk1 pathway. J Biol Chem 280:27800-27808.
Pennacchietti S, Michieli P, Galluzzo M, Mazzone M, Giordano S, Comoglio PM. 2003. Hypoxia promotes invasive growth by transcriptional activation of the met protooncogene. Cancer Cell 3:347-361.
Pepper MS, Vassalli JD, Orci L, Montesano R. 1993. Biphasic effect of transforming growth factor-beta 1 on in vitro angiogenesis. Exp Cell Res 204:356-363.
Perez-Gomez E, Del Castillo G, Juan Francisco S, Lopez-Novoa JM, Bernabeu C, Quintanilla M. 2010. The role of the TGF-beta coreceptor endoglin in cancer. ScientificWorldJournal 10:2367-2384.
Porta C, Paglino C, Imarisio I, Bonomi L. 2007. Uncovering Pandora's vase: the growing problem of new toxicities from novel anticancer agents. The case of sorafenib and sunitinib. Clin Exp Med 7:127-134.
Pruneri G, Bertolini F, Baldini L, Valentini S, Goldaniga M, Soligo D, Carboni N, Viale G, Lambertenghi-Deliliers G. 2003. Angiogenesis occurs in hairy cell leukaemia (HCL) and in NOD/SCID mice transplanted with the HCL line Bonna-12. Br J Haematol 120:695-698.
Pruneri G, Ponzoni M, Ferreri AJ, Decarli N, Tresoldi M, Raggi F, Baldessari C, Freschi M, Baldini L, Goldaniga M, Neri A, Carboni N, Bertolini F, Viale G. 2002. Microvessel density, a surrogate marker of angiogenesis, is significantly related to survival in multiple myeloma patients. Br J Haematol 118:817-820.
Psaila B, Lyden D. 2009. The metastatic niche: adapting the foreign soil. Nat Rev Cancer 9:285-293.
Regal JF. 2004. Murine Asthma Models. Current Protocols in Toxicology 21:18.13.11-18.13.21.
Rendell MS, Milliken BK, Finnegan MF, Finney DE, Healy JC, Bonner RF. 1998. The microvascular composition of the healing wound compared at skin sites with nutritive versus arteriovenous perfusion. J Surg Res 80:373-379.
Rennel ES, Varey AH, Churchill AJ, Wheatley ER, Stewart L, Mather S, Bates DO, Harper SJ. 2009. VEGF(121)b, a new member of the VEGF(xxx)b family of VEGF-A splice isoforms, inhibits neovascularisation and tumour growth in vivo. Br J Cancer 101:1183-1193.
Ricci-Vitiani L, Pallini R, Biffoni M, Todaro M, Invernici G, Cenci T, Maira G, Parati EA, Stassi G, Larocca LM, De Maria R. 2010. Tumour vascularization via endothelial differentiation of glioblastoma stem-like cells. Nature 468:824-828.
Rosen L, Gordon M, Hurwitz H, Mendelson D, Kleinzweig D, Adams B, Theuer C. 2008. Early evidence of tolerability and clinical activity from a phase 1 study of TRC105 (anti-CD105 antibody) in patients with advanced refractory cancer. Eur. J. Cancer Supplements 6:126.
Rosen LS, Gordon MS, Hurwitz HI, Wong MK, Adams BJ, D. A. 2009. Early evidence of tolerability and clinical activity from a phase I study of TRC105 (anti-CD105 antibody) in patients with advanced refractory cancer. J Clin Oncol 27:15.

Saad RS, El-Gohary Y, Memari E, Liu YL, Silverman JF. 2005. Endoglin (CD105) and vascular endothelial growth factor as prognostic markers in esophageal adenocarcinoma. Hum Pathol 36:955-961.

Saad RS, Jasnosz KM, Tung MY, Silverman JF. 2003. Endoglin (CD105) expression in endometrial carcinoma. Int J Gynecol Pathol 22:248-253.

Sandlund J, Hedberg Y, Bergh A, Grankvist K, Ljungberg B, Rasmuson T. 2006. Endoglin (CD105) expression in human renal cell carcinoma. BJU Int 97:706-710.

Sarraf P, Mueller E, Jones D, King FJ, DeAngelo DJ, Partridge JB, Holden SA, Chen LB, Singer S, Fletcher C, Spiegelman BM. 1998. Differentiation and reversal of malignant changes in colon cancer through PPARgamma. Nat Med 4:1046-1052.

Scharpfenecker M, van Dinther M, Liu Z, van Bezooijen RL, Zhao Q, Pukac L, Lowik CW, ten Dijke P. 2007. BMP-9 signals via ALK1 and inhibits bFGF-induced endothelial cell proliferation and VEGF-stimulated angiogenesis. J Cell Sci 120:964-972.

Schimming R, Marme D. 2002. Endoglin (CD105) expression in squamous cell carcinoma of the oral cavity. Head Neck 24:151-156.

Schmierer B, Hill CS. 2007. TGFbeta-SMAD signal transduction: molecular specificity and functional flexibility. Nat Rev Mol Cell Biol 8:970-982.

Seaman S, Stevens J, Yang MY, Logsdon D, Graff-Cherry C, St Croix B. 2007. Genes that distinguish physiological and pathological angiogenesis. Cancer Cell 11:539-554.

Seon BK, Haba A, Matsuno F, Takahashi N, Tsujie M, She X, Harada N, Uneda S, Tsujie T, Toi H, Tsai H, Haruta Y. 2011. Endoglin-targeted cancer therapy. Curr Drug Deliv 8:135-143.

Seon BK, Matsuno F, Haruta Y, Kondo M, Barcos M. 1997. Long-lasting complete inhibition of human solid tumors in SCID mice by targeting endothelial cells of tumor vasculature with antihuman endoglin immunotoxin. Clin Cancer Res 3:1031-1044.

Serrati S, Margheri F, Pucci M, Cantelmo AR, Cammarota R, Dotor J, Borras-Cuesta F, Fibbi G, Albini A, Del Rosso M. 2009. TGFbeta1 antagonistic peptides inhibit TGFbeta1-dependent angiogenesis. Biochem Pharmacol 77:813-825.

Shaner NC, Steinbach PA, Tsien RY. 2005. A guide to choosing fluorescent proteins. Nat Methods 2:905-909.

Shao ES, Lin L, Yao Y, Bostrom KI. 2009. Expression of vascular endothelial growth factor is coordinately regulated by the activin-like kinase receptors 1 and 5 in endothelial cells. Blood 114:2197-2206.

Shariat SF, Karam JA, Walz J, Roehrborn CG, Montorsi F, Margulis V, Saad F, Slawin KM, Karakiewicz PI. 2008. Improved prediction of disease relapse after radical prostatectomy through a panel of preoperative blood-based biomarkers. Clin Cancer Res 14:3785-3791.

She X, Matsuno F, Harada N, Tsai H, Seon BK. 2004. Synergy between anti-endoglin (CD105) monoclonal antibodies and TGF-beta in suppression of growth of human endothelial cells. Int J Cancer 108:251-257.

Shiozaki K, Harada N, Greco WR, Haba A, Uneda S, Tsai H, Seon BK. 2006. Antiangiogenic chimeric anti-endoglin (CD105) antibody: pharmacokinetics and immunogenicity in nonhuman primates and effects of doxorubicin. Cancer Immunol Immunother 55:140-150.

Siemann DW, Bibby MC, Dark GG, Dicker AP, Eskens FA, Horsman MR, Marme D, Lorusso PM. 2005. Differentiation and definition of vascular-targeted therapies. Clin Cancer Res 11:416-420.

Siemann DW, Shi W. 2008. Dual targeting of tumor vasculature: combining Avastin and vascular disrupting agents (CA4P or OXi4503). Anticancer Res 28:2027-2031.

Sini P, Samarzija I, Baffert F, Littlewood-Evans A, Schnell C, Theuer A, Christian S, Boos A, Hess-Stumpp H, Foekens JA, Setyono-Han B, Wood J, Hynes NE. 2008. Inhibition of multiple vascular endothelial growth factor receptors (VEGFR) blocks lymph node metastases but inhibition of VEGFR-2 is sufficient to sensitize tumor cells to platinum-based chemotherapeutics. Cancer Res 68:1581-1592.

Soriano P. 1999. Generalized lacZ expression with the ROSA26 Cre reporter strain. Nat Genet 21:70-71.

St-Jacques S, Cymerman U, Pece N, Letarte M. 1994. Molecular characterization and in situ localization of murine endoglin reveal that it is a transforming growth factor-beta binding protein of endothelial and stromal cells. Endocrinology 134:2645-2657.

Suzuki S, Sano K, Tanihara H. 1991. Diversity of the cadherin family: evidence for eight new cadherins in nervous tissue. Cell Regul 2:261-270.

Suzuki Y, Ohga N, Morishita Y, Hida K, Miyazono K, Watabe T. 2010. BMP-9 induces proliferation of multiple types of endothelial cells in vitro and in vivo. J Cell Sci 123:1684-1692.

Tabata M, Kondo M, Haruta Y, Seon BK. 1999. Antiangiogenic radioimmunotherapy of human solid tumors in SCID mice using (125)I-labeled anti-endoglin monoclonal antibodies. Int J Cancer 82:737-742.

Takahashi N, Haba A, Matsuno F, Seon BK. 2001a. Antiangiogenic therapy of established tumors in human skin/severe combined immunodeficiency mouse chimeras by anti-endoglin (CD105) monoclonal antibodies, and synergy between anti-endoglin antibody and cyclophosphamide. Cancer Res 61:7846-7854.

Takahashi N, Kawanishi-Tabata R, Haba A, Tabata M, Haruta Y, Tsai H, Seon BK. 2001b. Association of serum endoglin with metastasis in patients with colorectal, breast, and other solid tumors, and suppressive effect of chemotherapy on the serum endoglin. Clin Cancer Res 7:524-532.

Takahashi Y, Cleary KR, Mai M, Kitadai Y, Bucana CD, Ellis LM. 1996. Significance of vessel count and vascular endothelial growth factor and its

receptor (KDR) in intestinal-type gastric cancer. Clin Cancer Res 2:1679-1684.
Takei Y, Kadomatsu K, Yuzawa Y, Matsuo S, Muramatsu T. 2004. A small interfering RNA targeting vascular endothelial growth factor as cancer therapeutics. Cancer Res 64:3365-3370.
Talmadge JE, Fidler IJ. 2010. AACR centennial series: the biology of cancer metastasis: historical perspective. Cancer Res 70:5649-5669.
Tammela T, Zarkada G, Wallgard E, Murtomaki A, Suchting S, Wirzenius M, Waltari M, Hellstrom M, Schomber T, Peltonen R, Freitas C, Duarte A, Isoniemi H, Laakkonen P, Christofori G, Yla-Herttuala S, Shibuya M, Pytowski B, Eichmann A, Betsholtz C, Alitalo K. 2008. Blocking VEGFR-3 suppresses angiogenic sprouting and vascular network formation. Nature 454:656-660.
Tan GH, Tian L, Wei YQ, Zhao X, Li J, Wu Y, Wen YJ, Yi T, Ding ZY, Kan B, Mao YQ, Deng HX, Li HL, Zou CH, Fu CH. 2004. Combination of low-dose cisplatin and recombinant xenogeneic endoglin as a vaccine induces synergistic antitumor activities. International Journal of Cancer 112:701-706.
Tanaka F, Otake Y, Yanagihara K, Kawano Y, Miyahara R, Li M, Yamada T, Hanaoka N, Inui K, Wada H. 2001. Evaluation of angiogenesis in non-small cell lung cancer: comparison between anti-CD34 antibody and anti-CD105 antibody. Clin Cancer Res 7:3410-3415.
Tanigawa N, Amaya H, Matsumura M, Shimomatsuya T. 1997. Association of tumour vasculature with tumour progression and overall survival of patients with non-early gastric carcinomas. Br J Cancer 75:566-571.
ten Dijke P, Arthur HM. 2007. Extracellular control of TGFbeta signalling in vascular development and disease. Nat Rev Mol Cell Biol 8:857-869.
ten Dijke P, Goumans MJ, Pardali E. 2008. Endoglin in angiogenesis and vascular diseases. Angiogenesis 11:79-89.
Tozer GM, Kanthou C, Baguley BC. 2005. Disrupting tumour blood vessels. Nat Rev Cancer 5:423-435.
Tsujie M, Tsujie T, Toi H, Uneda S, Shiozaki K, Tsai H, Seon BK. 2008. Anti-tumor activity of an anti-endoglin monoclonal antibody is enhanced in immunocompetent mice. Int J Cancer 122:2266-2273.
Tsujie M, Uneda S, Tsai H, Seon BK. 2006. Effective anti-angiogenic therapy of established tumors in mice by naked anti-human endoglin (CD105) antibody: differences in growth rate and therapeutic response between tumors growing at different sites. Int J Oncol 29:1087-1094.
Twombly R. 2002. First clinical trials of endostatin yield lukewarm results. J Natl Cancer Inst 94:1520-1521.
Uneda S, Toi H, Tsujie T, Tsujie M, Harada N, Tsai H, Seon BK. 2009. Anti-endoglin monoclonal antibodies are effective for suppressing metastasis and the primary tumors by targeting tumor vasculature. Int J Cancer 125:1446-1453.
Unger RE, Krump-Konvalinkova V, Peters K, Kirkpatrick CJ. 2002. In vitro expression of the endothelial phenotype: comparative study of primary

isolated cells and cell lines, including the novel cell line HPMEC-ST1.6R. Microvasc Res 64:384-397.
Valdevenito JP, Gallegos I, Fernandez C, Acevedo C, Palma R. 2007. Correlation between primary tumor pathologic features and presence of clinical metastasis at diagnosis of testicular seminoma. Urology 70:777-780.
van Beijnum JR, Rousch M, Castermans K, van der Linden E, Griffioen AW. 2008. Isolation of endothelial cells from fresh tissues. Nat Protoc 3:1085-1091.
van de Loosdrecht AA, Ossenkoppele GJ, Beelen RH, Broekhoven MG, Drager AM, Langenhuijsen MM. 1993. Apoptosis in tumor necrosis factor-alpha-dependent, monocyte-mediated leukemic cell death: a functional, morphologic, and flow-cytometric analysis. Exp Hematol 21:1628-1639.
Vantyghem SA, Wilson SM, Postenka CO, Al-Katib W, Tuck AB, Chambers AF. 2005. Dietary genistein reduces metastasis in a postsurgical orthotopic breast cancer model. Cancer Res 65:3396-3403.
Verheul HM, Hammers H, van Erp K, Wei Y, Sanni T, Salumbides B, Qian DZ, Yancopoulos GD, Pili R. 2007. Vascular endothelial growth factor trap blocks tumor growth, metastasis formation, and vascular leakage in an orthotopic murine renal cell cancer model. Clin Cancer Res 13:4201-4208.
Volkel T, Holig P, Merdan T, Muller R, Kontermann RE. 2004. Targeting of immunoliposomes to endothelial cells using a single-chain Fv fragment directed against human endoglin (CD105). Biochim Biophys Acta 1663:158-166.
Wang JM, Kumar S, Pye D, Haboubi N, al-Nakib L. 1994. Breast carcinoma: comparative study of tumor vasculature using two endothelial cell markers. J Natl Cancer Inst 86:386-388.
Wang JM, Kumar S, Pye D, van Agthoven AJ, Krupinski J, Hunter RD. 1993. A monoclonal antibody detects heterogeneity in vascular endothelium of tumours and normal tissues. Int J Cancer 54:363-370.
Wang R, Chadalavada K, Wilshire J, Kowalik U, Hovinga KE, Geber A, Fligelman B, Leversha M, Brennan C, Tabar V. 2010a. Glioblastoma stem-like cells give rise to tumour endothelium. Nature 468:829-833.
Wang Y, Nakayama M, Pitulescu ME, Schmidt TS, Bochenek ML, Sakakibara A, Adams S, Davy A, Deutsch U, Luthi U, Barberis A, Benjamin LE, Makinen T, Nobes CD, Adams RH. 2010b. Ephrin-B2 controls VEGF-induced angiogenesis and lymphangiogenesis. Nature 465:483-486.
Weidner N, Folkman J, Pozza F, Bevilacqua P, Allred EN, Moore DH, Meli S, Gasparini G. 1992. Tumor angiogenesis: a new significant and independent prognostic indicator in early-stage breast carcinoma. J Natl Cancer Inst 84:1875-1887.
Weidner N, Semple JP, Welch WR, Folkman J. 1991. Tumor angiogenesis and metastasis--correlation in invasive breast carcinoma. N Engl J Med 324:1-8.
Weissleder R, Pittet MJ. 2008. Imaging in the era of molecular oncology. Nature 452:580-589.

Wels J, Kaplan RN, Rafii S, Lyden D. 2008. Migratory neighbors and distant invaders: tumor-associated niche cells. Genes Dev 22:559-574.

Whelan MC, Senger DR. 2003. Collagen I initiates endothelial cell morphogenesis by inducing actin polymerization through suppression of cyclic AMP and protein kinase A. J Biol Chem 278:327-334.

Wikstrom P, Lissbrant IF, Stattin P, Egevad L, Bergh A. 2002. Endoglin (CD105) is expressed on immature blood vessels and is a marker for survival in prostate cancer. Prostate 51:268-275.

Williams RL, Courtneidge SA, Wagner EF. 1988. Embryonic lethalities and endothelial tumors in chimeric mice expressing polyoma virus middle T oncogene. Cell 52:121-131.

Wong NS, Buckman RA, Clemons M, Verma S, Dent S, Trudeau ME, Roche K, Ebos J, Kerbel R, Deboer GE, Sutherland DJ, Emmenegger U, Slingerland J, Gardner S, Pritchard KI. 2010. Phase I/II trial of metronomic chemotherapy with daily dalteparin and cyclophosphamide, twice-weekly methotrexate, and daily prednisone as therapy for metastatic breast cancer using vascular endothelial growth factor and soluble vascular endothelial growth factor receptor levels as markers of response. J Clin Oncol 28:723-730.

Wong VC, Chan PL, Bernabeu C, Law S, Wang LD, Li JL, Tsao SW, Srivastava G, Lung ML. 2008. Identification of an invasion and tumor-suppressing gene, Endoglin (ENG), silenced by both epigenetic inactivation and allelic loss in esophageal squamous cell carcinoma. Int J Cancer 123:2816-2823.

Yamashita H, Ichijo H, Grimsby S, Moren A, ten Dijke P, Miyazono K. 1994. Endoglin forms a heteromeric complex with the signaling receptors for transforming growth factor-beta. J Biol Chem 269:1995-2001.

Yang DJ, Kim EE, Inoue T. 2006. Targeted molecular imaging in oncology. Ann Nucl Med 20:1-11.

Yoshitomi H, Kobayashi S, Ohtsuka M, Kimura F, Shimizu H, Yoshidome H, Miyazaki M. 2008. Specific expression of endoglin (CD105) in endothelial cells of intratumoral blood and lymphatic vessels in pancreatic cancer. Pancreas 37:275-281.

Yu JL, Rak JW, Coomber BL, Hicklin DJ, Kerbel RS. 2002. Effect of p53 status on tumor response to antiangiogenic therapy. Science 295:1526-1528.

Zhou J, Yu Z, Zhao S, Hu L, Zheng J, Yang D, Bouvet M, Hoffman RM. 2009. Lentivirus-based DsRed-2-transfected pancreatic cancer cells for deep in vivo imaging of metastatic disease. J Surg Res 157:63-70.